



Tan, Moh Chuan (2021) *Design of antenna array and data streaming platform for low-cost smart antenna systems*. PhD thesis.

<http://theses.gla.ac.uk/82055/>

Copyright and moral rights for this work are retained by the author

A copy can be downloaded for personal non-commercial research or study, without prior permission or charge

This work cannot be reproduced or quoted extensively from without first obtaining permission in writing from the author

The content must not be changed in any way or sold commercially in any format or medium without the formal permission of the author

When referring to this work, full bibliographic details including the author, title, awarding institution and date of the thesis must be given

Enlighten: Theses  
<https://theses.gla.ac.uk/>  
[research-enlighten@glasgow.ac.uk](mailto:research-enlighten@glasgow.ac.uk)

# **Design of Antenna Array and Data Streaming Platform for Low-Cost Smart Antenna Systems**

Tan Moh Chuan

Matriculation Number:

Submitted in fulfilment of the requirements for the  
Degree of Doctor of Philosophy

School of Engineering  
College of Science and Engineering  
University of Glasgow



University  
of Glasgow

January 2021

# Abstract

The wide range of wireless infrastructures such as cellular base stations, wireless hotspots, roadside infrastructures, and wireless mobile infrastructures have been increasing rapidly over the past decades. In the transportation sector, wireless technology refreshes require constantly introducing newer wireless standards into the existing wireless infrastructure. Different wireless standards are expected to co-exist, and the air space congestion worsens if the wireless devices are operating in different wireless standards, where collision avoidance and transmission time synchronisation become complex and almost impossible. Huge challenges are expected such as operation constraints, cross-system interference, and air space congestion. Future proof and scalable smart wireless infrastructures are crucial to harmonise the un-coordinated wireless infrastructures and improve the performance, reliability, and availability of the wireless networks.

This thesis presents the detailed design of a novel pre-configurable smart antenna system and its sub-system including antenna element, antenna array, and radio frequency (RF) frontend. Three types of 90° beamforming antenna array (with low, middle and high gain) were designed, simulated, and experimentally evaluated. The RF frontend module or transmit and receive (T/R) module was designed and fabricated. The performance of the T/R module was characterised and calibrated using the recursive calibration method, and drastic sidelobe level (SLL) improvement was achieved using the amplitude distribution technique. Finally, the antenna arrays and T/R modules are integrated into the pre-configurable smart antenna system, the beam steering performance is experimentally evaluated and presented in this thesis.

With the combination of practical know-how and theoretical estimation, the thesis highlights how the modern smart antenna techniques that support most cutting-edge wireless technology can be adopted into the existing infrastructure with minimum distraction to the existing systems. This is in line with the global Smart City initiative, where a huge number of Internet of Things (IoT) devices being wired, or wireless are expected to work harmoniously in the same premises. The concept of the pre-configurable smart antenna system presented in this thesis is set to deliver a future-proof and highly scalable and sustainable infrastructure in the transportation market.

# Declaration

**Name:** Tan Moh Chuan

**Matriculation Number:**

With the exception of chapters 1 to 3 which contain introductory material and literature review, chapters 4 to 7 already been published, all works in this thesis were carried out by the author unless otherwise explicitly stated.

Permission to use has been granted from RFNet Technologies Pte Ltd to use the training materials from the company as shown in *Table 2.2 Deployment cost for the roadside infrastructure covering 10 km distance (in US\$)*. Permission letter can be found in *Appendix A: Permission Request Form*.

The copyright of this thesis rests with the author. No copy, distribution, and re-production are permitted without prior agreement from the author.

The author declares that this thesis does not include work forming part of a thesis presented successfully for another degree, and the thesis has been produced in accordance with the University of Glasgow's Code of Good Practice in Research.

Signature: \_\_\_\_\_

Date: \_\_\_\_\_



# Acknowledgments

*The author would like to acknowledge and express sincere appreciation to the Singapore Economic Development Board (EDB), Singapore, and RFNet Technologies Pte Ltd (RFNet), Singapore for financing and providing a good environment and facilities to support the research.*

*I would like to thank my supervisors Dr. Minghui Li, Dr. Qammer H. Abbasi and Professor Muhammad Ali Imran for providing their professional guidance, laboratories, and IT resource to make my research work possible and completed within the stipulated timeline. It was a great experience to tag on their networks that indirectly enhance the visibility of my research works.*

*I would like to express my appreciation to my co-workers in RFNet Technologies Pte Ltd, Dai Shao Wei, Murdifi bin Muhammad, Tan Geok Sun, and Nelson Teh Saw Hooi who have participated actively in the project discussion and thank for their support during the prototype testing.*

*Finally, a special thanks to my parent, See Eik Kui, family, and friends for providing unconditional support that allows me to have a clear mind throughout the course.*

# Publications and Book Arising from This Thesis

## [Book]

1. M. C. Tan, M. Li, Q. H. Abbasi and M. A. Imran. Antenna Design Challenges and Future Directions for Modern Transportation Market. Springer. (In production, to appear in March 2021).

## [Journal]

2. M. C. Tan, M. Li, Q. H. Abbasi and M. A. Imran, "Design and Characterization of T/R Module for Commercial Beamforming Applications," in *IEEE Access*, vol. 8, pp. 130252-130262, 2020, doi: 10.1109/ACCESS.2020.3009531.
3. M. C. Tan, M. Li, Q. H. Abbasi and M. A. Imran, "A Wideband Beamforming Antenna Array for 802.11ac and 4.9 GHz in Modern Transportation Market," in *IEEE Transactions on Vehicular Technology*, vol. 69, no. 3, pp. 2659-2670, March 2020, doi: 10.1109/TVT.2019.2963111.

## [Conference] – Best Student Paper Award

4. M. C. Tan, M. Li, Q. H. Abbasi and M. Imran, "Sensor Aided Beamforming in Vehicular Environment," *2020 International Conference on UK-China Emerging Technologies (UCET)*, Glasgow, United Kingdom, 2020, pp. 1-4, doi: 10.1109/UCET51115.2020.9205411.

## [Conference]

5. M. C. Tan, M. Li, Q. H. Abbasi and M. A. Imran, "An Amplitude Distribution Network in the T/R Module for Beamforming Applications" Proc. *IEEE International Symposium on Antennas and Propagation (AP-S)*, Montréal, Canada, 2020.
6. M. C. Tan, M. Li, Q. H. Abbasi and M. Imran, "A Recursive Calibration Approach for Smart Antenna Beamforming Frontend," *2020 14<sup>th</sup> European Conference on Antennas and Propagation (EuCAP)*, Copenhagen, Denmark, 2020, pp. 1-5, doi: 10.23919/EuCAP48036.2020.9135881.
7. M. C. Tan, M. Li, Q. H. Abbasi and M. Imran, "A Flexible Low-Cost Hybrid Beamforming Structure for Practical Beamforming Applications," *2019 IEEE*

*International Symposium on Radio-Frequency Integration Technology (RFIT)*, Nanjing, China, 2019, pp. 1-3, doi: 10.1109/RFIT.2019.8929162.

8. D. T. R. Liang, M. C. Tan, M. Li, Q. H. Abbasi and M. Imran, "Radome Design with Improved Aerodynamics and Radiation for Smart Antennas in Automotive Applications," *2019 IEEE International Symposium on Radio-Frequency Integration Technology (RFIT)*, Nanjing, China, 2019, pp. 1-3, doi: 10.1109/RFIT.2019.8929217.
9. M. C. Tan, M. Li, Q. H. Abbasi and M. Imran, "A Wideband Beam forming Antenna Array for 802.11ac and 4.9 GHz," *2019 13<sup>th</sup> European Conference on Antennas and Propagation (EuCAP)*, Krakow, Poland, 2019, pp. 1-5.
10. M. C. Tan, M. Li, Q. H. Abbasi and M. Imran, "A smart and low-cost enhanced antenna system for industrial wireless broadband communication," *12<sup>th</sup> European Conference on Antennas and Propagation (EuCAP 2018)*, London, 2018, pp. 1-4, doi: 10.1049/cp.2018.1218.

# Contents

|   |            |
|---|------------|
| <b>Abstract.....</b>  | <b>i</b>   |
| <b>Declaration.....</b>   | <b>ii</b>  |
| <b>Acknowledgments .....</b>  | <b>iii</b> |
| <b>Publications and Book Arising from This Thesis.....</b>                            | <b>iv</b>  |
| <b>List of Tables .....</b>   | <b>x</b>   |
| <b>List of Figures.....</b>   | <b>xi</b>  |
| <b>List of Acronyms, Constants and Symbols .....</b>                                  | <b>xiv</b> |
| <b>1 Introduction.....</b>  | <b>1</b>   |
| 1.1 Research Motivation.....  | 3          |
| 1.2 Research Objectives .....   | 4          |
| 1.3 Key Contributions .....   | 5          |
| 1.4 Thesis Outline.....   | 6          |
| <b>2 Wireless Infrastructure in the Transportation Market and the Challenges.....</b> | <b>9</b>   |
| 2.1 Wireless Infrastructure in the Transportation Market .....                        | 9          |
| 2.2 Mode of Communications .....  | 14         |
| 2.3 Wireless Cell Planning .....  | 16         |
| 2.4 Wireless Infrastructure Cost Proposition .....                                    | 20         |
| 2.4.1 Cost Factors of the Communication Infrastructure.....                           | 21         |
| 2.4.1.1 Environmental Protection .....  | 22         |
| 2.4.1.2 Electromagnetic Compatibility and Electromagnetic Interference (EMC/EMI) ..   | 22         |
| 2.4.2 Project Cost Estimation – a Case Study .....                                    | 23         |
| 2.5 The Key Challenges .....  | 26         |
| 2.6 The Advantages of the Smart Antenna.....  | 26         |
| 2.7 Summary .....   | 28         |
| <b>3 Beamforming Antenna Concept and System .....</b>                                 | <b>29</b>  |
| 3.1 Direction of Arrival .....  | 29         |
| 3.2 Type of Beamforming Antenna.....  | 32         |
| 3.2.1 Analogue Beamforming.....   | 32         |
| 3.2.1.1 Selectable Antenna Element .....  | 32         |
| 3.2.1.2 Beam Switching Slotted Array .....  | 32         |
| 3.2.1.3 Butler Matrix.....  | 33         |
| 3.2.1.4 Electronically Steerable Parasitic Array Radiator Antenna (ESPAR).....        | 35         |

|          |  |           |
|----------|--|-----------|
| 3.2.1.5  | Rotman Lens .....  | 35        |
| 3.2.1.6  | Blass Matrix .....   | 36        |
| 3.2.1.7  | Wullenweber Array .....  | 37        |
| 3.2.2    | Digital Beamforming .....  | 37        |
| 3.2.3    | Hybrid Beamforming .....   | 38        |
| 3.3      | Smart Antenna System .....                                       | 40        |
| 3.3.1    | Antenna Array .....  | 42        |
| 3.3.2    | Antenna Elements .....   | 43        |
| 3.4      | The Proposed Modern Pre-Configurable Smart Antenna System.....   | 44        |
| 3.5      | Summary .....  | 44        |
| <b>4</b> | <b>Designing the Antenna Element .....</b>                       | <b>46</b> |
| 4.1      | Conventional Microstrip Patch Antenna Element.....               | 46        |
| 4.2      | Enhanced Antenna Element Design and Optimisations.....           | 48        |
| 4.3      | Size of the Ground Plane.....                                    | 52        |
| 4.4      | Radiated Measurement of the Antenna Arrays .....                 | 52        |
| 4.4.1    | Antenna Radiated Measurement Topology.....                       | 53        |
| 4.4.2    | Radiation Measurement of the Single Element Antenna .....        | 56        |
| 4.5      | Summary .....  | 57        |
| <b>5</b> | <b>Designing the Antenna Arrays.....</b>                         | <b>58</b> |
| 5.1      | Optimise the Element Separation .....                            | 58        |
| 5.1.1    | Evaluation of the Elements Separation vs Gain and Beamwidth..... | 59        |
| 5.1.2    | Evaluation of Elements Separation vs Sidelobe Level .....        | 60        |
| 5.2      | Designing the Feeding Network for the Phased Array.....          | 62        |
| 5.3      | Forming the $n \times 4$ Antenna Arrays.....                     | 64        |
| 5.3.1    | $1 \times 4$ Low Gain Antenna Array.....                         | 65        |
| 5.3.2    | $2 \times 4$ Middle Gain Antenna Array .....                     | 66        |
| 5.3.3    | $4 \times 4$ High Gain Antenna Array .....                       | 67        |
| 5.4      | Simulated Result of the $n \times 4$ Antenna Arrays.....         | 69        |
| 5.4.1    | Beam Steering Results of the $1 \times 4$ Array.....             | 70        |
| 5.4.2    | Beam Steering Results of the $2 \times 4$ Array.....             | 71        |
| 5.4.3    | Beam Steering Results of the $4 \times 4$ Array.....             | 72        |
| 5.5      | Antenna Array Prototyping and Experimental Evaluation.....       | 73        |
| 5.5.1    | Assembling the Prototype Antenna Array .....                     | 74        |
| 5.6      | Conducted Measurement of the Antenna Arrays .....                | 77        |
| 5.6.1    | Radiation Results of the Antenna Arrays.....                     | 82        |
| 5.7      | Beamforming Evaluation .....                                     | 84        |

|          |  |            |
|----------|--|------------|
| 5.7.1    | Simulation Results of the Beamforming Antenna Array .....                  | 84         |
| 5.7.2    | Experimental Verifications on the Beamforming Array .....                  | 86         |
| 5.8      | Summary .....  | 89         |
| <b>6</b> | <b>Designing and Characterizing the RF Beamforming Frontend .....</b>      | <b>90</b>  |
| 6.1      | Introduction on T/R module .....   | 90         |
| 6.2      | T/R Module Design .....  | 93         |
| 6.2.1    | Receiver.....  | 94         |
| 6.2.2    | Transmitter .....  | 96         |
| 6.2.3    | RF Switches .....  | 96         |
| 6.2.4    | Power Supply .....   | 97         |
| 6.2.5    | Electrical Interface and Control .....                                     | 97         |
| 6.2.6    | Key Components in the T/R module.....                                      | 98         |
| 6.3      | Schematic and PCB Design.....  | 99         |
| 6.4      | The Prototype of the T/R module.....                                       | 102        |
| 6.5      | Characterization of the RF Performance .....                               | 103        |
| 6.5.1    | Characterizing the RF Output Power .....                                   | 106        |
| 6.5.2    | Characterizing the RF Phase Error.....                                     | 108        |
| 6.5.3    | Characterizing the Amplitude Distribution.....                             | 109        |
| 6.6      | Measurement Results and Discussion .....                                   | 111        |
| 6.7      | Summary .....  | 115        |
| <b>7</b> | <b>The Novel 360 Degree Pre-configurable Antenna Systems.....</b>          | <b>116</b> |
| 7.1      | The Proposed Novel Pre-Configurable Smart Antenna System .....             | 116        |
| 7.2      | Beamforming Concept in the 360° Pre-configurable Smart Antenna System .... | 120        |
| 7.3      | Proposed DOA Estimation Using the Pre-configurable Smart Antenna System    | 122        |
| 7.3.1    | Sector Scanning.....   | 122        |
| 7.3.2    | Direction-Finding.....   | 123        |
| 7.4      | Comparison with the State-of-the-art Antennas .....                        | 124        |
| 7.5      | Summary .....  | 124        |
| <b>8</b> | <b>Future Directions of Beamforming System .....</b>                       | <b>126</b> |
| 8.1      | Future Directions .....  | 126        |
| 8.1.1    | The Concept of Sensor Aided Beamforming.....                               | 127        |
| 8.1.2    | Sensor Aided Beamforming System .....                                      | 128        |
| 8.1.3    | Simulation Result and Discussion.....                                      | 132        |
| <b>9</b> | <b>Conclusions.....</b>  | <b>136</b> |
|          | <b>Bibliography .....</b>  | <b>138</b> |
|          | <b>Appendix A: Permission Request Form.....</b>                            | <b>152</b> |

|  |            |
|--|------------|
| <b>Appendix B: PCB Gerber Artwork File for the Antenna Array.....</b>    | <b>154</b> |
| <b>Appendix C: Specification of the Antenna Substrate Material .....</b> | <b>158</b> |
| <b>Appendix D: Schematic Diagram of the T/R Module.....</b>              | <b>159</b> |
| <b>Appendix E: PCB Gerber Artwork File of the T/R Module.....</b>        | <b>160</b> |
| <b>Appendix F: Bill-of-Materials (BOM) of the T/R Module .....</b>       | <b>164</b> |

# List of Tables

|  |     |
|--|-----|
| Table 2.1 Coverage estimation for access points serving moving clients.....  | 20  |
| Table 2.2 Deployment cost for the roadside infrastructure covering 10 km distance (in US\$). .....   | 25  |
| Table 3.1 Phase associated with selected port feed for the $4 \times 4$ Butler Matrix.....   | 33  |
| Table 3.2 Comparison of the beamforming techniques. ....   | 39  |
| Table 4.1 Conventional MPA antenna performance (without bandwidth and gain enhancement). ....  | 48  |
| Table 5.1 Simulation result of the $4 \times 4$ arrays using the proposed element spacing. ....  | 62  |
| Table 5.2 Parameters calculated for the $\frac{1}{4} \lambda$ impedance transformation. ....   | 64  |
| Table 5.3 Design parameters of the $n \times 4$ antenna arrays. ....   | 69  |
| Table 5.4 Simulated beam steering patterns of the $1 \times 4$ antenna array at 5.5 GHz over the $\pm 40^\circ$ steering angle.....  | 70  |
| Table 5.5 Simulated beam steering patterns of the $2 \times 4$ antenna array at 5.5 GHz over the $\pm 40^\circ$ steering angle.....  | 71  |
| Table 5.6 Simulated beam steering patterns of the $4 \times 4$ antenna array at 5.5 GHz over the $\pm 40^\circ$ steering angle.....  | 72  |
| Table 5.7 Performance summary of the proposed antenna arrays. ....   | 73  |
| Table 5.8 Evaluation results of the $1 \times 4$ , $2 \times 4$ , and $4 \times 4$ antenna arrays at 5.5 GHz.....  | 83  |
| Table 5.9 Beamforming results of the proposed $4 \times 4$ array. (simulated and measured) ....  | 88  |
| Table 6.1 Key components specification in the T/R module. ....   | 98  |
| Table 6.2 Phase compensation for beamforming chains.....   | 111 |
| Table 6.3 Comparison with the state-of-the-art T/R modules. ....   | 115 |
| Table 7.1 Pre-configurable matrix for the proposed flexible smart antenna structure, number of arrays, and different antenna gain can be pre-configured to form a smart antenna system. .... | 119 |
| Table 7.2 Comparison between the proposed antenna system and the state-of-the-art beamforming antenna.....   | 124 |



# List of Figures

|   |    |
|---|----|
| Fig. 1.1 Wireless infrastructure in transportation environment for the wireless link between vehicles to infrastructures. ....  | 2  |
| Fig. 2.1 Typical communication components in a public vehicle. ....   | 12 |
| Fig. 2.2 Cell planning. (a) 3 non-overlapping channels. (b) 7 non-overlapping channels...   | 17 |
| Fig. 2.3 Conventional point to multipoint deployment. ....  | 18 |
| Fig. 2.4 Deployment with the smart antenna. ....  | 19 |
| Fig. 2.5 Wireless zone coverage in the vehicular environment for various application scenarios. ....  | 28 |
| Fig. 3.1 Estimation of the angle of arrival ....  | 30 |
| Fig. 3.2 Adaptive beamforming architecture. ....  | 31 |
| Fig. 3.3 Structure of the $4 \times 4$ Butler Matrix ....   | 33 |
| Fig. 3.4 A $8 \times 8$ Rotman lens layout. ....  | 36 |
| Fig. 3.5 A 3-elements Blass Matrix ....   | 37 |
| Fig. 3.6 Block diagram of the digital beamforming system.....   | 38 |
| Fig. 3.7 Beam switching method for the smart antenna that covers $360^\circ$ azimuth plane, reproduced from [16] - [21]. ....   | 40 |
| Fig. 4.1 Conventional rectangular MPA antenna element ....  | 47 |
| Fig. 4.2 Conventional circular MPA antenna element.....   | 47 |
| Fig. 4.3 Capacitive feed dual-substrate MPA. (a) Top view. (b) Side view .....  | 50 |
| Fig. 4.4 Simulation results of the capacitive feed MPA element. (a) Simulated $S_{11}$ result. (b) Gain characteristic over 4 to 8 GHz band. (c) Far-field radiation pattern..... | 51 |
| Fig. 4.5 Simulation on the effect of the size of the ground plane at 5.5 GHz.....   | 52 |
| Fig. 4.6 Antenna measurement setup in open space. (a) Antenna measurement setup. (b) Antenna orientation (top view). ....   | 54 |
| Fig. 4.7 Photo of the far-field antenna measurement setup. ....   | 55 |
| Fig. 4.8 The radiation pattern of the single element antenna. ....  | 57 |
| Fig. 5.1 The $4 \times 4$ array illustration for “Far Field” simulation.....  | 59 |
| Fig. 5.2 The impact of element spacing on array gain and beamwidth. ....  | 60 |
| Fig. 5.3 The impact of element spacing to the sidelobe level at $0^\circ$ and $30^\circ$ beam. ....   | 61 |
| Fig. 5.4 Antenna feeding networks to integrate the antenna elements into the array for beamforming applications. (a) Series feed. (b) corporate feed. ....                        | 63 |
| Fig. 5.5 Corporate feed design, indicates the microstrip line width for the impedance matching.....   | 63 |
| Fig. 5.6 Microstrip feed on the $n \times 4$ antenna array.....   | 65 |
| Fig. 5.7 Top PCB of the $1 \times 4$ antenna array. ....  | 66 |
| Fig. 5.8 Bottom PCB of the $1 \times 4$ antenna array.....  | 66 |
| Fig. 5.9 Top PCB of the $2 \times 4$ antenna array. ....  | 67 |
| Fig. 5.10 Bottom PCB of the $2 \times 4$ antenna array.....   | 67 |
| Fig. 5.11 Top PCB of the $4 \times 4$ antenna array. ....   | 68 |
| Fig. 5.12 Bottom PCB of the $2 \times 4$ antenna array.....   | 68 |
| Fig. 5.13 Raw PCBs from the factory. (a) Top PCB. (b) Bottom PCB. ....  | 74 |
| Fig. 5.14 The geometrical view of the $4 \times 4$ antenna array. (a) Stack up view. (b) Exploded view.....   | 75 |

|           |  |     |
|-----------|--|-----|
| Fig. 5.15 | Photos of the fabricated antenna arrays. (a) Top side. (b) Bottom side.....  | 77  |
| Fig. 5.16 | Returned loss measurement results. (a) $1 \times 4$ antenna array. (b) $2 \times 4$ antenna array. (c) $4 \times 4$ antenna array. ....  | 78  |
| Fig. 5.17 | Simulation and measured inter-port isolation results. (a) $1 \times 4$ array. (b) $2 \times 4$ array. (c) $4 \times 4$ array.....  | 80  |
| Fig. 5.18 | The measured radiation pattern of the proposed antenna arrays at 5.5 GHz. ....   | 83  |
| Fig. 5.19 | Simulated beamforming performance of the antenna arrays at 5.5 GHz. (a) $1 \times 4$ array. (b) $2 \times 4$ array. (c) $4 \times 4$ array.....                                  | 85  |
| Fig. 5.20 | Block diagram of the $4 \times 4$ beamforming antenna system. ....   | 87  |
| Fig. 5.21 | Measured beamforming results of the $4 \times 4$ array at 5.5 GHz.....   | 88  |
| Fig. 6.1  | Block Diagram of the T/R module for $n \times 4$ array. ....   | 94  |
| Fig. 6.2  | Phase shifter in a beamforming linear array. ....  | 95  |
| Fig. 6.3  | T/R modules mounted on the interface controller board. ....  | 98  |
| Fig. 6.4  | The PCB cross-sectional view of the T/R module.....  | 100 |
| Fig. 6.5  | The impedance-controlled traces (orange traces). ....  | 101 |
| Fig. 6.6  | PCB layers stack-up of the T/R module. ....  | 101 |
| Fig. 6.7  | The prototype of the T/R module. ....  | 103 |
| Fig. 6.8  | The prototype of the test fixture. ....  | 103 |
| Fig. 6.9  | Calibration setup. (a) Setup for transmitting power calibration. (b) Setup for phase calibration.....  | 104 |
| Fig. 6.10 | Iteration flow for power and phase calibration.....  | 105 |
| Fig. 6.11 | Output power and $P_{det}$ , that can be used to determine the RF output power level of the T/R module. ....   | 106 |
| Fig. 6.12 | Power attenuation performance. ....  | 107 |
| Fig. 6.13 | Output power calibration. ....   | 107 |
| Fig. 6.14 | Phase performance of the T/R module, demonstrates that the phase error has been corrected by calibration.....  | 108 |
| Fig. 6.15 | Amplitude distribution model on the $4 \times 4$ array.....  | 109 |
| Fig. 6.16 | 4 T/R modules stacked-up for amplitude distribution characterization.....  | 110 |
| Fig. 6.17 | Simulated results of the SLL performance with different amplitude distribution factors at 5.5 GHz. ....  | 111 |
| Fig. 6.18 | Measured beamforming result with $4 \times 4$ array at 5.5 GHz. ....   | 112 |
| Fig. 6.19 | Measured results of the SLL performance with different amplitude distribution factors at 5.5 GHz. ....   | 113 |
| Fig. 6.20 | 360° beamforming system consists of the 4 units of T/R modules and antenna arrays.....   | 114 |
| Fig. 7.1  | Arrays with pre-configurable gain. (a) $1 \times 4$ array (low gain). (b) $2 \times 4$ array (mid gain). (c) $4 \times 4$ array (high gain). ....                                | 117 |
| Fig. 7.2  | Pre-configurable antenna system. (a) 90° sector with one sub-array. (b) 180° sector with 2 sub-arrays. (c) 270° sector with 3 sub-arrays. (d) 360° sector with 4 sub-arrays..... | 118 |
| Fig. 7.3  | The flexible beamforming antenna structure. (a) Isometric CAD view. (b) 360° beamforming pattern. ....   | 121 |
| Fig. 7.4  | Sector scanning to detect the coarse direction of the target.....  | 123 |
| Fig. 7.5  | Direction- finding to identify the fine direction of the target. ....  | 124 |
| Fig. 8.1  | Combination of sensor fusion and light direction of arrival for future beamforming antenna system .....  | 129 |
| Fig. 8.2  | Operation scenario of the IoT sensors aided beamforming system. ....   | 130 |

|  |     |
|--|-----|
| Fig. 8.3 Top view of the sensors aided beamforming system.....   | 130 |
| Fig. 8.4 Access Points (blue) and mobile waypoints (green) for beamforming simulation.<br>.....  | 133 |
| Fig. 8.5 Distance between the mobile client and the Access points, to demonstrate the<br>nearest AP that the mobile client is connected to while it is moving from point A to<br>B. .... | 133 |
| Fig. 8.6 Simulated beam angle for the mobile client and Access Points at location $m_1$ to<br>$m_{16}$ . ....  | 134 |
| Fig. 8.7 Beamforming at location $m_2$ where the mobile client is connected to $AP_1$ .....  | 135 |

# List of Acronyms, Constants and Symbols

## Acronyms

---

|       |   |
|-------|---|
| 3G    | Third Generation Wireless               |
| 5G    | Fifth Generation Wireless               |
| ACC   | Adaptive Cruise Control                 |
| ACT   | Arrays at Commercial Timescales         |
| ADC   | Analogue to Digital Converter           |
| AI    | Artificial Intelligent                  |
| AP    | Access Points                           |
| ATT   | Attenuator                              |
| AVC   | Advanced Video Coding                   |
| BLE   | Bluetooth low energy                    |
| BOM   | Bill of Material                        |
| BWA   | Broadband Wireless Access               |
| CAN   | Controller Area Network                 |
| CAPEX | Capital Investment                      |
| CAT-5 | Category-5                              |
| CCTV  | Closed Circuit Television               |
| CMOS  | Complementary Metal Oxide Semiconductor |
| COTS  | Commercially Off the Shelf              |
| CPWG  | Coplanar Waveguide                      |
| CR    | Cognitive Radio                         |
| CSRR  | Complementary Split Ring Resonators     |
| CST   | Computer Simulation Technology          |
| CVSS  | Cyclic Variable Step Size               |
| CWS   | Collision Warning System                |
| DAC   | Digital to Analogue Converter           |
| DGS   | Defective Ground Structure              |
| DOA   | Direction of Arrival                    |
| DR    | Dead Reckoning                          |

|         |  |
|---------|--|
| DSP     | Digital Signal Processing  |
| DSRC    | Dedicated Short Range Communications                               |
| DVD     | Digital Video Disc   |
| EBG     | Electromagnetic BandGap  |
| EIRP    | Effective Isotropic Radiated Power                                 |
| EMC     | Electromagnetic Compatibility                                      |
| EMI     | Electromagnetic Interference                                       |
| ESPAR   | Electronically Steerable Parasitic Array Radiator                  |
| ESPRIT  | Estimation of Signal Parameters via Rational Invariance Techniques |
| FIT     | Finite Integration Technique                                       |
| FMS     | Fleet Management System  |
| FOMCON  | Fractional Order Modelling and Control                             |
| FPGA    | Field Programmable Grid Array                                      |
| FR4     | Flame Retardant 4  |
| GaAs    | Gallium Arsenide   |
| GaN     | Gallium Nitride  |
| GOA     | United States Government Accountability Office                     |
| GPS     | Positioning System   |
| GPU     | Graphic Processing Unit  |
| GSC     | Generalized Sidelobe Canceller                                     |
| GUI     | Graphic User Interface   |
| HBF     | Hybrid Beamforming   |
| HD      | High Definition  |
| HetVNET | Heterogeneous Vehicular NETwork                                    |
| HF      | High Frequency   |
| HPBW    | Half Power Beamwidth   |
| IDF     | Intermediate Device Box  |
| IEC     | International Electrotechnical Committee                           |
| IF      | Intermediate Frequency   |
| IoT     | Internet of Thing  |
| IP      | International Protection   |
| IRT     | Innovation, Research and Technology                                |
| ISM     | Industrial, Scientific, and Medical                                |
| IT      | Information Technology   |

|       |   |
|-------|---|
| ITS   | Intelligent Transportation System       |
| LCD   | Liquid Crystal Display                  |
| LED   | Light Emitting Diode                    |
| LNA   | Low Noise Amplifier                     |
| LO    | Local Oscillator                        |
| LSAS  | Large Scale Antenna Systems             |
| LTCC  | Low Temperature Co-fired Ceramic        |
| LTE   | Long Term Evolution                     |
| MAC   | Medium Access Control                   |
| MCM   | Multichip Module                        |
| MEMS  | Micro Electro Mechanical Systems        |
| MIMO  | Multiple Input Multiple Output          |
| ML    | Machine Learning                        |
| MMIC  | Monolithic Microwave Integrated Circuit |
| MPA   | Microstrip Patch Antenna                |
| MPAR  | Multifunction Phased Array Radar        |
| MPEG  | Moving Picture Experts Group            |
| mRSU  | mobile RSU                              |
| MUSIC | Multiple Signal Classification          |
| OCC   | Operation and Command Center            |
| OPEX  | Operational Expenditure                 |
| PA    | Power Amplifier                         |
| PCB   | Printed Circuit Board                   |
| PDA   | Personal Digital Assistant              |
| PIDS  | Passenger Information Display System    |
| PIN   | Positive Intrinsic Negative             |
| PIR   | Pyroelectric Infrared                   |
| RF    | Radio Frequency                         |
| RFIC  | Radio Frequency Integrated Circuits     |
| RIA   | Railway Industry Association            |
| RLD   | Rotman Lens Designer                    |
| ROI   | Return of Investment                    |
| RSSI  | Receiver Signal Strength                |
| RSU   | RoadSide Infrastructure                 |
| RWSN  | Renewable Wireless Sensor Network       |

|       |   |
|-------|---|
| RX    | Receive                                   |
| S/FTP | Shield Foil Screened Twisted Pair         |
| SA    | Spectrum Analyzer                         |
| SDA   | Small Director Array                      |
| SDN   | Software Defined Network                  |
| SI    | System Integrator                         |
| SIFS  | Short Interframe Space                    |
| SiGe  | Silicon Germanium                         |
| SLL   | Sidelobe Level                            |
| SMA   | Sub Miniature Version A                   |
| SMT   | Surface Mount Technology                  |
| SNR   | Signal to Noise Ratio                     |
| SP4T  | Single Pole Four Throw                    |
| SPDT  | Single Pole Double Throw                  |
| sRSU  | static RSU                                |
| SVD   | Singular Value Decomposition              |
| SZPA  | Simplified Zero Placement Algorithm       |
| T/R   | Transmit and Receive                      |
| TETRA | Trans European Trunked Radio System       |
| TIS   | Train Information System                  |
| TMS   | Train Management System                   |
| TTL   | Transistor Transistor Logic               |
| TX    | Transmit                                  |
| UHF   | Ultra High Frequency                      |
| V2I   | Vehicle to Infrastructure                 |
| V2V   | Vehicle to Vehicle                        |
| VA    | Video Analytic                            |
| VHF   | Very High Frequency                       |
| VNA   | Vector Network Analyser                   |
| VoD   | Video on Demand                           |
| VoIP  | Voice over IP                             |
| WAVE  | Wireless Access in Vehicular Environments |
| Wi-Fi | Wireless Fidelity                         |
| WiGiG | Wireless Gigabits                         |
| WLAN  | Wireless Local Area Network               |

**Physical Constants**

|                 |   |
|-----------------|---|
| $c$             | $3 \times 10^8$ m/s, speed of light in free space                     |
| $R$             | 6,371 kilometers, radius of the earth                                 |
| $\varepsilon_o$ | $8.85 \times 10^{-12}$ F / m, electric permeability of the free space |
| $\mu_o$         | $4\pi \times 10^{-7}$ H / m, magnetic permeability of the free space  |
| $\pi$           | 3.14, pi  |

**Symbols**

|                     |  |
|---------------------|--|
| $a_k$               | Relative Amplitude of the Weight for the kth Antenna Element |
| $be$                | Bearing  |
| $d$                 | Distance between 2 points                                    |
| $f_c$               | Center Frequency   |
| $lat$               | Latitude in Degree   |
| $lon$               | Longitude in Degree  |
| $\phi_c$            | Compensated Phase  |
| $\phi_k$            | Phase shift of the weight for the kth antenna element        |
| $P_{ctrl}$          | Power Control  |
| $P_{det}$           | Power Detection  |
| $\theta$            | Angle of Arrival   |
| $w_k$               | Complex Weight for the kth Antenna Element                   |
| $z_o$               | Characteristic Impedance                                     |
| $\mathcal{E}_{eff}$ | Effective Dielectric Constant                                |
| $\mathcal{E}_r$     | Relative Permittivity of the Substrate Material              |
| $\lambda$           | Wavelength   |



# 1 Introduction

The smart antenna in a wireless communication system is a well-known technique commonly adopted to mitigate air space congestion, overcome wireless interference, and lower the system deployment cost. The advancement in the hybrid beamforming technique and adoption of the commercially available components into the smart antenna system have reduced the cost drastically. This has created a clear path for the smart antenna to expand its service into the commercial and industrial applications such as transportation sector, government, public service, and industrial applications. Amongst all, the transportation sector has benefited most from the advancement of smart antenna technology, simply due to the nature of the application scenarios where the wireless infrastructures are expected to serve the uncoordinated mobile clients such as commuters, vehicle to infrastructure, vehicle to vehicle communication and so on. This has cultivated the continuous interests amongst which the researchers continue to embark in improving the smart antenna systems that best suit the transportation industry.

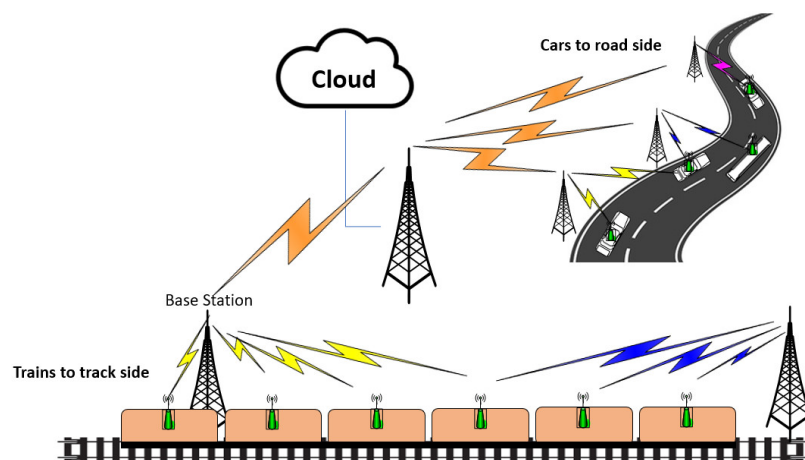
A good commuting experience in the transportation sector is not only measured by the affordability of the transportation cost and the conveniences in terms of the transportation networks and infrastructure framework that allow commuters to reach out to every destination within the city conveniently. A reliable wireless connectivity is highly demanded to provide commuters with a seamless infotainment experiences during the journey. The advancement in the internet technology is supported by highly reliable wireless infrastructures such as Fourth Generation Wireless (4G), Fifth Generation Wireless (5G), 802.11ac, and 802.11ax standards. The standards have incorporated Multiple Input Multiple Output (MIMO) technologies to improve the throughput and reliability performance of the wireless infrastructures. In addition, internet-enabled devices such as smartphones, Internet of Thing (IoT) sensors, and Personal Digital Assistants (PDA) have further pushed the mobile broadband applications to the higher level. Various mobile related applications have been made available such as video streaming, internet conferencing, mobile gaming, and social networking.

In the transportation environment, wireless infrastructures are deployed for public usage such as infotainment accessed via mobile phones and tablets through a wireless hotspot. The wireless infrastructures are also used for the applications that require uploading huge amount of data such as smart city related applications for sensors and Internet of Things (IoT) data

harvesting and devices management, government enforcement such as closed-circuit television (CCTV) installed at the public area for public safety purpose and many more.

Technology refresh is a common term used in the modern transportation sector, where the new wireless technology is introduced to the existing infrastructure. Due to the operation constraint, some of the legacy wireless devices may not be easily replaced with the new technology, therefore, the new wireless technology is expected to sit on top and co-exist with the existing devices. Huge challenges are expected such as operation constraints, cross-system interference, and air space congestion. This thesis is focusing on the popular frequency band between 4.9 GHz - 5.9 GHz band that allows transmission of high throughput broadband data. 4.9 GHz is the licensed band allocated for public safety spectrum [1] and 5GHz band covers the Industrial, Scientific, and Medical (ISM) band and is the worldwide licensed-free spectrum [2] commonly used in broadband WiFi applications.

This thesis is focus on the wireless link between cars to the road-side base stations or trains to the trackside base stations with fixed access points serving multiple mobile clients, referring to Fig. 1.1. The vehicles are installed with wireless clients that connected wirelessly to the wireless infrastructures installed at the roadside, and the wireless client roams across the roadside base stations while it is on the move to achieve seamless connectivity between the wireless client and the base stations. To achieve good wireless coverage for the intended wireless service area, careful wireless cell planning is necessary to determine the numbers of equipment needed, the wireless channel allocation, re-use of the non-overlapping channels, and the transmit power level to ensure the optimum wireless performance. The wireless cell planning may lead to the trade-off between performance and cost.



**Fig. 1.1** Wireless infrastructure in transportation environment for the wireless link between vehicles to infrastructures.

## ***1.1 Research Motivation***

The proven wireless technology and user's expectation have given a strong justification for the industry to demand a highly efficient and reliable wireless infrastructure with high availability. The popularity of wireless infrastructures, especially in the transportation sector, has led to over-congested airspace contributed by the increase in wireless infrastructures. The technology advancement may turn into a disaster if the air space congestion remains unattended. A smart antenna system [43] with a wide operating band from 4.9 to 5.9 GHz, a pre-configurable gain of 10 to 17 dBi, and a pre-configurable coverage sector is expected to mitigate the un-coordinated air space congestion issue.

Over the years, researchers and industry partners are working hard to mitigate the air space congestion issues using various approaches, such as more coordinated wireless planning, regulatory enforcement to restrict the frequency usage and limit the radiated power, and introduction of the new frequency spectrum for public usage. The smart antenna concept is one of the most powerful solutions that address the air space congestion issues from the source itself. In the smart antenna system, both the base station and mobile client are coordinated and only focus the radiating beam and receiving beam to each other with narrow beamwidth and cancels interference from other directions. The technique is aimed to focus the transmitter's radio frequency (RF) energy to the destination with minimum interference to the surrounding devices, similarly, at the receiver, it will focus its hearing beam to the radiating source and null off all the other directions to minimise the interference from the surrounding devices. Hence, the smart antenna technique is expected to mitigate the mutual interference issues between the transmitting and receiving devices.

The wireless infrastructure is deployed to support the day-to-day operation in the transportation sector, and the implementation cost is the key challenge due to its stringent requirements on safety, electromagnetic compatibility, and high availability. During the wireless infrastructure upgrade, the system integrators shall make sure minimum disruptions to the existing operations while performing the upgrade. Therefore, the equipment cost is crucial to the entire project budget, and reducing the number of equipment needed without compromising the functionality of the system is another interesting area for the researchers and system integrators to continue exploring. The smart antenna technique is expected to reduce the amount of equipment by multiple folds and is expected to operate and provide the same coverage as compared to the conventional wireless deployment methods.

## 1.2 Research Objectives

As discussed earlier, it is important to have a low-cost field-friendly smart antenna system to mitigate the air space congestion, lower the deployment and maintenance cost, that works well in the un-coordinated wireless environment in the transportation sector. In addition, it shall allow a seamless integration into the existing wireless infrastructure by leveraging on the transportation infrastructures and operation scenarios. The key objectives of this research are derived in line with the above in mind, the objectives are listed as follow:

- i) To assess the importance of the smart antenna in the transport-related industry, including the constraint and challenges, by taking into consideration the various applications and operation requirements that lead to the overwhelming of wireless infrastructure in the transportation sector. Identify the gap and propose suitable mitigation with the novel “Modern Pre-Configurable Smart Antenna System”.
- ii) To study the cost that constitutes the wireless infrastructure deployment in the transportation industry through a case study. This was carried out with an in-depth understanding of the cost implications due to regulatory, environmental protections, and Electromagnetic Compatibility and Electromagnetic Interference (EMC/EMI) requirement. The study aimed to further justify why the pre-configurable smart antenna system is vital to address or mitigate the various challenges encompassed in the wireless infrastructure deployment in the transportation environment.
- iii) The research is targeted to achieve a low-cost smart antenna system, this objective can be achieved by the low-cost hybrid beamforming structure that leverages on application scenarios, usage of the commercially available off the shelf components, and commercial affordable manufacturing process.
- iv) To research and design the antenna array structure including the elements that can operate in a wide frequency band from 4.9 to 5.9 GHz, a pre-configurable gain (between 10 to 17 dBi which can be pre-configured during the smart antenna deployment), a low sidelobe level, and is capable of performing beamforming that is suitable for application in the transportation sector.
- v) To research and design a low-cost and high-performance Transmit and Receive (T/R) module that can be integrated with the antenna array to form a smart antenna system. To achieve that, the components shall be selected from commercially available off the shelf components and manufactured by the low-cost commercial manufacturing technology.
- vi) To research and design a novel pre-configurable smart antenna structure aimed to reduce the number of equipment in the wireless infrastructure deployment in the transportation

environment, and the smart antenna structure shall outperform the conventional smart antenna system in terms of cost and performance.

- vii) To assess the current smart antenna technology and provide the future direction on how the smart antenna can evolve in the IoT world.

### 1.3 Key Contributions

The wireless air space congestion and huge deployment cost in the transportation sector are the real problem. A novel low-cost pre-configurable smart antenna has been presented in the work, the research contributions include the development of the antenna element, antenna arrays, data streaming platform (transmit and receive module) and finally the pre-configurable smart antenna system. The field-friendly pre-configurable smart antenna structure proposed in this thesis is expected to mitigate the sticky air space congestion issues as well as reducing the number of equipment needed in the field. The key contributions arising from this thesis are summarised below.

- i) Optimizing the wide operating band MPA element to cover the 4.9 GHz – 5.9 GHz band that can be materialized by the dual-substrates technique by integrating the MPA on two thick substrates consisting of air and the F4BTM-2 substrate.
- ii) Designing the flexible antenna array structure from the proposed element, and the structure can be prefabricated to support multiple gains 11.16, 14.59, and 17.25 dBi for  $1 \times 4$ ,  $2 \times 4$ , and  $4 \times 4$  arrays, respectively. Each array can support a narrow beamwidth of  $25^\circ$  that allows beam steering in the azimuth plane. The array can be picked and matched to integrate into the pre-configurable antenna system.
- iii) Designing a commercially affordable T/R module that operates in 4.9 – 5.9 GHz band for commercial and industrial applications. The T/R module was designed, calibrated, and characterized for use in the beamforming smart antenna systems. The proposed recursive calibration process managed to correct the phase error to  $\pm 1^\circ$  and amplitude error to  $\pm 0.2$  dB. In addition, the amplitude distribution of 0.5-1-1-0.5 combination has successfully suppressed the side-lobe level (SLL) to -28.7 dB for  $0^\circ$ , -22.71 dB for  $\pm 20^\circ$  and -12.77 dB for  $\pm 40^\circ$  beam steering.
- iv) Proposing a novel 360 pre-configurable antenna structure with the pre-configurable sector and gain. Each sector covers  $90^\circ$  scanning angle, the antenna structure can be preconfigured to enable coverage over the  $90^\circ/180^\circ/270^\circ/360^\circ$  area, up to 4 arrays to support  $360^\circ$  coverage. In addition, the gain of the pre-configurable antenna system can be selected from the  $1 \times 4$ ,  $2 \times 4$ , and  $4 \times 4$  arrays.

- v) To assess the evolution of the smart antenna industry by combining with the sensor fusion from existing IoT sensors such as GPS, accelerometer, gyroscope, odometer, and Bluetooth low energy (BLE). By leveraging on the operation behaviour and IoT infrastructure, the geographical locations of the mobile client can be determined and further computed into useful location-based information that helps the roadside APs and mobile terminal to coordinate and determine the accurate beamforming angle within them.

## 1.4 Thesis Outline

The rest of the thesis is organised as follow:

Chapter 2 covers the initial task to explore the importance of wireless infrastructure in the transportation sectors, includes the various applications in the transportation market which make use of the wireless roadside and rail side infrastructures. Applications span from data transfer of basic vehicular information, passenger infotainment, public safety, remote monitoring, and Internet of Thing (IoT) that called upon a reliable and secured wireless infrastructure. Field deployment methods such as cell planning and a comprehensive case study on the cost proposition in the wireless infrastructure deployment in the vehicular environment have been studied and presented in detail, and the performance and cost-benefit from CAPEX and OPEX have given a solid justification for the existence of smart antenna.

Chapter 3 covers the literature research on the various beamforming techniques utilised in the smart antenna industry such as analogue beamforming, digital beamforming, and hybrid beamforming. Follows by the review on the existing state-of-the-art antenna systems, including the antenna element, phased array, and the 360° coverage smart antenna system. Finally, a novel smart antenna structure “A Modern Pre-Configurable Smart Antenna System” was proposed. The proposed system is adopting the hybrid beamforming technique, which allows pre-configuration on both gain and coverage sector and performs electronic beam steering up to 360° in the azimuth plane.

Chapter 4 covers the necessary steps to optimise the antenna elements, which start with the single element design, simulation, and optimisation. Followed by steps to define the size of the antenna ground plane that eventually determines the overall size of the antenna. Finally, the radiating performance of the antenna element was evaluated, and results were presented. The measurement setup and topology are explained in detail with supporting photos, the same measurement topology was used in all the radiating measure in this work.

Chapter 5 runs through the design of the phased array by integrating the elements into 3 types of arrays  $1 \times 4$ ,  $2 \times 4$ , and  $4 \times 4$  with low, medium, and high gain. The array element spacing was studied and simulated to define the optimum performance and the trade-off between the gain, bandwidth, and sidelobe performance are highlighted. The prototype of the antenna arrays are fabricated using the commercially available printed circuit board (PCB) fabrication process followed by the soldering process to construct the array that consists of 2 pieces of PCBs. Finally, the arrays are experimentally evaluated on their conducted and radiated performance. The performance of the  $360^\circ$  pre-configurable antenna system was evaluated and tabulated in a table to compare with the state-of-the-art  $360^\circ$  beamforming antenna systems.

Chapter 6 presents the design, characterisation, and performance evaluation of the prototype beamforming T/R module for beamforming application in a linear phased array that operates in the commercial frequency band of 4.9 – 5.9 GHz band. The low-cost design was achieved by adopting the commercially available off the shelf components and mass volume production strategy. The design processes are explained in detail, including the functional blocks of the T/R module, schematic, PCB design, and fabrication of the prototype. The T/R module has been fabricated and experimentally evaluated, the recursive calibration method was introduced to calibrate the amplitude and phase errors of the T/R module. The performance of the T/R module is then validated with the phased array that was designed earlier in this project to verify the beam steering capability and finally, the sidelobe level (SLL) was optimised using the amplitude distribution method.

Chapter 7 presents the construction of the pre-configurable antenna system, and the configurations were derived from an in-depth understanding of the field deployment scenarios. The pre-configurable smart antenna system consists of 1 to 4 arrays with low, middle, or high gain, that capable of providing  $360^\circ$  azimuth coverage with a narrow half-power beamwidth and high beam-steering resolution. The benefits of the proposed smart antenna system against the state-of-the-art antenna system were presented.

Chapter 8 provides a moving forward overview of the smart antenna evolution in the modern transportation sector. By taking advantage of the pre-installed and fixed roadside or rail side infrastructure combined with the IoT sensors to form a futuristic smart antenna system. The antenna beamforming can be derived from the sensors data via a sensor fusion module together with the information of the known locations of the roadside infrastructures. The useful location-based information can be generated to help the roadside base stations and mobile terminals to coordinate and determine the accurate beamforming angle within

them while the mobile clients are on the move. The highly complex Field-Programmable Grid Array (FPGA) cost that is usually used in the conventional beamforming smart antenna system can be reduced. This is expected to reduce the smart antenna cost further while proving more accurate beamforming capability.

Chapter 9 concludes the thesis. Additional supporting materials such as design outputs and some critical specifications are included in Appendix A to D to provide additional information that is helpful to support the thesis content.



## 2 Wireless Infrastructure in the Transportation Market and the Challenges

### *2.1 Wireless Infrastructure in the Transportation Market*

As wireless technology emerges, sending a big amount of data from mobile terminals over the wireless infrastructure to the backend server becomes possible. A lot of opportunities have been created in digital data mining, migration from analogue system to digital system, and automates partial of the operations and control via wireless infrastructures. This phenomenon is in line with the local government initiative to promote the smart, connected, and sustainable smart city. This has improved the operations of the local industries such as transportation, factory automation, autonomous vehicles, and city surveillance. Among all, the transportation section has benefited most due to the nature that the automotive vehicles are physically isolated from the ground system and the only mode of communication is wireless. A book on the Railway related Broadband Wireless Communications [3], the French Innovation, Research and Technology (IRT) has demonstrated the equipment and infrastructures that were installed to cover the in-vehicle internet access and other related applications that aimed to bridge between the industry and academic research. The coverage including the railway wireless standards requirement as well as operational applications and passenger applications.

The consolidated works related to vehicular communication and networks were reported in [4], the topics covered by this book include i) Vehicle to Vehicle (V2V) and Vehicle to Infrastructure (V2I) communication, ii) medium access control (MAC) layer in vehicular communications, iii) vehicular communications protocols such as opportunistic routing, iv) dynamic spectrum access, v) security and privacy, vi) connected vehicle in Intelligent Transportation System (ITS), and vii) simulation and modelling work in vehicular networks and location-based applications. The report provides the insight with join opinions

---

*This chapter is reproduced from paper #10 in the publication list on page iv, where the thesis author is the main author in this paper.*

from different authors who are expert in their research field in particular to the vehicular networking.

In the transportation market, wireless infrastructures are deployed for various type of applications, the most common applications are highlighted below,

**Smart City:** various type of sensors was deployed at the roadside and as well as vehicles to constantly upload device health data to the backend for device health monitoring, control, and big data analysis. For example, the smart streetlight, where the ambient sensors are deployed on the street lamps to monitor the environmental condition such as temperature, humidity, and dimmer level, all the smart lamp poles are wirelessly linked and the data collected is sent to the backend wirelessly for analytic. For smart car park applications, the cars are equipped with wireless sensors that communicate with the car park infrastructures for parking charges and parking management and monitoring.

Power meter and water meter turned smart with built-in wireless, all the smart meters in a city are wirelessly connected to the back end management server, where remote monitoring and meter reading can be done easily that is essential to reduce the human cost. Another example is for disaster management, where multi-functional sensors such as seismic sensors and flood sensors can be installed at the prominent area to have early detection and warning on earthquake, flood, and typhoon that can save millions of humans' life if the disaster can be detected earlier and warning can be disseminated on time. All the sensors can be controlled and managed wirelessly via a central device management system located remotely.

**Closed-circuit television (CCTV):** as part of the public security initiative, local government and enforcer have installed public CCTV along the public roadsides and within the mobile vehicles to monitor the crowd condition and ensure the safety of the residents and passengers. In the past, the CCTV footage was stored in the local storage and re-cycle itself due to the limited storage. With the advancement of wireless technology and cloud storage, the CCTV footage is sent wirelessly to the backend server for storage and further video analytic process. Artificial intelligent (AI) and machine learning (ML) can be incorporated at the backend with powerful machines such as high-end graphic processing unit (GPU), and FPGA to enable video analytic, MI, and inferencing. Such equipment is not possible to be installed at the edge or mobile terminal due to their high cost and power consumption.

**Passenger Information:** most of the public transports, stations, terminals, and interchanges had equipped with passenger information display system (PIDS). It can be in the form of audio and visual display such as light-emitting diode (LED) display or graphic

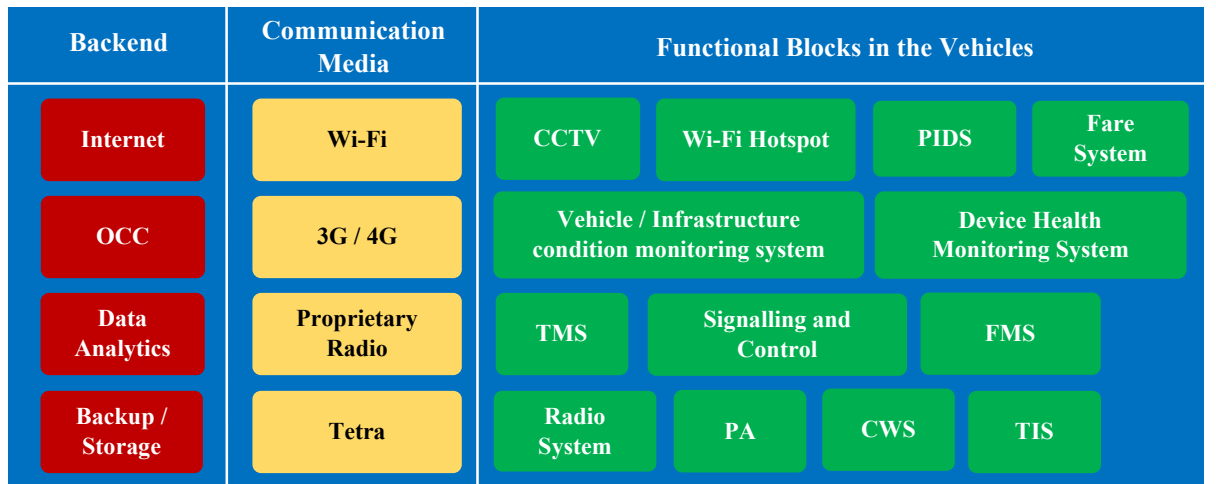
liquid crystal display (LCD). Passenger information such as current stop, next stop, interchange information, time of travel, emergency announcement, and intercom are disseminated to provide commuters with the timely update and create a pleasant and comfortable journey. The modern transportation system also comes with large signages where the stations' information and nearby attractions can be pushed to the signages that are located at the prominent area. Due to the locations of the PIDSs are scattered around the city, hence wireless communication is the most convenient communication network to connect them with the back end.

**Passenger Infotainments:** the advancement of wireless technology has also improved the lifestyle of the commuters, the mobile terminals installed in the automotive such as public buses and trains are wirelessly linked to the backend server, the mobile clients are expected to roam seamlessly across the wireless infrastructures installed along the roadside or rail side. Many types of public transports are equipped with signages for advertisement and posting of real-time announcement or commuter's related information. Wireless hotspots are available within the public buses and trains to provide entertainment during the bus or train journey such as internet serving, video on demand (VoD), voice over IP (VoIP), live streaming, and video/television conferencing. This has indirectly jacked up the usage expectation where a reliable infrastructure is expected to overcome issues such as air space congestion and un-coordinated infrastructures deployment from the different service providers.

**Operations and Services:** this is related to the command and control of the vehicles, including schedule planner, destination routing, signalling, obstacle detection, driving assistance, collision warning system (CWS), fare management system, driver management systems, real-time information exchange between the mobile vehicle and backend allows remote monitoring, and automates part of the operations remotely. For preventive and corrective maintenance, the central maintenance system can remotely record and monitors the sensors installed onboard. The sensors include, tyre pressure sensors, flood sensors, CCTV footage that monitors the entire sector of the rail structure for early detection of crack or deformation, the sensors data collected from the road or rail side can be analysed as part of the predictive and corrective maintenance exercise that improve the system reliability.

A flat functional map of the various communications component in the modern transportation sector is presented in Fig. 2.1. In the practical scenario, the automotive vehicles are on the move and it requires a seamless communication with the backend that provides the communication link between the vehicle to the backend operation and

command center (OCC). To uploads vehicular information and data collected during the journey and provide infotainment and internet connectivity to the commuters during their journey. All the above require a stable, reliable, and robust wireless infrastructure. The fact is that the communication media adopted in the transportation environment usually comes with different wireless systems that work on different standards and operating frequencies, that makes the co-existence task challenging. The network or wireless engineers need to design the system very carefully to ensure the co-existence between different communication equipment with multiple wireless standards to work harmonically within same premises in the transportation environment.



**Fig. 2.1** Typical communication components in a public vehicle.

In the transportation sector, Trans-European Trunked Radio System (TETRA) radio is widely used as a radio system for data and voice communication, voice communication includes the communication between the field operation personnel and the control center, and public address (PA) announcement. TETRA radio also used as a data communication link to transfer a small amount of data over the network such as short emergency messaging, and device health monitoring. The TETRA system operates in the very high frequency (VHF) band around 150 MHz and ultra-high frequency (UHF) band from 300 MHz to 1 GHz, the frequency selection highly dependent on the local authority who allocates the frequency spectrum in the respective country. The communication distance of the TETRA system depends on the allowable effective isotropic radiated power (EIRP) allowed by the local government. However, due to the radio propagation nature of the VHF and UHF frequency, the signal can be penetrated very far even for operation scenario where physical line of sight coverage is not possible such as the congested transportation environment, tunnel and within the buildings, this has made the TETRA radio a popular choice for mission-critical voice and data communication in the transportation sector.

For other mission-critical communication such as train management system (TMS), train signalling and control, interfacing with train information system (TIS), fleet management system (FMS), and CWS, that require higher data throughput, low latency, and secured connections. The proprietary radio communication system that may operate in different frequencies such as 2.4 GHz is used, however, the choice is highly dependent on the transport operators themselves. Such proprietary radio has built-in necessary Information Technology (IT) security profiles and collision avoidance that make it reliable to handle mission-critical communications. Usually, such a system comes as a standard built-in system provided by the vehicle manufacturer such as rolling stock and bus manufacturer as a standard package. Due to most of the usages are for mission-critical applications, the proprietary system was developed a long time back and its reliability and safety have been fully tested, verified, and proven over the years. In general, such a system will not be easily replaced.

When moving up to higher throughput applications such as CCTV surveillance, PIDS, vehicle/infrastructure condition monitoring systems, device health monitoring system, and fare systems, wireless networking standards such as 802.11 Wi-Fi that operated in the unlicensed band on 2.4 GHz and 5 GHz and cellular standards such as LTE and 5G can be deployed. The 802.11 standards are preferred over the cellular due to the licensed free spectrum and commercially affordable compared to cellular where the transport operators will need to pay for monthly service subscription fees to the telecom operators throughout the operation years. Over the years, we are seeing more adoption towards cellular usage thanks to the reduction of subscription cost due to massive competition amongst the telecom operators and the reduction in equipment cost. The data collected from the train is transmitted in real-time, delayed, or opportunist transmission to the back end or OCC where remote monitoring, command, and control or storage and further data analytic take place. In the IoT world, for instance, the data collected from vehicle/infrastructure monitoring system and TIS can be further processed using data analytic, machine learning (ML), and artificial intelligence (AI) to generate visualisation in term of the graphic user interface (GUI) or interactive dashboard to provide the stakeholder with an overview of the overall system performance.

With the help of technology, the big data can be further translated into useful data to determine the likelihood of components failure that may lead to system failure which can be further translated into predictive and preventive maintenance to further enhance and improve the reliability of the system. With the powerful processor at the backend, the CCTV footage transmitted to the backend can be further processed using highly complex video analytic

(VA) technology. The VA with the help of ML and AI allows the system to provide alerts when it identifies any suspicious objects or persons, and public bullying, this can serve as part of crime prevention activities in the transport industries.

The smart gadgets had emerged rapidly into our daily life, smartphones or tablets with internet connectivity becomes part of our accessories when we are in the moves. Lifestyle has been improved and the user expectation in the internet connectivity has risen, the PIDS provides real-time information about the journey, travelling time, current location, and destination as well as providing geographical highlight especially for the tourists. The in-vehicle wireless hot spot becomes popular with the introduction of smart devices, while in the moves, the commuters are expected to keep in touch with their friends through the social platform, perform works or entertainment that requires seamless connectivity to the internet. The Wi-Fi hot spot usually operates in the 2.4 GHz or 5 GHz band, which is the built-in feature in modern smart devices. The internet connectivity of the mobile vehicle is obtained through backhaul wireless connections to the backend either via another Wi-Fi infrastructure or cellular such as 4G. In recent days, new infrastructure deployment has considering Wi-Fi as roadside or trackside infrastructure to provide seamless data connectivity when the vehicle is in the moves.

## ***2.2 Mode of Communications***

Wireless communications in the transportation sector can be divided into 2 major areas, V2I and V2V. In the V2I infrastructure, the RSUs are installed at the roadside or nearby buildings to provide communication between the vehicular networks and the moving vehicles it is convenient to use existing cellular network or Wi-Fi technology to handle the necessary data throughput. In the case of V2V communications, the preferred technology can be LTE device-to-device standards or dedicated short-range communication (DSRC) technology, and it has gradually set a foundation for the future autonomous vehicle. In this section, the authors have included some interesting works that were presented in the academic world to demonstrate and enhance the communication performance in the V2I and V2V communications network.

In [5], the authors had demonstrated the comprehensive and comparative study in a city environment covers the communication hardware and software details as well as system integration models for two important vehicle communication types, V2V, and V2I communications. The software-defined network (SDN) concept that enables efficient data

services in vehicular networks was defined. The networking scheme presented includes DSRC for the vehicle-to-vehicle communications, In-cabin Wi-Fi for hot spot applications, and vehicle light communications. The book also covers the type of antennas for V2V and V2I communication and the physical layer according to the IEEE 802.11p standard, the IEEE 802.11p V2V and V2I communication technology is an amendment to the IEEE 802.11 standard that added Wireless Access in Vehicular Environments (WAVE) in Wi-Fi-based to support ITS applications.

The V2I and V2V communications based on Heterogeneous Vehicular NETWORK (HetVNET) frameworks have been illustrated in [6] for the requirement in safety as well as non-safety services in the ITS, the V2I and V2V communication were evaluated based on LTE cellular and DSRC technology which provides real-time and efficient information exchange among vehicles. By evaluating the various protocols on medium access control and networks layers, the authors have concluded that the LTE and DSRC are the best solutions to support the HetVNET networks for V2I and V2V communication respectively, where the cellular network provides wide coverage for the automotive users and the DSRC communication provides the reliable connection between vehicle to vehicle with low latency which is crucial for safety-critical communications.

In practical vehicular communication, the cellular networks provide a wide coverage range to the vehicular, however, it has a limited bandwidth when the number of vehicles that need to be served by a single base station increases. The bandwidth offload via roadside Wi-Fi infrastructure was proposed in [7] where the vehicles will aggressively cache the data when it passes the base station for offline browsing. The experiment was done in the highway and the results revealed that both unicast and broadcast-based systems have their communication throughput degraded when the density of the vehicle increases. The authors have proposed a method to incorporate device-to-device data scavenging that allows the vehicle to share information within them when the vehicles are passing the base stations, the method has successfully improved the throughput and reliability of the connections.

One of the main functions of the roadside infrastructure is to upload the CCTV data or provide real-time viewing of the CCTV footage in the vehicles at the backend 802.11p in the vehicular environment. H.264 also referring to advanced video coding (AVC) is the most popular standard for coding of high definition (HD) digital video, it compresses the video to approximately half of the space of Moving Picture Experts Group (MPEG-2), the digital video disc (DVD) standard and maintaining the same high-quality video. H.264 is a very common coding technique used in CCTV surveillance system. In [8], the H.264/AVC codec

extension has been proposed, the proposal was based on the 3-D discrete wavelet transform comes with a rate control algorithms and low-complexity unequal packet loss protection to achieve scalable video coding, good video visual quality was achieved with the V2I communication distance within 600 meters.

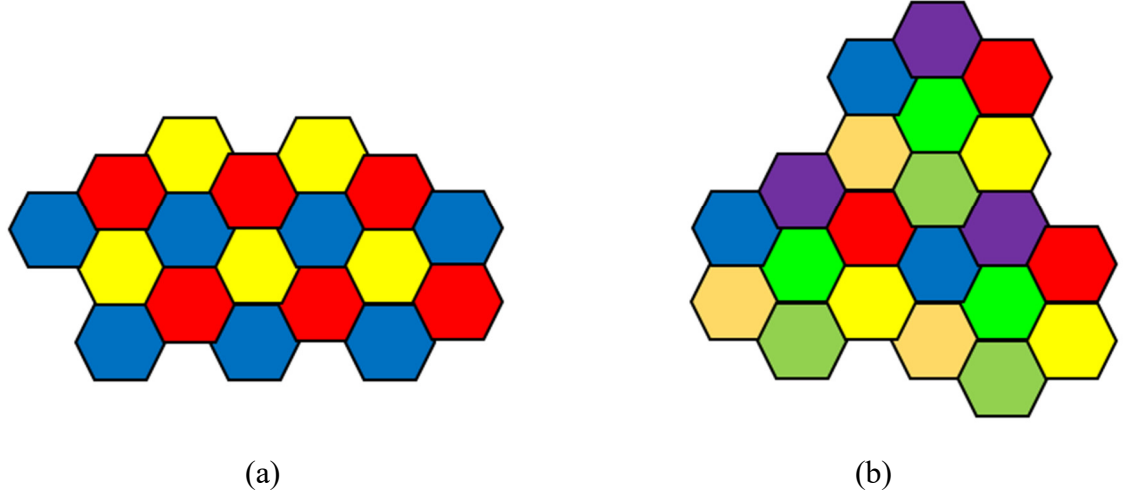
The roadside infrastructure is also referring to the RSU, as the cost of the roadside deployment is very high due to the stringent requirement of the equipment to sustain in the harsh outdoor environment and fieldwork such as cabling and equipment mounting structure. The study was carried out to reduce the deployment cost in [9] by introducing the concept of sub-category RSU called mobile RSU (mRSU) and static RSU (sRSU). By taking the advantage of the buses that have a fixed travelling route, bigger volume to house the RSU, the experiment and analysis results on the replacement ratio has been conducted based on the contact time, intercontact time, and throughput. The results revealed that the mRSUs can replace sRSUs with a certain replacement ratio without degrading the system throughput. The results can be used as a guideline to determine the utilisation ratio of mRSU and sRSU that achieve the optimum performance and cost trade-offs.

### ***2.3 Wireless Cell Planning***

The wireless cell panning is commonly used in wireless infrastructure deployment planning to determine the number of base stations is needed to provide optimum coverage to the service area, performance criteria such as coverage range of each base station, and reuse of frequency or channel are considered during the wireless cell planning. In the conventional wireless cell deployment, to ensure minimum interference from adjacent cells and maximise the usage of available frequency channels, a set of non-overlapping frequencies are used in the cluster, each cluster consists of multiple hexagonal cells, the cluster patterns are reused to create the entire coverage area. A low-cost hybrid beamforming antenna structure has been presented in [10], the paper highlighted the cell planning requirement for the conventional and smart antenna system, and the benefits with the smart antenna are highlighted along with the low-cost hybrid beamforming architecture. The cell planning scheme for 3 non-overlapping frequencies and 7 non-overlapping frequencies are shown in Fig. 2.2, different frequencies are represented by different colours. The cell deployment scheme can be chosen depending on the type of communication system, for instance, 7 non-overlapping cell planning scheme can be deployed on 802.11a/ac system that operates on 24 non-overlapping channels, while 802,11bgn with only 3 non-overlapping channels shall adopt 3 non-overlapping cell planning scheme. The 7 non-overlapping cell



planning scheme has the advantage over the 3 non-overlapping cell planning scheme in term of co-channel interference due to the frequency reuse is 3 cells away compare to only 2 cells away for the 3 non-overlapping cell planning scheme.



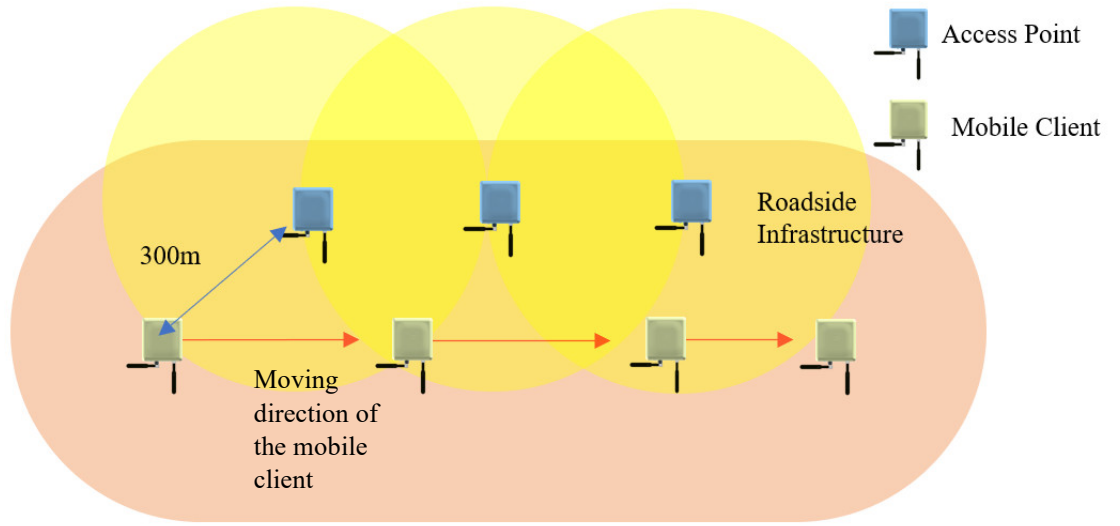
**Fig. 2.2** Cell planning. (a) 3 non-overlapping channels. (b) 7 non-overlapping channels.

In the practical deployment, the cell size was calculated using Free Space Lost formula in [11] and include the environmental loss factor.

$$FSL = 20 \log \left( \frac{4\pi f d}{c} \right) \quad (2.1)$$

Where:  $f$ : frequency of interest  
 $d$ : distance between the transmitter and the receiver.  
 $c$ : speed of light ( $3 \times 10^8$  m/s)

In most practical wireless deployment, especially in the transportation environment, the base station is required to communicate with multiple mobile or stationary clients within the service area. Fig. 2.3 shows the conventional method to set up the base station at roadside or tunnel to serve the moving vehicle or train, omni antenna is used for 360° coverage. Yellow cells represent the access points (AP) coverage and orange cell represents the coverage for the mobile clients. The overlapping between the APs coverage zone is to ensure it can provide maximum coverage to the entire route that the mobile clients are expected to travel.



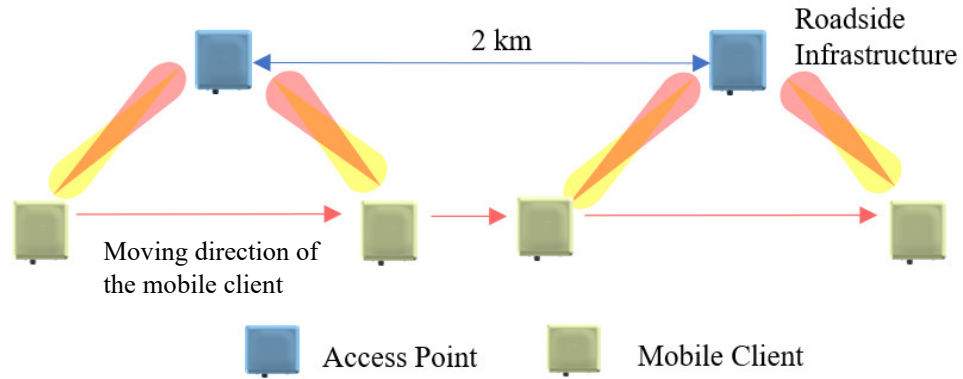
**Fig. 2.3** Conventional point to multipoint deployment.

For traditional AP deployment, the APs and the mobile terminals are both transmitting at 17 dBm power with 10 dBi antenna gain, the calculated cell size is approximately 300 m. Imagine the mobile client is moving from the left side of the coverage zone to the right, and it supposed to roam across the access points installed along the roadside. The potential issues anticipated from the existing deployment are:

- i. Small communication radius leads to more AP is needed to cover the entire service area. For example, a 10 km road requires around 34 APs.
- ii. Mutual RF interference between the adjacent cells if they are operating on the same frequency.
- iii. Higher installation cost and more installation materials.
- iv. Higher CAPEX and OPEX contributed by more equipment.

To overcome the current limitations, a smart antenna system is proposed, which allows the AP to steer the RF beam towards the mobile client and interference nulling by making use of beamforming technique. In addition, the concentration of transmitter and receiver radiating beam has concentrated the radiating power to a narrow beam which translated into higher antenna gain, the concentration of radiating beam also provides a good interference immunity as the transmitter and receiver only radiate and listen to the narrow-intended beam. Adaptive beamforming can be incorporated to dynamically steer the beam on-the-fly by tracking the client's direction using the direction of arrival technique. With this technique, when the clients are roaming within the service area, both the radiating beam of the access point and mobile client will steer and adjust to each other. Fig. 2.4 exhibits the

radiation beam of the access points and the client dynamically steer to follow the direction of the access points and clients.



**Fig. 2.4** Deployment with the smart antenna.

The benefits gained from the smart antenna are:

- i. Longer coverage distance due to the higher gain antenna, and thus fewer access points are needed. For example, a 10 km road requires 5 access points.
- ii. Reduce adjacent cell interference due to narrower beamwidth.
- iii. Low deployment and maintenance cost.
- iv. Energy saving in equipment usage.

Table 2.1 estimates the useable link distance between the access point for conventional deployment and smart antenna deployment serving the wireless clients in the transportation environment. 10 dB margin was included to act as the buffer for possible attenuation caused by environmental factors such as building, tree, and moisture. The calculated cell size for the conventional omni antenna deployment is approximately 300 m, whereas the coverage increases to 800 m if the access points are equipped with smart antennas while the mobile clients are installed with omni directional antenna, the range can be further improved to 2 km if both the access points and clients are equipped with the smart antenna. This simulation is based on the theoretical line of sight simulation, in real life, the signal propagation loss due to non-line of sight scenario must be considered.

**Table 2.1** Coverage estimation for access points serving moving clients.

| Type of antenna  | TX Power (dBm) | TX Ant Gain (dBi) | Distance (Meter) | RX Ant gain (dBi) | Calculated RSSI (dBm) | Target RSSI (dBm) | Margin (dB) |
|--|----------------|-------------------|------------------|-------------------|-----------------------|-------------------|-------------|
| Conventional (omni antenna)  | 17             | 10                | 300 m            | 10                | -59.8                 | -70               | 10.2        |
| Access points with smart antenna and mobile clients with omni antenna. | 17             | 18                | 800 m            | 10                | -60.3                 | -70               | 9.7         |
| Smart Antenna on both access points and mobile clients                 | 17             | 18                | 2000 m           | 18                | -60.3                 | -70               | 9.7         |

Note: TX (Transmitter), RX (receiver), RSSI (receiver signal strength indicator)

The benefit of the smart antenna in the transportation sector is obvious. The improvement in the coverage distance with smart antenna technique implies lower CAPEX due to fewer access points is needed and lower deployment cost because of minimum equipment and less wiring is needed, this will also benefit the OPEX where less equipment is needed to be taken care of during the whole maintenance regime. In the next section, we will explore the components that constitute the cost of the infrastructure's deployment, which includes the equipment need to be environmentally protected as well as the requirement specified in the environmental specifications and standards.

## 2.4 Wireless Infrastructure Cost Proposition

The deployment of wireless infrastructure in the transportation sectors can be divided into two schemes, new infrastructure, and upgrade on existing infrastructure. The introduction of new infrastructure is straight forward where new infrastructure such as communication equipment and new cabling and automotive stocks are introduced, the project owner usually will do the pre-assessment on the overall wireless deployment plan taking care of the various type of applications and co-existence between multiple wireless standards, wireless cell planning can be coordinated easily within the same contract or tender. More challenging when coming to an infrastructure upgrade, infrastructure upgrade or commonly called technology refresh that comes with the introduction of the latest technology into the existing systems while preserving the existing wireless system that is currently supporting the operations. In this context, 802.11ac/ax, Wireless Gigabits (WiGig)

or 5G wireless technology is introduced into the existing infrastructure that may still operate in older technology such as Third Generation (3G) wireless technology, 802.11a/b/g or due to the old infrastructure was unable to support the increasing demand in broadband wireless communication which was driven by the advancement in wireless technology.

The new technology being introduced may operate in the same frequency band as the current wireless systems that already in place and serving the operational needs of the existing infrastructure. The introduction of new wireless infrastructure has indirectly introduced more wireless devices to operate within the same premises and fight for the limited frequency spectrum, the problem gets worsen if the devices are sharing the same frequency spectrum but operating in different wireless standards, where collision avoidance and transmission time synchronisation become complex and almost impossible. Therefore, the system integrator (SI) is required to perform the wireless cell planning very carefully with the existing stake owner taking into consideration the limited frequency spectrum being allocated by the Infocomm authority.

The associated cost for both deployment scheme can be further derived by considering their CAPEX and OPEX, in most of the township or government project, the CAPEX is the main considering point while keeping the OPEX as low as possible. When comes to the infrastructure upgrade, the SI will need to consider deploying new cables and equipment on top of the existing structure, this will require additional efforts and cost to assess the interference that may potentially be introduced to the existing system due to the new equipment as well as protecting the current structure or cable that was deployed previously to support the existing equipment.

### **2.4.1 Cost Factors of the Communication Infrastructure**

In the transportation environment, the infrastructure cost is not simply the cost of the equipment itself, the cost is distributed over to every single step that required to ensure the infrastructure can sustain the harsh environment, minimise the interference to other equipment and importantly it does not produce any hazards to the public. Additional supporting equipment is needed to protect the system which constitutes a major portion of the cost. The next few paragraphs highlight some major requirements, specifications, or standards that are mandatory for every piece of equipment to fulfil before it can be installed in the field.

### **2.4.1.1 Environmental Protection**

Taking a closer look at the transportation environment, in general, the equipment is mainly installed outdoor with environmental protection. The outdoor environment is subjected to the effect of weather change such as temperature, humidity, rain, sunshine, and snow. Being part of an equatorial region such as Singapore, thunderstorms, high humidity, and severe rainfall are affecting the reliability of the equipment. Northern areas such as the United States, Europe, China, and Japan may experience wider temperature change across the year with snow during the winter and temperatures more than 40 °C during summer. Therefore, it is costly for such kind of equipment that requires special treatment electronically or mechanically to fulfil the environmental protection or International Protection (IP) as specified in the international standards International Electrotechnical Committee (IEC) 60529, the IP rating specified the degree of intrusion protection against the solid objects, accidental contact, dust, and water into the electronic device housed inside the enclosures. In [12], it was highlighted that the Trade Association for UK or Railway Industry Association (RIA) that supplies the equipment and services to the railway industry has published the environmental standards IEC 61373 [13] to deal with the environmental protection required for the equipment in the railway environment. As of today, the IEC 61373 standards is widely adopted by equipment manufacturers across the world.

### **2.4.1.2 Electromagnetic Compatibility and Electromagnetic Interference (EMC/EMI)**

The transportation environment is also experiencing severe EMC interference, especially in the rail environment, where the high traction voltage that powering the rolling stocks will generate a huge amount of EMC that may potentially interfere and degrades the performance of the nearby electronic equipment. Another source of EMC surge is from lightning, where a huge amount of electromagnetic surge can be induced or coupled via ground or cable into the nearby equipment and potentially damages the electronic inside the equipment. A lightning arrestor or EMI suppressor can be installed to isolate the equipment from the vulnerable parts of the system. On the other hand, every electronic equipment will generate unwanted electromagnetic wave when in operation, the equipment that installed in the transportation environment must be designed with EMC treatment to control and restrict the unwanted EMC radiation below the allowable limit, this is crucial in order not to interfere with other mission-critical equipment that forms part of the transportation system to ensure safe operation of the vehicles.

The EN 50121 standards [12] addresses and defines the EMC/EMI requirement in the railway application environment. The family standards split into different parts of standards that deal with the different area of EMC/EMI requirement, for instance, EN 50121-2: Electromagnetic Emission to the outside environment, EN 50121-3-1 defines the Electromagnetic Emissions from Rolling Stock, EN 50121-3-2 defines the Electromagnetic Environment for on Board Equipment, EN 50121-4 defines the Electromagnetic Environment for Signalling and Telecommunications Equipment, EN 50121-5 defines the Electromagnetic Environment for Fixed Installations Equipment, and many more.

The requirements of environmental protection, EMC/EMI and surge immunity described above is translated into the total project cost. For example, a smart antenna that intended to be deployed in such environment will need to have an IP rated enclosure, built-in lightning arrestor, EMC/EMI suppressor that is necessary to isolate or suppress any EMC/EMI issue in the field, the outdoor equipment becomes costly due to the usage of industry-grade components to guarantee its performance and survival in the harsh environment. Usually, the equipment manufacturer will need to certify the product in the third-party accredited test lab before it can be deployed and operates in the transportation environment. The additional environment protection design and certification is expected to take up 50% of the overall equipment cost. Therefore, it is obvious to say that the number of equipment needed in a transportation system is key to determine the overall system cost.

#### **2.4.2 Project Cost Estimation – a Case Study**

A report on smart antenna deployment was presented by Vector Fields Limited to Ofcom in 2006 [14] far before the smart antenna technology was widely used in the commercial world. The project was initiated to investigate the adaption of the adaptive smart antenna in the Broadband Wireless Access (BWA) and Wireless Local Area Network (WLAN) or Wi-Fi, the evaluation was carried out using the 802.11a hardware. The study result shows that there was a significant benefit in smart antenna technology, the benefits are explained in 3 areas, i) the increase in the communication cell range of 40-70%, ii) reduction in spectrum utilization by 60-70%, and iii) network cost reduction by up to 50% that translates to a total business cost reduction of up to one third. This has provided positive motivation to the smart antenna industry significantly.

In [15] a study report was carried out by United States Government Accountability Office (GAO) to provide the cost estimates to support the deployment of DSRC for V2I

communication in the United States. The report highlighted that the total potential average, non-recurring costs, or CAPEX of deploying connected vehicle infrastructure per site is \$51,650. There are several types of recurring costs or OPEX, associated with V2I deployments, including equipment maintenance and replacement every 5 to 10 years, security, and personnel costs. The CAPEX and OPEX are computed by combining all the cost events in the deployment of the overall systems and the cost can be optimised by reducing the number of equipment installed on-site.

To better explain the cost propagation for the infrastructure deployment in the transportation market, a practical case study is presented here by comparing the infrastructure deployment using traditional and smart antenna techniques explained earlier in Fig. 2.3 and Fig. 2.4, the case study will also include all the necessary consideration that makes up the systems cost such as cabling, equipment protections, test, and commissioning, as well as maintenance cost. The case study was carried out to demonstrate the general wireless infrastructure deployment in the Singapore transportation sector targeting the wireless infrastructure for public buses and railway systems. The wireless system proposed in this study is an 802.11ac wireless LAN operating in the 5 GHz band. The case study is to serve as a guideline for general deployment using 802.11ac access point, the cost may vary depending on the requirement, type, and size of the contract. The maintenance cost tabulated below also highly depends on the maintenance regime agreed between the stakeholder and the contractor. The breakdown of the project implementation cost is presented in Table 2.2.

The regulatory certification cost is a one-time cost that is applied to all the products to be deployed in the field, the equipment cost includes the main access point products, antennas, EMC protection devices, lightning arrestors, and environment protection enclosures to house all the supporting devices. Installation cost is derived by taking into consideration the field-installed devices will need to draw power and data through cable from the intermediate device box (IDF) that includes the labour cost to install the devices and its cabling, the data is connected to the back end via ethernet connection, it is necessary to use armour grade type of cable or minimum Category-5 (Cat-5) shielded foil screened twisted pair (S/FTP) with protective trunking. The installation cost includes the mounting brackets and poles that erect the antennas to a certain height for optimum RF performance. Test and commissioning is a process designed to test and make sure the configurations of the equipment are set correctly and the performance of the system is up to its expectation.

The setup cost, equipment cost, and installation cost are categorized under the CAPEX cost. The OPEX is mainly referring to running cost incurred over the operation years, the



OPEX cost includes corrective and preventive maintenance and extended warranty, the warranty of the infrastructure equipment in the transportation market usually called for a minimum of 7 years period, however, most of the electronic equipment are providing 1 to 3 years of limited warranty, therefore, the extended warranty cost shall be provided to give provision of warranty up to 7 years or beyond.

**Table 2.2** Deployment cost for the roadside infrastructure covering 10 km distance (in US\$).

|                              | Items  | Cost per unit | * Scenario 1<br>(35 APs) | * Scenario 2<br>(13 APs) | * Scenario 3<br>(6 APs) |
|------------------------------|--|---------------|--------------------------|--------------------------|-------------------------|
| <b>Setup Cost</b>            |  |               |                          |                          |                         |
| 1.                           | Regulatory Certification                                       | \$ 50,000     | \$ 50,000                | \$ 50,000                | \$ 50,000               |
| <b>Equipment Cost</b>        |  |               |                          |                          |                         |
| 2.                           | Industrial 802.11ac Wireless LAN                               | \$ 750        | \$ 25,250                | \$ 9,750                 | \$ 4,500                |
| 3.                           | Omni Antenna   | \$100         | \$ 3,500                 | --                       | --                      |
| 4.                           | Smart Antenna frontend   | \$ 400        | --                       | \$ 5,200                 | \$ 2,400                |
| 5.                           | EMC filter   | \$ 120        | \$ 4,200                 | \$ 1,560                 | \$ 720                  |
| 6.                           | Lightning arrestor   | \$ 50         | \$ 1,750                 | \$ 650                   | \$ 300                  |
| 7.                           | Environmental proof enclosure                                  | \$ 300        | \$ 10,500                | \$ 3,900                 | \$ 1,800                |
| <b>Installation Cost</b>     |  |               |                          |                          |                         |
| 8.                           | Cat-6 cable (Material and installation cost per 100m)          | \$ 1,000      | \$ 35,000                | \$ 13,000                | \$ 6,000                |
| 9.                           | Structure to mount the equipment                               | \$ 500        | \$ 17,500                | \$ 6,500                 | \$ 3,000                |
| 10.                          | Test and commissioning   | \$ 100        | \$ 3,500                 | \$ 1,300                 | \$ 600                  |
| <b>Total CAPEX</b>           |  |               | <b>\$ 151,200</b>        | <b>\$ 91,860</b>         | <b>\$ 69,320</b>        |
| <b>Cost Benefit on CAPEX</b> |  |               | --                       | <b>39 %</b>              | <b>54 %</b>             |
| <b>Maintenance</b>           |  |               |                          |                          |                         |
| 11.                          | Corrective maintenance for each wireless access point (yearly) | \$ 200        | \$ 70,000                | \$ 26,000                | \$ 12,000               |
| 12.                          | Preventive maintenance for each wireless access point (yearly) | \$ 100        | \$ 35,000                | \$ 13,000                | \$ 6,000                |
| 13.                          | Extended warranty (yearly)                                     | \$ 75         | \$ 2,625                 | \$ 975                   | \$ 450                  |
| <b>Total OPEX</b>            |  |               | <b>\$ 107,625</b>        | <b>\$ 39,975</b>         | <b>\$ 18,450</b>        |
| <b>Cost benefit on OPEX</b>  |  |               | --                       | <b>63 %</b>              | <b>83 %</b>             |

Source: Training material that consists of general costing guidelines for the transportation-related project in RFNet, Singapore computed in May 2020.

*\*Scenario 1, conventional deployment with omni directional antenna*

*\*Scenario 2: hybrid deployment with access points equipped with the smart antenna and mobile terminals deployed with omni directional antenna.*

*\*Scenario 3: deployment with smart antenna equipped on both access points and mobile terminals.*

Finally, we can see that the CAPEX investment can achieve approximately 39 % cost saving for hybrid smart antenna system while cost saving of 54 % for full smart antenna deployment, more importantly, the smart antenna system has drastically improved the OPEX by approximately 63 % for hybrid smart antenna system and nearly 83 % for the full smart antenna system. The cost-benefit brought by the smart antenna technology can potentially create a huge opportunity for the business owners where the return of investment (ROI) can be easily justified.

## ***2.5 The Key Challenges***

Now we are clear that the main challenges for the infrastructure deployment in the transportation sector are the air space congestion and deployment cost, below are the summary of the challenges and mitigation objective that we are trying to achieve with the smart antenna system.

- i. **High CAPEX:** Reduction of the number of field equipment will significantly contribute to the reduction of the CAPEX cost, this can be achieved by introducing the beamforming technique into the antenna systems, further cost reduction on the smart antenna system that allows pre-configuration to allow only necessary sub-array to be installed.
- ii. **Wireless Interference:** Reduction of the Mutual interference between adjacent cells if they are operating on the same frequency, this can be achieved by beam steering where the radiating beam of the transmitter and receiver antenna are always pointing to each other with a narrow beam and nulls all other direction.
- iii. **High OPEX:** as discussed earlier, the smart antenna technique has significantly reduced the number of equipment needed to be deployed, this will lead to a reduction in the OPEX cost, operating cost such as preventive and corrective maintenance can be controlled if there is a lesser number of field equipment need to be maintained.

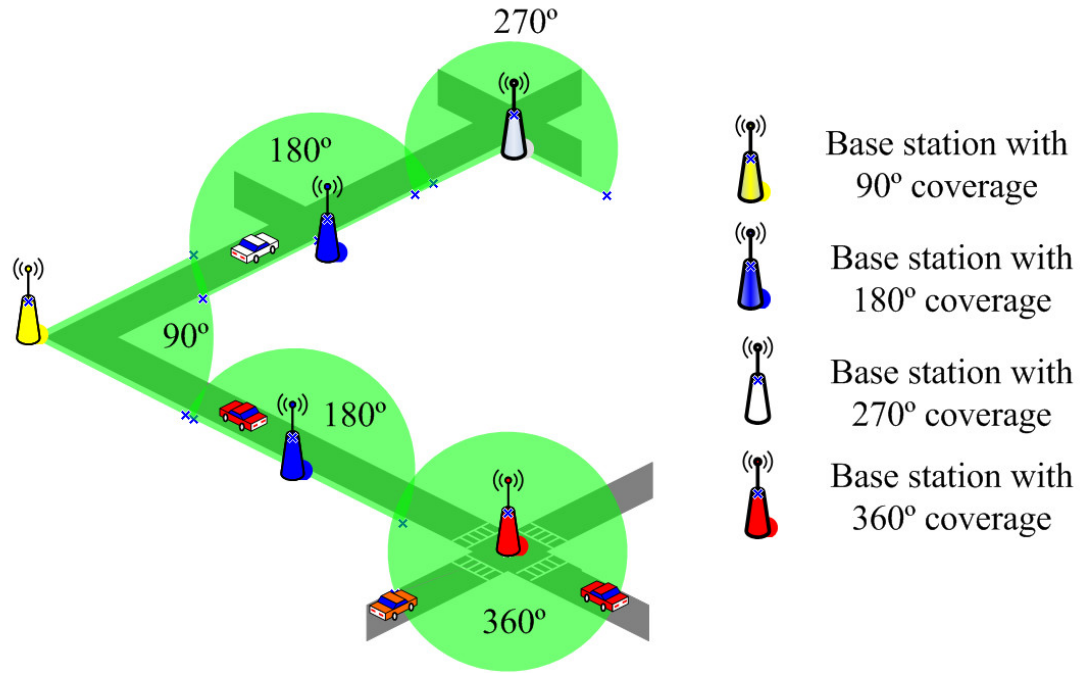
## ***2.6 The Advantages of the Smart Antenna***

There is always a fixed constraint on the wireless link between mobile terminals in the moving vehicles and the base stations installed along the roadside, this is mainly due to the mobility of the mobile terminals, the antenna beam for the roadside infrastructure and the mobile terminals are not always fixed. As described in Table 2.1, the traditional wireless deployment was implemented by an omni-directional antenna that provides 360° coverage for the access point and the mobile client, this method has limited the coverage radius of the base station and the omni antenna implies the base station can transmit and receive the signal to and from all the direction, the base station can be easily interfered and interfering others, the SI is trying hard to avoid this while maintaining the system cost especially in the area with air space congestion.

To strike the balance between the cost and performance, the modern pre-configurable antenna shall be equipped with beamforming function and provide the capability to be pre-configured before installation and re-configured during the operation based on the deployment scenario illustrated in the following paragraph. This technique can tremendously improve interference performance, cost reduction, and increase the field deployment friendliness.

In the dynamic transportation environment, specific radiating beam and the communication distance of the antenna [38] may apply to different application scenarios as described in Fig. 2.5. A big traffic junction (red cell) will require a base station with the entire 360° coverage with maximum antenna gain, a small junction (white cell) may need a base station with 270° wireless coverage with lower antenna gain, a roadside infrastructure installed at the roadside (blue cell) just requires a 180° wireless coverage and a right-angled road (yellow cell) will just require a small 90° beam coverage. To increase the field deployment friendliness further, the gain of the antenna system can be pre-configured to the low, middle, and high gain before the installation, hence, it can be customised to what is needed to best fit the application scenario. On top of that, the beamforming feature can be realised in the proposed antenna array by integrating the array with the beamforming frontend and processor. The proposed pre-configurable smart antenna structure aimed to achieve the lowest CAPEX and OPEX that fit well in the volatile transportation sector. The proposed pre-configurable antenna system comes with beamforming capability that outperformed the conventional smart antenna and reconfiguration antenna system with the following benefits,

- i) The number of equipment needed is reduced (with beamforming technique)
- ii) Lower cost and minimise waste materials (with pre-configurable structure)
- iii) Maintenance-friendly and good maintainability (with fewer components)
- iv) Fewer arrays, less processing effort resulted in faster processing time. (the beamformer just need to concentrate on the selected arrays) and
- v) Enhanced interference performance (radiate and received on a narrow and concentrated beam on the specific array installed).



**Fig. 2.5** Wireless zone coverage in the vehicular environment for various application scenarios.

## 2.7 Summary

It is undeniable that the big chunk of the cost that was spent in the wireless infrastructure deployment goes to the equipment and installation cost that was mainly contributed by the number of equipment and the added cost to certify the product and enable it to be deployed in the harsh transportation environment. The natural approach towards cost and interference friendliness is to reduce the numbers of equipment in the field, this can be achieved via the smart antenna technique with pre-configurable structure and re-configurable beam to focus the RF radiation solely on the targeted directly.

### 3 Beamforming Antenna Concept and System

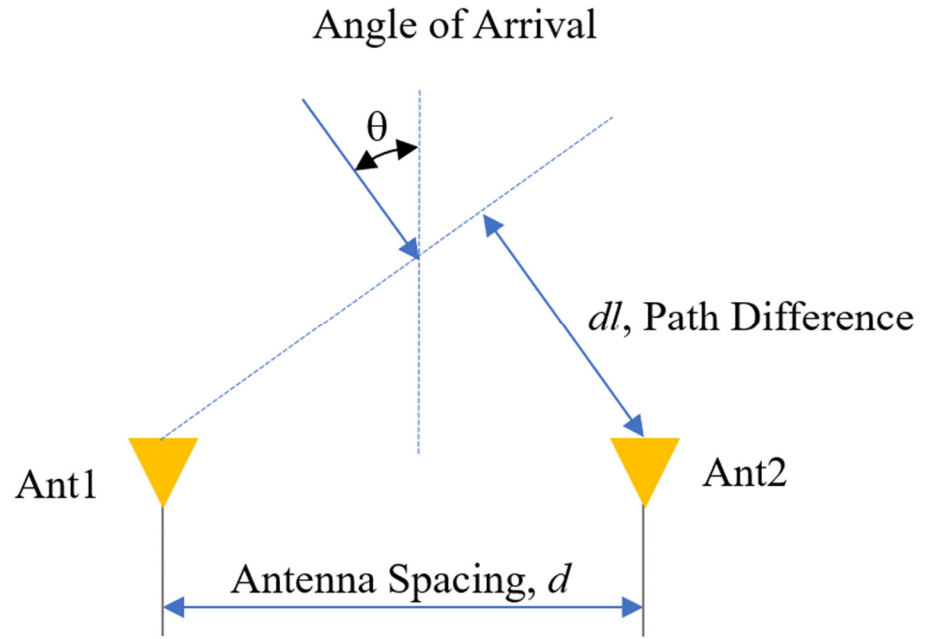
Smart antenna technology is implemented using the antenna array with beamforming technique realized either by analogue or digital means, the techniques are being introduced increasingly with the development of other technologies including the software-defined radio, cognitive radio (CR), MIMO radio, and many others.

Smart antenna technology enables the radiation pattern and beam direction of the transmitter and receiver to alter and adapt to the changing environments. The radiating beam of the antenna can be shaped to concentrate the energy of the RF beam into a narrow beam and steer according to the target direction by combining the RF energy from the multiple elements in the phased array, thus improving the overall capacity and reduce the co-channel interference. The direction of arrival (DOA) of the receiver can be calculated using the beamforming technique and DSP/FPGA processing, in addition, the adaptive beamforming algorithm is able to adapt dynamically to the changing environment by adjusting the weight of the signal fed to the antenna array elements.

The Two main functions of the smart antenna are described as, i) **DOA estimation**, which is to enable the antenna to detect the direction of the intended transmitter's signal, as a result, the antenna can achieve the optimum performance with minimum interference to and from other nearby devices, the information received by the antenna array is passed to the signal processor to provide the required analysis, ii) **Beam steering**, once the DOA is determined, the beamforming front end can be controlled to change the phase and amplitude of the RF signal that feeds into the individual port in the phased array where the beam steering can be achieved.

#### 3.1 *Direction of Arrival*

The beamforming antenna consists of at least 2 antenna elements separated by a predefined distance,  $d$ . Take an example, when the radio is in receiving mode, the angle of arrival can be defined by calculating the phase difference when the same signal source received by 2 antennas separated by a distance  $d$  [46], the angle of arrival calculated can be represented by Fig. 3.1.



**Fig. 3.1** Estimation of the angle of arrival

Assuming a waveform traveling from direction  $\theta$  arrives at antenna 1, the same signal traveling with an additional path  $dl$  before it reaches antenna 2, this gives,

$$dl = d \sin \theta \quad (3.1)$$

This results in the received signal with  $\phi$ , the phase difference between the 2 antennas.

$$\begin{aligned} \phi &= 2\pi dl / \lambda \\ \phi &= 2\pi d \sin \theta / \lambda \end{aligned} \quad (3.2)$$

The direction of the wave can be calculated by the angle of arrival from the phase difference:

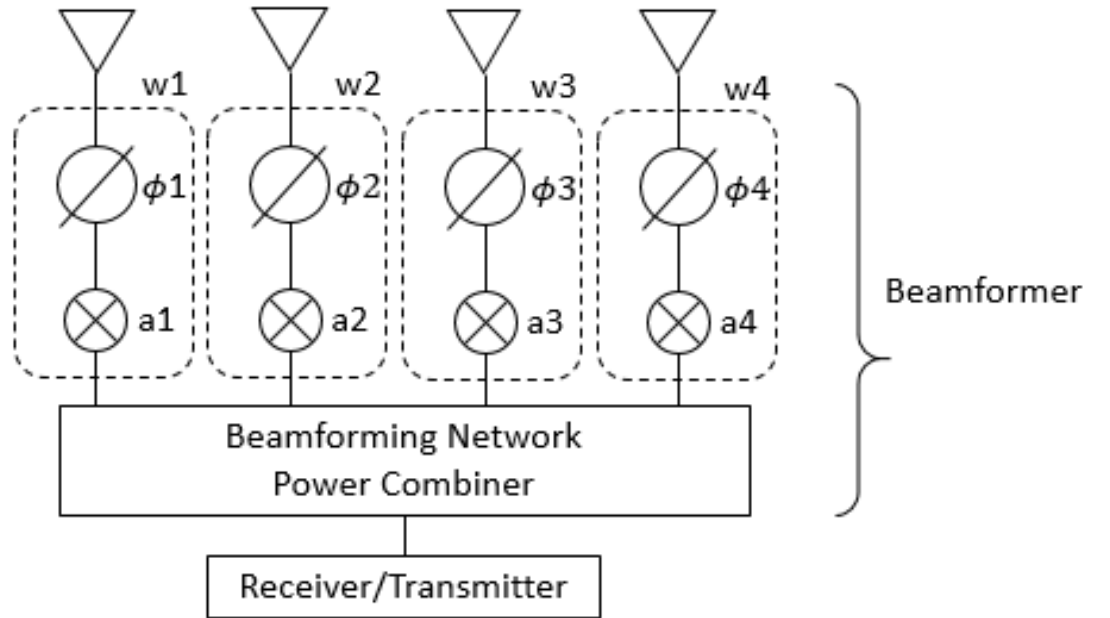
$$\theta = \sin^{-1}(\phi \lambda / 2\pi d) \quad (3.3)$$

Where  $d$  is the distance between the two antenna elements,  $dl$  is the additional path for the same signal receive by antenna 2 compared to antenna 1,  $\lambda$  is the wavelength of the RF signal,  $\phi$  is the phase difference between the 2 antennas and  $\theta$  is the angle of arrival or direction of the signal.

The above principle is applicable for receiver antenna, when used as a transmitter, the angle of transmission beam can be simulated by varying the phase of the microwave source feed into each antenna port, this can be done by introducing the phase shifter to shift

the respective phase before feeding into the antennas, this is also known as analogue beamforming. Alternatively, the beamforming can be implemented digitally using sophisticated digital processing such as FPGA.

The adaptive beamforming article presented in the Spectrum Signal Processing article [46], highlighted that in the beamforming process, both the amplitude and phase of the antenna element are controlled. Combined amplitude and phase control can be used to adjust sidelobe levels and steer nulls better than can be achieved by phase control alone. The combined relative amplitude  $a_k$  and phase shift  $\phi_k$  for each antenna is called a “complex weight” and is represented by a complex constant  $w_k$  (for the  $k^{th}$  antenna). The complex weights  $w_k$  for the antenna elements are carefully chosen to give the desired peaks and nulls in the radiation pattern of the antenna array. The complex weights function of the adaptive beamforming as shown in Fig. 3.2 can be derived using formula (3.4).



**Fig. 3.2** Adaptive beamforming architecture.

$$w_k = a_k e^{j\phi_k}$$

$$w_k = a_k \cos \phi_k + j a_k \sin \phi_k \quad (3.4)$$

Where:

$w_k$  is a complex weight for the  $k^{th}$  antenna element.

$a_k$  is the relative amplitude of the weight.

$\phi_k$  is the phase shift of the weight.

## **3.2 *Type of Beamforming Antenna***

The literature review covers various types of beamforming techniques, including analogue beamforming, digital beamforming, and hybrid beamforming. Hybrid beamforming is implemented using a combination of digital and analogue beamforming technique, whose objective is to simplify the beamforming design as well as reducing the implementation cost while maintaining the beamforming performance close to the digital beamforming.

### **3.2.1 Analogue Beamforming**

Over the years, there were quite many works done on analogue beamforming smart antenna, following sections included some reviews done on the previous research works.

#### **3.2.1.1 Selectable Antenna Element**

The patent proposed by Ruckus [47] consists of multiple antennas, embedded into a product, the antennas were implemented using microstrip line technology on PCB material such as flame retardant 4 (FR4) making the solution low-cost and commercially affordable. With the whole antennas embedded inside the product housing that resulted in the materials and manufacturing cost even lower. Each of the antenna elements provides a directional radiation pattern. The antenna elements are electrically selectable via a pin diode. This technique can be a good candidate for commercial product such as home routers, hot spot AP where the deployment cost is low and does not require long-range coverage, however, it will not be a direct fit for the outdoor and industrial applications that require higher gain and small beamwidth.

#### **3.2.1.2 Beam Switching Slotted Array**

Multiple sets of the equally spaced slotted array are connected in series to a coplanar waveguide [48], switching diode shorting strips are mounted across each slot that enables and disables the desired slot to achieve beamforming. The antenna is fabricated on FR4 PCB material. The proposed design works on LTE Band 7 (2500 ~ 2690 MHz) Femtocell, it's capable of providing 9.9 ~ 10.7 dBi gain, with beam switching at 62°, 82°, and 108° on horizontal beamwidth around 80° beamwidth. However, the proposed design has an elevated sidelobe for a large tilt angle. The fixed angle switching slot antenna with wide beamwidth

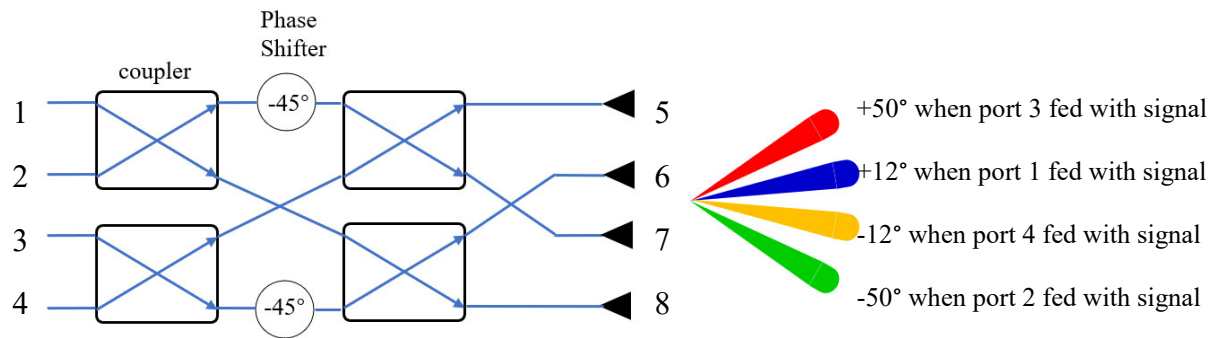


and limited steering angle may not be suitable for our application that requires a narrow bandwidth and fine steering angle over  $360^\circ$ .

### 3.2.1.3 Butler Matrix

Butler Matrix is another popular and practical technique uses in analogue beamforming, it's passive and reciprocal symmetrical microwave structure that can be easily implemented using the microstrip line technique. The Butler Matrix structure consists of 3 main components, they are the 3 dB couplers, cross over, and  $45^\circ$  phase shifter. The Butler matrix has N input ports and N output ports that drive N antenna elements to provide N numbers of radiating beams. The Butler matrix structure can be implemented on the low-cost FR4 PCB. The spacing distance between the antenna element is set to  $0.5\lambda$ .

The typical  $4 \times 4$  Butler Matrix is shown in Fig. 3.3. The direction of the radiation beam will steer depends on which input port is fed with a signal. The phase difference and antenna beam associated with the selected port fed is shown in Table 3.1.



**Fig. 3.3** Structure of the  $4 \times 4$  Butler Matrix

**Table 3.1** Phase associated with selected port feed for the  $4 \times 4$  Butler Matrix

| Input | Output      |             |             |             | phase diff   | Beam direction | feed                    |
|-------|-------------|-------------|-------------|-------------|--------------|----------------|-------------------------|
|       | P5          | P6          | P7          | P8          |              |                |                         |
| P1    | $135^\circ$ | $90^\circ$  | $45^\circ$  | $0^\circ$   | $-45^\circ$  | $50^\circ$     | Signal feed from port 3 |
| P2    | $45^\circ$  | $180^\circ$ | $-45^\circ$ | $90^\circ$  | $135^\circ$  | $12^\circ$     | Signal feed from port 1 |
| P3    | $90^\circ$  | $-45^\circ$ | $180^\circ$ | $45^\circ$  | $-135^\circ$ | $-12^\circ$    | Signal feed from port 4 |
| P4    | $0^\circ$   | $45^\circ$  | $90^\circ$  | $135^\circ$ | $45^\circ$   | $-50^\circ$    | Signal feed from port 2 |

The literature review has picked up some of the previous work done on the Butler Matrix smart antenna. The  $4 \times 4$  Butler Matrix array antenna was designed to operate at frequency 2350 MHz for LTE application [49], it's able to achieve 20 dB port-to-port isolation, the beamforming array is capable of switching the beam at  $20^\circ$ ,  $-20^\circ$ ,  $+40^\circ$ , and  $-40^\circ$  with an HPBW of  $33.8^\circ$ ,  $39.8^\circ$ ,  $40.3^\circ$ , and  $35.6^\circ$  and gain is about 6.11 dBi. The final butler matrix with antenna array occupied the size of 280mmx260mm, considering the size and service beam of  $\pm 40^\circ$ , this may not be feasible for the smart antenna that targeted to steer over  $360^\circ$ .

Another work was presented on 4x4 Butler matrix beamforming antenna with wide bandwidth and narrow beamwidth was presented in [50]. The proposed design operates on 2.3 GHz, 2.6 GHz as well as 2.4 GHz band, the design was able to achieve 400 MHz service bandwidth with the gain between 6 - 7.5 dBi. The radiation beam covered  $+15^\circ$ ,  $-15^\circ$ ,  $+45^\circ$ ,  $-45^\circ$ . The HPBW is around 25 MHz. However, the design shows a big insertion loss around 10 dB due to the lossy FR4 material.

Butler matrix smart antenna that was designed for WLAN, operate at 5.25 GHz [51], the  $4 \times 4$  Butler Matrix antenna was implemented using RT/duroid 5880 substrate with a relative permittivity  $\epsilon_r = 2.2$ , the port-to-port isolation was greater than 20 dB. The radiation beam switch from  $+16^\circ$ ,  $-15^\circ$ ,  $+38^\circ$  and  $-39^\circ$ . However, the design suffers a huge sidelobe level (SSL) corresponding to beam  $+38^\circ$  and  $-39^\circ$  due to mutual coupling between the antenna element and mismatches between the feeding network and the antenna.

Another piece of work that utilizing Butler Matrix was designed to operate at 2.4 to 2.48 GHz band [52], PCB substrate Rogers RT/Duroid 5880 relative permittivity  $\epsilon_r = 2.2$  was used in the design with a systematically approach. First, the author evaluated the single antenna element with 7.0244 dBi gain with the operating frequency from 2.443 to 2.473 GHz and  $99.1^\circ$  HPBW, next, the single patch was integrated into a  $4 \times 4$  antenna array with  $0.45\lambda$  spacing, measured performance of 11.0452 dBi gain and  $25.2^\circ$  HPBW with service bandwidth of 30 MHz was achieved from the antenna array. The  $4 \times 4$  Butler matrix array is capable of switching between  $+14.3^\circ$ ,  $-14.3^\circ$ ,  $+47.8^\circ$ , and  $-47.8^\circ$ . The overall size of this proposed Butler matrix antenna is  $21.3 \times 18.6$  cm and this is similar to other Butler matrix antenna arrays in size.

### 3.2.1.4 Electronically Steerable Parasitic Array Radiator Antenna (ESPAR)

ESPAR is another popular technique used in low-cost antenna development, in a simple form of explanation, a single driver element is surrounded by multiple parasitic elements, the radiation pattern of the ESPAR antenna is formed by varying the reactance of the parasitic element.

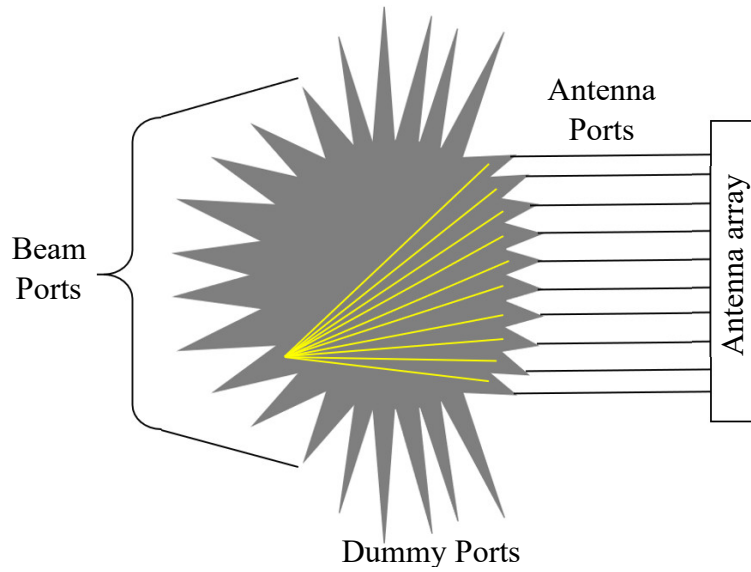
Many research works were carried out in the past, one of the examples, the folded monopole element was used to realize the ESPAR antenna that operates from 2.3 to 2.55 GHz [53]. The proposed design consists of a feeding port via a sub-miniature version A (SMA) connector, connected to the driven element, in this case, a  $\frac{1}{4} \lambda$  monopole element located at the middle of the antenna, the driven element is surrounded by 6 pieces of parasitic folded monopole elements, varactors were installed at each parasitic element that can be used to vary the reactance of the parasitic element to form the antenna beam. The design was able to achieve 4 dBi gain with a wide beamwidth close to  $90^\circ$  to steer across  $360^\circ$ .

### 3.2.1.5 Rotman Lens

Beamforming can also be realized by a Rotman, the lens is used to focus energy from one of the input ports to the radiated antennas. The Rotman lens can be implemented using copper etched over the dielectric materials. The operation principle of the Rotman lens can be explained as follow, in the transmitting mode, the RF signal is injected into one of the input ports depends on the desired beam direction. The RF signal is directed into the antenna array ports with their respective travelling distance that translated to the steering angle of the radiating beam, in the receive mode, as shown in Fig. 3.4, the RF energy is received from all the antenna ports and focused to one of the beam ports based on the direction of the receiving beam. To achieve the high beam resolution, large numbers of beam ports need to be incorporated, resulted in more components count and reduction of the beam port isolation due to the decrease of the physical distance between the adjacent beam ports. This is undesirable in the practical application where the complexity and size matters. The layout illustration of the Rotman lens is shown in Fig. 3.4.

The design of the Rotman lens can be carried out by the software called Rotman Lens Designer (RLD) [54], in which the Rotman lens design parameters can be tuned to optimize the network performance such as the beam pattern, insertion loss, sidelobe level, phase and amplitude errors. The results of the  $8 \times 8$  Rotman lens design suing RLD was able to achieve insertion loss ranges from 2.7 to 3.9 dB for the 5.5 GHz operating frequency, and it is capable

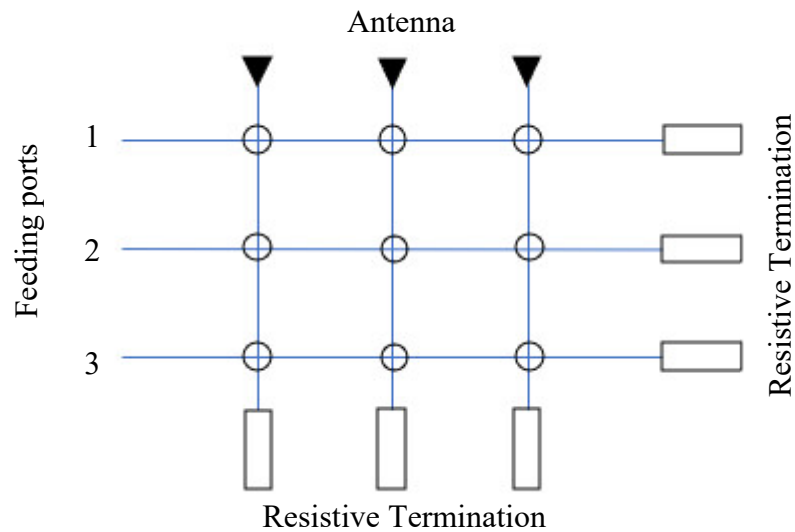
of steering evenly radiated beam of  $-45^\circ$  to  $+45^\circ$  with the size of  $310 \times 344$  mm relatively large for practical antenna application.



**Fig. 3.4** A 8x8 Rotman lens layout.

### 3.2.1.6 Blass Matrix

The Blass Matrix beamforming technique uses transmission line and directional couplers to form time delays required to shape the radiation pattern of the antenna array for the beamforming application. Blass Matrix is lossy because of the resistive termination. Fig. 3.5 shows A 3-elements Blass matrix antenna array, Port 2 provides equal delays to all antenna elements, resulting in a perpendicular beam. The other two ports provide progressive time delays between elements and produce beams that are off perpendicular. The 5 inputs 32 elements Blass matrix antenna was proposed [55], the author making use of a waveguide cross coupler operates from frequencies 11.235 GHz to 11.825 GHz.



**Fig. 3.5** A 3-elements Blass Matrix

### 3.2.1.7 Wullenweber Array

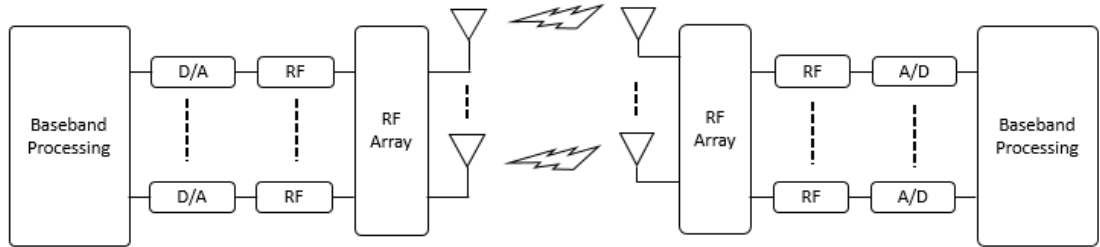
A Wullenweber array is a directional array developed mainly for high frequency (HF) applications, the Wullenweber array consists of large amounts of evenly spaced omnidirectional or directional antenna elements. Multiple elements are used at a time to form the radiation beam. The advantage of Wullenweber antenna is its ability to scan over  $360^\circ$  with minimum variation in its beam characteristic. The nature of Wullenweber structure leads to its big antenna size.

### 3.2.2 Digital Beamforming

The advancement in Digital Signal Processing (DSP) has accelerated the adoption of Digital beamforming in the smart antenna industry. Thanks to the flexibility of high-speed digital processing that enables the digital beamforming work to carry out efficiently and widely in the wireless industries, for instance, the recent 802.11 WLAN development has incorporated the digital beamforming as part of the fundamental offering in the 802.11an and 802.11ac MIMO products.

Digital beamforming involves software and hardware realization to form the beam digitally using FPGA. The RF signal is received using a linear array antenna consisting of multiple antenna elements. Fig. 3.6 shows the basic block diagram of the digital beamforming system. Each antenna has its own RF subsystem, which includes a low noise amplifier (LNA), mixer, and local oscillators (LO) to down-convert the received signal to

the intermediate frequency (IF). The IF signal is then filtered and passed to the digital subsystem for further baseband processing. Baseband and beamforming processing is carried out by digital signal processing (DSP) or FPGA. The design is highly complex and usually, the cost of implementation is high.



**Fig. 3.6** Block diagram of the digital beamforming system.

The FPGA based 16 antenna elements digital beamforming system was developed [56], since each RF chain required its own Mixer, it is important to ensure the RF signal received from each antenna are in equal phase, this can be realized by making use of a common reference clock to feed into each mixer. The RF signal is down converted to a lower frequency or intermediate frequency (IF) that can be handled by the analogue to digital converter (ADC), the ADC will digitize the IF signal and feed into FPGA for beamforming processing.

At first, the FPGA will perform channelization to split the wideband signal into smaller bandwidth, the output of each channel is passed to their respective beamformer module, a low-pass filter is in place to filter out unwanted harmonics and noise. The baseband IQ signal is generated for DSP to perform the beamforming weight calculation.

For the transmitter, the baseband IQ signal is multiplied with the calculated beamforming weight follow by a digital to analogue converter (DAC) to convert the baseband signal to IF frequency, the IF frequency is further upconverted to RF frequency by a mixer. A low-pass filter is necessary to filter out the unwanted noise and harmonics generated by the mixer during the up-conversion process. The RF signal is amplified by an external power amplifier before its feeds into the radiating elements.

### 3.2.3 Hybrid Beamforming

Various low-cost analogue beamforming techniques had been discussed earlier, and costly digital beamforming technique that requires a dedicated RF chain for each antenna

element. The digital beamforming requires a complex processing algorithm that make it extremely costly for commercial or industrial implementation. Another technique called hybrid beamforming was evaluated, this technique combines the best of both analogue and digital beamforming in a hybrid structure. Hybrid beamforming architecture consists of a low-dimensional digital beamformer and the analogue beamforming frontend consists of analogue phase shifters, RF switches, power amplifier, and low noise amplifier. In [57], the authors concluded that if the number of RF chains is twice the total number of data streams, the hybrid beamforming structure can realize any fully digital beamformer performance, regardless of the number of antenna elements.

The hybrid beamforming technique is a wise choice for industrial and commercial smart antenna system simply because of the cost-benefit and simplicity in implementation. The hybrid beamforming can also easily incorporate with the DOA estimation and Adaptive beamforming function which are the key requirements in smart antenna implementation. On the other hand, digital beamforming requires a dedicated RF chain for each antenna element, the implementation is complex and costly. For low-cost architecture, hybrid beamforming that combined analogue and digital beamforming is preferred. The summary of the pros and cons between the three beamforming techniques are highlighted in Table 3.2.

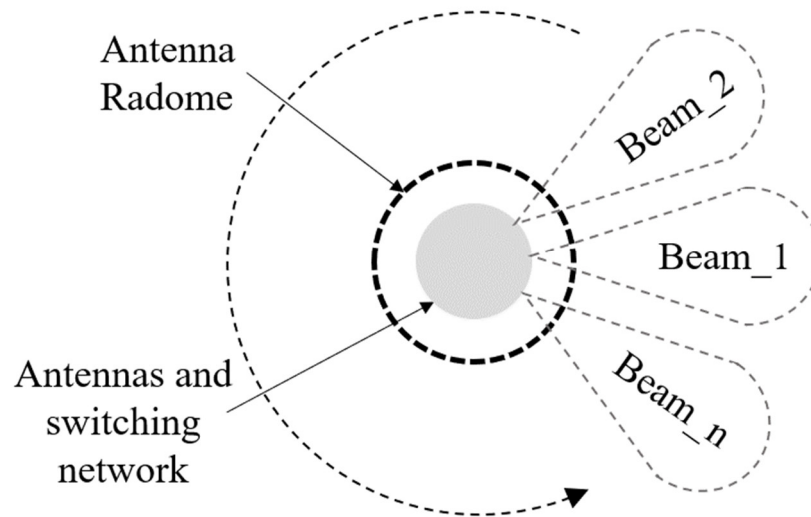
**Table 3.2** Comparison of the beamforming techniques.

|                             | Complexity | Beamforming Resolution | Cost   | Pros. and Con.   |
|-----------------------------|------------|------------------------|--------|--|
| <b>Analogue Beamforming</b> | Low        | Rough                  | Low    | <ul style="list-style-type: none"> <li>• The engineer did not need to control the phase and amplitude of the radio.</li> <li>• Suitable for fixed beam application.</li> </ul>   |
| <b>Digital Beamforming</b>  | High       | Fine                   | High   | <ul style="list-style-type: none"> <li>• Sophisticated beamforming algorithm to control the phase and amplitude of the radio.</li> <li>• Realised in high-cost processing platforms such as FPGA or DSP.</li> <li>• Suitable for Software Defined Radio, military, and satellite Radio.</li> </ul> |
| <b>Hybrid Beamforming</b>   | Medium     | Moderate               | Medium | <ul style="list-style-type: none"> <li>• Combining the best of both digital and analog beamforming techniques.</li> <li>• Lower cost and yet achieving comparable result as digital beamforming.</li> <li>• Commercial and industrial.</li> </ul>  |

In this thesis, the pre-configurable smart antenna system is designed and implemented using the hybrid beamforming technique, where the antenna element is designed and integrated into a bigger array, the RF beamforming frontend also known as the T/R module is designed and integrate with the antenna array to form the beamforming smart antenna system. Many research works have been carried out in the beamforming and smart antenna related area, in this work, the focus is on 3 areas, i). the smart antenna system, ii). the phased antenna array and, iii). the single antenna element that formed the phased antenna array.

### 3.3 Smart Antenna System

The smart antenna system allows the transmitter and receiver to radiate and receive its RF signal from the calculated direction with the best reception quality and lowest operating beamwidth to avoid mutual interference with the neighboring devices. The beam switching method for the conventional smart antenna that covers a  $360^\circ$  azimuth plane can be explained in Fig. 3.7, the antenna was designed to operate at a fixed number of beams and each beam occupied the fixed beamwidth, for instance, a 6 switched beams antenna will have a  $60^\circ$  beamwidth on each beam. During the smart antenna operation, one of the beams is activated at one time according to the targeted direction of the transmitter and receiver.



**Fig. 3.7** Beam switching method for the smart antenna that covers  $360^\circ$  azimuth plane, reproduced from [16] - [21].

In the smart antenna literature, most of the works were concentrated around the reconfigurable structure and beamforming antenna. In this thesis, the research area has been



broadened into the usage scenarios and practical application that combines multiple phased arrays with wide operating band and beamforming capability to address the different application scenarios in the dynamic transportation sector as described in Fig. 2.5. In the past, a reconfigurable polarization beamforming antenna [16] that operates in 5 radiating beams covering the whole  $360^\circ$  with 3 polarizations in the 2.4GHz band was proposed, the reconfigurable was realized by changing the bias voltage of the positive intrinsic negative (PIN) diodes on the parasitic elements and the polarized reconfigurable square patch, the realized gain for the 5 beams are between 2.5 to 3.5 dBi.

Similarly, in [17], the authors have proposed a reconfigurable beam switching antenna with dual-polarization, the design was constructed by radial waveguide as center probes surrounded by radiating elements, the polarization and the radiating beam are controlled by 36 pieces of PIN diodes, the proposed antenna was targeted for the WLAN at 5 GHz band between 5.18–5.825 GHz. The prototype was tested with the realized gain of around 12 dBi and the half power beamwidth (HPBW) of around  $30^\circ$  that allows the antenna to switch among the 12 fixed beams within the  $360^\circ$  azimuth plane.

The smart antenna that can be reconfigured by beam switching has been proposed In [19] making use of a patch as radiating element and six parasitic elements that can be controlled by the PIN diodes, the design was able to achieve the beam switching up to six directions over  $360^\circ$  with the azimuth beamwidth of  $42^\circ$  and the peak gain of around 10 dBi. Another reconfigurable switched beam antenna system [18] was designed using the slotted array that is capable of performing beam scanning in the elevation plane, the design was targeted for LTE femtocells, the HPBW was around  $25^\circ$  with the down-tilt angles of  $13^\circ$  and  $32^\circ$  that capable to switch between 3 elevation beams ( $62^\circ$ ,  $82^\circ$ , and  $108^\circ$ ) via the series-fed structure, the achievable antenna gain was around 9.9 dBi.

In [20], the electronically steerable parasitic array radiators (ESPARs) has been proposed, the parasitic elements consist of 12 folded monopole antennas which were surrounded by a short monopole antenna at the middle of the antenna structure. Each folded monopole was controlled by a PIN diode and the driven element was implemented using the short monopole antenna, the beam switched over the  $360^\circ$  in the azimuth plane was configured via the PIN diodes. The operating frequency of the antenna was from 1.8 – 2.2 GHz and 2.85 – 3.15 GHz with the realized gain of 6.5 for 2 GHz and 5.5 dBi for 2.9 GHz. The combination of PIN diode switching can generate up to 12 beams with  $30^\circ$  beams steering resolution.

Another 360° beam-steering antenna was proposed with gain enhancement and size reduction by adopting the Yagi-Uda arrangement using the small director array (SDA) [21], the reconfigurable was achieved using switched parasitic elements via the PIN diode to steer the beam from 0° to 360° in the azimuth plane. The antenna operates from 2.4 – 2.5 GHz with 10 dBi measured gain. The antenna was designed to operate up to 6 beams with a 60° beam-steering resolution.

A 360° beam-steering antenna has been implemented by combining a monopole and patch as simultaneous radiation elements as reported in [22], the antenna consists of two ports, one connected to the dipole and the other to the patch. By injecting the RF signal to the ports with different phases, 4 beams can be selected over the entire 360° azimuth plane, each selected beam comes with two symmetrical beams. The proposed antenna operates from 2.235 – 2.725 GHz and the measured gain is between 2.1 and 3.1 dBi.

The reconfigurable techniques in [16] - [21] are the popular techniques adopted for beam steering antenna, where the PIN diodes were used to switch the radiating beam of the antenna. However, such technique has its limitations due to the fixed beams and wide beamwidth that limit the antenna system for the operations that required a narrower and fine resolution on the steering angle, as the technology migrates into digital beamforming that requires more precise beamforming angle, fine beam-steering resolution, and small beamwidth to fulfil the high interference rejection requirement.

### 3.3.1 Antenna Array

The phased array plays an important part in our proposed smart antenna system, the choice of the antenna array design will determine the smart antenna performance such as operating bandwidth, gain, and sidelobe level. Antenna arrays design seems to be a popular topic in the literature, however, the applications were mainly focused on the area such as 5G [23][29]-[33], X-band [34], LTE [36], 2.4GHz band [37] and 2.35 GHz to 2.8 GHz / 5 GHz to 5.5 GHz [38]. In the Wi-Fi arena such as 802.11a/an/ac, the literature was mainly focused on array miniaturization, enhance the radiation performance, structure and left with limited work on enabling the array to operate in a wider band that covers the 4.9 GHz licensed band and 5.1 – 5.9 GHz unlicensed band. For instance, in [39], a  $2 \times 4$  dual-polarization antenna array that operates from 5.15 – 5.85 GHz with the realized gain of 12 dBi was proposed. In another work [40], the complementary split ring resonators (CSRR) method was used to reduce the size of the 5 GHz patch antenna, however, the gain suffered at only -0.16 dBi and limited operating bandwidth around 80 MHz, similarly, in [41], the 8 elements MIMO antenna with 6.5 dBi gain and narrow operating frequency bandwidth from 4.985 to 5.15

GHz has been proposed. Furthermore, in [45], a 3 monopole patches antenna array with inverted L and inverted Z came with slightly wider bandwidth covering from 5 to 6 GHz with achievable gain from 2 to 3.7 dBi was proposed. In this work, a wideband and high-gain phased array that operates from 4.9 – 5.9 GHz band is introduced, the proposed wideband array is further integrated into the pre-configurable smart antenna system.

### 3.3.2 Antenna Elements

The type of antenna elements in the phased array will determine the performance and radiation characteristics of the phased array. One of the popular antenna elements that is widely used in the phased array design is the microstrip patch antenna (MPA) [24], the reason was due to the flexible MPA structure, simple to manufacture, and lower cost. The flexible structure allows easy customization and performance enhancement such as gain and bandwidth improvement. The MPA has been enhanced through various methods such as altering the structure of the MPA, changing the material of the dielectric substrate, and different feeding methods, as a result, the gain and operation bandwidth limitation have been improved over the years. A 14% bandwidth ratio wideband multilayer patch antenna structure was proposed in [25], however, the design may not be suitable for large array integration due to the nature of the stacked capacitive coupling through air structure that may not be manufacture friendly. An open slot was introduced on the radiating patch in [27] to enhance the bandwidth ratio to 22% but it suffered a lower gain of around 3.25 dBi. The electromagnetic bandgap (EBG) [26] and defective ground structure (DGS) [28] techniques have delivered the bandwidth ratio of 18.68% and 63.65% respectively with the bigger element size. An ultra-wideband dual substrate MPA with a small capacitive feed was proposed in [35], the bandwidth ratio was around 50% and exceeding 7 dBi gain, the capacitive coupling was realized by the spacing between the radiating patch and the feeding pad on the same PCB layer that increases the manufacturability of the antenna, the dual substrate capacitive feed MPA elements can be a potential candidate for further integration and optimized into a beamforming array.

### 3.4 *The Proposed Modern Pre-Configurable Smart Antenna System*

The conventional smart antenna was aimed to combat the sticky interference issue due to air space congestion. This thesis is aiming to further enhance the smart antenna by taking into consideration various scenarios in the practical deployment [43]. The idea of this smart beamforming antenna systems is aimed to improve the wireless communication in the transportation environment in 3 areas, i) **performance**: interference and range performance can be improved by concentrating the antenna transmit power and receiving to the direction of the target and nulls for other direction, ii) **cost**: the range coverage improvement has reduced the number of base stations needed, in addition, the pre-configuration method allows only the necessary sub-array to be installed based on the coverage and range requirement, hence it saves the material cost, iii) **maintainability**: with the less number of equipment installed in the field that implies fewer resources and cost is needed to maintain the system throughout the operating years. The thesis is targeting an antenna structure with a wide operating frequency band that can be pre-configured to different coverage sector and gain with a narrow beam that supports beamforming feature within the sector, the proposed pre-configurable smart antenna structure is expected to improve the interference rejection and deployment cost in the dynamic transportation environment. The smart antenna system is expected to deliver the following features,

- a. A Wide operating band that covers the 4.9 – 5.9 GHz band that can be materialized by the dual-substrates technique by integrating the MPA on two thick substrates consist of air and the F4BTM-2 substrate.
- b. Different arrays with choice of gain can be pre-selected from the prefabricated  $1 \times 4$ ,  $2 \times 4$ , and  $4 \times 4$  arrays, for example, 11.16, 14.59, and 17.25 dBi.
- c. Pre-configurable sector (each sector covers  $90^\circ$  scanning angle) can be pre-configured to enable coverage over the  $90^\circ/180^\circ/270^\circ/360^\circ$  area, up to 4 arrays to support  $360^\circ$  coverage.
- d.  $24^\circ$  beamwidth with beam steering function.

### 3.5 *Summary*

The beamforming antenna concept has been studied, including various beamforming techniques such as analogue beamforming, digital beamforming, and hybrid beamforming.

The hybrid beamforming is adopted in this work due to the simplicity, flexibility, and cost-effectiveness. The building blocks of the 360° smart antenna system were studied including the single antenna element, antenna array, and method to realize the 360° smart antenna system. The study result has led to a conclusion that the pre-configurable 360° antenna system has demonstrated a great advantage over the conventional methods for application in the transportation environment, the performance, cost, and maintainability benefit have been highlighted.

## 4 Designing the Antenna Element

This section will run through the necessary steps towards designing and optimising the antenna element. Starting from the selection of the type of antenna element by comparing the simulation results with the conventional circular and rectangular patch element without enhancement. Followed by parameters optimisation on the targeted single antenna element to enhance the operating bandwidth, gain and sidelobe level. Finally, the ground plane simulation was carried out to identify the ground plane effect using the time domain approaches, Finite Integration Technique (FIT) solver from Simulia Computer Simulation Technology (CST) Studio Suite (Darmstadt, Germany) [61]. The performance of the antenna element was experimentally evaluated.

### 4.1 Conventional Microstrip Patch Antenna Element

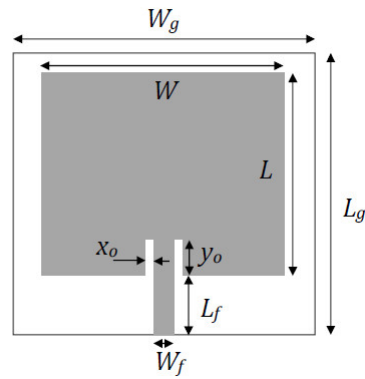
Among many types of antenna element structure, the MPA structure is the popular type of element, it is simple to design and easily integrated into the antenna array that supports higher gain, the small form factor of the MPA also make it popular for application in mobile devices, vehicular applications, and long-range communication antennas. The MPA structure consists of four parts (patch, port feed, substrate, and ground plane) as described in Fig. 4.1 and Fig. 4.2. A thin copper patch is laid over a non-conductive dielectric substrate with the finite ground plane at the opposite side of the substrate. The patch is made of copper foil coated with anti-corrosion material such as gold, the substrate materials use in PCB usually consists of fibreglass with a dielectric constant between 2 to 4.5. Copper foil or solid metal plate can be used as a ground plane depends on the type of application.

Over the years, many shapes of the MPA were designed and presented in the literature, and the most popular shapes are the rectangular and circular shape MPA [58]. The design consideration for the circular patch is relatively simple compared to rectangular patch, for example, the circular patch has only one degree of freedom, which is to control the radius of the MPA patch, however, the rectangular patch has two degrees of freedom where both length and width of the MPA patch need to be controlled. The characteristic of the

---

*This chapter is reproduced from paper #3 in the publication list on page iv, where the thesis author is the main author in this paper.*

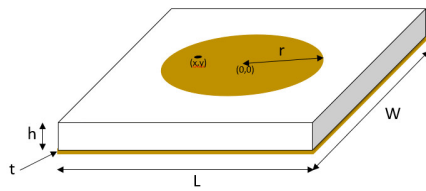
conventional rectangular and circular shape MPA without any gain and bandwidth enhancement was reproduced and simulated using the CST FIT solver, the parameter of the rectangular and circular MPA are presented in Fig. 4.1 and Fig. 4.2 and the result for 5.5 GHz operating frequency are tabulated in Table 4.1. The conventional MPA antenna normally comes with a narrower operating bandwidth around 4 % and lower gain of less than 5 dBi. In practical application, many works, and techniques have been carried out to overcome the limitation and improve the performance of the MPA to make it more useable, the next section covers the performance parameters enhancement of the MPA such as gain, operating bandwidth, and in-band gain ripple.



Where:

|  |         |
|--|---------|
| $W_g$ : width of the Ground/Substrate                          | 26.4 mm |
| $L_g$ : length of the Ground/Substrate                         | 22.2 mm |
| $W$ : width of the Patch                                       | 16.8 mm |
| $L$ : length of the Patch                                      | 12.6 mm |
| $L_f$ : length of the feed                                     | 8.8 mm  |
| $W_f$ : width of the feed                                      | 2.9 mm  |
| $x_o$ : the gap between the antenna and inset feed             | 1.0 mm  |
| $y_o$ : length of the inset feed                               | 4.0 mm  |
| $t_p$ : thickness of the patch                                 | 0.2 mm  |
| $h_s$ : height of the substrate                                | 1.6 mm  |
| $\epsilon_r$ : relative permittivity of the substrate material | 4.3     |

**Fig. 4.1** Conventional rectangular MPA antenna element



Where:

|  |         |
|--|---------|
| $r$ : patch radius   | 7.3 mm  |
| $t$ : patch thickness  | 0.1 mm  |
| $h$ : substrate thickness                                      | 1.6 mm  |
| $x$ : feeding point, x   | 2.6 mm  |
| $y$ : feeding point, y   | 0.0 mm  |
| $L$ : length of the ground plane                               | 29.0 mm |
| $W$ : width of the ground plane                                | 29.0 mm |
| $\epsilon_r$ : relative permittivity of the substrate material | 4.3     |

**Fig. 4.2** Conventional circular MPA antenna element

**Table 4.1** Conventional MPA antenna performance (without bandwidth and gain enhancement).

| Characteristic                         | Conventional Rectangular Patch | Conventional Circular Patch |
|--|--------------------------------|-----------------------------|
| Frequency                              | 5.573 GHz                      | 5.336 GHz                   |
| Operating band                         | 5.47 – 5.69 GHz                | 5.21 – 5.46 GHz             |
| Bandwidth                              | 0.22 GHz                       | 0.25 GHz                    |
| Bandwidth ratio                        | 3.90 %                         | 4.70 %                      |
| Gain                                   | 1.76 dBi                       | 4.78 dBi                    |
| Gain characteristic (4.9GHz to 5.6GHz) | -5.42 to 1.69 dBi              | 0.24 to 4.54 dBi.           |
| In-band gain ripple                    | 7.10 dB                        | 4.30 dB                     |

## 4.2 Enhanced Antenna Element Design and Optimisations

The antenna array was built by multiple single antenna elements placed in the plane vertically and horizontally. The single elements constructed with the dual substrate and feed via capacitive coupling techniques in [35] was chosen in our design. The geometrical view of the dual substrate capacitive feed MPA is shown in Fig. 4.3, the large patch as shown in Fig. 4.3(a) acts as the radiator, and the small patch functions as a capacitive feeding network to allow the energy feed through from the coaxial feed to the radiating patch. The capacitive feed that isolates the radiating patch from the co-axial feed by a thin air gap will reduce the potential mismatch that may occur between the co-axial feeding cable and the patch, on the other hand, the bandwidth and gain of the MPA antenna can be enhanced by the dual layers of the substrate structure. The radiating patch of the antenna was designed on an F4BTM-2 substrate with relative permittivity,  $\epsilon_r = 3$ , to resonate at 5.5 GHz. The length,  $L$  and width,  $W$  of the patch were calculated using the formula from the literature [24] listed below.

$$W = \frac{1}{2f_c\sqrt{\mu_o\epsilon_o}}\sqrt{\frac{2}{\epsilon_r + 1}} = \frac{c}{2f_c}\sqrt{\frac{2}{\epsilon_r + 1}} \quad (4.1)$$

where,

$W$  : the width of the patch

$f_c$  : the center frequency

$\mu_o$  : magnetic permeability of free space

$\epsilon_o$  : electric permeability of free space

$\epsilon_r$  : dielectric constant of the substrate



$c$  : speed of light.

$$L = \frac{c}{2f_c\sqrt{\epsilon_{eff}}} - 2\Delta L \quad (4.2)$$

Where,

$L$  : the length of the patch

$\epsilon_{eff}$  : the effective dielectric constant

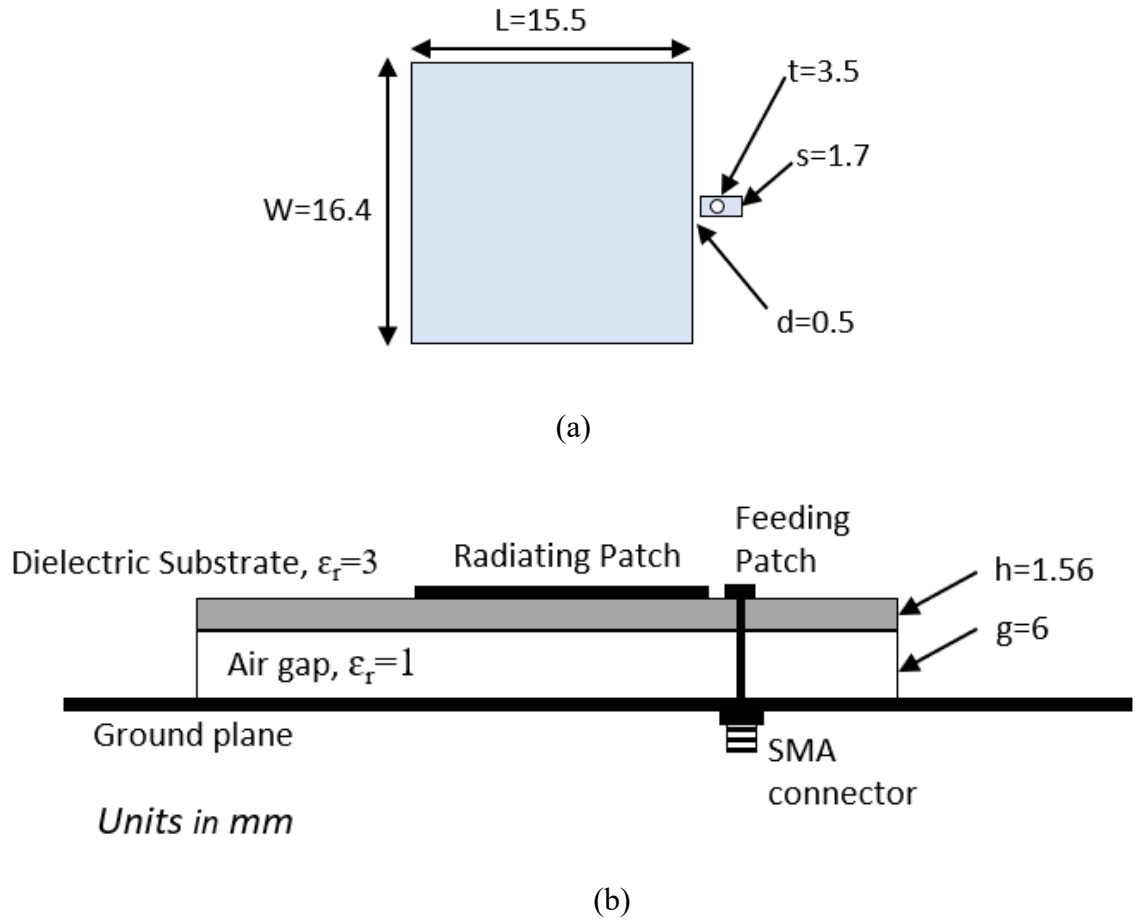
$\Delta L$  : the extended length of the patch that can be calculated using equations (5.3) and (5.4).

$$\epsilon_{eff} = \frac{\epsilon_r + 1}{2} + \frac{\epsilon_r - 1}{2} \left[ 1 + 12 \frac{h}{W} \right]^{-\frac{1}{2}} \quad (4.3)$$

where  $h$  is the height of the substrate.

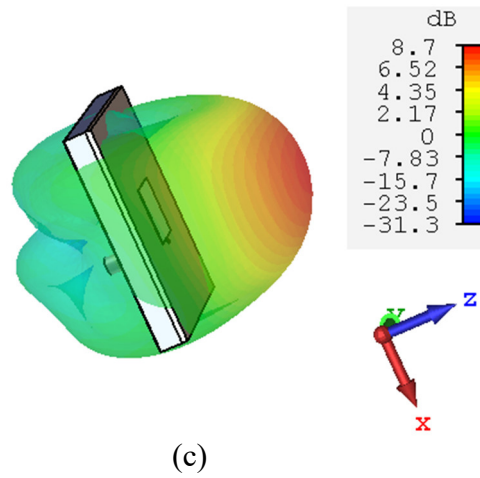
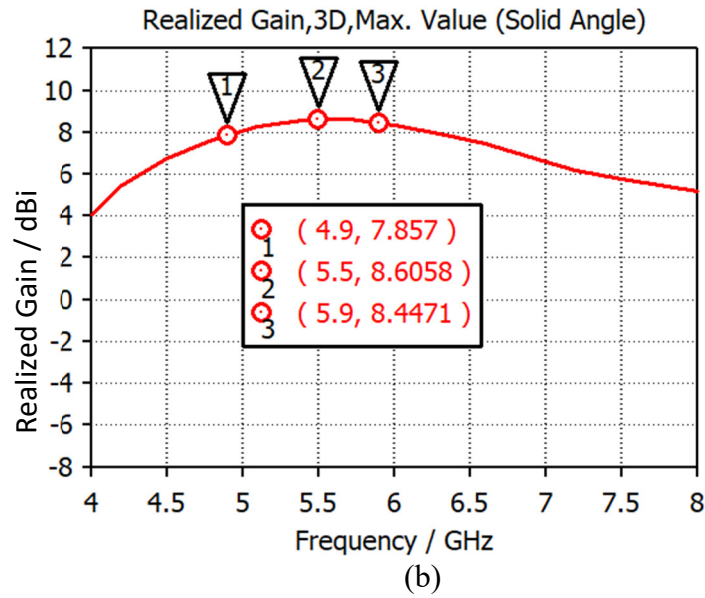
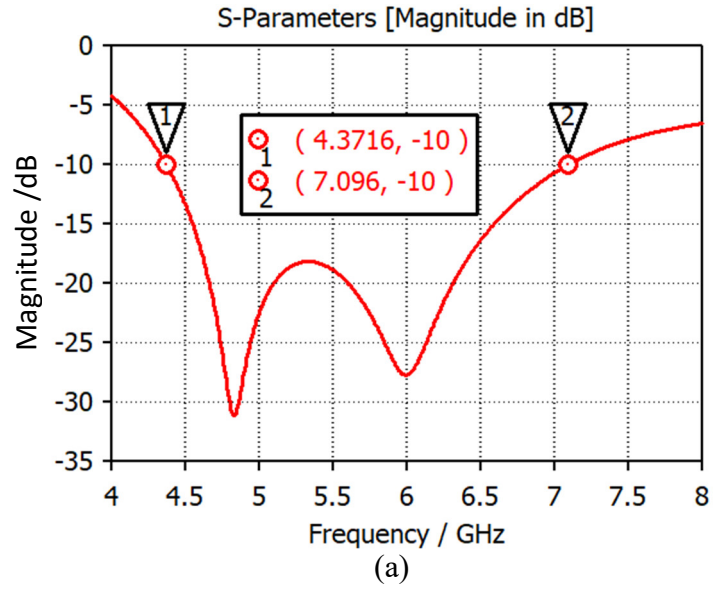
$$\Delta L = 0.412h \frac{(\epsilon_{eff} + 0.3)(\frac{W}{h} + 0.264)}{(\epsilon_{eff} - 0.258)(\frac{W}{h} + 0.8)} \quad (4.4)$$

The optimum operating frequency bandwidth can be optimised by adjusting the capacitive feed length ( $t$ ), width ( $s$ ), distance to patch ( $d$ ), and the space of airgap ( $g$ ). In this work, the design in [35] was used as a base and further optimize through parameter optimization to improve the frequency bandwidths to cover our interest band from 4.9 – 5.9 GHz as well as enhancing the antenna gain and cap the returned loss to below 10 dB, from the simulation result, about 15 % improvement was achieved on both operating bandwidth and gain compared to the original design parameter in [35].



**Fig. 4.3** Capacitive feed dual-substrate MPA. (a) Top view. (b) Side view

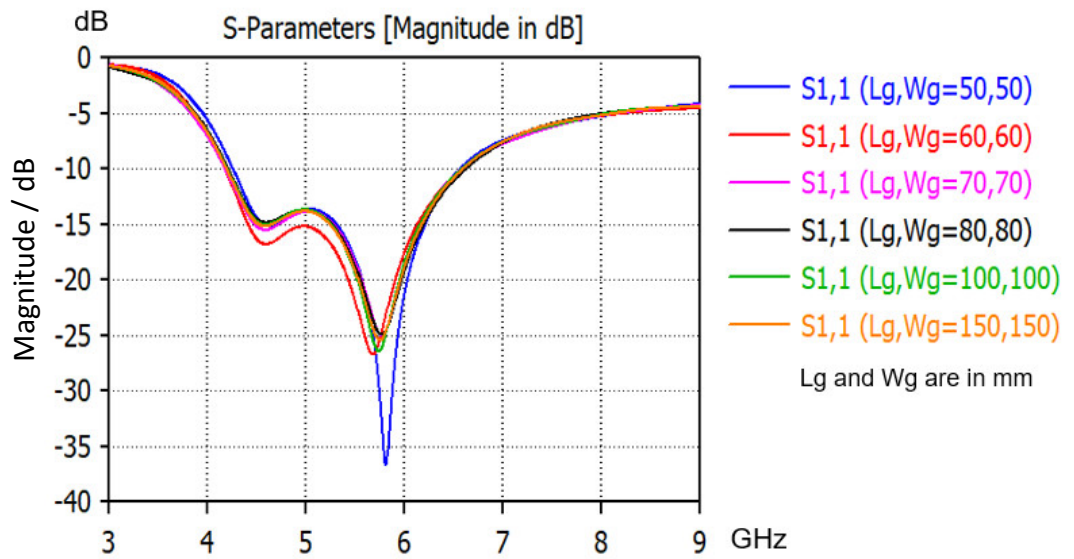
The antenna parameters were optimized and simulated using the CST FIT solver, the optimized parameters are shown in the geometrical model in Fig. 4.3. The simulation results of the single capacitive feed MPA element are presented in Fig. 4.4. The returned loss of 10 dB was achieved between 4.73 to 7.09 GHz which translates to around 43 % bandwidth ratio at 5.5 GHz center frequency. The maximum gain of 8.6 dBi at 5.5 GHz was achieved with the gain flatness of 0.8 dB over the 4.9 to 5.9 GHz band, which is quite reasonable for the entire 1 GHz bandwidth.



**Fig. 4.4** Simulation results of the capacitive feed MPA element. (a) Simulated S11 result. (b) Gain characteristic over 4 to 8 GHz band. (c) Far-field radiation pattern.

### 4.3 Size of the Ground Plane

The phased array was constructed by arranging multiple MPA elements to form a bigger array that directly contributes to the increase in ground plane size. The performance impact from the size of the ground plane is evaluated by observing the return loss of the element with respect to the ground plane size. The simulation results are captured in Fig. 4.5, the results have proofed that the variations of ground plane dimension has a minimum impact to the antenna performance, thus we concluded that the antenna element can be used to design into a phased array that usually occupied a big ground plane. The radiated performance of the single element is presented in the next section.



Note:  $L_g$  is the length of the ground plane and  $W_g$  is the width of the ground plane.

**Fig. 4.5** Simulation on the effect of the size of the ground plane at 5.5 GHz.

### 4.4 Radiated Measurement of the Antenna Arrays

To ease the measurement and iteration process, we have set up the open site to perform the far-field measurement of the antenna radiation pattern including the gain, sidelobe level, and beam steering performance, the measurement setup is demonstrated in Fig. 4.6. a receiving antenna with the known gain was placed at a distance  $D$  away from the antenna under test, the far-field distance  $D$  was chosen to be larger than the theoretical minimum far-field distance computed using formula  $2A^2/\lambda$  [42], where  $A$  is the maximum dimension of the antenna and  $\lambda$  is the wavelength of the frequency of interest, with  $A = 18.27$  cm and  $\lambda =$

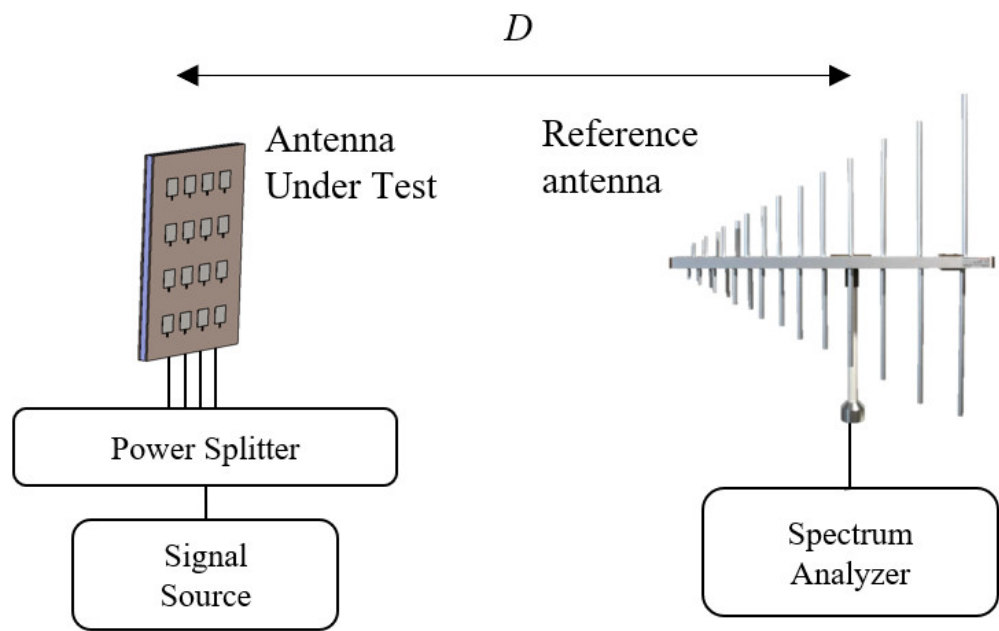
5.45 cm, the minimum far field distance calculated as 1.22 meter, for simplicity  $D = 3$  meters is used in the measurement. The radiated power transmitted from the antenna under test is captured by the receiving antenna and feed into the spectrum analyser for measurement and data logging. This section will cover the far-field antenna radiation pattern measurement at its nominal  $0^\circ$  beam. A power splitter is used to split the RF source into 4 dedicated antenna ports with a similar phase that are connected to the antenna under test. For  $0^\circ$  beam measurement, the 4 antenna ports are injected with the signal with equal phase.

#### 4.4.1 Antenna Radiated Measurement Topology

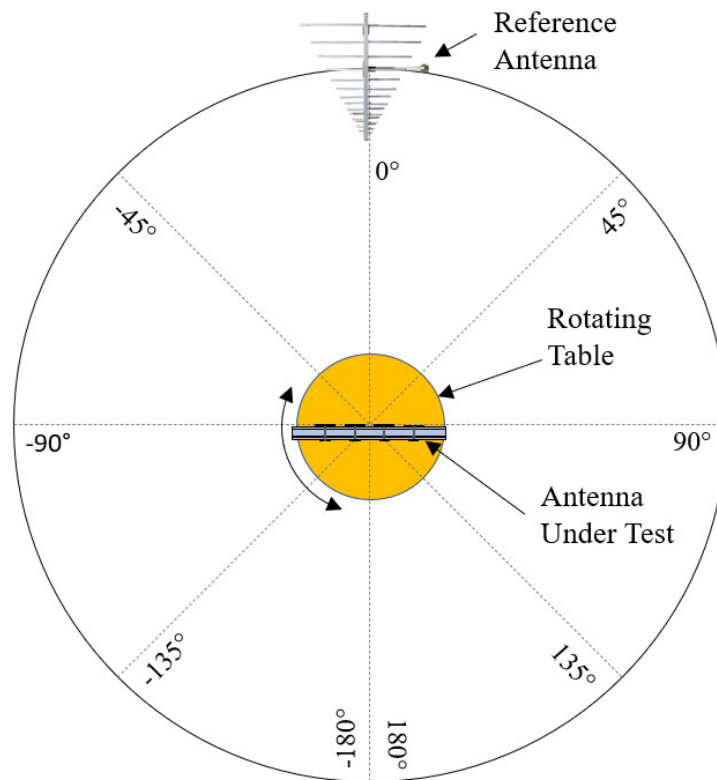
Open site technique [60] along with the Free Space Loss (FSL) method [11] was adopted to measure the antenna radiation pattern of the prototype arrays. Thus, the antenna gain of the receiver can be calculated using Friis equation as shown below:

$$G_r + G_t = 20\log\left(\frac{4\pi f D}{c}\right) + P_r - P_t + \alpha \quad (4.5)$$

where  $G_r$  and  $G_t$  are referring to the realized gain in (dBi) of the golden antenna (receiver antenna) and the target antenna (transmitter antenna) respectively, the interest frequency is represented by  $f$ , distance between the transmitter antenna and receiver antenna is represented by  $D$ ,  $c = 3 \times 10^8$  m/s denotes the speed of light,  $P_r$  is the power received by the reference antenna in (dBm),  $P_t$  represents the power transmitted by the signal source in (dBm), the attenuator factor due to connectors and cables is shown as  $\alpha$ .



(a)

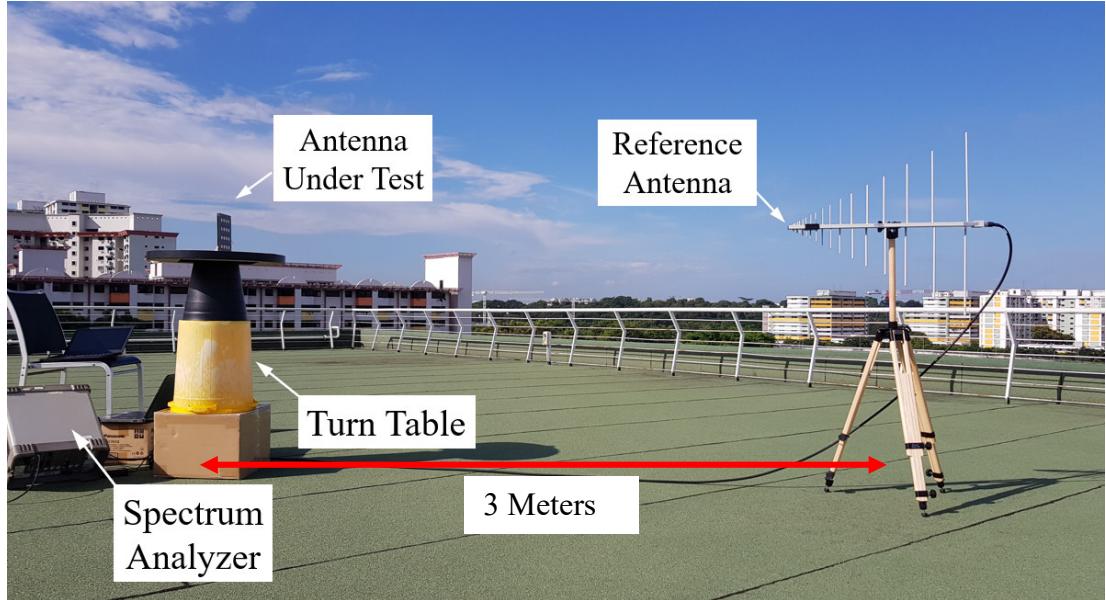


(b)

**Fig. 4.6** Antenna measurement setup in open space. (a) Antenna measurement setup. (b) Antenna orientation (top view).

In the measurement setup presented in Fig. 4.6(a), the log-periodic antenna part number LP-04 is used as a reference antenna, the antenna is manufactured by Narda (Milano, Italy) with the gain provided by the manufacturer is 6 dBi at 5.5 GHz. The spectrum analyser E4407B from Agilent (Santa Clara, United States) is used to measure the power received by the reference antenna. A pre-calibrated off the shelf 802.11ac wireless dongle part number WUSB-3002 is used as a signal source to provide the transmit output power of 23 dBm at the frequencies between 5.1 – 5.9 GHz. In the measurement setup with  $D = 3$ , the calculated FSL is 56.79 dB, the measurement system was pre-calibrated to include the offset of the FSL and  $\alpha$ , attenuation factor.

To emulate the radiating angle during the measurement, the antenna under test is placed on the turntable as shown in Fig. 4.6(b) and constantly rotates through the azimuth plan in the step of  $5^\circ$  over the  $360^\circ$  sector to simulate the  $360^\circ$  radiation pattern. The receiver antenna will pick up the RF field while the transmitter antenna rotates, the measured power can be converted to the antenna gain using equation (6.1) and presented as antenna radiation pattern by plotting the full set of measurement data over the  $360^\circ$  chart. The photo of the measurement setup is shown in Fig. 4.7, the measurement was done at the open site at the building top to minimise the measurement uncertainty due to multipath RF reflection.

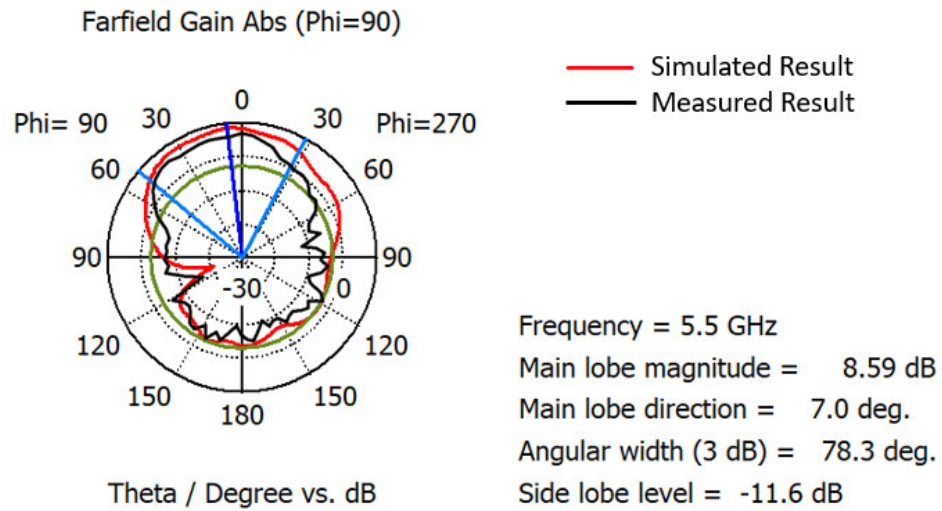


**Fig. 4.7** Photo of the far-field antenna measurement setup.

#### **4.4.2 Radiation Measurement of the Single Element Antenna**

The single element was experimentally evaluated using the measurement setup in Fig. 4.7, the RF beamwidth observed is around  $80^\circ$  and matched well with the simulated result as shown in Fig. 4.8. The far-field antenna gain is measured at 3 frequencies 4.9, 5.5, and 5.9 GHz with the gain of 7.3, 6.87, and 5.5 dBi respectively, compared to the simulated results of 7.42, 8.59, and 8.69 dBi, there is a variation of gain at the high band, this might be due to the frequency response of the coaxial cable and RF connectors.





**Fig. 4.8** The radiation pattern of the single element antenna.

## 4.5 Summary

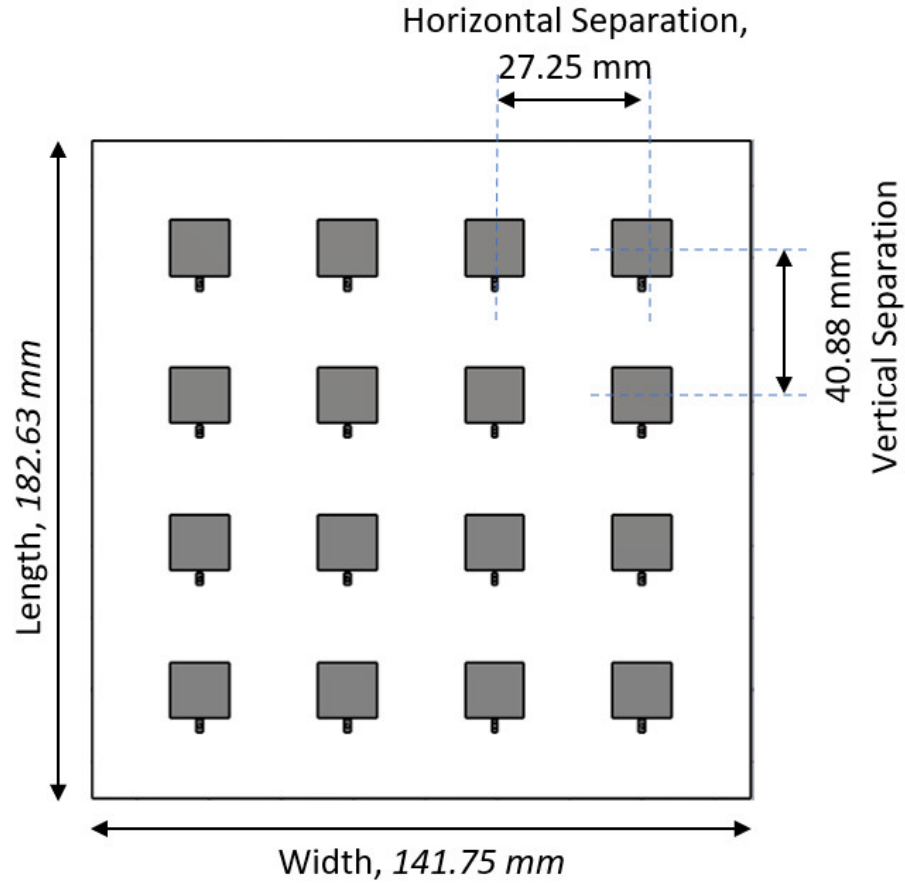
This section has concluded that the proposed MPA element with dual substrate structure and capacitive feed technique is able to achieve the desired gain and operating bandwidth, the minimum performance impact on the size of the ground plane has concluded that the proposed antenna element can be used to design into a phased array that usually occupied a big ground plane. The dedicated open space test site has been set up to evaluate the radiated performance of the element, a moderate agreement was observed between the experimental and the measured result.

## 5 Designing the Antenna Arrays

This section covers the necessary steps to design the antenna arrays using the enhanced MPA element. First, the optimum arrays performance was simulated by adjusting the spacing of the elements, once the optimum elements spacing are determined, the vertical elements are combined via the microstrip feeding network to the RF feeding port, the elements are arranged symmetrically to form a linear array with 4 RF ports that allow beamforming function to take place. 3 types of arrays  $1 \times 4$ ,  $2 \times 4$ , and  $4 \times 4$  with low, middle, and high gain were designed. The antenna array prototypes are fabricated and experimentally evaluated to validate the gain, sidelobe level, HPBW, and beam steering capability against the simulation results.

### 5.1 Optimise the Element Separation

The antenna array or commonly called a phased array that consists of multiple single-antenna elements placed vertically and horizontally in the same plane, the spacing of the elements are equally spaced in the array form. Phased arrays are used to synthesize a specific radiating pattern that cannot be achieved with a single element antenna [58], to achieve that, the spacing between the element needs to be properly defined and optimized to achieve optimum performance in terms of gain, sidelobe, and beamwidth. Before the integration of the single element into the bigger array, the first thing is to determine the necessary element spacing, that may impact the performance and size of the final phased array, the proposed  $4 \times 4$  array as shown in Fig. 5.1 was first evaluated using CST FIT solver. The gain, sidelobe, and beamwidth performance with respect to the element spacing in the antenna array are presented in Fig. 5.2 and Fig. 5.3.

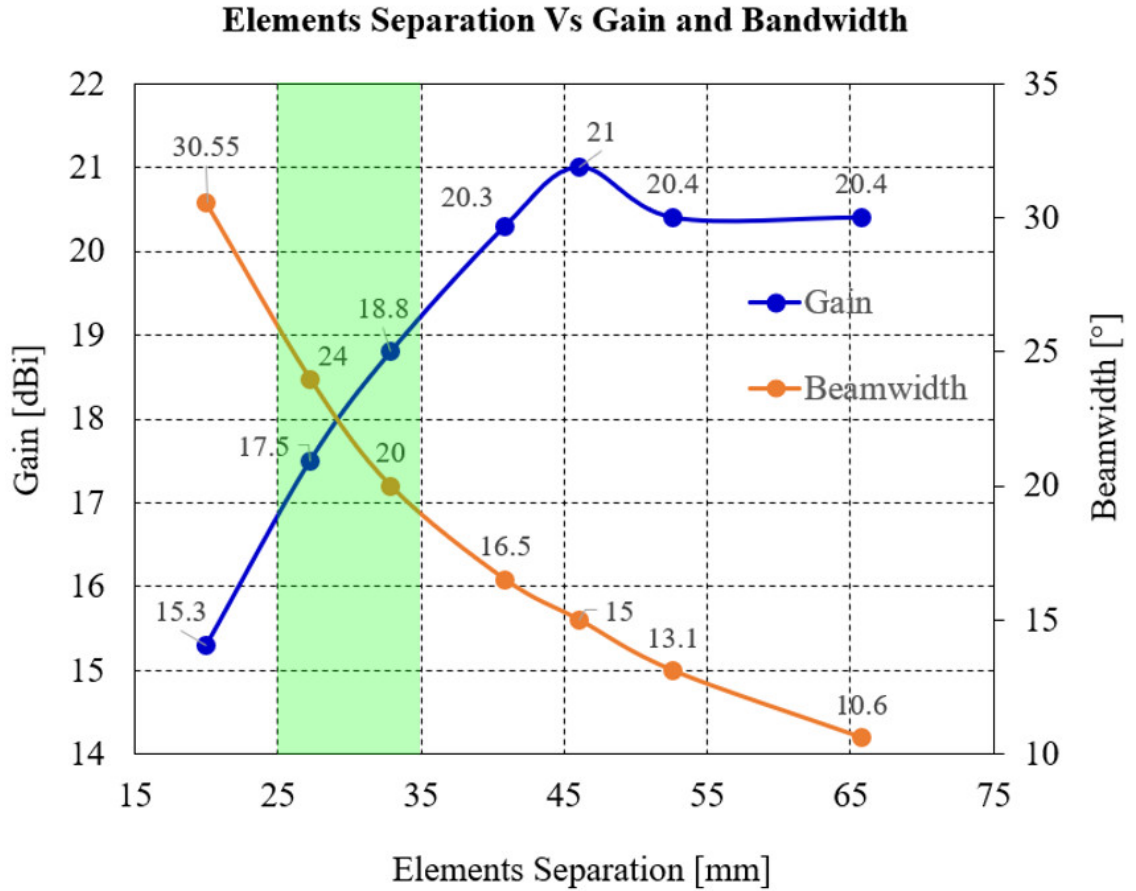


**Fig. 5.1** The  $4 \times 4$  array illustration for “Far Field” simulation.

### 5.1.1 Evaluation of the Elements Separation vs Gain and Beamwidth

Fig. 5.2 presents the relationship between the operating beamwidth and the gain of the  $4 \times 4$  phased array with respect to the element separation, as the element separation increases, the gain will gradually increase until it reaches the maximum gain of 21 dBi at 46.03 mm element separation or slightly less than  $1\lambda$  (wavelength), the gain became saturated when the element separation increases beyond  $1\lambda$ . Separately, the operating beamwidth became narrower in the exponential rate with the increases in the element separation, for instance, the beamwidth at 20 mm element separation decreases in the rate of 30% for 10 mm increase in the element spacing, the rate of the beamwidth decreases is lower when the element separation increases. The trade-off between the gain and operating beamwidth seems straight forward and easy to understand if the antenna array is used as a point-to-point link where the gain is maximised while maintaining the beamwidth to as narrow as possible. when comes to beamforming array, we will need to consider another factor which is the sidelobe level (SLL), usually, the best SLL appear at  $0^\circ$  beam, however, it tends to increase when the beam

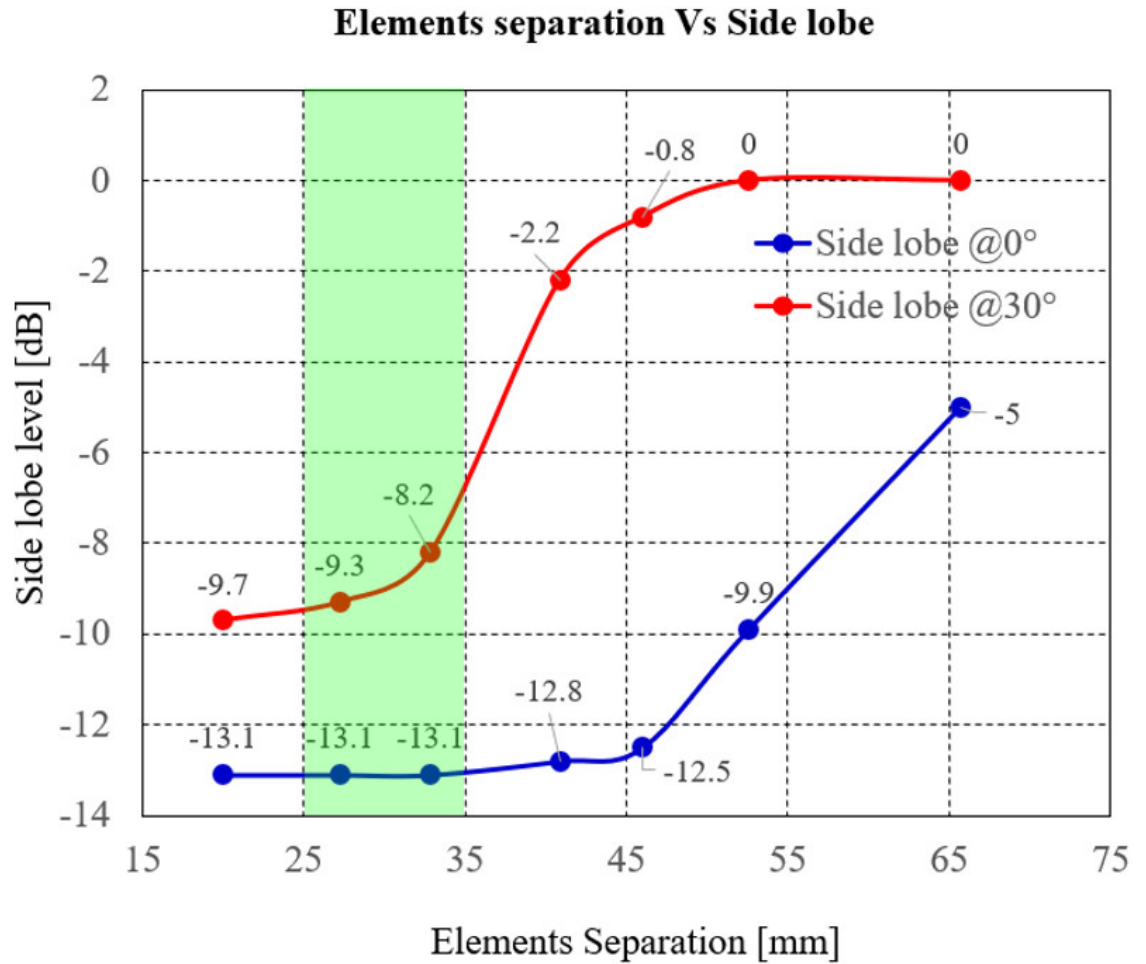
is steered away from its  $0^\circ$  beam, hence, the SLL is another contributor to the performance trade-off that required much attention.



**Fig. 5.2** The impact of element spacing on array gain and beamwidth.

### 5.1.2 Evaluation of Elements Separation vs Sidelobe Level

The impact of elements spacing on SLL performance when the radiating beam steered from  $0^\circ$  to  $30^\circ$  is presented in Fig. 5.3. For evaluation purposes, the performance of the  $30^\circ$  beam is tested to demonstrate the SLL impact due to the steered beam, and similar effects are applied for other angles. As expected, the lowest SLL level of -13.1 dB is observed at the  $0^\circ$  beam, and the SLL starts to increase rapidly when the element spacing increased beyond 45 mm. In the case of  $30^\circ$  beam, the best SLL observed was around -9.7 dBm and the SLL increases rapidly at a higher rate when the element spacing increases. For both cases, the grating lobe occurred with 2 end-fire maxima when the element spacing reached around  $1\lambda$ . Therefore, we concluded that the optimum element separation should keep between 25 mm to 35 mm. This will ensure optimum gain, beamwidth, and SLL performance.



**Fig. 5.3** The impact of element spacing to the sidelobe level at 0° and 30° beam.

Thus far, the performance trade-off such as beamwidth, gain, and SLL are demonstrated. As the proposed smart antenna is focusing on the azimuth beam steering, the possible element spacing in Fig. 5.2 and Fig. 5.3 are highlighted in green, 27.25 mm ( $0.5 \lambda$ ) was chosen for horizontal separation which produces optimum gain and SLL performance. 40.875 mm ( $0.75 \lambda$ ) for vertical separation that gives the good beamwidth and gain performance as well as better mutual coupling between the vertical spaced elements. The performance of the array is further simulated using the proposed element spacing, promising results were observed and tabulated in Table 5.1. For other application such as a point-to-point link that usually targeted for higher gain and does not require beamforming function, the element spacing can be set to 45 mm, that will produce 21 dBi gain, 15° beamwidth, and -12.5 dB SLL, which is reasonably good for such application.

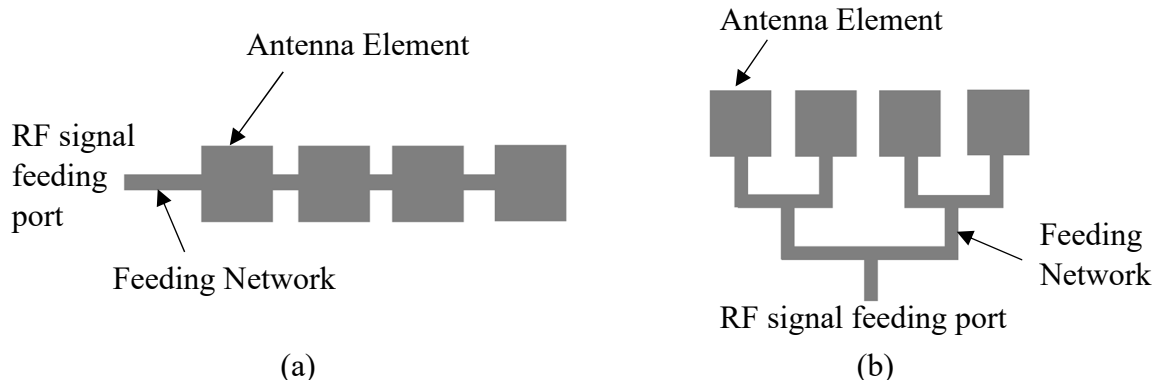
**Table 5.1** Simulation result of the  $4 \times 4$  arrays using the proposed element spacing.

| RF Parameters       | Performance |
|---------------------|-------------|
| Gain                | 17.5 dBi    |
| Operating Beamwidth | 24°         |
| SLL (at 0° beam)    | -13.1 dB    |
| SLL (at 30° beam)   | -9.3 dB     |

The  $1 \times 4$  configurations of antenna array designed using the similar MPA configuration was presented in [44] that operates in 4.19 – 6.58 GHz band with the bandwidth ratio of 44.38 %, the  $1 \times 4$  array provides 12.6 dBi gain, -12.9 dB SLL at 0° steering beam and 24.4° beamwidth, in addition, the antenna array is also capable to perform  $\pm 40^\circ$  beam steering.

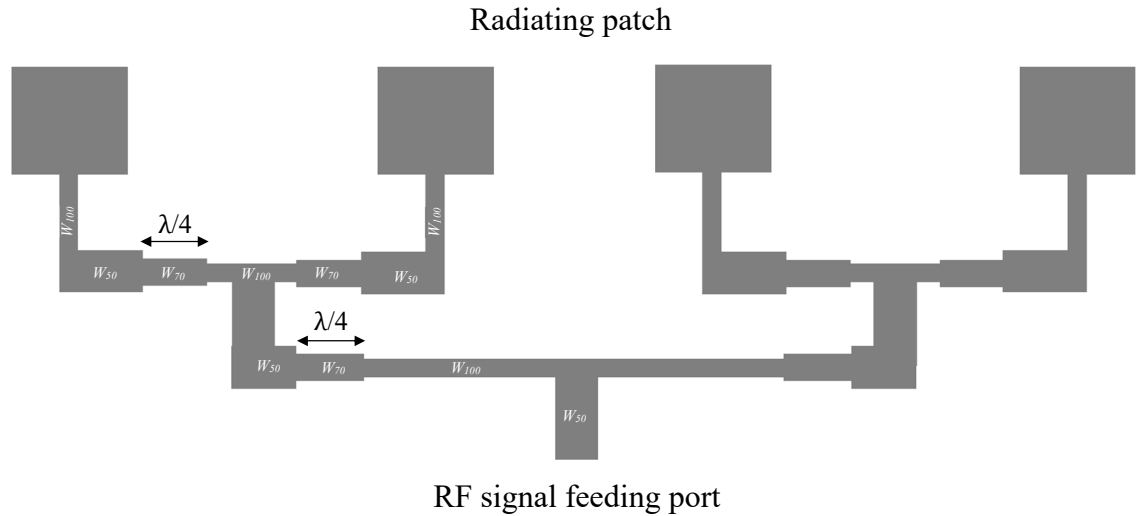
## 5.2 Designing the Feeding Network for the Phased Array

Now, the spacing of the elements has been fixed, next is to integrate the vertically spaced elements into a single feed point via the microstrip feeding network. The  $n \times 4$  beamforming array is formed by arranging the 4 columns of the vertical arrays horizontally. There are 2 types of popular microstrip feeding networks for MPA array design, they are single line feed (series feed) and multiple lines feed (corporate feed) [58] as shown in Fig. 5.4. The simplest way is to use series feed, however, the drawback is the series feed is subjected to mutual performance effects such as elements coupling and microstrip line reflections if changes are made to the feed line or antenna element. For beamforming phased array, corporate feed method is recommended which is less susceptible to design changes, though it required a little bit more space to implement the feeding, however, the concern can be overcome by a good PCB layout technique to lay the feeding line between the available space available between the element spacing.



**Fig. 5.4** Antenna feeding networks to integrate the antenna elements into the array for beamforming applications. (a) Series feed. (b) corporate feed.

In this work, the corporate feed method is adopted. The  $n$  numbers of vertical elements (for instance  $n = 2$  for  $2 \times 4$  array and  $n = 4$  for  $4 \times 4$  array) are jointed at the bottom side of the bottom PCB via the microstrip line with  $\frac{1}{4} \lambda$  impedance transform between the element and the feeding co-axial. The geometry view of the corporate feed array is shown in Fig. 5.5. The parameters are shown in Table 5.2.



**Fig. 5.5** Corporate feed design, indicates the microstrip line width for the impedance matching.

The width of the microstrip line,  $W_f$  is etched over the F4BTM-2 PCB substrate with  $\epsilon_r = 3$ , and thickness of  $h_s = 1.56$  mm can be calculated using the following equation [59].

$$W_f = \frac{8 \sqrt{\frac{A}{11} \left(7 + \frac{4}{\epsilon_r}\right) + \frac{1}{0.81} \left(1 + \frac{1}{\epsilon_r}\right)}}{A} \times h_s \quad (5.1)$$

$$A = e^{\left(\frac{z_0 \sqrt{\epsilon_r + 1}}{42.4}\right)} - 1 \quad (5.2)$$

At the operating frequency of 5.5 GHz, the trace widths  $W_f$  and the length of the quarter wavelength stub are calculated in Table 5.2:

**Table 5.2** Parameters calculated for the  $\frac{1}{4} \lambda$  impedance transformation.

| Microstrip line   | Width / Length |
|---|----------------|
| 50 $\Omega$ line width, $W_{50}$                        | 3.89 mm        |
| 70 $\Omega$ line width, $W_{70}$                        | 2.21 mm        |
| 100 $\Omega$ line width, $W_{100}$                      | 1.04 mm        |
| Length of the Quarter wavelength, $\frac{1}{4} \lambda$ | 6.58 mm        |

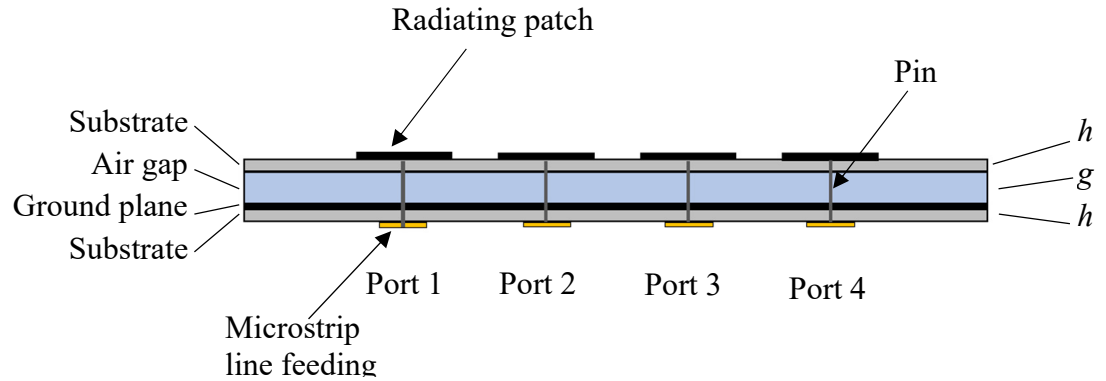
In summary, the bandwidth ratio of the MPA has been improved using the capacitive feed dual substrate technique, the bandwidth ratio improved to 43 % compared to 4 – 7 % for a typical MPA without any bandwidth enhancement. The HPBW, SLL and gain performance were optimised by iterating the element's spacing in the array, which is a practical simulation approach to determine the trade-off between the array's performance parameters which is important as it optimised the performance that suits the application, in our case, we are trying to achieve maximum gain while keeping the HPBW and SLL low. The corporate fed structure adopted can also simplify the design of the  $1 \times 4$ ,  $2 \times 4$ , and  $4 \times 4$  arrays that can be installed into the smart antenna systems that required different gain based on the field scenario as described in Fig. 7.1 and Fig. 7.2.

### 5.3 Forming the $n \times 4$ Antenna Arrays

The proposed antenna array is designed using the capacitive feed MPA with a stack-up structure combining the air and PCB substrate discussed earlier in Section 4.2. The radiating elements are located at the top side of the top PCB using F4BTM-2 with  $\epsilon_r = 3$  as substrate, the air gap sandwiched within the radiating PCB (top) and the grounding/feeding PCB (bottom) to act as the second substrate. The bottom PCB consists of a solid ground



plane on the top layer that will act as the reflector to the radiating element as well as providing a good mutual coupling rejection between the radiating element and the feeding line which is located at the opposite side of the solid ground plane. The detailed cross-sectional view of the PCB stack-up construction is captured in Fig. 5.6.

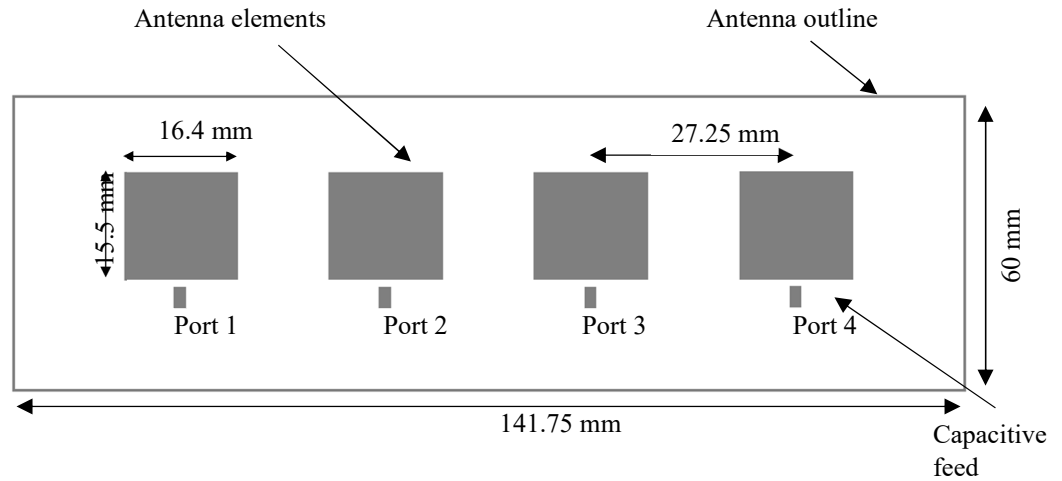


**Fig. 5.6** Microstrip feed on the  $n \times 4$  antenna array.

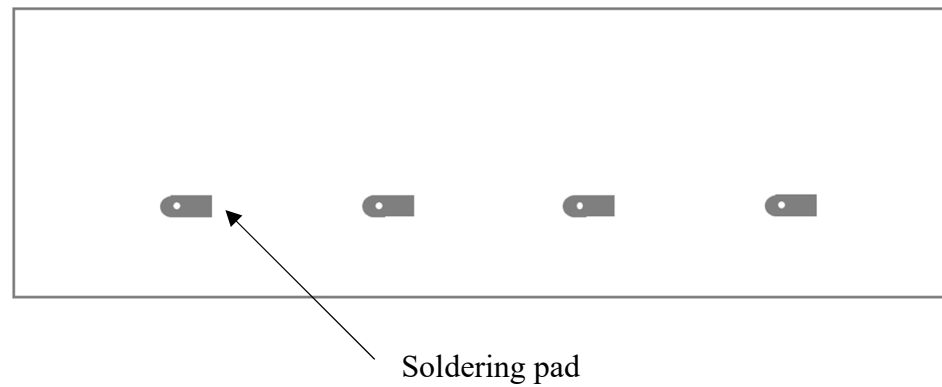
To address the requirement of the pre-configurable antenna system, we have created three variances of arrays using the same MPA element but with the reduced number of elements for lower gain version, i.e.,  $1 \times 4$  array (with 4 elements),  $2 \times 4$  array (with 8 elements) and  $4 \times 4$  array (with 16 elements).

### 5.3.1 $1 \times 4$ Low Gain Antenna Array

The  $1 \times 4$  array is constructed by arranging the MPA element horizontally with the pre-calculated element spacing of  $d = \lambda/2$  or 27.25 mm in the stack-up structure as shown in Fig. 5.6, the external dimension of the antenna is determined by the minimum size of the ground plane and additional space to cater for mechanical mounting structure between the top and bottom PCB. The length and width of the  $1 \times 4$  antenna array are 141.75 mm  $\times$  60 mm. The 4 soldering points allow the co-axial cable to be attached to facilitate connection to external equipment or RF frontend. The top PCB and the bottom PCB of the  $1 \times 4$  antenna array are presented in Fig. 5.7 and Fig. 5.8.



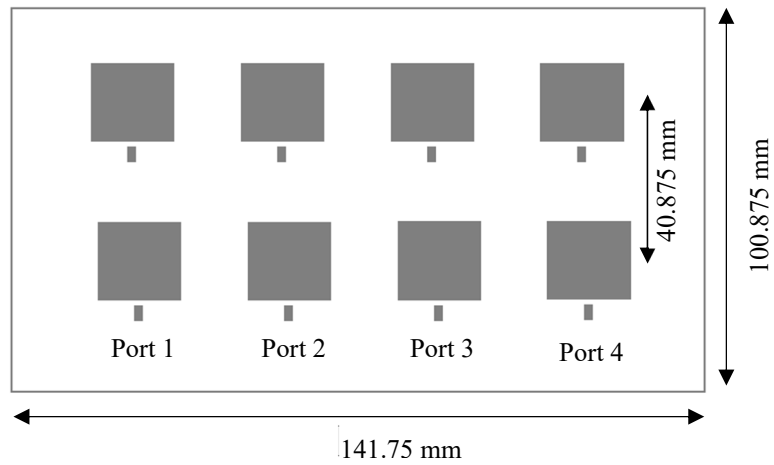
**Fig. 5.7** Top PCB of the  $1 \times 4$  antenna array.



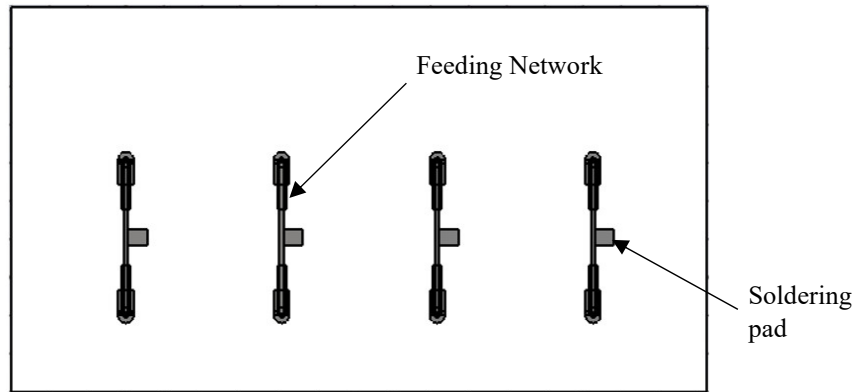
**Fig. 5.8** Bottom PCB of the  $1 \times 4$  antenna array.

### 5.3.2 $2 \times 4$ Middle Gain Antenna Array

For the  $2 \times 4$  array, 8 identical MPA elements are arranged in 2 rows, each horizontal row consists of 4 MPA elements with the element spacing of 27.25 mm which is similar to the  $1 \times 4$  array, the row spacing is set to 40.875 mm as simulated earlier. The length and width of the  $2 \times 4$  antenna array are 141.75 mm  $\times$  100.875 mm. The top PCB consists of the radiating elements and shown in Fig. 5.9 and the bottom PCB consists of the solid ground plane and the microstrip feeding network as shown in Fig. 5.10 that combined the 2 vertical elements into a single feeding point.



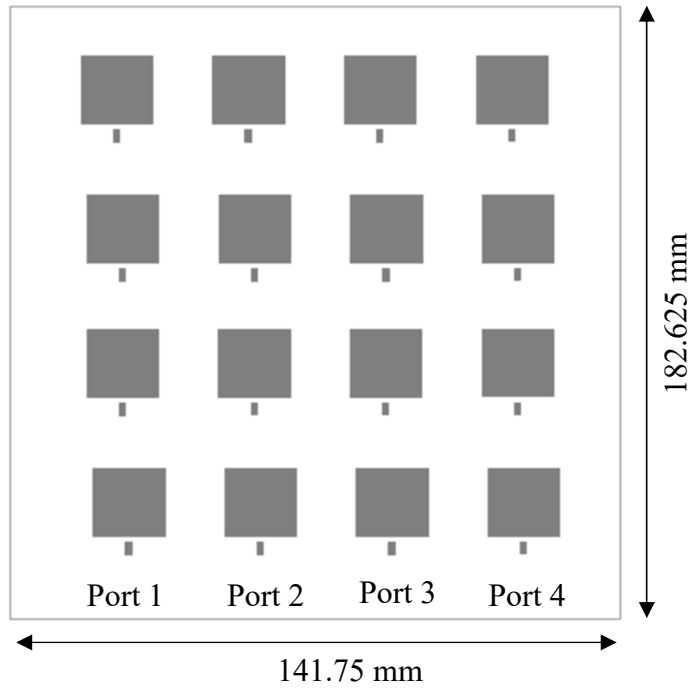
**Fig. 5.9** Top PCB of the  $2 \times 4$  antenna array.



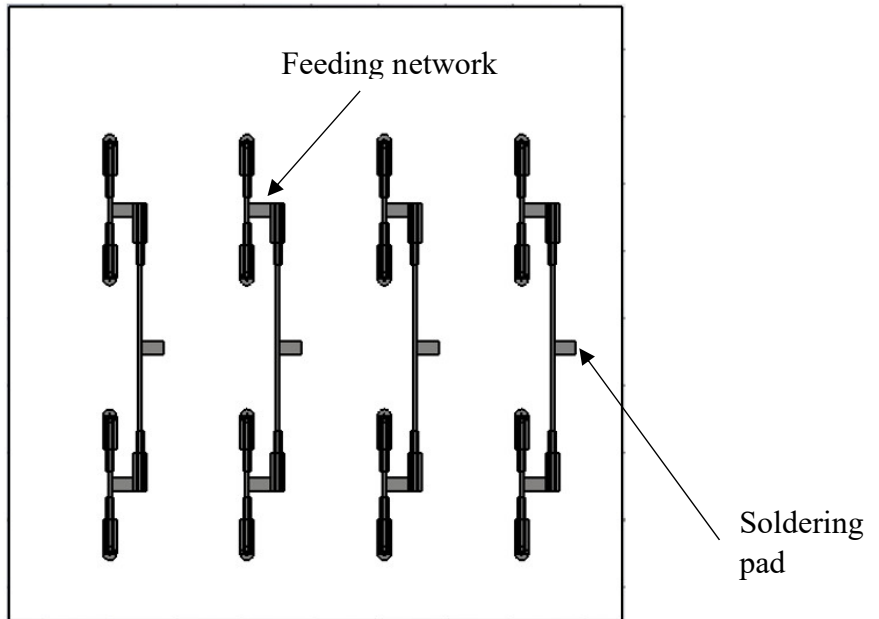
**Fig. 5.10** Bottom PCB of the  $2 \times 4$  antenna array.

### 5.3.3 $4 \times 4$ High Gain Antenna Array

The  $4 \times 4$  array consists of 16 identical elements arranged in 4 rows and 4 columns, similar to the  $1 \times 4$  and  $2 \times 4$  array, the spacing of the horizontal and vertical elements is set to 27.25 mm and 40.875 mm respectively, this makes the overall dimension of the antenna PCB to 141.75 mm  $\times$  182.625 mm. The top view and bottom view of the  $4 \times 4$  array are presented in Fig. 5.11 and Fig. 5.12. Similarly, the bottom PCB consists of the microstrip feeding networks that combined all the vertical spaced elements into a single feed port.



**Fig. 5.11** Top PCB of the  $4 \times 4$  antenna array.



**Fig. 5.12** Bottom PCB of the  $2 \times 4$  antenna array.

The dimensions of the respective array parameters are shown in Table 5.3. Except for the length of the arrays, the rest of the design parameters are common to all the arrays. The common width for the arrays is 141.75 mm while the length of the arrays depends on the type of configuration, the smallest array with  $1 \times 4$  configurations measured 60 mm in length,  $2 \times 4$  array will take up 100.875 mm length and the biggest  $4 \times 4$  array occupied 182.625 mm length.

**Table 5.3** Design parameters of the  $n \times 4$  antenna arrays.

| Parameter    | Description   | Value     |
|--------------|---|-----------|
| $h$          | The thickness of the die-electric substrate         | 1.56 mm   |
| $g$          | The thickness of the air-substrate                  | 6.00 mm   |
| $L$          | Length of the single element                        | 15.50 mm  |
| $W$          | Width of the single element                         | 16.40 mm  |
| $t$          | Length of the capacitive feed                       | 3.50 mm   |
| $s$          | Width of the capacitive feed                        | 1.70 mm   |
| $d$          | Air gap between capacitive feed and antenna element | 0.50 mm   |
| $y$          | Horizontal separation of the antenna elements       | 27.25 mm  |
| $x$          | Vertical separation of the antenna elements         | 40.88 mm  |
| $L_{ant}$    | Length of the $1 \times 4$ antenna array            | 60.00 mm  |
|              | Length of the $2 \times 4$ antenna array            | 100.88 mm |
|              | Length of the $4 \times 4$ antenna array            | 182.63 mm |
| $W_{ant}$    | Width of the antenna array                          | 141.75 mm |
| $\epsilon_r$ | Relative permittivity of the substrate material     | 3         |

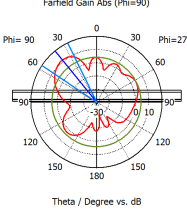
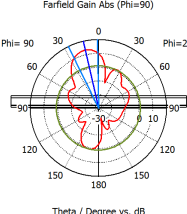
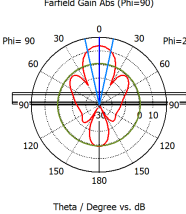
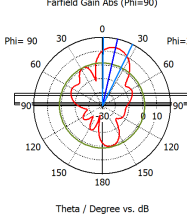
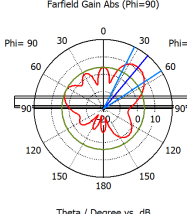
### 5.4 Simulated Result of the $n \times 4$ Antenna Arrays

The performance of the antenna arrays is simulated using CST FIT solver, the beam steering capability of the  $1 \times 4$  array antenna can be simulated by injecting the signal into port 1 to port 4 with different phases. The beamforming antenna is targeted to work within  $90^\circ$  steering beam, therefore radiating beam within  $\pm 45^\circ$  was evaluated.

### 5.4.1 Beam Steering Results of the $1 \times 4$ Array

The simulated results are presented in Table 5.4, the 1<sup>st</sup> row represents the required phase shift on the antenna ports P1 to P4 to steer the radiation beam between  $\pm 45^\circ$ . The beam directions associated with the different phase shifts are tabulated. From the table, we can derive that the proposed antenna able to cover the operating angle of  $\pm 45^\circ$  with a small gain variation of 1.5dB over the operating angle, the maximum gain of 13.6dBi can be achieved at  $0^\circ$ . The sidelobe level is -12.9 dB at  $0^\circ$  beam and gradually reduced to -7.2 dB at the beam edges.

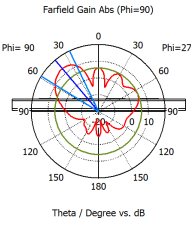
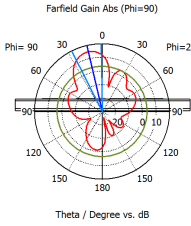
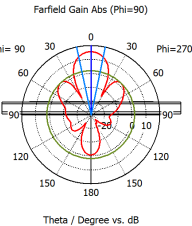
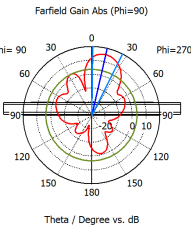
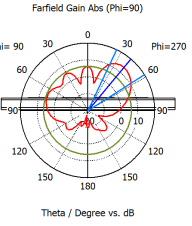
**Table 5.4** Simulated beam steering patterns of the  $1 \times 4$  antenna array at 5.5 GHz over the  $\pm 40^\circ$  steering angle.

| Radiating beam according to excitation phase per port |  |   |  |  |   |
|---|--|---|--|--|---|
| Phase shift per port                                  | P1: $45^\circ$ ,<br>P2: $180^\circ$ ,<br>P3: $-45^\circ$ ,<br>P4: $90^\circ$   | P1: $0^\circ$ ,<br>P2: $45^\circ$ ,<br>P3: $90^\circ$ ,<br>P4: $135^\circ$  | P1: $0^\circ$ ,<br>P2: $0^\circ$ ,<br>P3: $0^\circ$ ,<br>P4: $0^\circ$   | P1: $135^\circ$ ,<br>P2: $90^\circ$ ,<br>P3: $45^\circ$ ,<br>P4: $0^\circ$   | P1: $90^\circ$ ,<br>P2: $-45^\circ$ ,<br>P3: $180^\circ$ ,<br>P4: $45^\circ$  |
| Beam Direction  | $-39^\circ$  | $-13^\circ$   | $0^\circ$  | $+13^\circ$  | $+40^\circ$   |
| Realized Gain   | 11.1 dBi   | 13.4 dBi  | 13.6 dBi   | 13.4 dBi   | 11.2 dBi  |
| Side Lobe Level                                       | -7.3 dB  | -12.4 dB  | -12.9 dB   | -12.3 dB   | -7.2 dB   |
| 2D Radiation Pattern                                  |  <p>Farfield Gain Abs (Phi=90)</p> <p>Frequency = 5.5 GHz<br/>Main lobe magnitude = 11.1 dB<br/>Main lobe direction = <math>-39.0^\circ</math><br/>Angular width (3 dB) = <math>29.9^\circ</math><br/>Side lobe level = -7.3 dB</p> |  <p>Farfield Gain Abs (Phi=90)</p> <p>Frequency = 5.5 GHz<br/>Main lobe magnitude = 13.4 dB<br/>Main lobe direction = <math>-13.0^\circ</math><br/>Angular width (3 dB) = <math>25.3^\circ</math><br/>Side lobe level = -12.4 dB</p> |  <p>Farfield Gain Abs (Phi=90)</p> <p>Frequency = 5.5 GHz<br/>Main lobe magnitude = 13.6 dB<br/>Main lobe direction = <math>0.0^\circ</math><br/>Angular width (3 dB) = <math>24.4^\circ</math><br/>Side lobe level = -12.9 dB</p> |  <p>Farfield Gain Abs (Phi=90)</p> <p>Frequency = 5.5 GHz<br/>Main lobe magnitude = 13.4 dB<br/>Main lobe direction = <math>13.0^\circ</math><br/>Angular width (3 dB) = <math>25.3^\circ</math><br/>Side lobe level = -12.3 dB</p> |  <p>Farfield Gain Abs (Phi=90)</p> <p>Frequency = 5.5 GHz<br/>Main lobe magnitude = 11.2 dB<br/>Main lobe direction = <math>40.0^\circ</math><br/>Angular width (3 dB) = <math>30.3^\circ</math><br/>Side lobe level = -7.2 dB</p> |

### 5.4.2 Beam Steering Results of the $2 \times 4$ Array

Table 5.5 presented the simulated results of the  $2 \times 4$  array, the maximum gain of 15.5 dBi is achieved at  $0^\circ$  beam, with gain variation from 2.2 dB or 13.3 to 15.5 dBi over the coverage angle of  $\pm 45^\circ$  and the sidelobe level is 13.8 dB at  $0^\circ$  beam and -7.3 dB at the beam edges.

**Table 5.5** Simulated beam steering patterns of the  $2 \times 4$  antenna array at 5.5 GHz over the  $\pm 40^\circ$  steering angle.

| Radiating beam according to excitation phase per port |   |  |  |  |   |
|---|---|--|--|--|---|
| Phase shift per port                                  | P1: $45^\circ$ ,<br>P2: $180^\circ$ ,<br>P3: $-45^\circ$ ,<br>P4: $90^\circ$  | P1: $0^\circ$ ,<br>P2: $45^\circ$ ,<br>P3: $90^\circ$ ,<br>P4: $135^\circ$   | P1: $0^\circ$ ,<br>P2: $0^\circ$ ,<br>P3: $0^\circ$ ,<br>P4: $0^\circ$   | P1: $135^\circ$ ,<br>P2: $90^\circ$ ,<br>P3: $45^\circ$ ,<br>P4: $0^\circ$   | P1: $90^\circ$ ,<br>P2: $-45^\circ$ ,<br>P3: $180^\circ$ ,<br>P4: $45^\circ$  |
| Beam Direction  | $-40^\circ$   | $-13^\circ$  | $0^\circ$  | $+13^\circ$  | $+40^\circ$   |
| Realized Gain   | 13.3 dBi  | 15.2 dBi   | 15.5 dBi   | 15.2 dBi   | 13.4 dBi  |
| Side Lobe Level                                       | -7.3 dB   | -11.8 dB   | -13.8 dB   | -11.8 dB   | -7.3 dB   |
| 2D Radiation Pattern                                  |  <p>Farfield Gain Abs (Phi=90)<br/>Phi= 90 30 0 30 Phi=270<br/>60 60<br/>120 120<br/>150 180 150<br/>Theta / Degree vs. dB</p> <p>Frequency = 5.5 GHz<br/>Main lobe magnitude = 13.3 dB<br/>Main lobe direction = <math>40.0^\circ</math><br/>Angular width (3 dB) = <math>32.6^\circ</math><br/>Side lobe level = -7.3 dB</p> |  <p>Farfield Gain Abs (Phi=90)<br/>Phi= 90 30 0 30 Phi=270<br/>60 60<br/>120 120<br/>150 180 150<br/>Theta / Degree vs. dB</p> <p>Frequency = 5.5 GHz<br/>Main lobe magnitude = 15.2 dB<br/>Main lobe direction = <math>13.0^\circ</math><br/>Angular width (3 dB) = <math>25.7^\circ</math><br/>Side lobe level = -11.8 dB</p> |  <p>Farfield Gain Abs (Phi=90)<br/>Phi= 90 30 0 30 Phi=270<br/>60 60<br/>120 120<br/>150 180 150<br/>Theta / Degree vs. dB</p> <p>Frequency = 5.5 GHz<br/>Main lobe magnitude = 15.5 dB<br/>Main lobe direction = <math>0.0^\circ</math><br/>Angular width (3 dB) = <math>24.3^\circ</math><br/>Side lobe level = -13.8 dB</p> |  <p>Farfield Gain Abs (Phi=90)<br/>Phi= 90 30 0 30 Phi=270<br/>60 60<br/>120 120<br/>150 180 150<br/>Theta / Degree vs. dB</p> <p>Frequency = 5.5 GHz<br/>Main lobe magnitude = 15.2 dB<br/>Main lobe direction = <math>13.0^\circ</math><br/>Angular width (3 dB) = <math>25.7^\circ</math><br/>Side lobe level = -11.8 dB</p> |  <p>Farfield Gain Abs (Phi=90)<br/>Phi= 90 30 0 30 Phi=270<br/>60 60<br/>120 120<br/>150 180 150<br/>Theta / Degree vs. dB</p> <p>Frequency = 5.5 GHz<br/>Main lobe magnitude = 13.4 dB<br/>Main lobe direction = <math>40.0^\circ</math><br/>Angular width (3 dB) = <math>32.3^\circ</math><br/>Side lobe level = -7.3 dB</p> |

### 5.4.3 Beam Steering Results of the $4 \times 4$ Array

From the simulated result of the  $4 \times 4$  array presented in Table 5.6, the realized gain of 17.9 dBi was achieved at  $0^\circ$  beam and 15.5 dBi and 15.8 dBi at  $-41^\circ$  and  $+41^\circ$  beam respectively. The sidelobe level is -13.6 dB at  $0^\circ$  which is amongst the highest compared to the  $1 \times 4$  and  $2 \times 4$  array.

**Table 5.6** Simulated beam steering patterns of the  $4 \times 4$  antenna array at 5.5 GHz over the  $\pm 40^\circ$  steering angle.

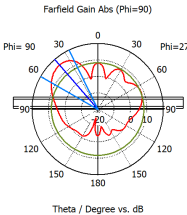
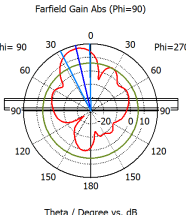
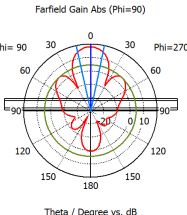
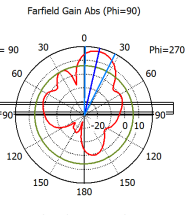
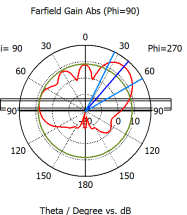
|  | Radiating beam according to excitation phase per port                        |                |               |                 |  |
|--|--|----------------|---------------|-----------------|--|
|  | Phase shift per port   | Beam Direction | Realized Gain | Side Lobe Level | 2D Radiation Pattern   |
|  | P1: $45^\circ$ ,<br>P2: $180^\circ$ ,<br>P3: $-45^\circ$ ,<br>P4: $90^\circ$ | $-41^\circ$    | 15.5 dBi      | -7.2 dB         |  <p>Frequency = 5.5 GHz<br/>Main lobe magnitude = 15.5 dB<br/>Main lobe direction = <math>-41.0^\circ</math><br/>Angular width (3 dB) = <math>34.2^\circ</math><br/>Side lobe level = -7.2 dB</p>   |
|  | P1: $0^\circ$ ,<br>P2: $45^\circ$ ,<br>P3: $90^\circ$ ,<br>P4: $135^\circ$   | $-13^\circ$    | 17.6 dBi      | -12.0 dB        |  <p>Frequency = 5.5 GHz<br/>Main lobe magnitude = 17.6 dB<br/>Main lobe direction = <math>-13.0^\circ</math><br/>Angular width (3 dB) = <math>25.9^\circ</math><br/>Side lobe level = -12.0 dB</p>  |
|  | P1: $0^\circ$ ,<br>P2: $0^\circ$ ,<br>P3: $0^\circ$ ,<br>P4: $0^\circ$       | $0^\circ$      | 17.9 dBi      | -13.6 dB        |  <p>Frequency = 5.5 GHz<br/>Main lobe magnitude = 17.9 dB<br/>Main lobe direction = <math>0.0^\circ</math><br/>Angular width (3 dB) = <math>24.5^\circ</math><br/>Side lobe level = -13.6 dB</p>   |
|  | P1: $135^\circ$ ,<br>P2: $90^\circ$ ,<br>P3: $45^\circ$ ,<br>P4: $0^\circ$   | $+13^\circ$    | 17.5 dBi      | -11.6 dB        |  <p>Frequency = 5.5 GHz<br/>Main lobe magnitude = 17.5 dB<br/>Main lobe direction = <math>13.0^\circ</math><br/>Angular width (3 dB) = <math>25.9^\circ</math><br/>Side lobe level = -11.6 dB</p> |
|  | P1: $90^\circ$ ,<br>P2: $-45^\circ$ ,<br>P3: $180^\circ$ ,<br>P4: $45^\circ$ | $+41^\circ$    | 15.8 dBi      | -7.3 dB         |  <p>Frequency = 5.5 GHz<br/>Main lobe magnitude = 15.8 dB<br/>Main lobe direction = <math>41.0^\circ</math><br/>Angular width (3 dB) = <math>33.8^\circ</math><br/>Side lobe level = -7.3 dB</p>  |

Table 5.7 summarized the overall performance of the proposed antenna arrays, all the proposed antenna arrays can steer over  $\pm 40^\circ$  with approximate 2.5dB gain variation over steering angle, the steering angle is wide enough for  $\pm 45^\circ$  sector coverage when operate at the half-power beamwidth. Array with different gain can be chosen and configured for various operating scenarios depends on the gain and coverage angle needed. Reasonable



sidelobe level at  $0^\circ$  was observed from the simulated results, for example, -12.9 dB for  $1 \times 4$  array, -13.8 dB for  $2 \times 4$  array and -13.6 dB for  $4 \times 4$  array, however, in this work, I have also confirmed that the sidelobe level can be further reduced by the recursive calibration process and proper assignment of the amplitude distribution that fed into the antenna ports from the transmitter and receiver module that was designed for this project. The sidelobe level enhancement results can be found in chapter 5.8.

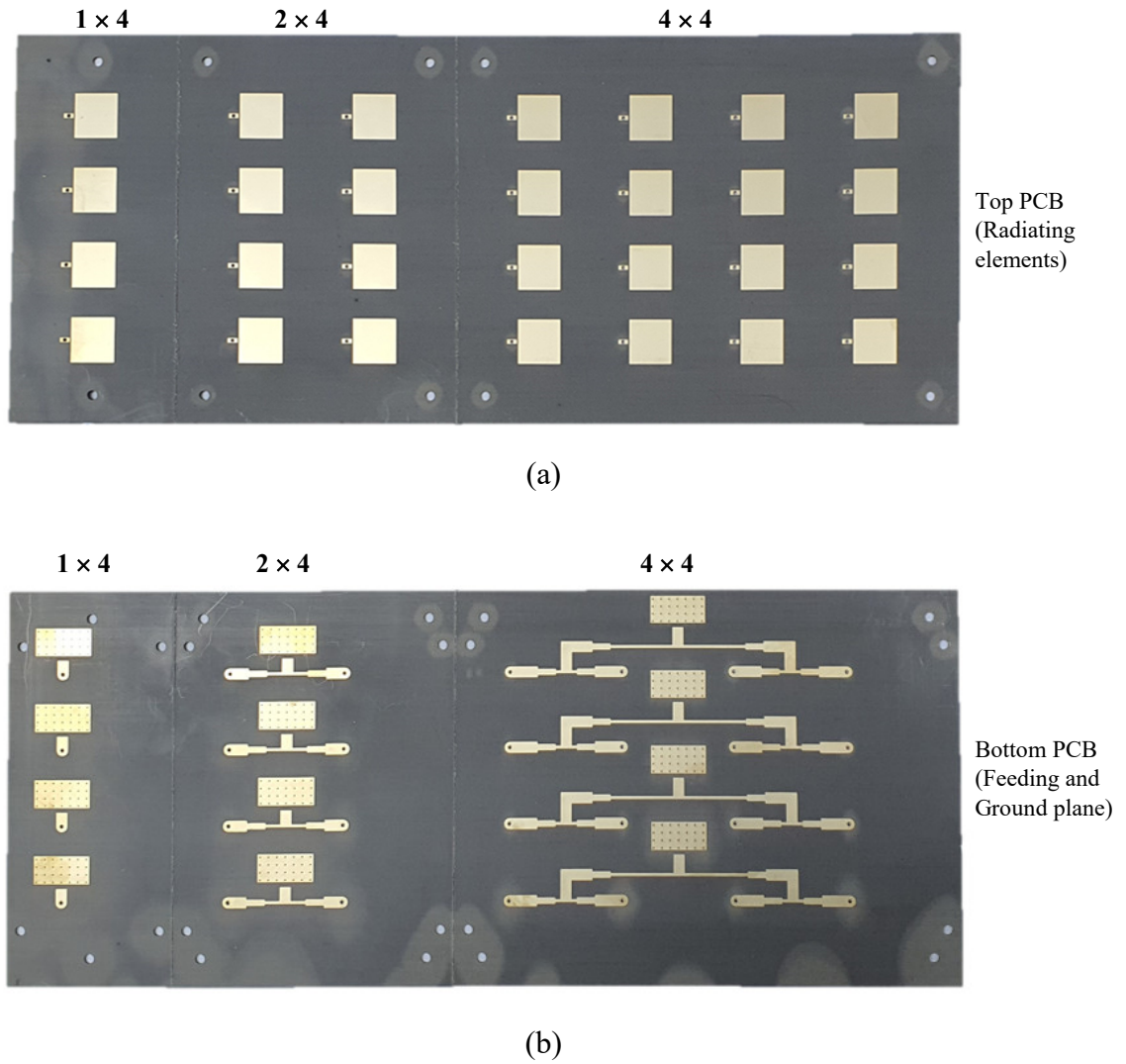
**Table 5.7** Performance summary of the proposed antenna arrays.

| Type of antenna array      | Dimension               | Gain [dBi] | Beam-width   | Sidelobe Level at $0^\circ$ | Steering capability | Gain over steering beam |
|----------------------------|-------------------------|------------|--------------|-----------------------------|---------------------|-------------------------|
| $1 \times 4$ antenna array | $141.8 \times 60.0$ mm  | 13.6       | $24.4^\circ$ | -12.9 dB                    | $\pm 40^\circ$      | 11.1 - 13.6 dBi         |
| $2 \times 4$ antenna array | $141.8 \times 100.9$ mm | 15.5       | $24.3^\circ$ | -13.8 dB                    | $\pm 40^\circ$      | 13.5 - 15.5 dBi         |
| $4 \times 4$ antenna array | $141.8 \times 182.6$ mm | 17.9       | $24.5^\circ$ | -13.6 dB                    | $\pm 40^\circ$      | 15.5 - 17.9 dBi         |

## 5.5 Antenna Array Prototyping and Experimental Evaluation

Once the antenna design is simulated and with the satisfactory result, the 3 antenna arrays are panelised into a single PCB panel, the antenna arrays are separated by a v-cut that allows the individual array to be separated from the main PCB panel during the assembly process, this method will significantly reduce the PCB manufacturing time and cost. The CST tool allows the designer to export that design files into gerber format which is the format commonly used by the PCB factory to generate the artwork and stencil that is required during the PCB fabrication process, the gerber artwork for the antenna panel is presented in *Appendix B: PCB Gerber Artwork File for the Antenna Array*.

The antennas were fabricated using the commercially available PCB fabrication technique. The PCBs that were fabricated and delivered from the factory are in panel form as demonstrated in Fig. 5.13, each array was separated by a V-cut for easy breaking before assembling into the respective antenna array. RO3003 material [24], [31] and [35] from Roger (Arizona, United States) is the popular materials used in the high-frequency PCB industry, for cost reason, we have chosen the lowest cost alternative substrate F4BTM-2 produced by Taizhou Wangling (Jiangsu, China) with equivalent electrical specification compared to RO4003 material, the new material is expected to pocket a 60% cost saving from the substrate material itself. The specification of the F4BTM-2 can be found in *Appendix C: Specification of the Antenna Substrate Material*. The antenna arrays are constructed according to the stack-up structure shown in Fig. 5.6.

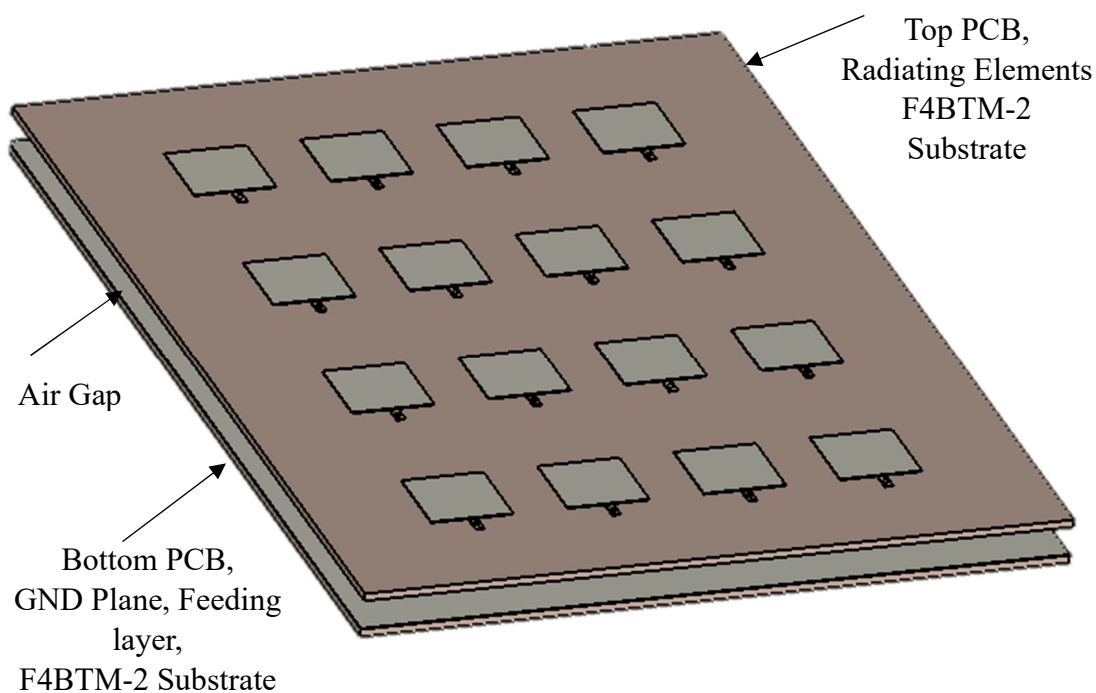


**Fig. 5.13** Raw PCBs from the factory. (a) Top PCB. (b) Bottom PCB.

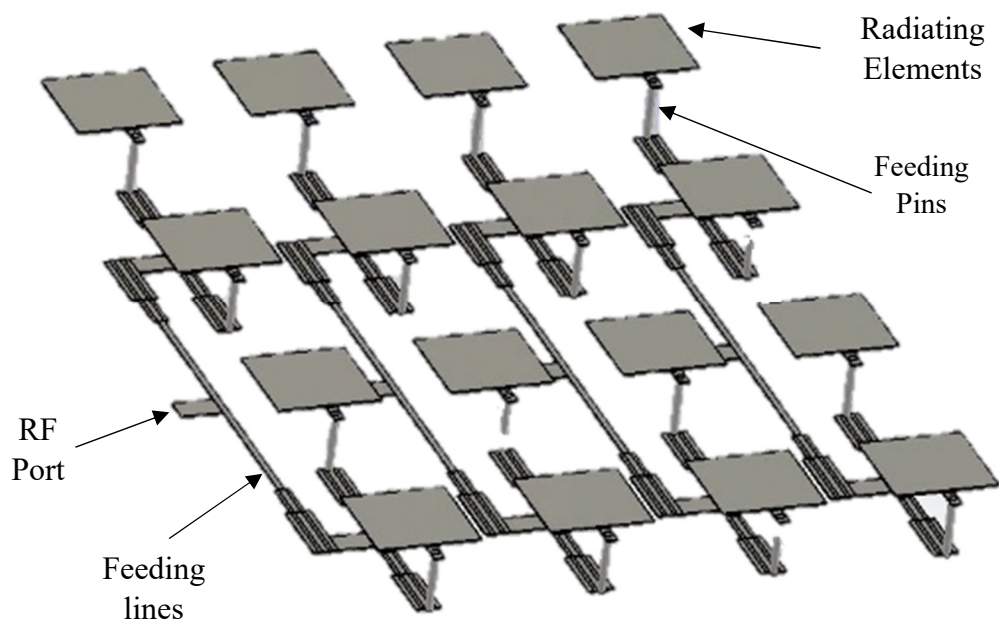
### 5.5.1 Assembling the Prototype Antenna Array

The construction of the  $4 \times 4$  array can be presented in Fig. 5.14, (a) represents the stack-up view and (b) illustrates the exploded view. The top and bottom PCBs are supported by the metal feeding pins and 4 pieces of nylon spacers, the feeding pins are installed to transfer the RF energy from the feeding networks from the bottom PCB to the capacitive feeding pads on the top PCB, the feeding pins are secured to both PCBs by solder. 2 nylon spacers (for  $1 \times 4$  array) and 4 nylon spacers (for  $2 \times 4$  and  $4 \times 4$  arrays) are installed at the edge of the array to provide additional support to the PCBs as well as to maintain the 6 mm air gap between the radiating PCB and the feeding PCB according to the design, the nylon spacers are secured by the nylon nuts and screws. Nylon spacers, nylon screws, and nylon nuts are chosen due to their excellent mechanical, thermal, and chemical properties, and minimum effects on the electromagnetic performance of the antenna. The similar

construction method is applied to  $1 \times 4$  and  $2 \times 4$  arrays but with a different number of elements.



(a)



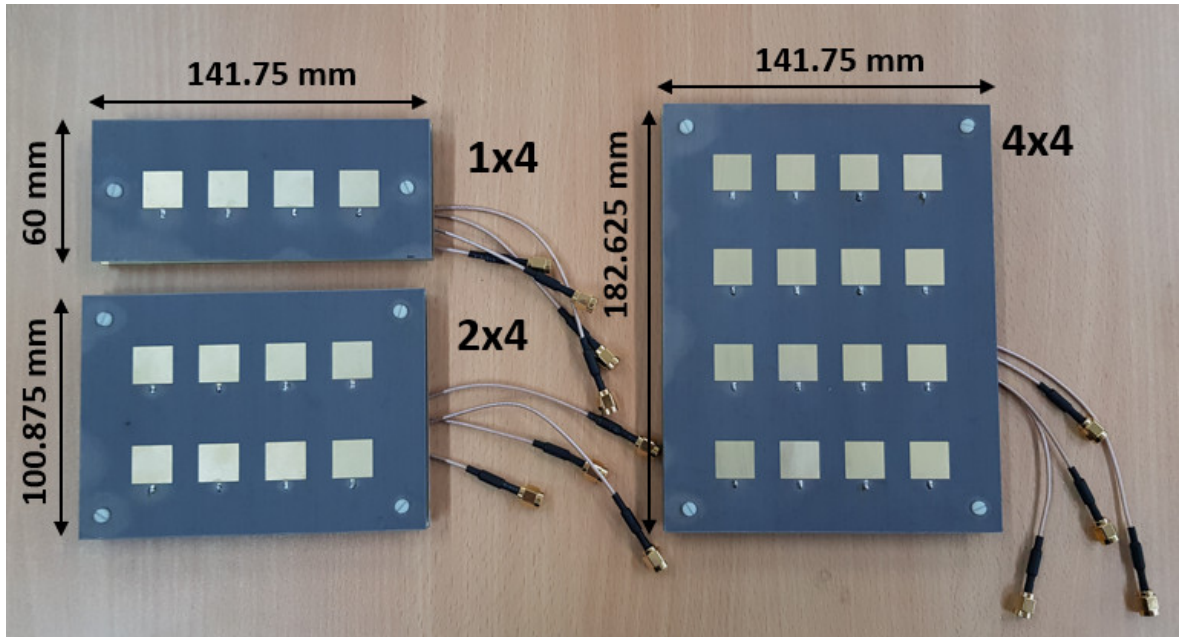
(b)

**Fig. 5.14** The geometrical view of the  $4 \times 4$  antenna array. (a) Stack up view. (b) Exploded view.

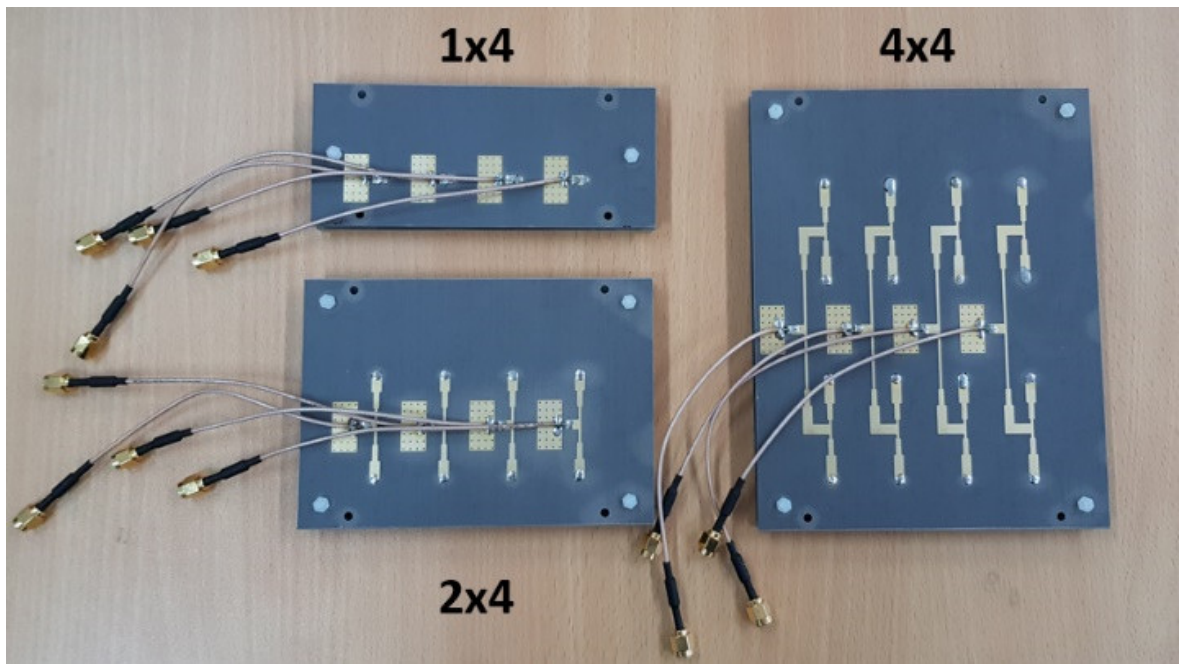
To make sure we get the best performance out of the array prototype, some precautions are worth considering during the assembly process of the antenna array.

- i) PCB warpage, as the PCB area especially for the  $4 \times 4$  array is bigger around 182.625 mm in length and 141.75 mm in width, the PCBs may potentially warp if the manufacturing control and packaging were not well-taken care of by the PCB manufacturing factory. We have included 4 pieces of 6 mm nylon stand-off at the 4 corners of the PCBs, this is to ensure the top and bottom PCB are spaced evenly over the whole surface area. In mass production, there might be some visible warpage due to PCB manufacturing tolerance, a few more nylon washers can be added at the middle or the side of the PCBs to properly hold the PCBs and offset the warpage.
- ii) The feeding pins and co-axial cables are soldered directly onto feeding copper pads of the PCBs, the soldering process must be properly controlled and ensure the good solder fillet and no dry joint at the solder joint. No excessive solder, as it may impact the characteristic impedance and matching of the microstrip line.
- iii) Ensure the RF co-axial at each feeding port are with equal length, this is to minimize the unnecessary phase variation due to unequal co-axial cable length at each port.

The co-axial cables are assembled to the antenna array by soldering the co-axial hot pin to the feeding copper pad and co-axial shield to the ground pad which was specially designed with sufficient copper opening for soldering purpose as demonstrated in Fig. 5.15(b), The other end of the co-axial cables are assembled with the SMA connector that can be connected to test equipment or RF frontend directly. The final prototype of the antenna arrays are shown in Fig. 5.15, with both top and bottom views. Each antenna array comes with 4 mechanical mounting holes to facilitate the assembly process, where multiple antenna arrays are mounted onto the radome to form a smart antenna structure that is designed to cover up to  $360^\circ$  scanning angle by combining multiple arrays with  $90^\circ$  coverage each.



(a)



(b)

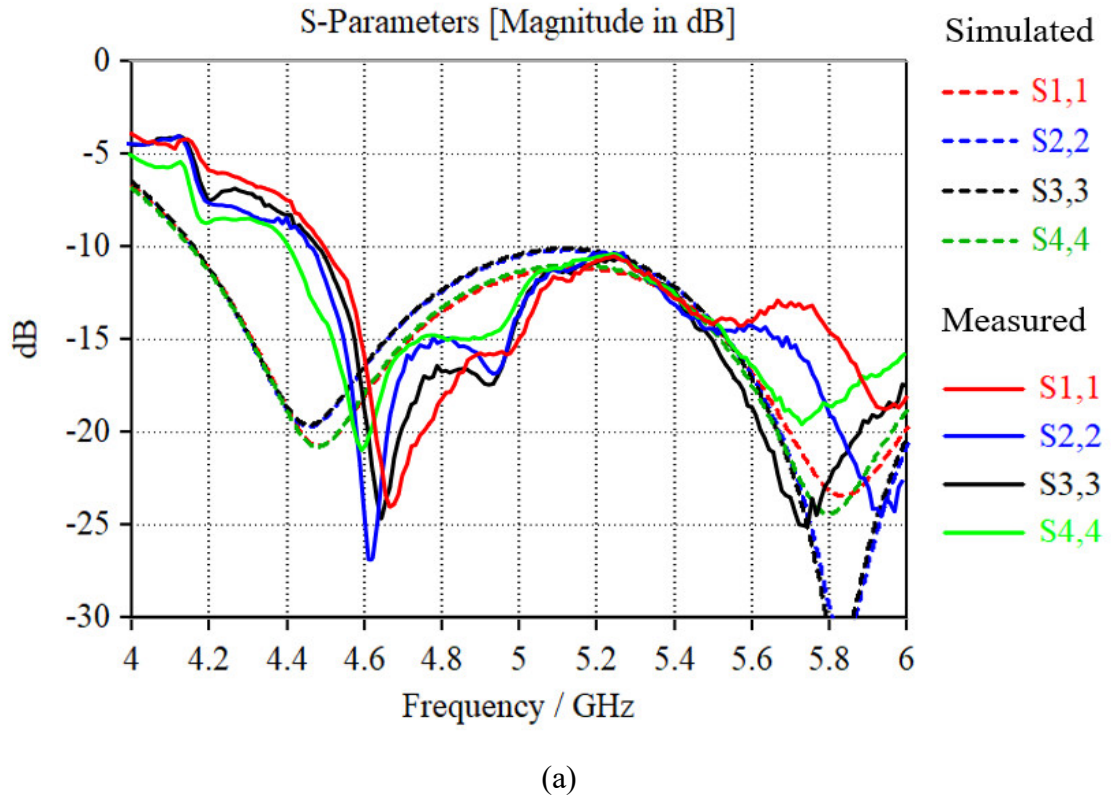
**Fig. 5.15** Photos of the fabricated antenna arrays. (a) Top side. (b) Bottom side.

## 5.6 Conducted Measurement of the Antenna Arrays

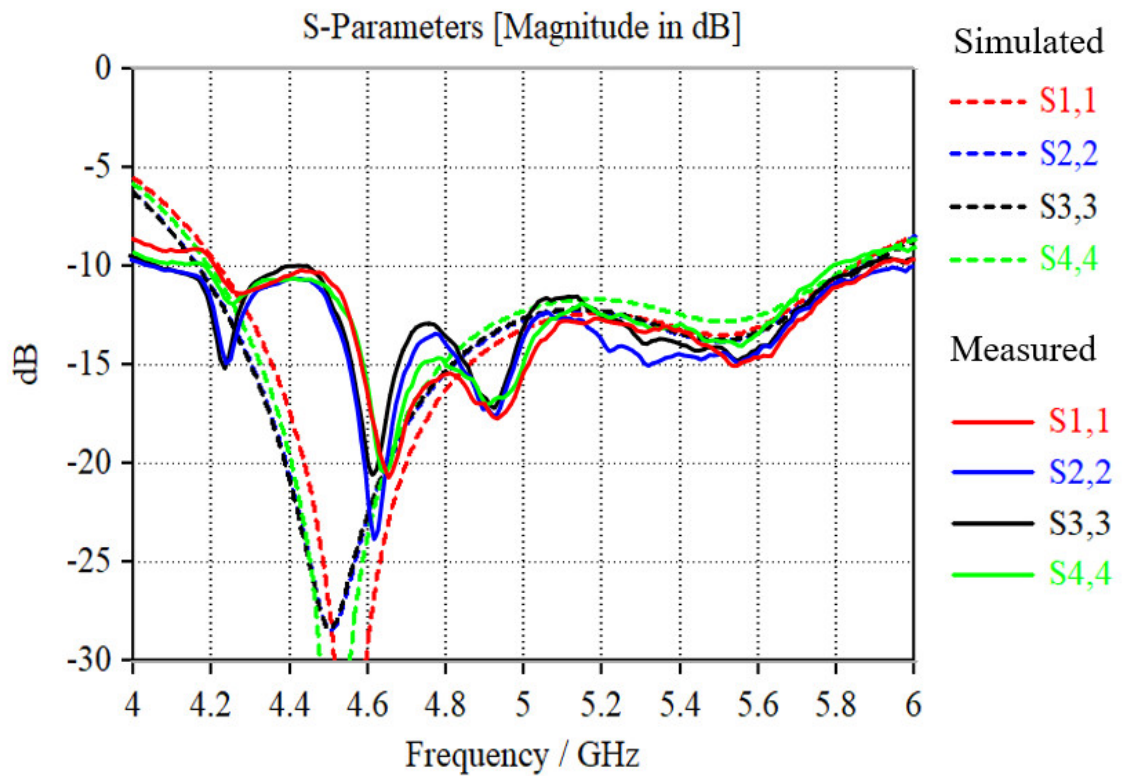
The returned loss and isolation between ports are measured in the conducted setup. The vector network analyser (VNA), model: VNA0406 e-SB manufactured by MegiQ (Eindhoven, Netherlands) with operating frequency from 400 MHz to 6 GHz is used to perform the measurement. The measured results of the S11 returned loss for the 3 types of proposed antenna arrays are presented in Fig. 5.16, all the antennas exhibited more than 10



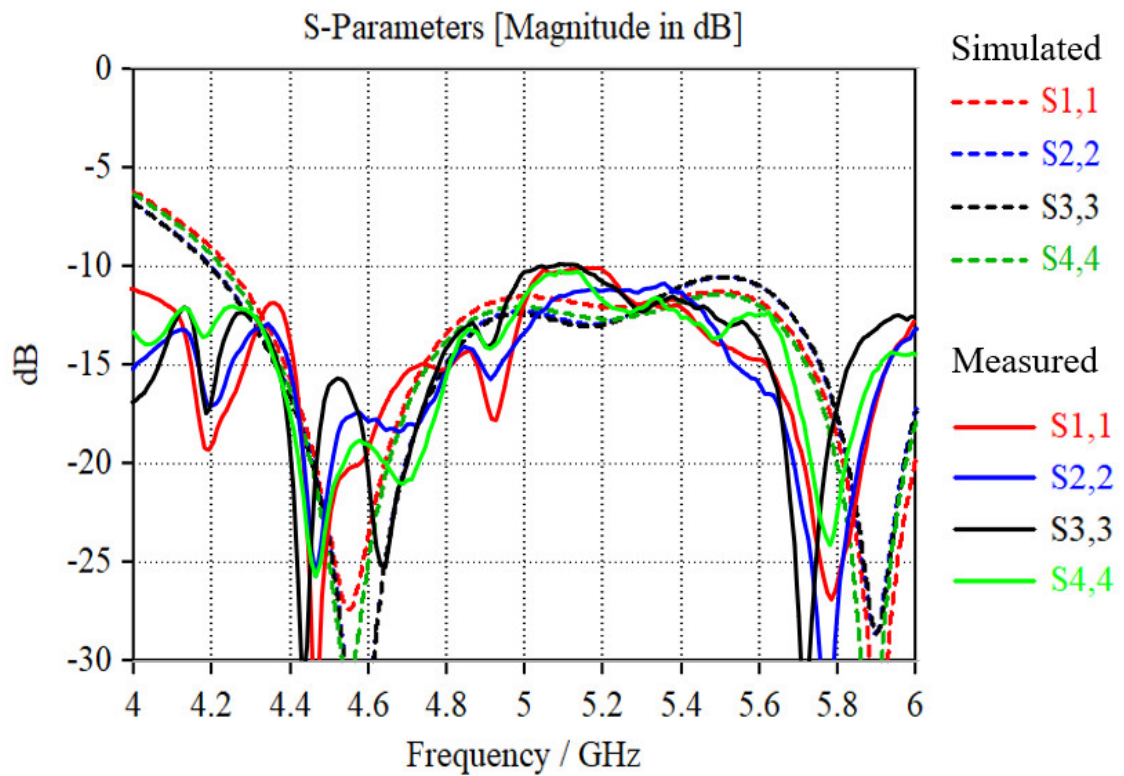
dB returned loss for the intended frequency band from 4.9 to 5.9 GHz, which is reasonable and within the antenna design requirement. A slight shift in the 1<sup>st</sup> resonance frequency point was observed around 4.5 GHz, which might be contributed by the manufacturing tolerance of the PCB, SMA connector as well as assembly tolerance. However, the overall design was able to fulfil the minimum 10 dB returned loss requirement set in our antenna design target over the 4.9 – 5.9 GHz frequency band.



**Fig. 5.16** Returned loss measurement results. (a)  $1 \times 4$  antenna array. (b)  $2 \times 4$  antenna array. (c)  $4 \times 4$  antenna array.



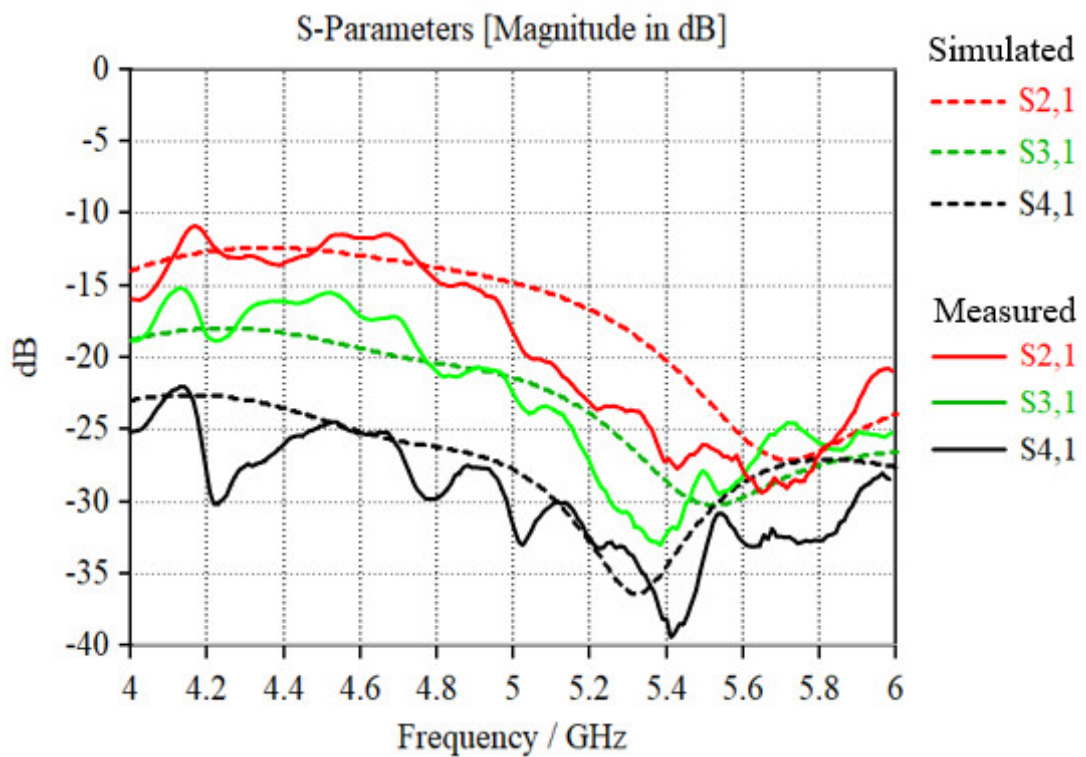
(b)



(c)

Fig. 5.16 (continued).

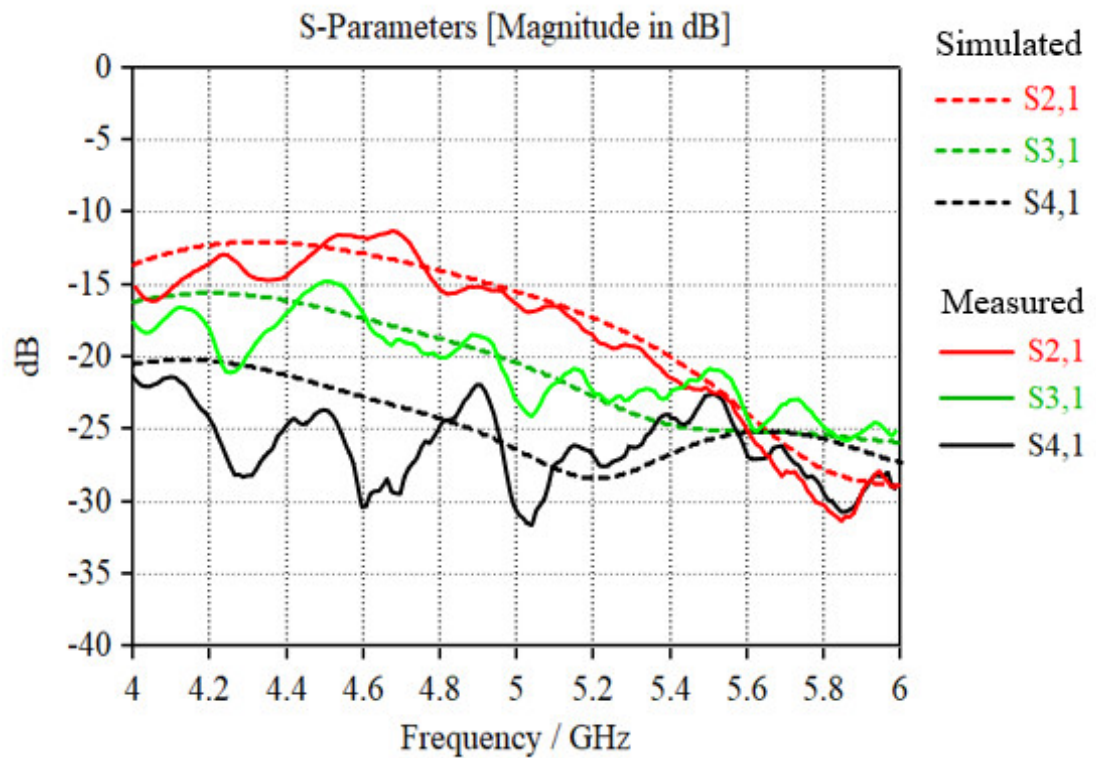
The port-to-port isolation was experimentally measured, for simplicity, due to the symmetric property of the antenna array, the inter port isolation measurement was conducted between the first port and the neighbouring ports, and the rest of the ports are expected to have the similar characteristic. **Error! Reference source not found.** Fig. 5.17 shows the measurement results of the port-to-port isolation, a moderate agreement was demonstrated when compared with the simulated results, components tolerance, PCB manufacturing tolerance and stack up tolerance during the assembly of the antenna array might have contributed to the slight variation in the measured results. However, the fair port-to-port isolation of a minimum 15 dB over the 4.9 to 5.9 GHz band is acceptable to eliminate the crosstalk that may potentially affect the performance of the array.



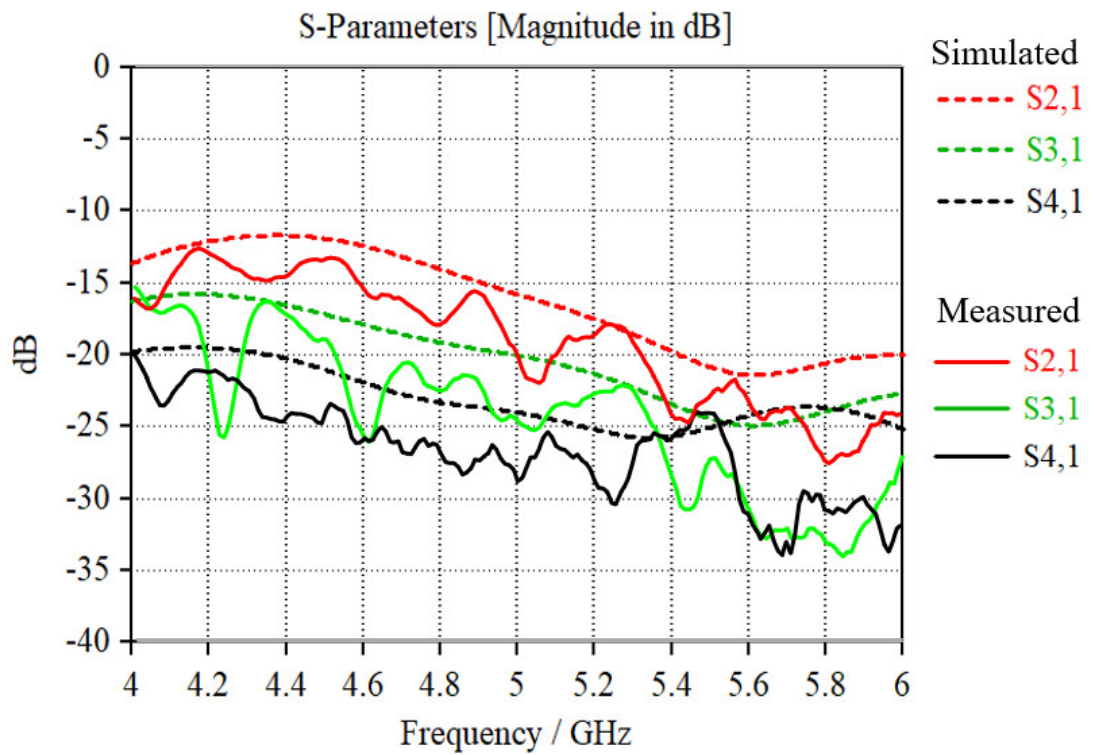
(a)

**Fig. 5.17** Simulation and measured inter-port isolation results. (a)  $1 \times 4$  array. (b)  $2 \times 4$  array. (c)  $4 \times 4$  array.





(b)



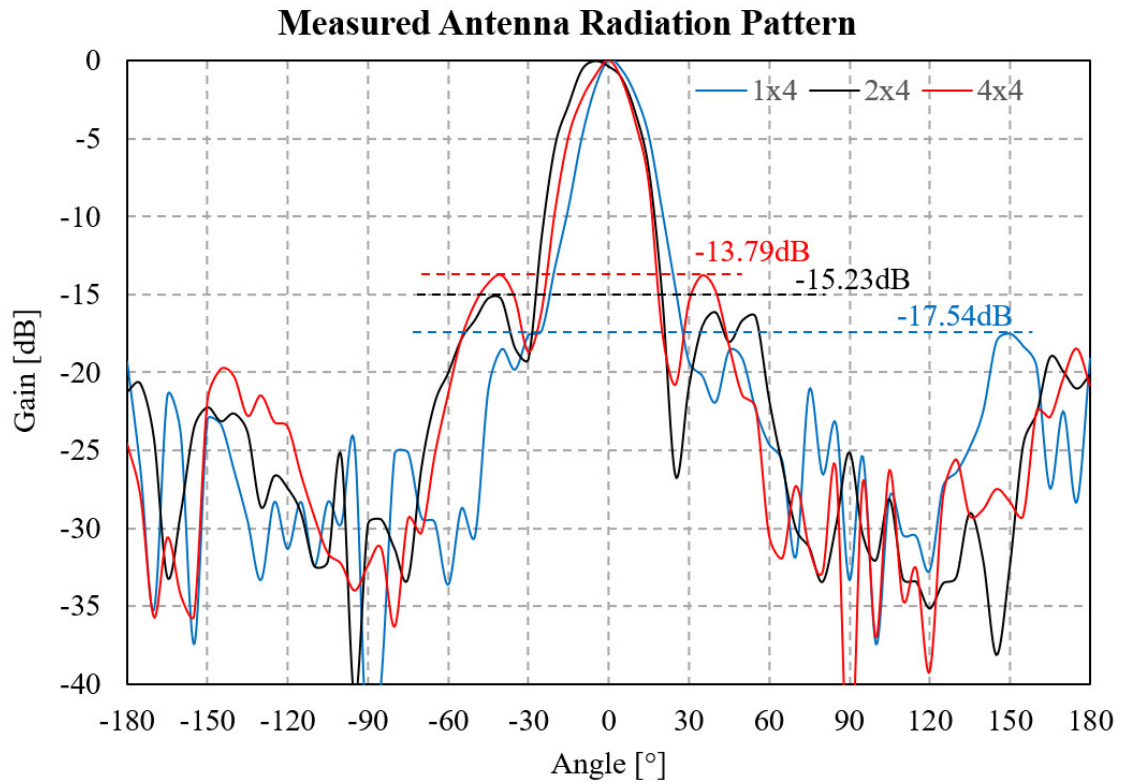
(c)

Fig. 5.17 (Continued)

### 5.6.1 Radiation Results of the Antenna Arrays

The radiated measurement was carried out using the same measurement topology presented in section 4.4. The boresight antenna gain at  $0^\circ$  and 5.5 GHz of the  $1 \times 4$ ,  $2 \times 4$ , and  $4 \times 4$  antenna arrays are shown in Fig. 5.18, and Table 5.8 tabulated the key antenna performance parameter such as the far-field gain, HPBW, SLL, with the comparison between both measured and simulated results.

Referring to the results in Fig. 5.18 and Table 5.8, the measured antenna gains for  $1 \times 4$ ,  $2 \times 4$ , and  $4 \times 4$  arrays are 11.16, 14.59, and 17.25 dBi respectively, which is tallied with the simulated results of 13.53, 15.4, and 17.8 dBi, some slight deviation that might be caused by the tolerance of PCB manufacturing, coaxial cable, connectors, as well as the environmental factors. Further evaluation on the realized gain was carried out for the entire interest band from 4.9 – 5.9 GHz for the low, middle, and high gain arrays, their respective gains variations across the frequency band are 11.16 to 12.27 dBi, 13.97 to 15.74 dBi, and 17.25 to 18.12 dBi with respect to the  $1 \times 4$ ,  $2 \times 4$ , and  $4 \times 4$  arrays, the gain flatness over the interest frequency band is kept within 2 dB which is reasonably good for the wideband antenna. The results show a moderate agreement with the simulated result of 12.90 to 14.10 dBi, 15.00 to 15.70 dBi and 17.25 to 18.12 dBi for the respective low, middle, and high gain arrays. There is a slight improvement of 4.5 dB for the SLL as compared to the simulation results, the measure SSL result for the low gain array is -17.54 dB compared to -12.9 dB of the simulated result, the main reason was due to the slight lower gain of the antenna prototype that leads to the improvement in the SSL level. In the case of HPBW, the measured result of less than  $24^\circ$  is also tallied well with the simulated result with the SLL value of around  $24^\circ$ .



**Fig. 5.18** The measured radiation pattern of the proposed antenna arrays at 5.5 GHz.

**Table 5.8** Evaluation results of the  $1 \times 4$ ,  $2 \times 4$ , and  $4 \times 4$  antenna arrays at 5.5 GHz.

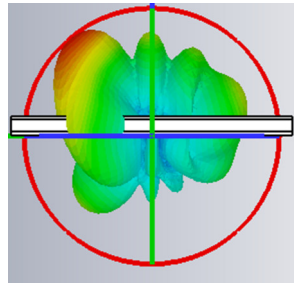
|                |     |           | 1 × 4 | 2 × 4 | 4 × 4 |
|----------------|-----|-----------|-------|-------|-------|
| Antenna Gain   | dBi | Simulated | 13.5  | 15.4  | 17.8  |
|                |     | Measured  | 11.2  | 14.6  | 17.2  |
| Sidelobe Level | dB  | Simulated | -12.9 | -13.8 | -13.6 |
|                |     | Measured  | -17.5 | -15.2 | -13.8 |
| 3dB Beamwidth  | °   | Simulated | 24.4° | 24.3° | 24.5° |
|                |     | Measured  | 20.0° | 24.0° | 20.0° |

## 5.7 *Beamforming Evaluation*

The beamforming performances of the  $1 \times 4$ ,  $2 \times 4$ , and  $4 \times 4$  arrays are covered in this section, including the results for both simulation and experimental measurement, the simulation was done using the CST FIT solver and the measurements are carried out using the measurement topology explained earlier. To the end of this section, we have included the construction method for the  $360^\circ$  beamforming antenna structure and presented a table to highlight the advantages of the proposed pre-configurable antenna structure over the related state-of-the-art antennas that have the same  $360^\circ$  steering coverage. A simple explanation of the DOA estimation process has been briefly explained at the end of this section.

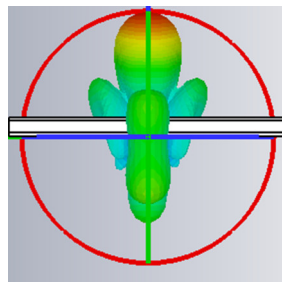
### 5.7.1 **Simulation Results of the Beamforming Antenna Array**

CST FIT solver is used to simulate and validate the beamforming performance of the antenna arrays, the phase of each antenna port from P1 to P4 are varied so that the beam direction of the antenna can be controlled. The phase shift of the individual antenna feeding ports from P1 to P4 with respect to the beam direction can be explained as follows, the phase shift of  $0^\circ/0^\circ/0^\circ/0^\circ$  for  $0^\circ$  beam direction,  $45^\circ/180^\circ/-45^\circ/90^\circ$  for  $-40^\circ$  beam direction, and  $90^\circ/-45^\circ/180^\circ/45^\circ$  for  $+40^\circ$  beam direction. The simulated results of the beamforming performance of the  $1 \times 4$ ,  $2 \times 4$ , and  $4 \times 4$  arrays can be found in Fig. 5.19, all the arrays demonstrated a  $\pm 41^\circ$  beam steering capability, when operating at HPBW, the steering angle shall cover up to  $\pm 45^\circ$ .



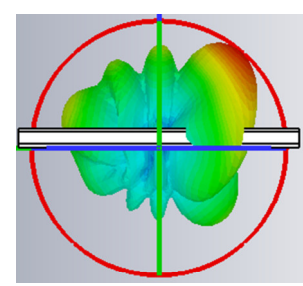
Frequency = 5.5 GHz  
Main lobe magnitude = 11.1 dB  
Main lobe direction = 39.0 deg.  
Angular width (3 dB) = 29.9 deg.  
Side lobe level = -7.3 dB

(i)  $-39^\circ$



Frequency = 5.5 GHz  
Main lobe magnitude = 13.6 dB  
Main lobe direction = 0.0 deg.  
Angular width (3 dB) = 24.4 deg.  
Side lobe level = -12.9 dB

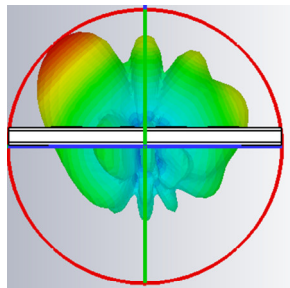
(ii)  $0^\circ$



Frequency = 5.5 GHz  
Main lobe magnitude = 11.2 dB  
Main lobe direction = 40.0 deg.  
Angular width (3 dB) = 30.3 deg.  
Side lobe level = -7.2 dB

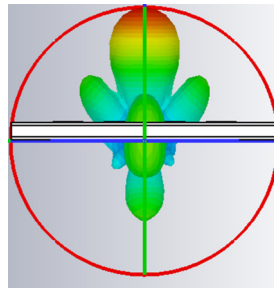
(iii)  $+40^\circ$

(a)



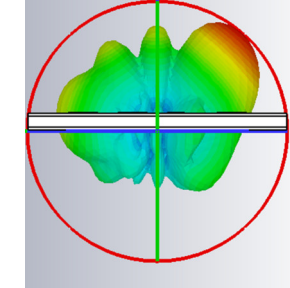
Frequency = 5.5 GHz  
Main lobe magnitude = 13.3 dB  
Main lobe direction = 40.0 deg.  
Angular width (3 dB) = 32.6 deg.  
Side lobe level = -7.3 dB

(i)  $-40^\circ$



Frequency = 5.5 GHz  
Main lobe magnitude = 15.5 dB  
Main lobe direction = 0.0 deg.  
Angular width (3 dB) = 24.3 deg.  
Side lobe level = -13.8 dB

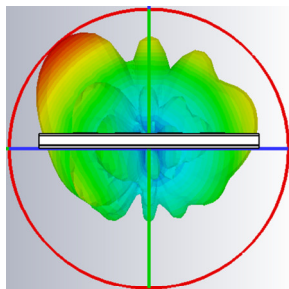
(ii)  $0^\circ$



Frequency = 5.5 GHz  
Main lobe magnitude = 13.4 dB  
Main lobe direction = 40.0 deg.  
Angular width (3 dB) = 32.3 deg.  
Side lobe level = -7.3 dB

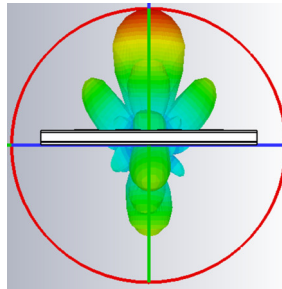
(iii)  $+40^\circ$

(b)



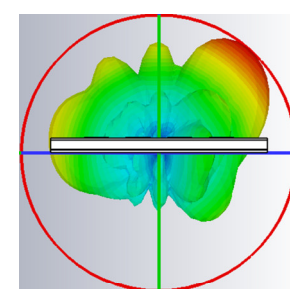
Frequency = 5.5 GHz  
Main lobe magnitude = 15.5 dB  
Main lobe direction = 41.0 deg.  
Angular width (3 dB) = 34.2 deg.  
Side lobe level = -7.2 dB

(i)  $-41^\circ$



Frequency = 5.5 GHz  
Main lobe magnitude = 17.9 dB  
Main lobe direction = 0.0 deg.  
Angular width (3 dB) = 24.5 deg.  
Side lobe level = -13.6 dB

(ii)  $0^\circ$



Frequency = 5.5 GHz  
Main lobe magnitude = 15.8 dB  
Main lobe direction = 41.0 deg.  
Angular width (3 dB) = 33.8 deg.  
Side lobe level = -7.3 dB

(iii)  $+40^\circ$

(c)

**Fig. 5.19** Simulated beamforming performance of the antenna arrays at 5.5 GHz.

(a)  $1 \times 4$  array. (b)  $2 \times 4$  array. (c)  $4 \times 4$  array.

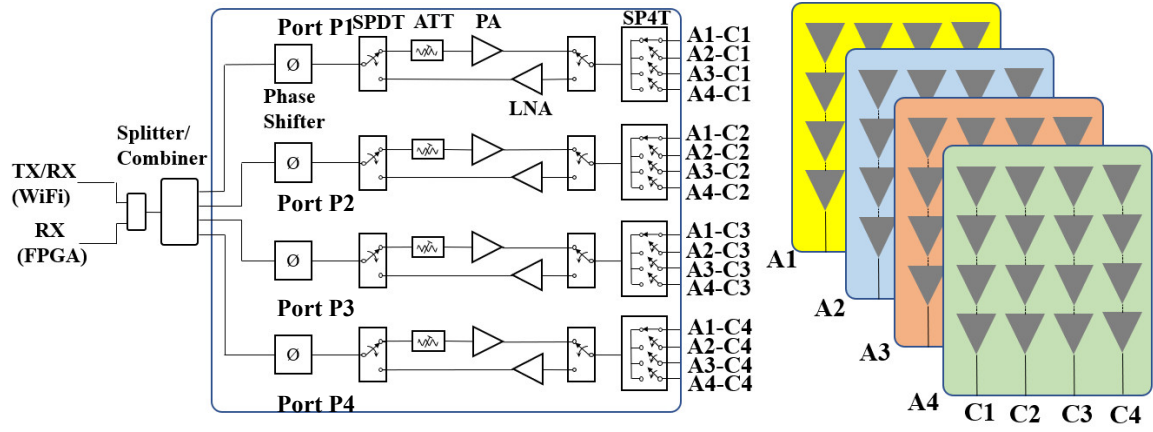
### 5.7.2 Experimental Verifications on the Beamforming Array

The beam steering performance of the proposed  $4 \times 4$  array is further evaluated using the flexible beamforming concept in [62] and the setup in Fig. 5.20. The flexible structure was constructed by integrating with maximum 4 sets of  $90^\circ$  phased arrays indicated as A1, A2, A3, and A4 to support  $90^\circ$ ,  $180^\circ$ ,  $270^\circ$ , and the entire  $360^\circ$  service sector, each of the phased array is connected via 4 horizontal feeding ports C1, C2, C3, and C4 to support the beamforming in the dedicated  $90^\circ$  sector. For  $360^\circ$  coverage, a total of 4 sets of arrays with 16 feeding ports are connected to the 4 RF beamforming chains or T/R module. The key building blocks of the RF chain are briefly explained below, the detailed design of the T/R module is covered in chapter 5.8.

- i. A Single Pole Four Throw (SP4T) switch for RF switching between the antenna column,
- ii. Two Single Pole Double Throw (SPDT) switches to switch the RF path between the transmitter and receiver,
- iii. A 6-bit digital phase shifter to control the phase of each antenna column,
- iv. A Low Noise Amplifier (LNA) for the receiver to boost the signal received from the antenna and,
- v. A Power Amplifier (PA) for power amplification during transmission,
- vi. An RF Attenuator (ATT) with a 30 dB attenuation range to control the transmit power level.

Another function of the LNA and PA is to compensate for the insertion loss exhibited by onboard components such as SPDT, SP4T, phase shifter, and power combiner.

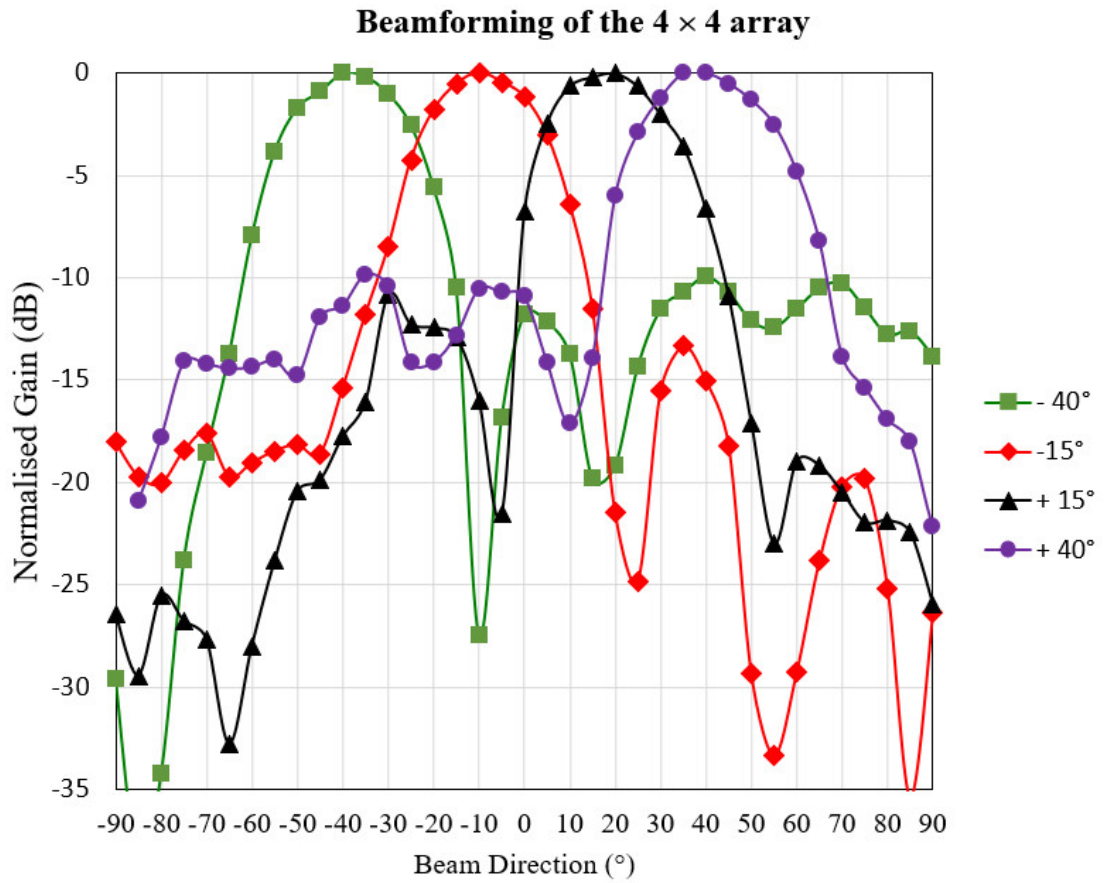
A power combiner is used to channel the RF signal from the 4 RF chains before it is connected to the radio transceiver and baseband processor as shown in Fig. 5.20. The antennas switching and the selection of transmitter/receiver mode are controlled by external processor units such as microcontroller or Field Programmable Gate Array (FPGA) via various interfaces such as Input-Output (IO) signals, Digital to Analogue Converter (DAC) and Analogue to Digital Converter (ADC) that directly interacts, manage, and control the respective block within the RF chains.



**Fig. 5.20** Block diagram of the  $4 \times 4$  beamforming antenna system.

To simplify the beamforming evaluation process, the evaluation was done on one of the  $90^\circ$  sectors and due to the similarity of the RF chains and arrays, the rest of the sectors are expected to have the similar beamforming performance. In this measurement, one of the 4 arrays in the beamforming antenna system is chosen, for instance, A4 was chosen in this case, and the 4 RF chains are toggled to switch to the respective antenna column in A4 via the SP4T switch. The phase shifter on each RF chains are controlled to generate the phase shift of the individual port P1/P2/P3/P4 that is necessary to shape the radiating beam for the array under test, for instance, the phase shift of  $0^\circ/0^\circ/0^\circ/0^\circ$  for  $0^\circ$  beam direction,  $45^\circ/180^\circ/-45^\circ/90^\circ$  for  $-40^\circ$  beam direction and  $90^\circ/-45^\circ/180^\circ/45^\circ$  for  $+40^\circ$  beam direction. The measurement setup and test environment are similar to Fig. 4.6 and Fig. 4.7. The beamforming result of the  $4 \times 4$  arrays is presented in Fig. 5.21. The measured results tallied with the expected beam steering results as expected by varying the phase difference of the individual port. The detailed measurement results and comparison with the simulated results are tabulated in Table 5.9.





**Fig. 5.21** Measured beamforming results of the  $4 \times 4$  array at 5.5 GHz.

Table 5.9 illustrates the simulated and measured beamforming performance of the  $4 \times 4$  array. A fair agreement was observed between the two results. Since all the arrays and RF chains are identical, the similar beamforming result is expected for the other arrays that cover the entire  $360^\circ$ . The simulated and measured beam scanning angle resolution of the proposed arrays was approximately  $2^\circ$ , this was achieved by using the phase shifter with the lowest phase resolution of  $5.625^\circ$ .

**Table 5.9** Beamforming results of the proposed  $4 \times 4$  array. (simulated and measured)

| Beam Angle     |     |           | $-40^\circ$ | $-15^\circ$ | $15^\circ$ | $40^\circ$ |
|----------------|-----|-----------|-------------|-------------|------------|------------|
| Antenna Gain   | dBi | Simulated | 15.8        | 17.6        | 17.5       | 15.5       |
|                |     | Measured  | 14.4        | 16.0        | 16.4       | 14.8       |
| Sidelobe Level | dB  | Simulated | -7.3        | -12.0       | -11.6      | -7.2       |
|                |     | Measured  | -10.0       | -13.3       | -12.3      | -9.8       |
| 3dB Beamwidth  | °   | Simulated | 33.8        | 25.9        | 25.9       | 34.2       |
|                |     | Measured  | 30.9        | 27.5        | 28.2       | 31.5       |



The proposed middle gain  $2 \times 4$  antenna (with 8 elements) is compared with the state-of-the-art 8-elements antenna array in [33], the gain of the proposed antenna at  $0^\circ$  is 14.6 dBi outperformed the design in [33] with just 6.9 dBi, in addition, the proposed array demonstrated superior SLL of -15.2 dB compare to less than -10 dB in [33]. Therefore, the proposed low, middle, and high gain array are suitable candidates that can be integrated into the beamforming antenna system which requires a superior gain and SLL performance.

## **5.8 Summary**

The optimum antenna separation has been decided which is 27.25 mm ( $0.5 \lambda$ ) for horizontal separation which produce optimum gain and SLL performance, and 40.875 mm ( $0.75 \lambda$ ) for vertical separation that gives the good beamwidth and gain performance as well as better mutual coupling between the vertical spaced elements. 3 types of antenna array  $1 \times 4$ ,  $2 \times 4$ , and  $4 \times 4$  were designed using the corporate feed method, fabricated and their performance was experimentally evaluated on their radiated and beam steering performance. The measured result agreed well with the simulation results. The results have concluded that the proposed antenna arrays are suitable and ready to be integrated into the pre-configurable smart antenna system.

# 6 Designing and Characterizing the RF Beamforming Frontend

In the smart antenna system, the T/R module is one of the core components as it accounts for nearly 45% of the overall smart antenna system cost. Due to the high implementation cost of the T/R module, the literature was mainly centered around the military and satellite radar applications. However, over the years, the cost of the T/R module has been reduced drastically by leveraging on the advanced manufacturing technology, volume production pricing, and adaptation of the commercially available off-the-shelf components, as a result, the adoption of the T/R module in the commercial and industrial application becomes possible. In this thesis, a commercially affordable T/R module that operates in the 4.9 – 5.9 GHz band for commercial and industrial applications has been proposed. The T/R module was designed, calibrated, and characterized for use in the beamforming smart antenna system. The design process including the circuit, schematic, and printed circuit board (PCB) were highlighted. The proposed recursive calibration process managed to correct the phase error to  $\pm 1^\circ$  and amplitude error to  $\pm 0.2$  dB. In addition, the amplitude distribution of 0.5-1-1-0.5 combination has successfully suppressed the side-lobe level (SLL) to -28.7 dB for  $0^\circ$ , -22.71 dB for  $\pm 20^\circ$  and -12.77 dB for  $\pm 40^\circ$  beam steering. This work is aimed to promote the adoption of the T/R module into commercial and industrial applications such as public or government infrastructure.

## 6.1 Introduction on T/R module

In the smart antenna industry, the hybrid beamforming (HBF) technique is one of the techniques that attracted many researchers due to its simplicity, cost-effectiveness, and being able to achieve comparable results as compared to digital beamforming. HBF combines both analogue and digital beamforming components that can perform beamforming digitally and maintain a low cost. The HBF architecture consists of a low-dimensional digital beamformer and a radio frequency (RF) beamformer implemented using the phase shifters, targeted to achieve low deployment cost and high scalability. The advantages of the HBF system has

---

*This chapter is reproduced from paper #2 in the publication list on page iv, where the thesis author is the main author in this paper.*

been reported in [72] applications in large scale antenna systems (LSAS), [73] wireless power transfer (WPT) and [74] antenna system with limited space and power.

RF beamforming frontend is one of the most important components in the HBF system. The RF beamforming frontend has been evolved over the years, and the subsystem has been modularized and miniaturized using the commercially off-the-shelf (COTS) components into the T/R module that increases the deployment friendliness and the cost benefits by mass-producing the T/R modules. In [75], the authors pointed out the importance of the T/R module that can be integrated as the slat and tile architecture for the multifunction phased array radar (MPAR), significant cost reduction of the T/R module was contributed by the increases in production volume and the advancement in automated assembly and test equipment. In [76], the authors highlighted that in the military phased array radar systems, detailed cost figures of the main segments are indicating that the T/R module of the phased array antenna accounts for nearly 45% of the system cost and justify the cost of the T/R module is crucial to determine the total system cost. In [77], the Arrays at Commercial Timescales (ACT) program constitutes a forward-looking approach to the design, construction, and upkeep of phased arrays accomplished through modular array component architectures T/R modules that leverage on commercial semiconductor technologies that evolve at much faster rates than traditional RF components.

Due to the high implementation cost, the early adoption of the T/R modules was mainly focused on military applications. The advancement in the manufacturing technology and commercially available radio frequency integrated circuits (RFIC) or chipset had further reduced the cost of the T/R module and contributes to the higher demand of such modules, the application of the T/R module has gained momentum and broadened its coverage into other frequency bands. For instance, an L and C-band T/R module for active phased array radar applications has been reported in [78], in [79], and [86] where various types of transceiver modules operate between X, W and Ka-band have been proposed using the silicon-germanium (SiGe) technology. In [80], the S-band T/R module was developed using gallium arsenide (GaAs) monolithic microwave integrated circuit (MMIC). In [81] the T/R module was developed into the C-Band using the multichip module (MCM). In X-band, [82], [83], and [84], the T/R module were developed using gallium nitride (GaN) MMIC, liquid cooling micro-channels structure integrated into low-temperature co-fired ceramic (LTCC) substrate and complementary metal-oxide-semiconductor (CMOS) RF system on a chip (SoC) with GaAs RF frontend IC respectively. In [85], the LTCC was used to design the T/R module.

Performance parameter characterizations are the key tasks that require much attention during the design of the T/R module. In the beamforming process [46], both the amplitude and phase of each antenna element are controlled. A combined amplitude and phase control or “complex weight” can be used to adjust the side-lobe level (SLL) and steer nulls more accurately as compared to the improvement by phase control alone. Therefore, the precision of the amplitude and the phase of the RF beamforming frontend is extremely important to ensure the accuracy of the beam steering. The RF beamformer frontend shall be properly characterized and calibrated to offset the phase and amplitude errors that were contributed by i) manufacturing tolerance such as printed circuit board (PCB) materials and process variations, ii) components tolerances, iii) performance variations due to frequency response and thermal effect.

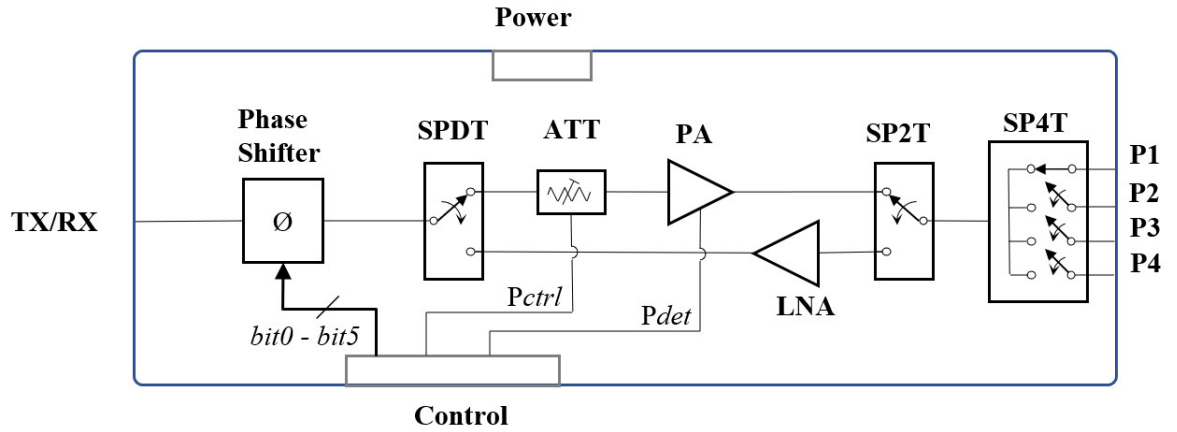
Amplitude calibration involves calibrating the transmit output power of the T/R module over the operating frequency, the value is utilized to set the amplitude distribution from the T/R module to each antenna port during the beamforming process. Some well-known amplitude distribution techniques are listed here, (i) Uniform distribution, where the amplitudes at all the antenna ports are set equal, and the best gain and-half power beamwidth (HPBW) can be achieved while the SLL suffered, (ii) Optimum distribution with the amplitudes being highest at the middle ports and gradually decreasing towards the side of the other ports, this technique produces the moderate gain, HPBW, and SLL performance, while (iii) Binomial distribution provides the best SLL performance but suffers from lower gain and wider HPBW. In [87], the authors revealed that the Tschebyscheff distribution delivers the best SLL compared with the uniform and binomial amplitude distributions of the linear patch antenna array. In [88], the authors demonstrated that the grating lobes appear if the amplitude distribution within a module and a system of modules are independent of each other. In [89], the amplitude taper function was applied to improve the SLL of the phased array antenna system, and approximately 10 dB improvement on the SLL level was demonstrated.

Phase calibration is required to correct the inherited phase error of the T/R module due to manufacturing tolerances. In [90], a phase optimization procedure based on the local search and the simulated annealing (SA) algorithm has been proposed to achieve more accurate beamforming of the phased array. A simple calibration procedure has been proposed in [91] to decrease the phase deviation during phase shift and gain control, the calibration results show that the phase error has been drastically mitigated.

In this work, we are focusing on the highly scalable T/R module that was designed to support commercial band in 4.9 – 5.9 GHz for linear phased array [92] applications in an HBF antenna system. The T/R module was designed using the commercially available off-the-shelf components using GaAs MMIC that is flexible to be integrated into the conventional phased array to form a smart beamforming antenna system. A simple iteration-based method is proposed to calibrate the amplitude and phase error of the T/R Module. The amplitude distribution of the beamforming system has been simulated and the results were experimentally validated. A customized T/R module has been developed instead of the off-the-shelf RF frontend which has limited control features that are important to realize the accuracy of the beamforming function, such as the wide dynamic gain control, high-resolution phase control, fast RF switching to support up to 4 antennas with the single chain and gain boost for transmitter and receiver.

## ***6.2 T/R Module Design***

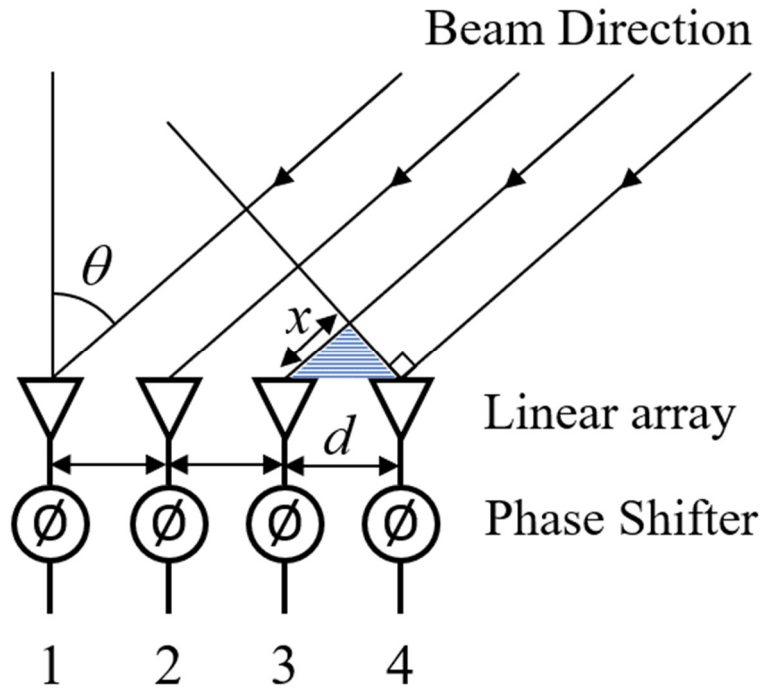
The block diagram of the T/R module is presented in Fig. 6.1. The T/R module has both transmitter and receiver functions that can be switched using the single pole two throw (SP2T) switch. Each T/R module consists of necessary components such as the power amplifier (PA), low noise amplifier (LNA), phase shifter, attenuator, RF switched and control peripherals to support the necessary functions required to steer the radiating beam of the phased array. The T/R module was designed to operate from 4.9 – 5.9 GHz. Each T/R module is designed to support an  $n \times 4$  antenna array with the built-in high-speed single pole four throw (SP4T) RF switch to switch between the element in the  $n \times 4$  array. Each  $n \times 4$  array is capable of performing  $90^\circ$  sector scanning, and only 4 sets of T/R modules are needed to support 4 units of  $n \times 4$  arrays to form a  $360^\circ$  beamforming antenna system. The T/R module was designed using COTS components and commercial manufacturing technology, that increases its scalability and further cost reduction by volume production, the recursive calibration was introduced to enhance the T/R module performance and necessary calibration during the mass production. The circuit design consideration of the T/R module is explained below.



**Fig. 6.1** Block Diagram of the T/R module for  $n \times 4$  array.

### 6.2.1 Receiver

The main function of the receiver is to amplify the RF signal received from the antenna and to keep the noise figure as low as possible to achieve good receiver sensitivity, hence the LNA must be placed as close as possible to the antenna. The receiver power budget is calculated as follow, the attenuation of the phase shifter is 5 dB, SP2Ts are 2.6 dB, SP4T is 1.7 dB, PCB and connector lose is 3 dB, with the input power of -90 dBm and the LNA gain of 14.5 dB, the calculated receiver output is -87 dBm, which is sufficient to compensate for the attenuation due to components. The attenuation factor of the individual COTS components is carefully selected to meet the power budget requirement. The phase shifter is placed at a common path where it can be shared between the transmitter and receiver via an SP2T switch, the 6-bits digital phase shifter with  $5.625^\circ$  resolution can be adjusted digitally via bit0 - bit5 to control the phase of the received signal during the beamforming operation.



**Fig. 6.2** Phase shifter in a beamforming linear array.

The beam steering direction,  $\theta$  can be varied by setting the phase shift,  $\Delta\phi$  of the two successive elements [93] as shown in Fig. 6.2 and it can be represented by equation (6.1) to (6.3). A shaded right-angle triangle can be drawn between the radiator plane and the beam direction that gives,

$$x = d \cdot \sin\theta \quad (6.1)$$

The distance  $x$  can be expressed with respect to the wavelength,

$$\frac{\lambda}{x} = \frac{360^\circ}{\Delta\phi} \quad (6.2)$$

where  $x$  is the shorter side of the triangle that lies on the beam,  $d$  is the separation of the elements,  $\theta$  is the direction of the beam steering, the array boresight is defined as  $0^\circ$ ,  $\lambda$  is the wavelength, and  $\Delta\phi$  is the phase difference between two successive elements. Substitute equation (6.1) into (6.2) gives,

$$\Delta\phi = \frac{360^\circ \cdot d \cdot \sin\theta}{\lambda} \quad (6.3)$$

A 5.5 GHz linear array with 27.25 mm elements separation, and the phase shift,  $\Delta\phi$  of  $45^\circ$  between the successive elements will produce a beam steering direction of  $14.5^\circ$ . The beam steering resolution is determined by the resolution of the phase shifter, a 6-bit phase shifter with  $5.625^\circ$  lowest bit resolution will give approximately  $2^\circ$  beam steering resolution.

### 6.2.2 Transmitter

The transmitter function is to boost the RF signal before it is transmitted to the air via the antenna, the PA is included to boost the RF signal and compensate for the insertion loss exhibited by the phase shifter, RF switches, and PCB traces. The internally matched 3-stages commercially available PA was used to minimise the antenna mismatch and possibly degrade the transmitter performance during the beamforming operation. An RF attenuator was included before the PA to attenuate the RF power before entering the PA, it provides a 30 dB dynamic transmit power range. Like the receiver, the phase of the transmitted signal can be adjusted by controlling a digital phase shifter located at the common path. The amplitude and phase are necessary to vary to set the weight of the RF signal that is required during the beamforming process. The transmitter power budget is calculated as follow, the attenuation of the phase shifter is 5 dB, SP2Ts are 2.6 dB, SP4T is 1.7dB, PCB and connector lose is 3 dB, with the target input power of 5 dBm, PA gain of 30 dB and attenuator range of 0 - 30 dB, the targeted output power calculated around -7.3 to 22.7 dBm with approximately 30 dB dynamic range. Similarly, the attenuation factor of the individual COTS components is carefully selected to meet the power budget requirement.

### 6.2.3 RF Switches

Two types of RF switches are used in the T/R module design, i) SP2T, to switch between the transmitter and receiver path and provides 51 dB isolation between the transmit and receive ports to minimise the self-excitation due to the signal feedback during transmit and receive operations. The HMC8038LP4CETR is widely used in Wireless Lan applications to switch between the transmitter and receiver path, it has a switching timing of 150 ns which is sufficient to support the half-duplex transceiver that has more than 150 ns wait time between the transmit and receive operations. For instance, 802.11 wireless LAN with the short interframe space (SIFS) duration of 10  $\mu$ s, the SIFS is the time from the end of the last symbol of the previous frame to the beginning of the first symbol of the preamble of the subsequent frame. In 802.11 WLAN, once SIFS duration elapses, the transmission can immediately start, ii) SP4T, is a high-speed RF switch to switch between each element in the phased array for the beam scanning operation [94] to channel the RF signals to the high-speed processor or FPGA for decoding. The SP4T has a switching time of around 19 ns, the estimated symbol processing time for the FPGA and processor can be computed by taking the symbol duration divided by 4 minuses away the switching time, for instance, the



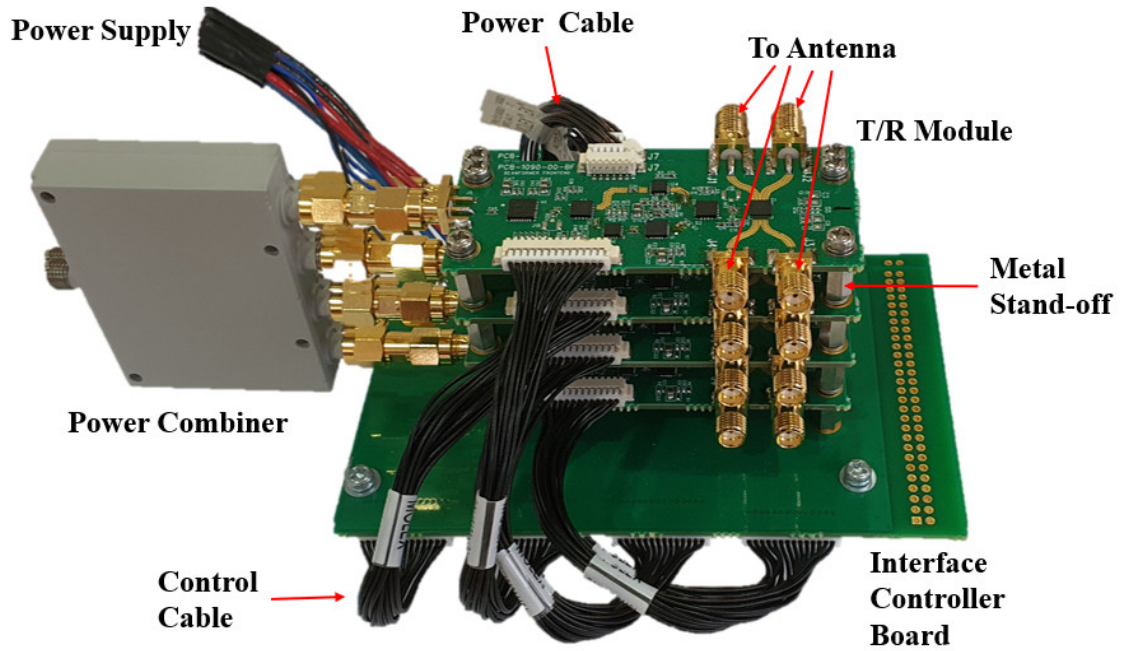
symbol duration for 802.11n WLAN is 6.8  $\mu$ s, this will allow the processor to have a 1.681  $\mu$ s to process the symbol received from each antenna element, thus the direction of arrival can be determined. In addition, to avoid the port mismatch that causes the signal reflected from the antenna ports, PA and LNA, the ports at the RF switches are made non-reflective with a 50-ohm termination design when the port is not active.

#### **6.2.4 Power Supply**

The T/R module is powered by the multiple power supplies +5 V, +3.3 V, -3.3 V, and -5 V, any stable commercially available power source can be used to power up the T/R module. When multiple T/R modules are cascaded for a bigger beamforming system, a common power supply can be used to power up all the T/R modules in the cascaded system.

#### **6.2.5 Electrical Interface and Control**

Now the design and the specifications of the T/R module are specified, the next step is to define the various control methodology and steps required to evaluate the T/R module and automatic adjustment on various RF parameters when the T/R modules are placed into the beamforming antenna systems. The power and control of the T/R module are connected to the external power supply and the interface controller via the 6-way and 14-way cable assembly from Molex, PicoBlade series. The interface controller board was designed such that it allows manual control via dip switches for digital control and resistive trimmer for analogue control, for instance as shown in Fig. 6.1, bit0 to bit5 transistor-transistor logic (TTL) for phase adjustment, analogue voltage signal *Pctrl* to control the transmit power of the RF chain and the analogue signal *Pdet* that can be used to monitor the transmit power generated by the PA. The T/R module was designed with 4 mounting holes to allow stack-up arrangement using brass stand-off. The picture of the 4 T/R modules in a stack-up arrangement is shown in Fig. 6.3.



**Fig. 6.3** T/R modules mounted on the interface controller board.

### 6.2.6 Key Components in the T/R module

The T/R module is designed using the commercially available components mounted on a commercially low-cost PCB. The key components used in the T/R module and their key specifications are listed in Table 6.1 below. The table also indicated the comparison with other COTS components that were evaluated but not suitable for this application due to their technical specification are lower than the design requirement.

**Table 6.1** Key components specification in the T/R module.

| Parts         | Part Number/<br>Maker     | Key Parameters   | Key Specifications   | Comparing with<br>other COTS parts  |
|---------------|---------------------------|--|--|---|
| Phase Shifter | HMC1133LP5E/<br>ADI [95]  | Operating Frequency<br>Insertion Loss<br>Phase Resolution<br>Phase Coverage<br>Phase Error<br>Supply voltage               | 4.8 - 6.2 GHz<br>5 dB<br>5.625°<br>360°<br>2.8°<br>± 5 V                             | P/N: <i>ASL 2009</i> from <i>Aelius</i> and P/N: <i>MAPS-011008</i> from <i>MACOM</i> do not cover the desired frequency range. |
| RF Attenuator | IDTF2258NLGK/<br>IDT [96] | Operating Frequency<br>Insertion Loss<br>Attenuation Range<br>Attenuation Slope<br>Control voltage range<br>Supply Voltage | 50 - 6000 MHz<br>2.7 dB<br>33.6 dB<br>33 dB/Volt<br>0 V to 3.6 V<br>3.15 V to 5.25 V | P/N: <i>HMC346AMS8GE</i> from <i>ADI</i> has a narrower attenuation range of only 28 dB.  |

| Parts               | Part Number/<br>Maker        | Key Parameters   | Key Specifications   | Comparing with<br>other COTS parts  |
|---------------------|------------------------------|--|--|---|
| Power Amplifier     | TQP5525/<br>Qorvo [97]       | Operating Frequency<br>Gain<br>P1dB<br>$P_{sat}$<br>Supply Voltage   | 4.9 – 5.925 GHz<br>32 dB<br>32 dBm<br>31.5 dBm<br>+3.3 to +5 V           | P/N: <i>HMC717ALP3E</i><br>from <i>ADI</i> has a lower gain of 14.5 dB and a lower P1dB of 18 dBm.                    |
| LNA                 | HMC717ALP3E/<br>ADI [98]     | Operating Frequency<br>Noise Figure<br>Gain<br>P1dB<br>Output $P_{sat}$<br>Supply Voltage  | 4.8 - 6 GHz<br>1.3 dB<br>14.5 dB<br>18 dBm<br>19 dBm<br>+5 V             | P/N: <i>SKY65981-11</i><br>from <i>Skyworks</i> does not cover the entire frequency band.                             |
| RF Switch<br>(SP2T) | HMC8038LP4CE<br>TR/ ADI [99] | Operating Frequency<br>Switch<br>Insertion loss<br>t rise<br>t fall<br>Port Isolation<br><i>RFC to RF1-2 (off)</i><br>Supply Voltage | 0.1 - 6 GHz<br>SP2T<br>1.3 dB<br>60 ns<br>60 ns<br>51 dB<br><br>+3.3 V   | P/N: <i>MASWSS0129</i><br>from <i>MACOM</i> has a higher insertion loss of 1.55 dB and lower port isolation of 30 dB. |
| RF Switch<br>(SP4T) | ADRF5044/<br>ADI [100]       | Operating Frequency<br>Switch<br>Insertion loss<br>t rise<br>t fall<br>Port Isolation<br><i>RFC to RF1-4 (off)</i><br>Supply Voltage | 0.1-30 GHz<br>SP4T<br>1.7 dB<br>4 ns<br>4 ns<br>55 dB<br><br>$\pm 3.3$ V | P/N: <i>MA4SW410</i> from <i>MACOM</i> has a slower switching speed of 50 ns.   |

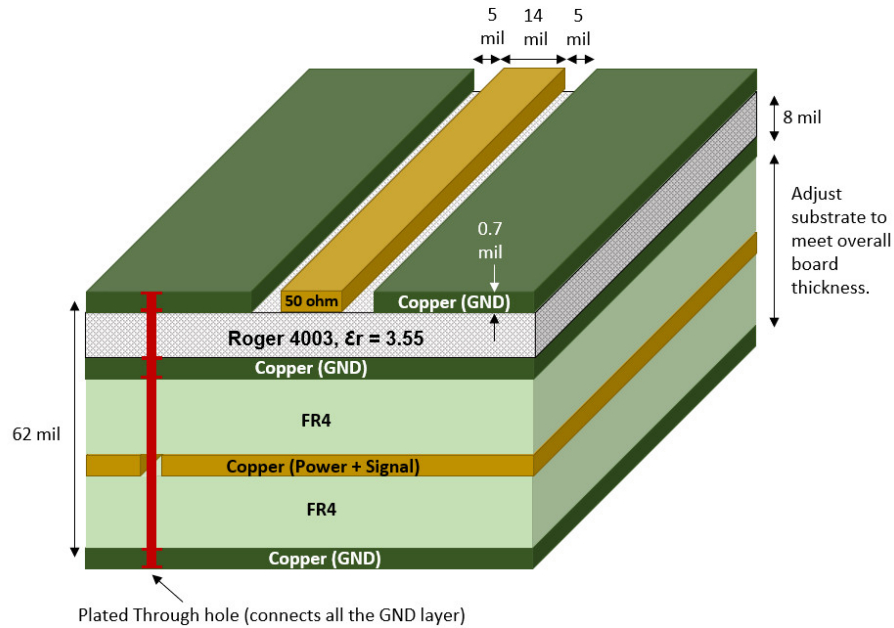
### 6.3 Schematic and PCB Design

The Schematic capture and PCB layout are designed using Power Logic and Power PCB from Mentor Graphic [101]. The T/R module is a 4-layer PCB board, each layer of copper is 0.7mil thickness and separated by the dielectric substrates. The top layer substrate is R04003 materials with 8 mils thickness for optimum RF performance, and the middle and bottom layers substrate are the lower cost FR-4 material. The total PCB thickness is 62 mils. The price of the PCB material fluctuates based on the market demand and supply, the general guideline of the cost factor ratio between the FR4 and RO4003 is 1 : 5, therefore it's justifiable to use RO4003 only for the critical layer and replace the rest of the layers with

the low-cost FR4 material. The schematic diagram of the T/R module is presented in *Appendix D: Schematic Diagram of the T/R Module*, and the PCB gerber file is presented in *Appendix E: PCB Gerber Artwork File of the T/R Module*.

The RF traces and the signal line are routed at the top layer, the second layer provides a solid ground plane for good RF performance, third and fourth layers provide additional ground and power supply routing. All the components are mounted at the top layer to ease the assembly process and troubleshooting. The stacked-up construction of the PCB is shown in Fig. 6.4.

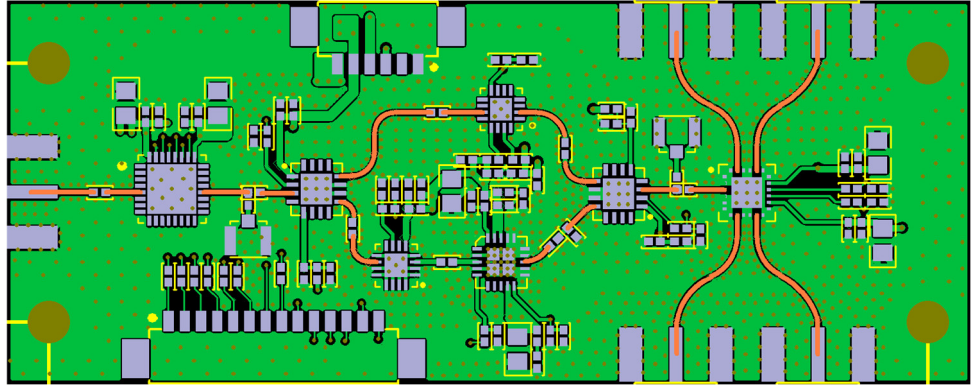
The transmission line is constructed using the coplanar waveguide (CPWG) model, where the characteristic impedance of the 14 mils traces with 5 mils ground plane spacing is 50-ohm. Substrate RO4003 with dielectric constant  $\epsilon_r = 3.55$  and 8 mils thickness is sandwiched between the impedance-controlled traces and the ground plane, and the thickness of the 2 layers of FR4 substrate is adjusted to meet the total board thickness of 62 mils.



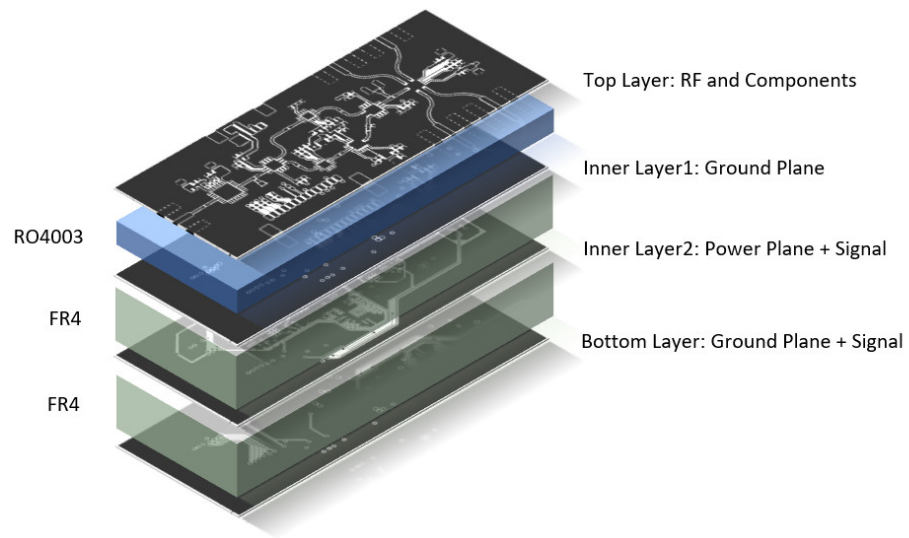
**Fig. 6.4** The PCB cross-sectional view of the T/R module.

The PCB layout was designed with the following consideration, i) impedance control, all the RF traces are laid on the top layer for better CPWG impedance control with a solid copper plane on the second layer separated by RO4003 substrate, and the impedance controlled traces are highlighted in orange as shown in Fig. 6.5, ii) Electro Magnetic Compatibility (EMC) consideration, the control signals, power plane and additional ground plane are laid on layer 3, layer 4 consists of a solid ground plane that acts as a shield for optimum EMC performance, iii) thermal consideration, the heat-generating components

such as PA will have its metal body soldered directly to the big copper plane on the top later of the PCB, and the bottom layer of the PCB will have an exposed copper to install the heatsink when needed, iv) cost consideration, the RO4003 substrate material cost is relatively higher compared to FR-4 material, therefore except the substrate between layer 1 and layer 2 is utilizing RO4003, FR-4 substrate is used for all other layers where the impedance control is not required. The PCB layout layers stack-up is shown in Fig. 6.6.



**Fig. 6.5** The impedance-controlled traces (orange traces).



**Fig. 6.6** PCB layers stack-up of the T/R module.

The electronic components to be mounted onto the T/R module PCB are listed in the bill of material (BOM). The BOM consists of necessary information of the components such as part number, descriptions, part specifications, manufacturers, vendors, reference designators, and quantity used, the information contains in the BOM is to provide necessary input to the buyer for them to procure the parts for prototyping and during the mass production stage. The BOM is also used by the production factory to assemble the components to the PCB on the correct and designated location called reference designator.

The listed BOM for the T/R module can be found in *Appendix F: Bill-of-Materials (BOM) of the T/R Module*.

The T/R module is assembled with components using surface mount technology (SMT). The solder paste is deposited onto the PCB solder pads using the stencil mask, components are placed onto the PCB using SMT machine for tape and reel part or manually for loose components, after which the board is passing through a reflow oven to solidify the solder thus holding the components in solid solder joint. The top view of the beamformer boards after assembly is shown in Fig. 6.7.

## ***6.4 The Prototype of the T/R module***

The prototype of the T/R module is presented in Fig. 6.7. The P1 – P4 and TX/RX ports can be easily connected to external RF equipment via the Sub-Miniature version A (SMA) connectors, the power supply, and control of the T/R module are connected to the external power supply and the interface controller or test fixture to allow external control during the performance evaluations.

A Test fixture has been developed to aid the evaluation of the T/R module and the prototype of the test fixture is shown in Fig. 6.8. The building block of the test fixture consists of i) the dip switches to digitally control the RF components of the T/R module such as SP2T, SP4T, phase shifter and turning on and off the PA and LNA, ii) an analogue control by the resistive trimmer to tune the analogue voltage that is required to adjust the attenuation of the attenuator, and iii) analogue voltage monitoring to monitor the voltage level of the power detector output which is used to determine the actual transmitted power. In addition, the common power supplies provide the power sources and distribute them to the multiple T/R modules when they are cascaded. Provision has been provided by pulling out all the signals to a header, that can be connected to a microcontroller of FPGA for automated control during testing and beamforming operation.



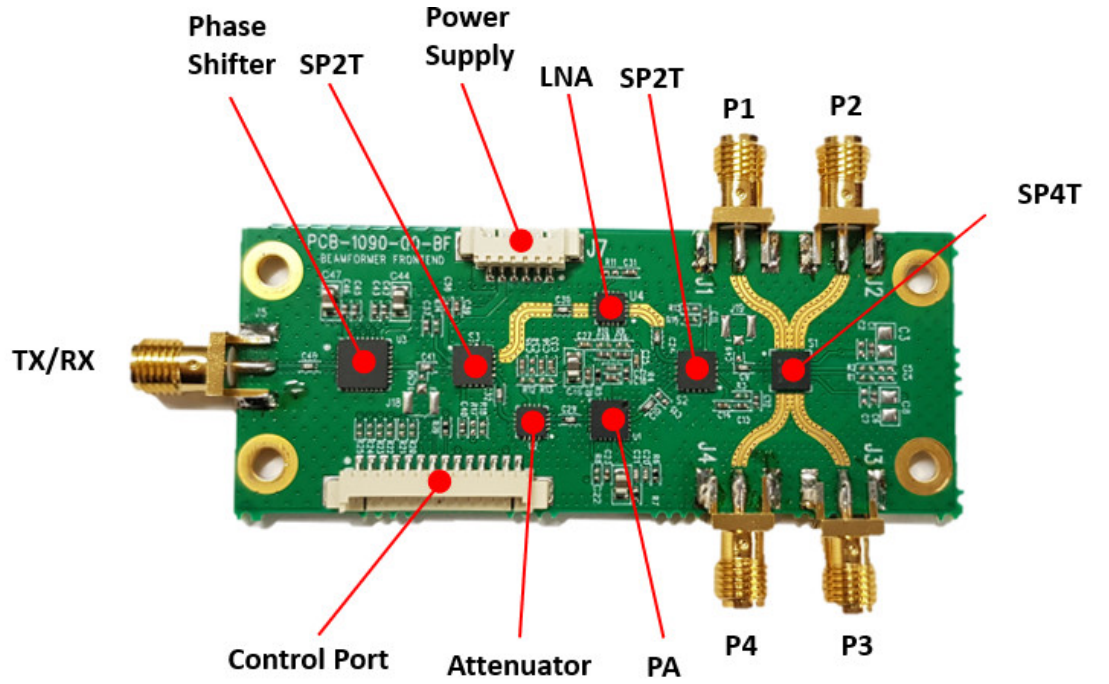


Fig. 6.7 The prototype of the T/R module.

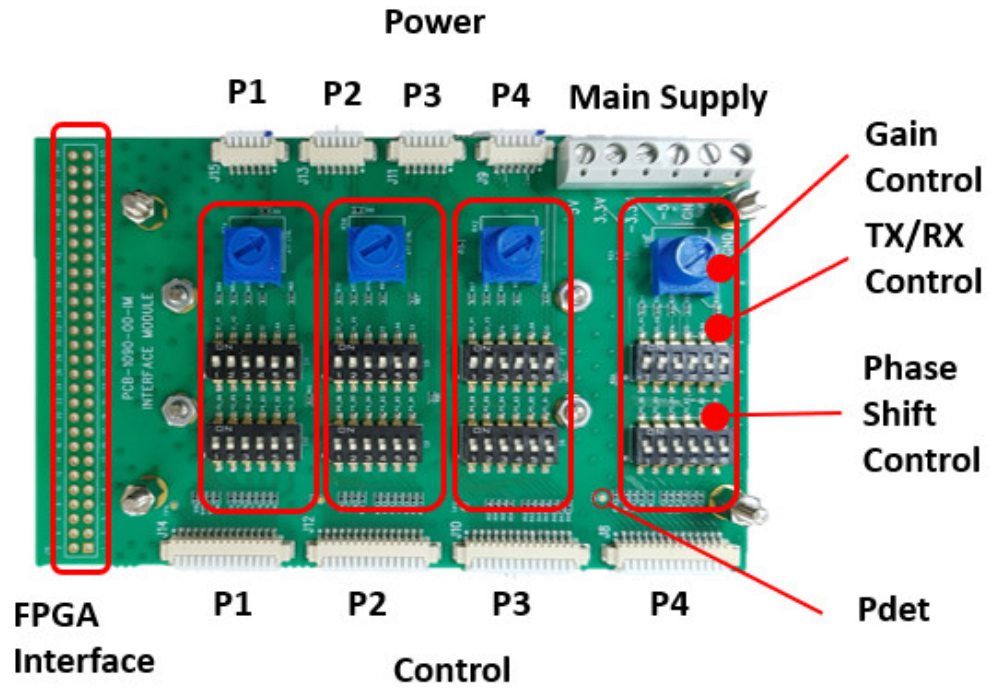
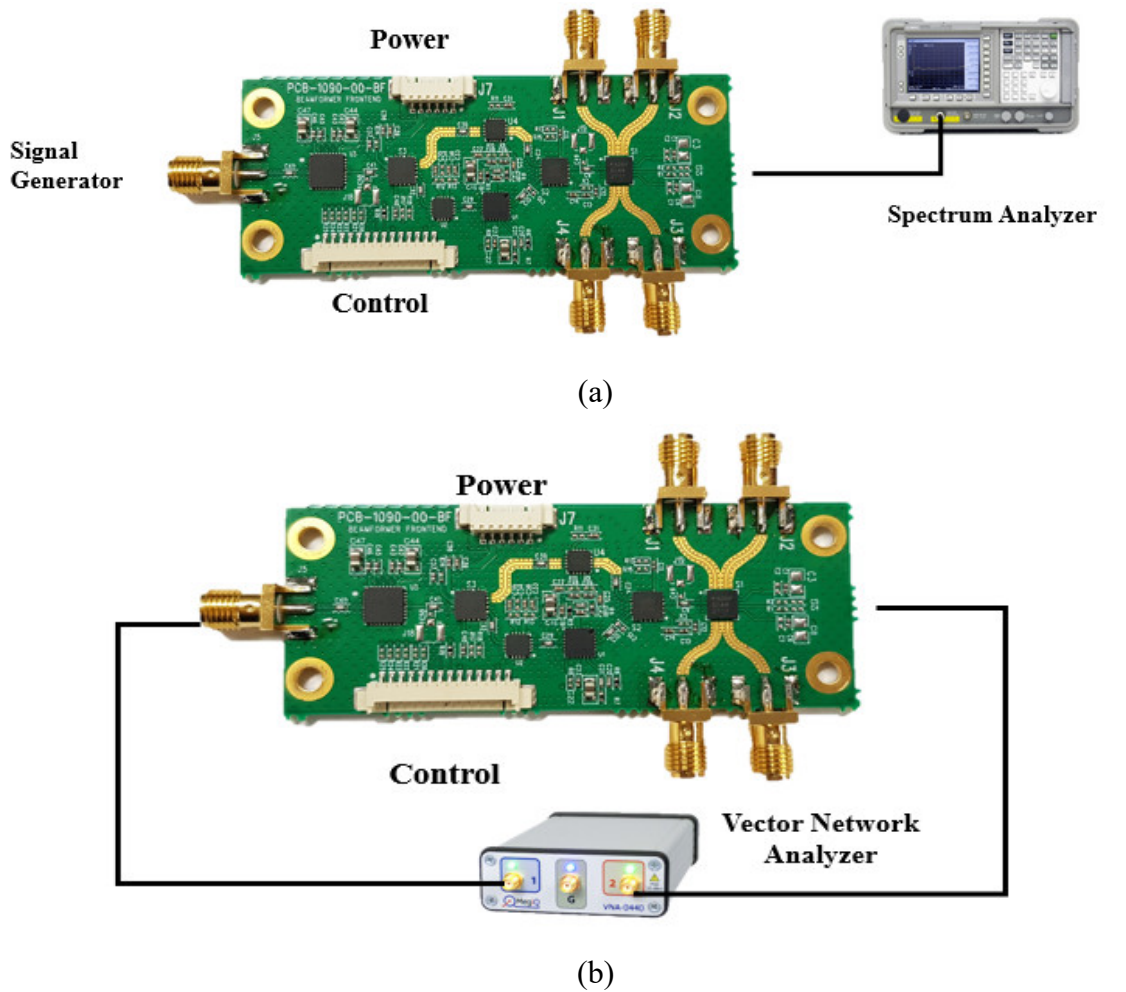


Fig. 6.8 The prototype of the test fixture.

## 6.5 Characterization of the RF Performance

The RF parameters such as transmit power or amplitude and phase errors are characterized using the recursive calibration approach, and the calibrated parameter are

stored in the memory and is used for self-compensation during the beamforming process. The SLL of the beam can be optimized by varying the amplitude of each antenna port which is represented by amplitude distribution. The calibration setup of the T/R module is shown in Fig. 6.9, the phase shifter is controlled by the 6 bits TTL signal, the output power is controlled by adjusting the RF attenuator via the analogue control signal  $Pctrl$  through an external power source, and the output power level is detected and converted to an analogue voltage,  $Pdet$  that is used to monitor the output power level during the calibration. A Spectrum Analyzer (SA) and a Vector Network Analyzer (VNA) are used to measure the transmit power and phase shift of the T/R module. The equipment is connected to the individual port namely P1 to P4 to perform the calibration on the respective port.

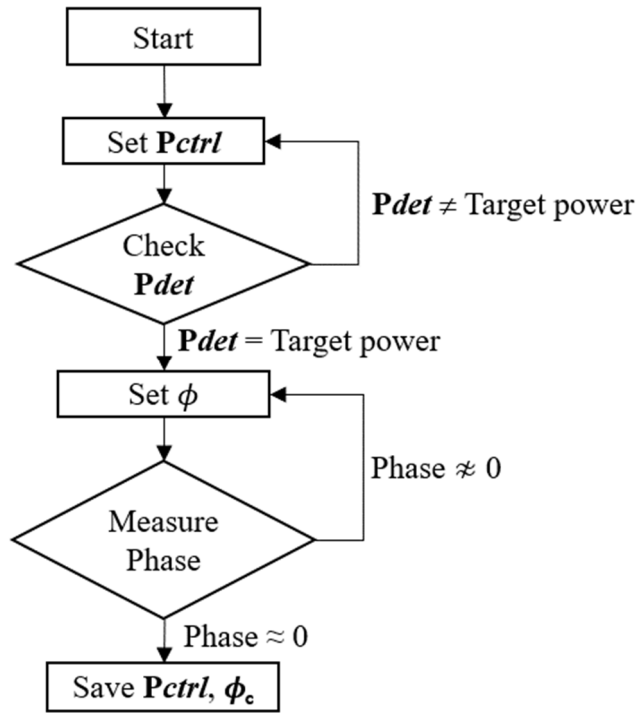


**Fig. 6.9** Calibration setup. (a) Setup for transmitting power calibration. (b) Setup for phase calibration.

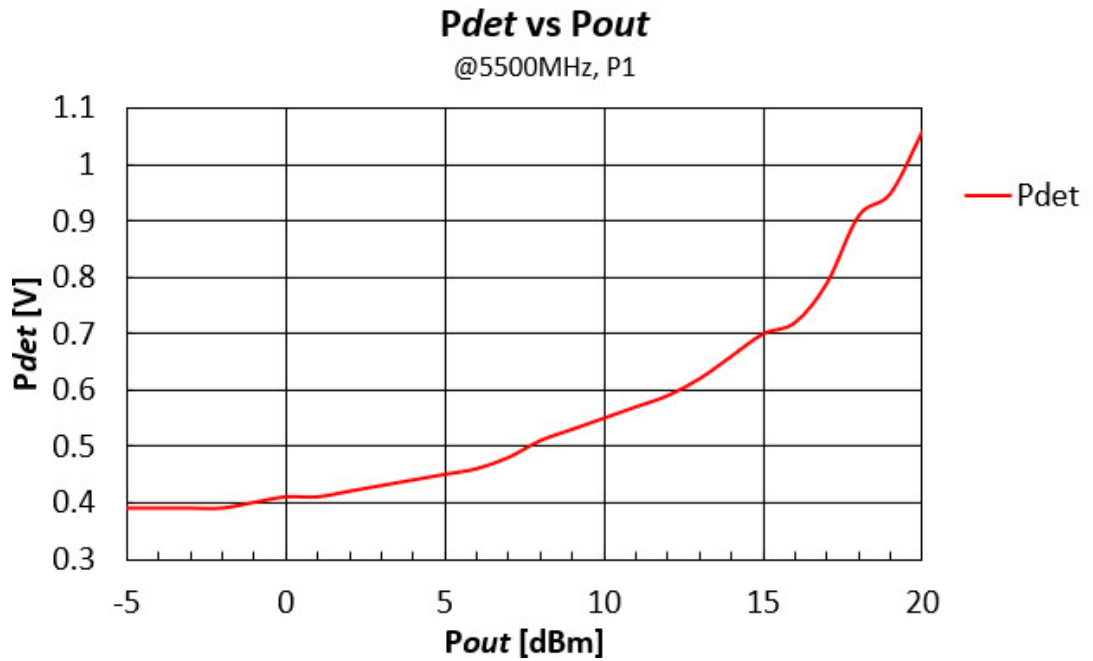
The transmit power response is first characterized using the spectrum analyzer as shown in Fig. 6.9a, followed by the phase offset calibration using VNA as shown in Fig. 6.9b. The iteration flow involved in the calibration of the transmit power and phase is



illustrated in Fig. 6.10. During the power detector  $P_{det}$  calibration, the  $P_{ctrl}$  voltage is adjusted between 0 V and +3 V, and the output power of the T/R module and  $P_{det}$  voltage is constantly measured, thus the relationship between  $P_{ctrl}$ ,  $P_{det}$ , and the output power can be plotted, refer to Fig. 6.11. Once the  $P_{det}$  characterization is done, the phase calibration can be carried out by controlling the  $P_{ctrl}$  and monitoring the  $P_{det}$  for constant power calibration, the phase error is observed by the VNA and iterated by controlling bit0 to bit5 of the phase shifter. The calibration process continues for other variables such as the frequency, and power, and repeats for Port 2, 3, and 4.



**Fig. 6.10** Iteration flow for power and phase calibration.

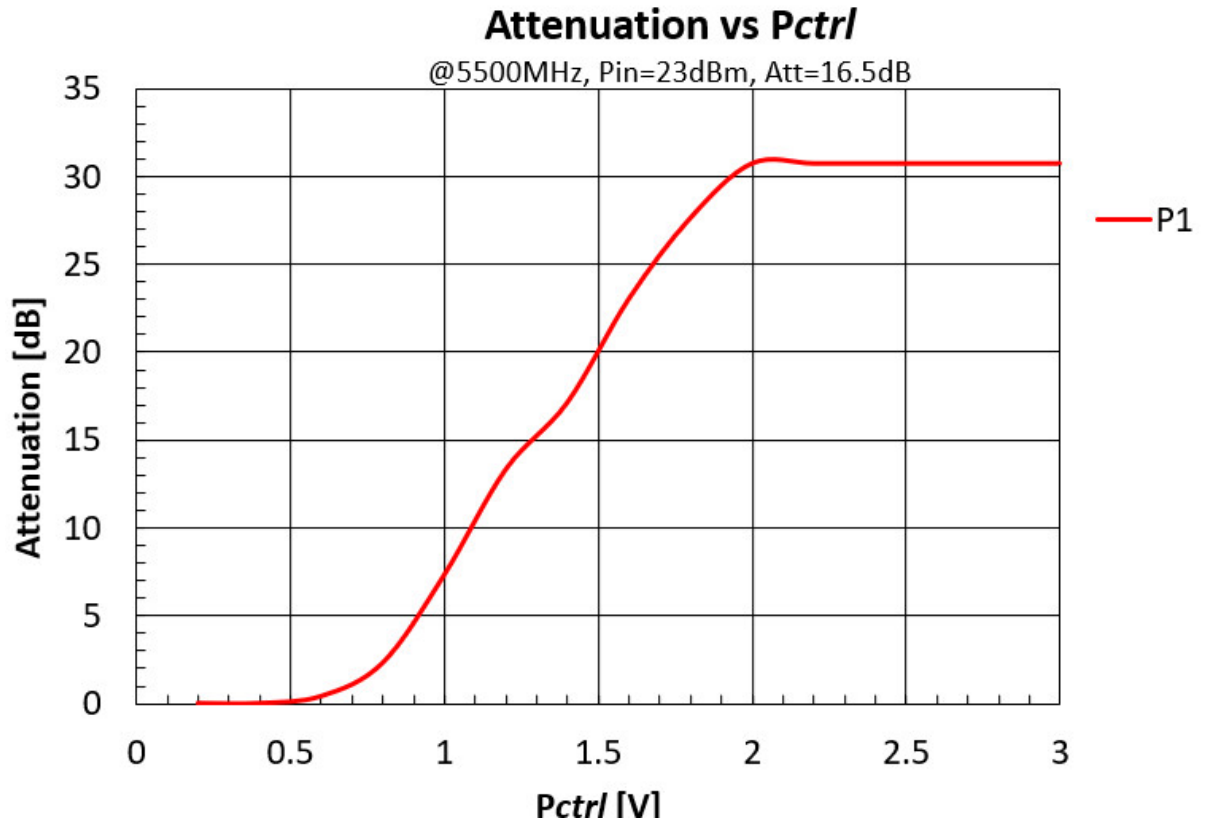


**Fig. 6.11** Output power and  $P_{det}$ , that can be used to determine the RF output power level of the T/R module.

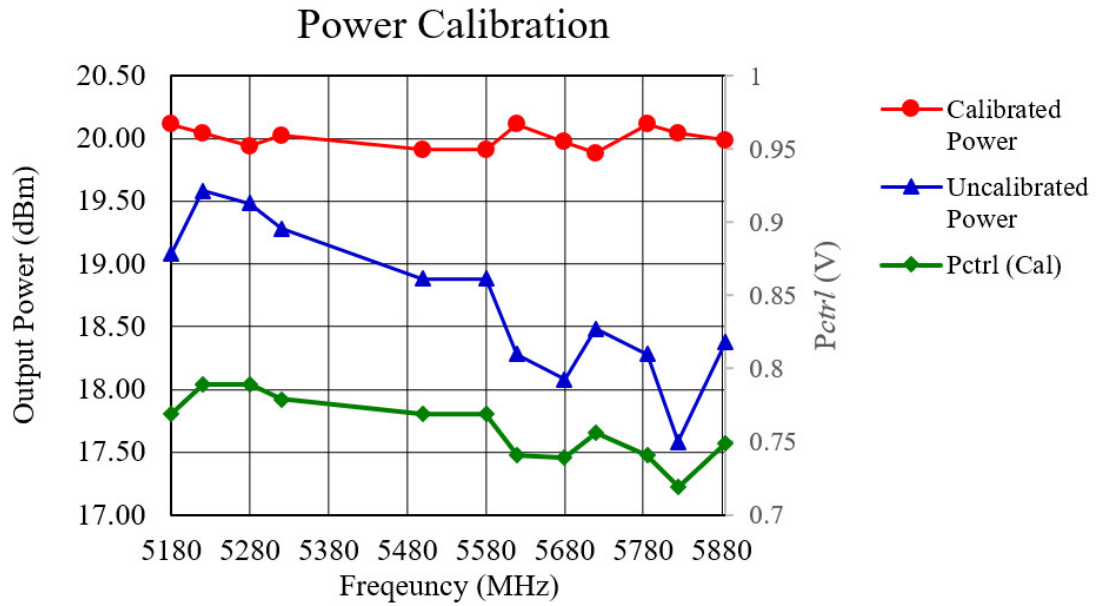
### 6.5.1 Characterizing the RF Output Power

The power control of the RF chain is achieved by controlling the attenuator. The attenuation performance of the RF chain is shown in Fig. 6.12, the control voltage,  $P_{ctrl}$  is ranged from +0.7 to +2.0 V, where +0.7 V gives 0 dB attenuation and the maximum attenuation of 30 dB occurs at +2.0 V.

In most cases, the output power of the RF chain varies according to the frequency and thermal response. The RF calibration will help to define the appropriate  $P_{ctrl}$  to produce a flat transmit power response over the intended operating condition. The frequency response chart for the transmit power is shown in Fig. 6.13, with  $P_{ctrl}$  being at +0.8 V, the transmit output power tolerance as shown in the blue line is around  $\pm 2$  dB over the frequency range from 5180 to 5880 MHz. The variation is probably due to the components and PCB manufacturing tolerances. The red line represents the transmit power after power calibration, the tolerance is improved to  $\pm 0.2$  dB. The  $P_{ctrl}$  voltage set to calibrate the transmit power is represented by the green line.



**Fig. 6.12** Power attenuation performance.



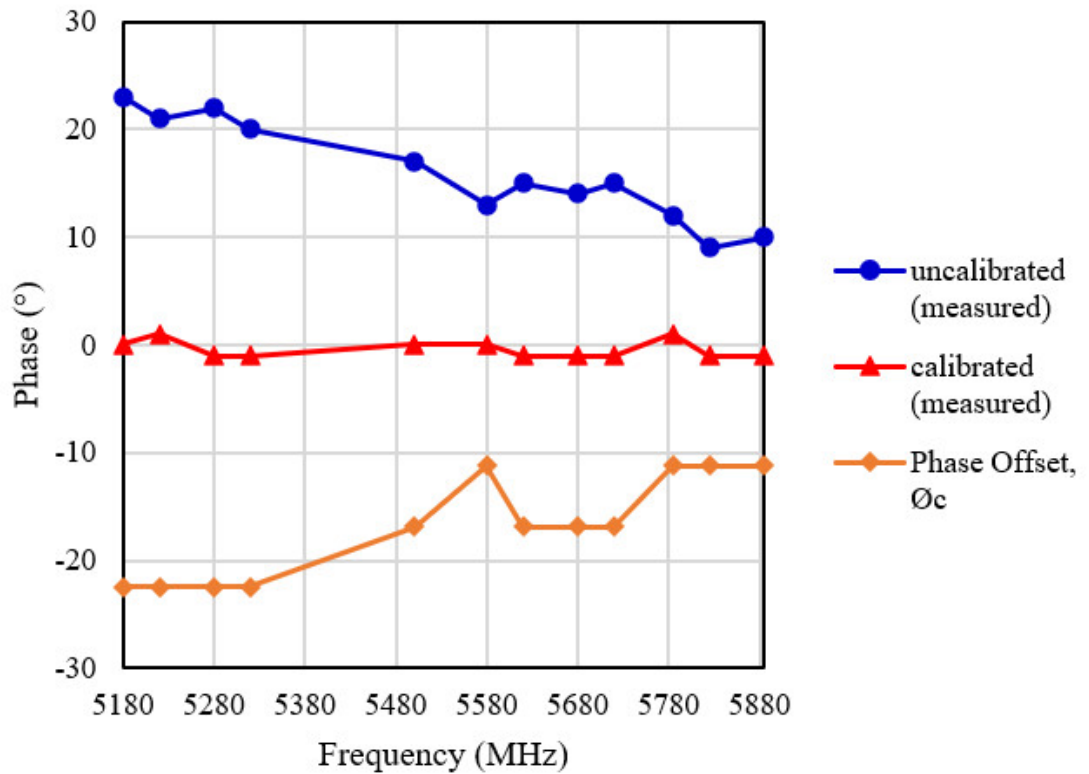
**Fig. 6.13** Output power calibration.

The gain flatness can be compensated automatically by initial calibration or calibration on-the-fly where the  $P_{det}$  can be monitored regularly and the output power can be adjusted using the  $P_{ctrl}$ , and the automated adjustment procedure will make sure each of the RF

chains transmit at its desired power. The maximum measured  $P_{out}$  of the transmitter path with 5 dBm input power is around 22 dBm compared to the simulated  $P_{out}$  of 22.7 dBm.

### 6.5.2 Characterizing the RF Phase Error

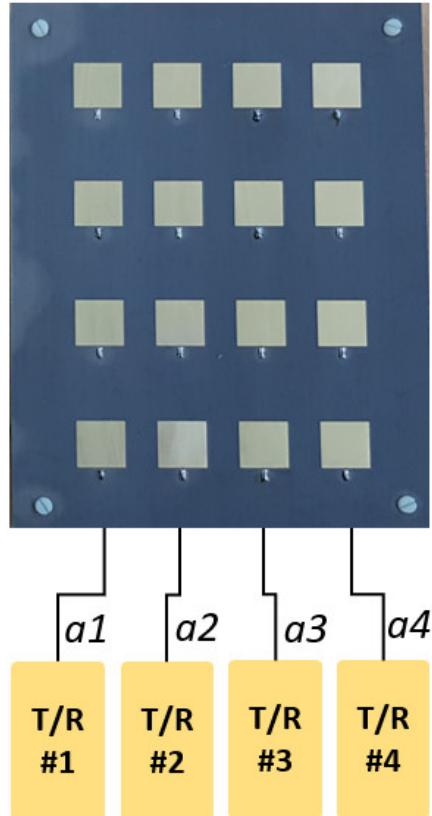
The frequency response, manufacturing tolerance, and components tolerance are the major contributors to the phase tolerance in the RF chain. The phase tolerance must be properly identified and compensated to provide an accurate beam steering performance of the beamforming system. The phase error was measured relative to the input phase to the T/R module, the similar phase calibration can be performed for receiver phase error correction. The phase error of the RF chain is measured using the VNA as described in Fig. 6.9b over the frequency band from 5180 to 5880 MHz, the phase calibration result is shown in Fig. 6.14. The uncalibrated phase error is shown in the blue line with  $13^\circ$  phase error, and the phase offset required to compensate for the phase error is described by the orange line,  $\phi_c$ . The red line represents the phase error after calibration with the phase error being improved to  $\pm 1^\circ$ .



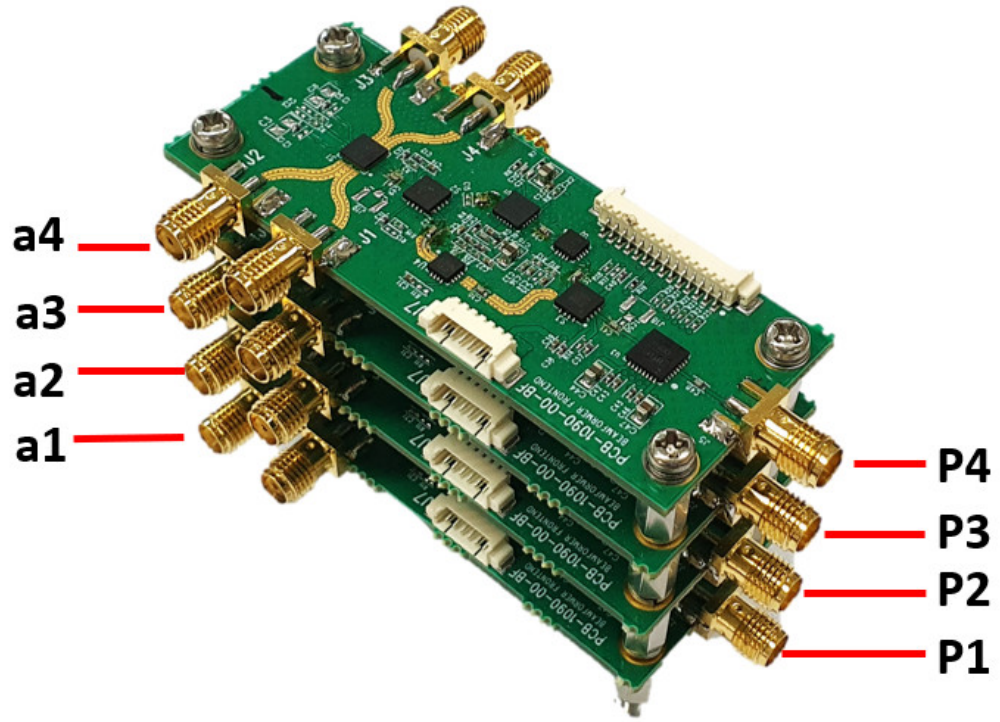
**Fig. 6.14** Phase performance of the T/R module, demonstrates that the phase error has been corrected by calibration.

### 6.5.3 Characterizing the Amplitude Distribution

The gain distribution model is presented in Fig. 6.15. The antenna array in [43] consists of 4 vertical elements combined into a single port using the corporate fed method, in this case, 4 units of T/R modules as shown in Fig. 6.16. are used to evaluate the amplitude distribution of the antenna system. The notation for the amplitude distribution is presented as  $a1-a2-a3-a4$  where  $a1$  is the amplitude ratio for port 1,  $a2$  is the amplitude ratio for port 2 and so on, the amplitude ratio ranged between 0 and 1 where 1 is the full power and 0.5 is half power.

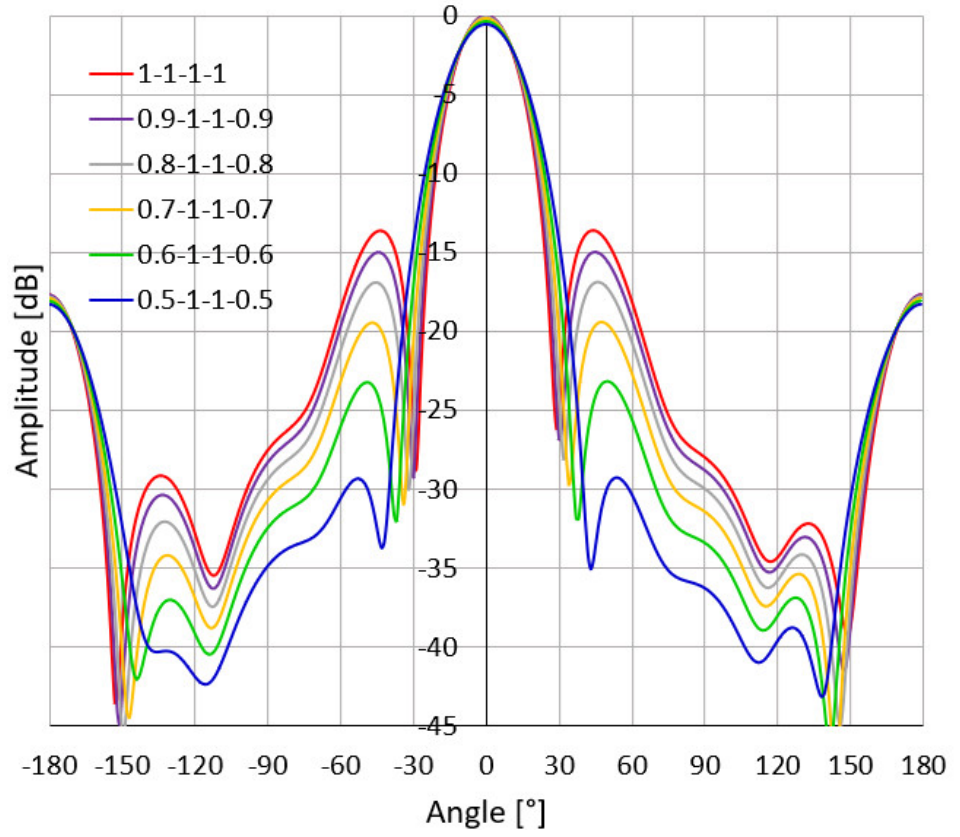


**Fig. 6.15** Amplitude distribution model on the  $4 \times 4$  array.



**Fig. 6.16** 4 T/R modules stacked-up for amplitude distribution characterization

The amplitude distributions of the T/R module integrated with the  $4 \times 4$  array is simulated using CST FIT solver, the simulation results at 5.5 GHz operating frequency are presented in Fig. 6.17. As we can observe from the results, the antenna radiation pattern is compromised between the gain, HPBW, and SLL, and the optimal results are observed when the amplitude distribution factor is 0.5-1-1-0.5 (optimum distribution) where the gain is 17.4 dBi, HPBW is  $29.2^\circ$  and SLL is -28.7 dB compared to the uniform amplitude distribution of 1-1-1-1 that produces the gain of 17.9 dBi, HPBW of  $24.5^\circ$  and SLL of -13.6 dB, thus, the optimum amplitude distribution delivers good SLL improvement of 15.1 dB for interference performance and reasonable gain and HPBW as compared to uniform distributions. The SLL improvement can further enhance the interference rejection in the smart antenna system. Further simulation has been carried out to evaluate the SLL improvement with amplitude distribution 0.5-1-1-0.5 for the entire steering angle supported by the array, SLL of -22.71 dBm and -12.55 dBm which is 11.1 dB and 5.27 dB improvement respectively were observed for  $\pm 20^\circ$  and  $\pm 40^\circ$  steering angle. However, the amplitude distribution was not able to suppress the grating lobe level at the end-fire around  $\pm 40^\circ$ .



**Fig. 6.17** Simulated results of the SLL performance with different amplitude distribution factors at 5/5 GHz.

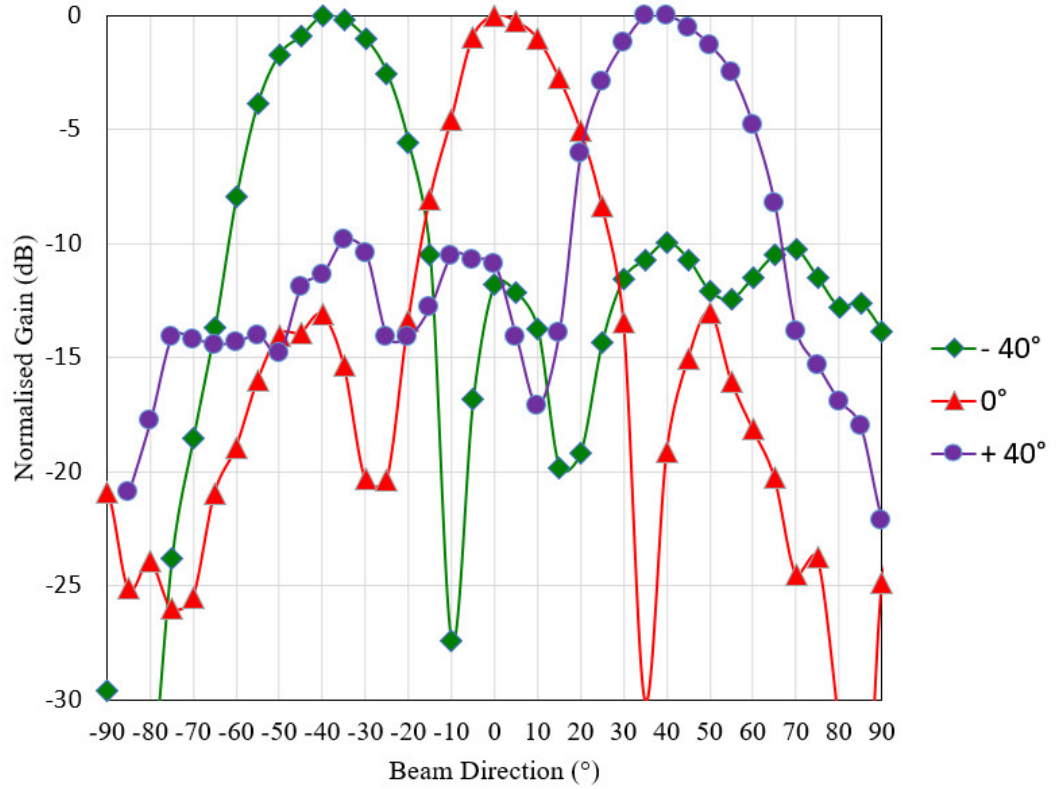
## 6.6 Measurement Results and Discussion

The beamforming performance of the antenna array is measured by asserting the RF signal into each port of the antenna array with different phase shift added by the phase offset  $\phi_c$  calibrated earlier. The phase difference to each port is set by controlling the bit0 to bit5 of the 6-bits phase shifter. The phase difference for each port to enable  $0^\circ$ ,  $+40^\circ$  and  $-40^\circ$  beam steering is presented in Table 6.2 below, where  $\phi_{c1}$ ,  $\phi_{c2}$ ,  $\phi_{c3}$ , and  $\phi_{c4}$  denote the calibrated offset value for each port.

**Table 6.2** Phase compensation for beamforming chains.

|                      | $-40^\circ$       | $0^\circ$   | $+40^\circ$       |
|----------------------|-------------------|-------------|-------------------|
| Chain 1 ( $^\circ$ ) | $\phi_{c1}$       | $\phi_{c1}$ | $45 + \phi_{c1}$  |
| Chain 2 ( $^\circ$ ) | $135 + \phi_{c2}$ | $\phi_{c2}$ | $270 + \phi_{c2}$ |
| Chain 3 ( $^\circ$ ) | $270 + \phi_{c3}$ | $\phi_{c3}$ | $135 + \phi_{c3}$ |
| Chain 4 ( $^\circ$ ) | $45 + \phi_{c4}$  | $\phi_{c4}$ | $\phi_{c4}$       |

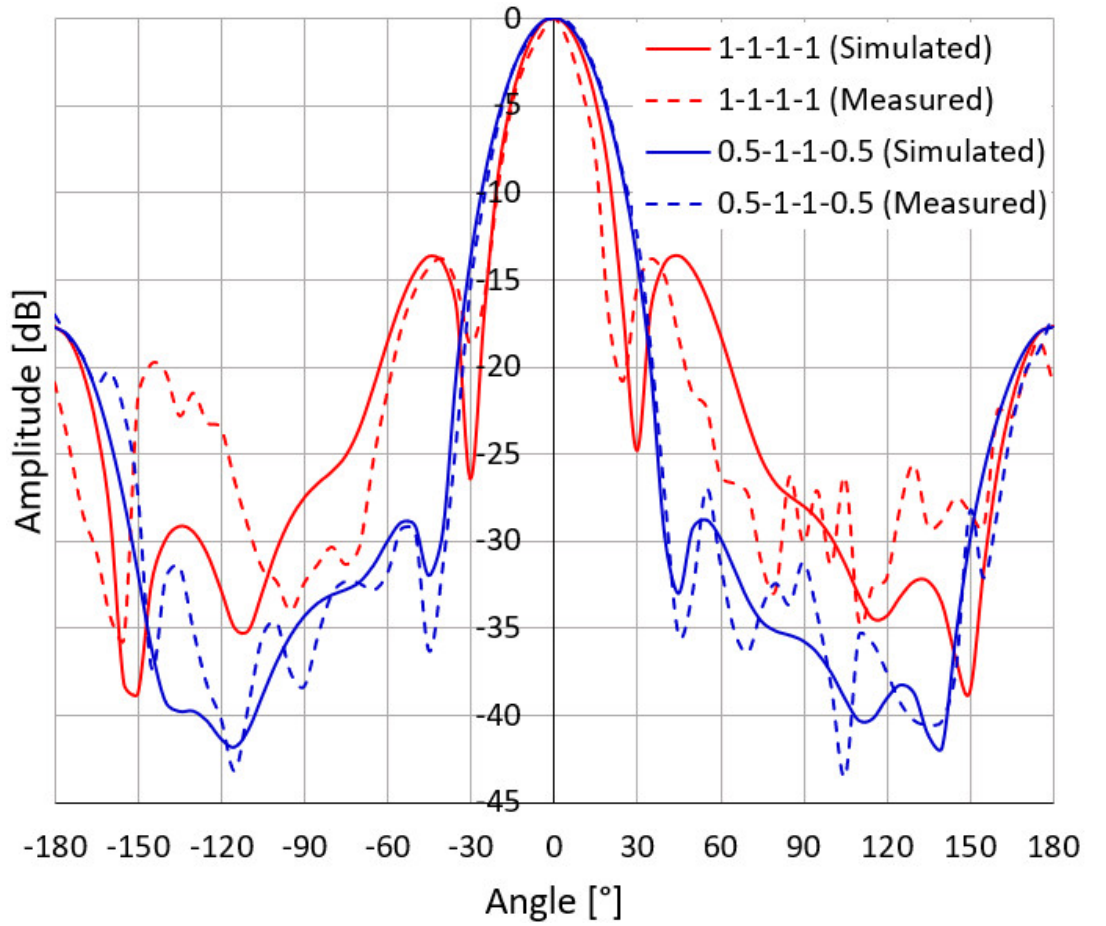
The beamforming results evaluated with the compensated phase and chain power are presented in Fig. 6.18, where the beam steering angle agreed well with the simulated results. The compensated phase  $\phi_c$  has successfully offset the phase difference between the RF chains. It was observed that the achievable beam-steering resolution angle is around  $2^\circ$  by using the 6-bits phase shifter at each RF chain.



**Fig. 6.18** Measured beamforming result with  $4 \times 4$  array at 5.5 GHz.

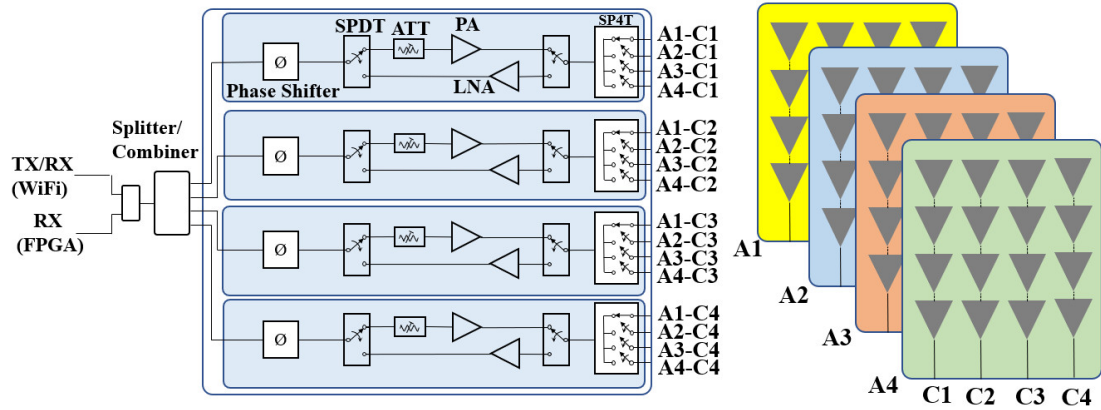
The SLL performance results at 5.5 GHz for  $0^\circ$  beam with amplitude distribution of 1-1-1-1 and 0.5-1-1-0.5 are experimentally validated using the T/R modules and the  $4 \times 4$  linear arrays and presented in Fig. 6.19. The optimum side-lobe and gain are achieved when the amplitude distribution is at 0.5-1-1-0.5 where the results are agreed well with the simulation results presented earlier.





**Fig. 6.19** Measured results of the SLL performance with different amplitude distribution factors at 5.5 GHz.

For a smart antenna system that requires  $360^\circ$  coverage, 4 of the T/R modules are cascaded and the RF ports are connected to the 4 antenna arrays respectively as shown in Fig. 6.20. for example, the port A1.C1 of the T/R module is connected to array A1 port C1, port A2.C1 is connected to array A2 port C1, and so on. Similar beam steering performance is expected for the rest of the other 3 sectors that makes  $360^\circ$  coverage of the smart antenna.



**Fig. 6.20** 360° beamforming system consists of the 4 units of T/R modules and antenna arrays

Table 6.3 tabulated the performance comparison with the state-of-the-art T/R modules, the proposed T/R module has the comparable or better performance compared to the state-of-the-art modules, the proposed recursive calibration process has managed to correct the phase error to  $\pm 1^\circ$  and amplitude error to  $\pm 0.2$  dB. In addition, the amplitude distribution of 0.5-1-1-0.5 combination has successfully suppressed the SLL to -28.7 dB for  $0^\circ$  beam, -22.71 dB for  $\pm 20^\circ$  beam, and -12.77 dB for  $\pm 40^\circ$ . The recursive calibration method has improved the SLL and phase error of the antenna system without the need to alter the geometry of the antenna design which is time-consuming and costly.

The proposed T/R module is also contributed to the overall cost reduction due to the utilization of COTS components and volume production. The material cost for the T/R module is around U\$193.7 for sample build and the cost drop significantly to U\$85.3 for a mass production volume of 2,500 pcs. Another cost-benefit for mass volume production is the manufacturing setup cost, which constitutes U\$200 for sample production and drops to U\$1 for volume production. The cost is around 5 to 10 times lower than other commercial T/R modules. Due to the low-cost structure by utilizing the COTS components, there is limited room for re-configuring the T/R module into other specifications such as different operating frequencies. However, the modular concept, simple design approach, and adaptation of COTS components make it easy to reproduce such T/R module in other operating specifications.

**Table 6.3** Comparison with the state-of-the-art T/R modules.

| Items                      | [83]           | [84]                          | [86]   | This work  |
|----------------------------|----------------|-------------------------------|--|--|
| Frequencies                | 8 – 12 GHz     | 9 – 10 GHz                    | 40 – 45 GHz                                      | 4.9 – 5.9 GHz  |
| Phase Shifter / resolution | 6-bit / 5.625° | LO Sync.                      | 4-bit / 22.5°                                    | 6-bit / 5.625°   |
| SLL                        | NA             | -7.6 dB<br>( $\pm 20^\circ$ ) | $\sim -13$ dB<br>( $\pm 45^\circ$ )<br>Figure 3. | -28.7 dB ( $0^\circ$ )<br>-22.71 dB ( $\pm 20^\circ$ )<br>-12.77 dB ( $\pm 40^\circ$ ) |
| Phase Error                | 5.463°         | 2.1°                          | $< 8.8^\circ$                                    | $\pm 1^\circ$  |
| Amplitude Error            | 1.25 dB        | NA                            | $< 1.3$ dB                                       | $\pm 0.2$ dB   |

Note: NA denotes information not available.

## 6.7 Summary

In this section, a beamforming T/R module for linear phased array application in the commercial frequency band 4.9 – 5.9 GHz band has been developed and demonstrated. The design consideration of the T/R module including circuits design, schematic, PCB, and interface controller boards has been discussed in detail. The performance of the T/R module has been calibrated and characterized using a simple recursive calibration approach, and the beamforming performance has been experimentally evaluated using the  $4 \times 4$  phased array. Leverage on the commercially available RF components and low-cost high volume manufacturing technology, the adoption of the T/R module is expected to accelerate the smart antenna deployment in the commercial infrastructure such as the 4.9 – 5.9 GHz band which is widely used as free access such as the wireless hotspot in commercial building and public areas. For future works, based on the design concepts of the T/R module that adopts the commercially off-the-shelf RF components and standard manufacturing technology, the T/R module can be easily developed into other un-licensed bands such as 2.4 GHz, 24 GHz, and 60 GHz which are commercially available for public use. In addition, the T/R module can be further miniaturized for better cost performance.

## 7 The Novel 360 Degree Pre-configurable Antenna Systems

As reviewed in Chapter 3, the conventional 360° beamforming antenna systems were mainly developed using the multiple fixed radiating beams that combined to provides 360° azimuth plane coverage, the beam control mechanism is supported by the PIN diodes that can be activated to turn on and off the radiating beam based at the intended radiating direction. The drawbacks of this method are poor beam steering resolution and wide HPBW. In this work, the novel pre-configurable 360° smart antenna system was designed by taking into consideration the performance, cost, and field deployment friendliness. It allows the gain and service sector to be pre-configured to suit the respective application scenarios, and the beamforming within the 90° sector is realized using the hybrid beamforming technique, with the array that supports narrow HPBW, and fine beam steering angle resolution that controlled by the dedicated phase shifter on each RF ports. This section will cover the details design and operation of the proposed pre-configurable beamforming antenna system.

### ***7.1 The Proposed Novel Pre-Configurable Smart Antenna System***

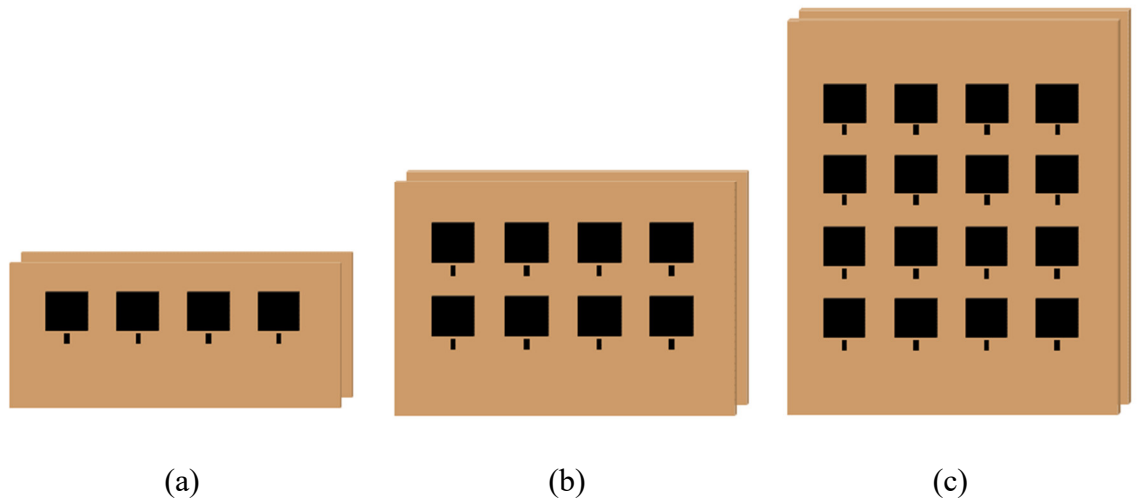
The illustrations of the pre-configurable smart antenna system are presented in Fig. 7.1 and Fig. 7.2. The phased array was designed with multiple capacitive feed MPA elements lay over the structure of the dual substrates to achieve a higher gain and wider operating bandwidth. The volatile antenna structure enables the pre-configurable ability of the smart antenna systems to tackle the needs to have the configurable gain and beam coverage angle in order to obtain the optimum setup that suite well in the dynamic vehicular environment, where different physical coverage beam and communication range can be pre-configured for different application scenarios as described earlier in Fig. 2.5.

Firstly, the antenna element was designed with high gain and wide operating bandwidth and constructed with the feed network into the modular sub-arrays, 3 types of modular linear sub-arrays that support 90° beam steering was pre-designed and fabricated with low, medium, and high gain as shown in Fig. 7.1, and then following the 2 simple configuration steps to form the 360° pre-configurable antenna system. The first step allowing the user to pick the

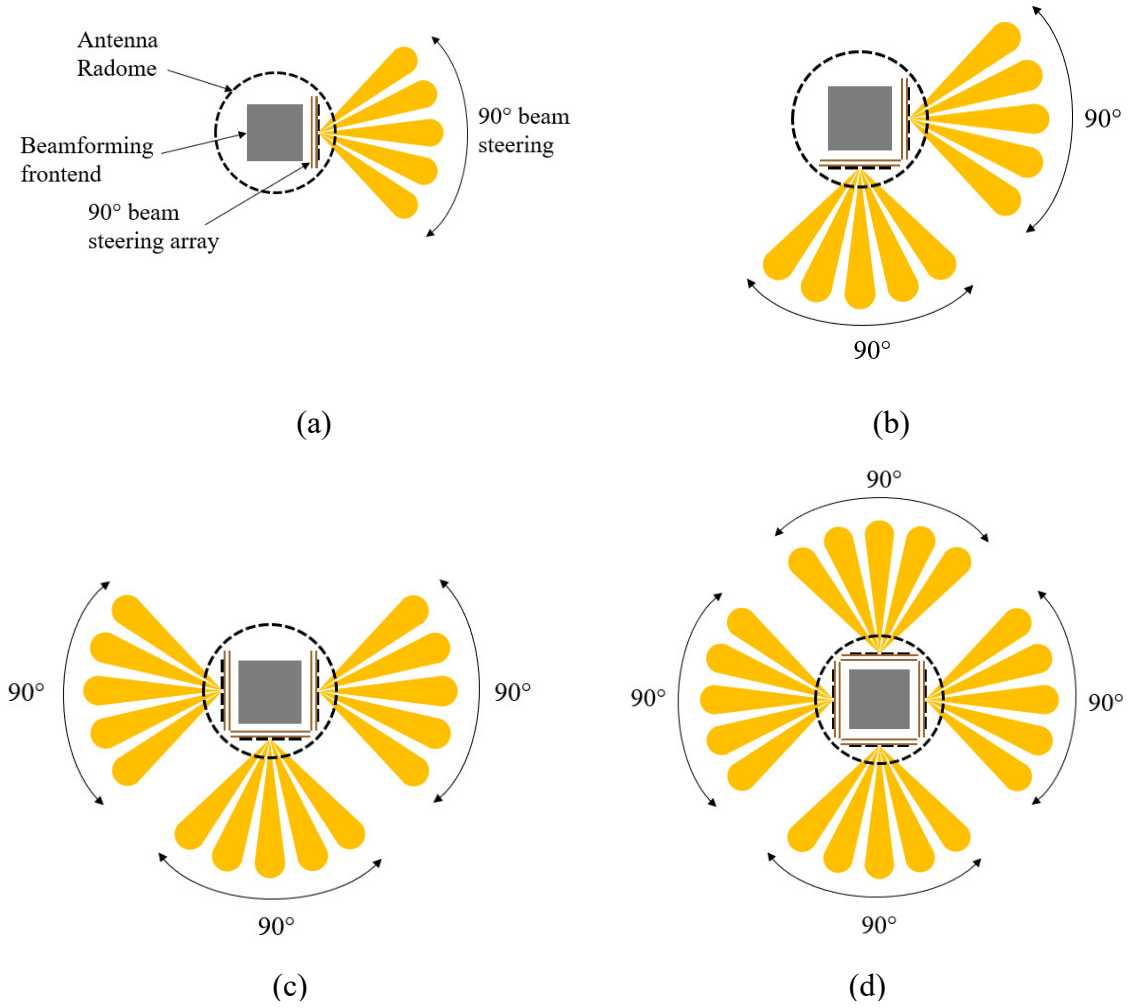
---

*Part of this chapter is reproduced from paper #2 in the publication list on page iv, where the thesis author is the main author in this paper.*

desired gain from the modular sub-arrays listed in Fig. 7.1. And the second step is shown in Fig. 7.2, the beam coverage of  $90^\circ$ ,  $180^\circ$ ,  $270^\circ$ , and  $360^\circ$  can be constructed by simply integrate the multiple sub-arrays onto the antenna systems; the similar method can be used to configure the middle gain and high gain antenna system, the cone shapes highlighted in orange colour represent the beams of the sub-array which can be electronically steered within the  $90^\circ$  sector. The space at the middle of the radome is reserved to house the RF beamforming frontend that consists of electronic components mounted on the PCB to perform and beam steering function.



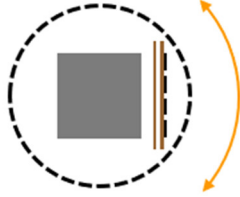

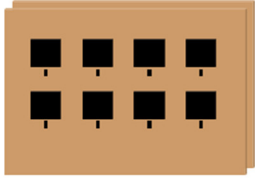


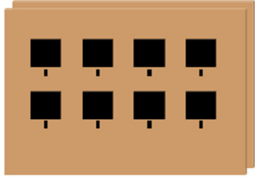
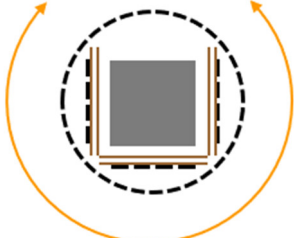
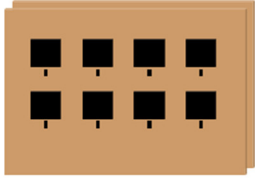
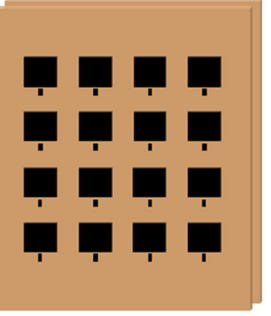
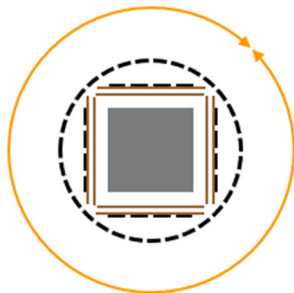
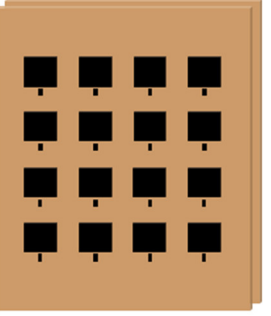
**Fig. 7.1** Arrays with pre-configurable gain. (a) 1 x 4 array (low gain). (b) 2 x 4 array (mid gain). (c) 4 x 4 array (high gain).



**Fig. 7.2** Pre-configurable antenna system. (a) 90° sector with one sub-array. (b) 180° sector with 2 sub-arrays. (c) 270° sector with 3 sub-arrays. (d) 360° sector with 4 sub-arrays

The usage scenarios and type of pre-configurable smart antenna can be summarised in Table 7.1. The application scenarios in Fig. 2.5 are extracted and translated to the desired coverage sector of the proposed pre-configurable smart antenna structure and presented as top view in the antenna illustration column. The flexible antenna structure can be pre-configured to cover 90°, 180°, 270°, and 360° respectively where the type of gain can be pre-selected from the  $1 \times 4$  array for low gain,  $2 \times 4$  array for middle gain, and  $4 \times 4$  array for high gain applications. The beam steering performance of each array can be referred to the radiation pattern of the single array in chapter 5.8 section 6.6, as all the arrays reside in the pre-configurable antenna system are identical, for the antenna system with more than one array, the same beam steering performance is applied to other arrays.

**Table 7.1** Pre-configurable matrix for the proposed flexible smart antenna structure, number of arrays, and different antenna gain can be pre-configured to form a smart antenna system.

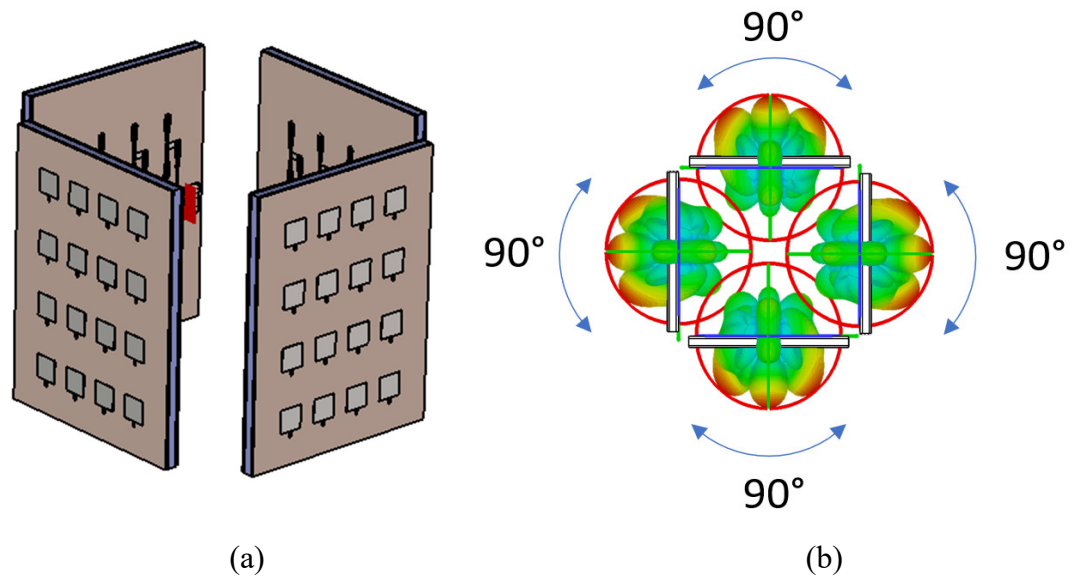
| Application Scenarios       | Type of configuration | Number of Arrays and Antenna illustration   | Choice of gain (Arrays)  |
|-----------------------------|-----------------------|---|--|
| Right angle road / track    | 90°                   | 1 array<br><br>90° coverage     | <br><br>or<br>   |
| Straight road or track      | 180°                  | 2 arrays<br><br>180° coverage  | <br><br>or<br>   |
| Traffic Junction            | 270°                  | 3 arrays<br><br>270° coverage | <br><br>or<br> |
| Roundabout or Main Junction | 360°                  | 4 arrays<br><br>360° coverage |   |

## ***7.2 Beamforming Concept in the 360° Pre-configurable Smart Antenna System***

The 360° beamforming antenna system consists of 4 sets of antenna arrays with each covering 90°, the beamforming is realised using the RF beamforming frontend also known as the transmit and receive (T/R) module as presented in [63]. [64] had highlighted some key design requirement for the T/R modules and necessary calibration technique required to offset the possible phase and amplitude error during manufacturing, the technique to reduce the SLL of the beamforming antenna system has been discussed in detail. In typical deployment especially in the transportation sector, the smart antenna is deployed outdoor or installed on the vehicle, therefore, the antenna element and electronics need to be properly housed inside the enclosure or radome to protect it from the harsh environment. In [65] a study was done to assess the potential RF degradation due to the antenna radome as well as the effect of the drag coefficient to the shape of the radome, the results revealed that the polymethyl methacrylate material has negligible impact to the radiation performance at 4.9 to 5.9 GHz, and demonstrated that the improved aerodynamic design of the radome has a minimum effect to the overall drag coefficient of the vehicle.

The beamforming antenna system is pre-configured according to the application scenarios described earlier in Fig. 2.5, the proposed flexible architecture allows a maximum of 4 sets of arrays to be integrated and form a smart antenna system. The 360° beamforming structure is constructed using the 4 units of  $4 \times 4$  arrays as demonstrated in Fig. 7.3 with both the isometric view and 360° radiation pattern simulated using the CST post-processing function. Overall antenna performance was measured with the gain between 14.38 – 17.25 dBi with 20° – 31.5° radiating beamwidth.





**Fig. 7.3** The flexible beamforming antenna structure. (a) Isometric CAD view. (b) 360° beamforming pattern.

The RF beamforming frontend or T/R module is controlled by an external processor such as FPGA or single-board computer, the function is briefly discussed in this section, the baseband processing consists of the DOA algorithm combined with the sophisticated beamforming algorithm to compute the necessary beamforming weight that controls the hybrid beamforming frontend to achieve the desired beamforming and interference nulling. Various works have been carried out to optimise the DOA algorithm, such as the DOA performance evaluation [66] on the 4-elements array using Root-Multiple Signal Classification (Root-MUSIC), Root-Weighted Subspace Fitting (Root-WSF), and Beamspace-Estimation of Signal Parameters via Rational Invariance Techniques (BSPRIT) algorithms, performance optimization such as reducing the DOA computational time [67] via the Root-Transformation Matrix (root-T) technique, for low Signal to Noise Ratio (SNR) environment scenario, the Cross Cumulant-MUSIC (CC-MUSIC) combined with the root-MUSIC algorithm [68] was proposed. In the area of beamforming algorithm, the blocking matrix for Generalized Sidelobe Canceller (GSC) [69] for the high-speed environment was proposed using a Simplified Zero Placement Algorithm (SZPA) to achieve reduced computational time to 0.268 ms from 1.541 ms compared to Singular Value Decomposition (SVD) method. In [70], the improvement on the convergence speed in the adaptive beamforming was proposed via the Cyclic Variable Step Size (CVSS) algorithm. The Kalman Filter was introduced in [71] to overcome the DOA angle mismatch when the changes of the DOA are too fast especially when the mobile terminal is very close to the receiver station.

### ***7.3 Proposed DOA Estimation Using the Pre-configurable Smart Antenna System***

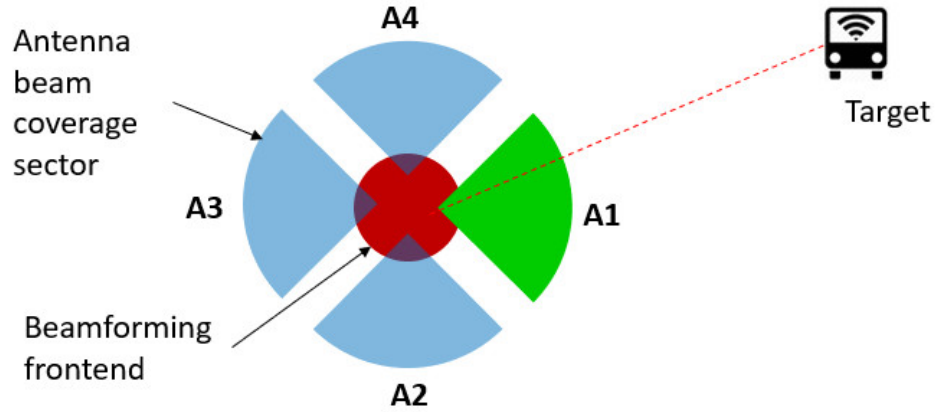
The objective of the direction of arrival (DOA) estimation is to detect the angle of arrival of the transmitting source using the receiving antenna array, the DOA information is used together with the beamforming algorithm to shape the antenna radiating and receiving beam towards the targeted direction and null off other directions, this technique aimed to mitigate the possible interference to and from other directions that are not intended. Utilising the proposed pre-configurable smart antenna array and the beamforming frontend or T/R module, the proposed DOA estimation can be carried out via 2 scanning steps, namely, sector scanning and direction-finding.

Each of the  $90^\circ$  sectors is designed to support i) full  $90^\circ$  scanning with only 1 antenna port is enabled, or ii) beam steering with  $25^\circ$  narrow beamwidth by enabling all the ports with phase control on each port. The features are very useful for direction of arrival (DOA) estimation in the  $360^\circ$  smart antenna system as presented in [62], where the sector scanning to determine the specific sector of the target, this can be performed by enabling one of the 4 columns on the 4 sector arrays. Once the target is locked to the targeted sector, the fine direction of arrival can be performed by enabling all the 4 columns on that particular array and zoom in the beam to the target with a narrow beamwidth of approximately  $25^\circ$ , beam scanning with  $25^\circ$  beamwidth and scanning resolution of up to  $2^\circ$  within the  $90^\circ$  sector is possible with the 6-bits digital phase shifter that is capable of producing the phase shift resolution as low as  $5.625^\circ$  on each RF chain.

#### **7.3.1 Sector Scanning**

Sector scanning is to scan the coarse direction of the targeted client over the  $360^\circ$  angle, as shown in Fig. 7.4, this requires 4 scanning iterations by switching between the 4 major sectors A1, A2, A3, and A4 with  $90^\circ$  coverage per sector, this can be done by switching between the antenna array and column by the RF switches, during the scanning process, the phase shifter is disabled, and only one of the antenna columns in the array is enabled to cover the wide  $90^\circ$  angle scanning. The illustration of the sector scanning is presented in Fig. 7.4, for example, the pre-configurable antenna with sector coverage A1, A2, A3, and A4 is scanning for the coarse direction of the target that is located at the right side of the antenna, the beamforming frontend will regularly switch its listening sector

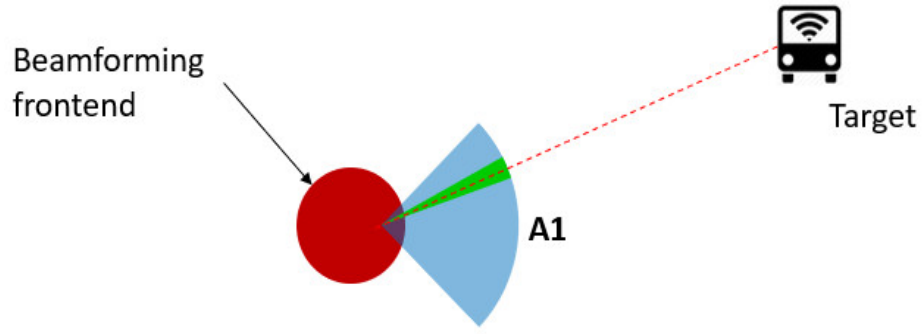
between A1 to A4 and listen to the signal strength of the targeted device, the targeted sector is locked when the receiver signal strength is the highest. Once the sector is determined, the beamforming will proceed to determine the fine direction of the target via the direction-finding method.



**Fig. 7.4** Sector scanning to detect the coarse direction of the target.

### 7.3.2 Direction-Finding

The next step is to focus on the particular antenna array sector to estimate the actual direction of the targeted client, refer to Fig. 7.5, for example, the target is located around sector A1, during the direction-finding process, all the 4 column elements C1, C2, C3, and C4 on array A1 is activated with respective phase differences to generate the antenna beam within the 90° array. It takes up to 4 iterations to determine the target in the 25° beam by scanning in 25° step over the 90° area, and additional 5 iterations can be added to finetune the scanning resolution to 5° by scanning the targeted 25° area in 5° step. With this, the actual direction of the target can be determined in the angular resolution of 25° or 5° depends on the number of iterations. Once the direction-finding is done, the antenna beamforming can be activated with respective beamforming weights to focus the receiving beam to the target as well as focusing the transmitting power in a narrow beam towards the target.



**Fig. 7.5** Direction- finding to identify the fine direction of the target.

## 7.4 Comparison with the State-of-the-art Antennas

- i) This section summarizes the pre-configurable antenna performance by comparing the key performance parameters with the similar 360° steering capability in the 802.11ac application field taking into consideration the application scenarios as elaborated earlier in Fig. 2.5. The comparison result can be found in Table 7.2.

**Table 7.2** Comparison between the proposed antenna system and the state-of-the-art beamforming antenna.

|   | [17]                     | [19]                                       | This work                          |
|---|--------------------------|--|------------------------------------|
| Type of Array Element                                 | Electro-magnetic Bandgap | Circular Patch with Six Parasitic Elements | Dual Substrate Capacitive Feed MPA |
| Number of Arrays                                      | 12                       | 6  | 4                                  |
| Operating Frequency (GHz)                             | 5.180 – 5.825            | 5.100 – 5.900                              | 4.900 – 5.900                      |
| Antenna Array Gain (dBi)                              | 12.0                     | 10.0                                       | 14.4 – 17.3                        |
| Azimuth Beamwidth                                     | 30.0°                    | 42.0°                                      | 27.5° – 31.5°                      |
| Beam Steering Method                                  | PIN Diode                | PIN diode                                  | SP4T and Phase Shifter             |
| Beam Steering Resolution                              | 30°                      | 60°  | Minimum 2°                         |
| Sidelobe Level (dB)<br>(from antenna radiation graph) | - 6.0 – -12.0            | -7.0                                       | -9.8 – -13.3                       |

## 7.5 Summary

The proposed antenna arrays and T/R modules were integrated into the pre-configurable smart antenna system. Both gain and coverage sectors can be pre-configured

before deployment, the pre-configuration method has been elaborated in detail. The advantages of the proposed pre-configurable antenna system over the state-of-the-art antenna systems are highlighted below,

- ii) **Wide operating band**, is realized by multiple substrate structure that enables the wide operating bandwidth, the proposed design covers the entire 4.9 – 5.9 GHz which include the 5 GHz unlicensed band and licensed band at 4.9 GHz,
- iii) **Novel array structure**, that radiated power are combined and concentrated in a small beamwidth that effectively improved the antenna gain to 14.38 to 17.25 dBi compared to 10 and 12 dBi, that makes it more suitable for long-range application such as transportation environment,
- iv) **Flexible beam steering capability**, dedicated phase shifter for each RF chain, and each sector is powered by 4 units of RF chains with the phase of each chain can be independently set,
- v) **Pre-configurable gain**, the gain of the antenna system can be pre-configured before it is installed, where the low, middle, and high gain arrays with different gain can be pre-selected and built into the 360° beamforming system.
- vi) **Pre-configurable sector**, the flexible structure can be pre-configured to 90°, 180°, 270°, and 360° coverage with each sector cover 90°.
- vii) **Fine beam steering angle**, the 6-bit digital phase shifter with 5.625° phase resolution enable the lowest beam resolution of 2°. The beamforming accuracy is improved with the fine beam steering resolution.

# 8 Future Directions of Beamforming System

## 8.1 Future Directions

The evolution of smart antenna system will not end here, the future direction of the smart antenna system is expected to emerge further with the aid of IoT sensors which have been widely available in the automotive vehicles. The concept of the sensors aided beamforming smart antenna system was presented in this thesis, combined with the IoT sensors, the technique is expected to speed up the computation of the direction of arrival (DOA) and lower the smart antenna deployment cost.

The advancement of internet of the things (IoT) has enabled the various type of sensors onboard the vehicles, the most relevant automotive sensors are GPS, accelerometer, gyroscope, and magnetometer, which can be easily integrated into communication gateway or being commercially available as off the shelf standalone module. Such sensors may already be available in many of the vehicles in the public transportation sector. The application of the sensors is not simply providing the raw data, it is combined through sensor fusion to produce the data in other forms that are more accurate and targeted to perform more tasks. The technique has been presented in the 2020 International Conference on UK-China Emerging Technologies (UCET), Glasgow, United Kingdom [102].

Over the years, many applications have benefited from sensor fusion technology. A study report on sensor fusion utilizations in healthcare was presented in [103], the paper provides a survey on different multi-sensor fusion techniques in IoT for healthcare, including their requirement and applications, fusion techniques were discussed such as fuzzy logic-based, Bayesian-based, Markov process-based, and Dempster-Shafer theory-based. The IoT sensor fusion in intelligent agriculture system [104] has been reported, regression trees method was used on the 8 different data related to light, temperature, humidity, rain, soil moisture, atmospheric pressure, air quality, and dew point were collected and the study was done to reduce the number of sensors by sensor fusion. For driving assistance or autonomous vehicles [105], the safety of future autonomous vehicles was discussed that includes the

---

*This chapter is reproduced from paper #4 in the publication list on page iv, where the thesis author is the main author in this paper.*

problem when the sensors data were shared between the vehicles [106], and the adaptive cruise control (ACC) system by utilizing cloud and sensor fusion by adaptive Kalman filter. Another application, the sensor fusion for indoor air quality monitoring [107] was implemented by using the fractional-order modelling and control (FOMCON) toolbox providing overall air quality alerts promptly for accurate prediction with enhanced performance against measurement noise and non-linearity. Sensor fusion was also utilized in the smart city for public space monitoring with IoT sensors [108], a data processing module was developed to capture public space utilization with a renewable wireless sensor network (RWSN) platform using pyroelectric infrared (PIR) and analogue sound sensor to monitor the public space utilization. In the mobile robot localization [109], data from various sensors such as accelerometers, gyroscopes, and low-cost encoders were combined to determine the continuous and accurate location of the mobile robots. To the best of our knowledge, there has been no research report so far concerning the usage of IoT sensors in the beamforming antenna system.

In this section, I am conducting a sensor aided beamforming antenna system study in the practical vehicular environment aimed to validate the alternative method to realize the beamforming antenna feature. A beamforming antenna is an electrically steerable antenna that concentrates its beam towards the interest direction and nulls off other direction, beamforming is a well-known technique to overcome the air space congestion and wireless interference in the wireless system. Combining the raw data from the onboard sensors such as GPS, accelerometer, gyroscope, odometer, BLE with sensor fusion to provide the accurate location, speed, and heading of the mobile client that can be used to perform the beam angle calculation.

### **8.1.1 The Concept of Sensor Aided Beamforming**

Considering the operation of the public buses and trains, the servicing routes for the buses are fixed according to their service map, similar to a train, where the rail tracks are fixed, and the trains always follow the dedicated route when in operation. This is one of the advantages that smart beamforming antenna designers can leverage on. With the fixed geographical location of the wireless infrastructure, and the fix location of the equipment being mounted in the vehicles, as well as the predetermined direction and route of the vehicle on the move, we can combine the information gathered from the onboard sensors such as GPS, accelerometer, gyroscope, odometer, and BLE, utilizing the sensors fusion method by combining the sensory data with the native beamforming algorithm to produce the

beamforming direction between the base stations and the mobile clients. This method is also set to reduce the complexity and processing effort of the native beamforming algorithm when combined with the sensor fusion.

GPS is the most common sensor in the vehicular industry, it received signal from multiple satellites and provide the useful positioning data, utilizing the simple and matured specification called National Marine Electronics Association, NMEA-0183 to communicate with the host processor. The protocol provides the geographical position of the receiver such as longitude, latitude, and altitude, as well as time, speed, and heading information. It is widely used in vehicle positioning and navigation-related applications.

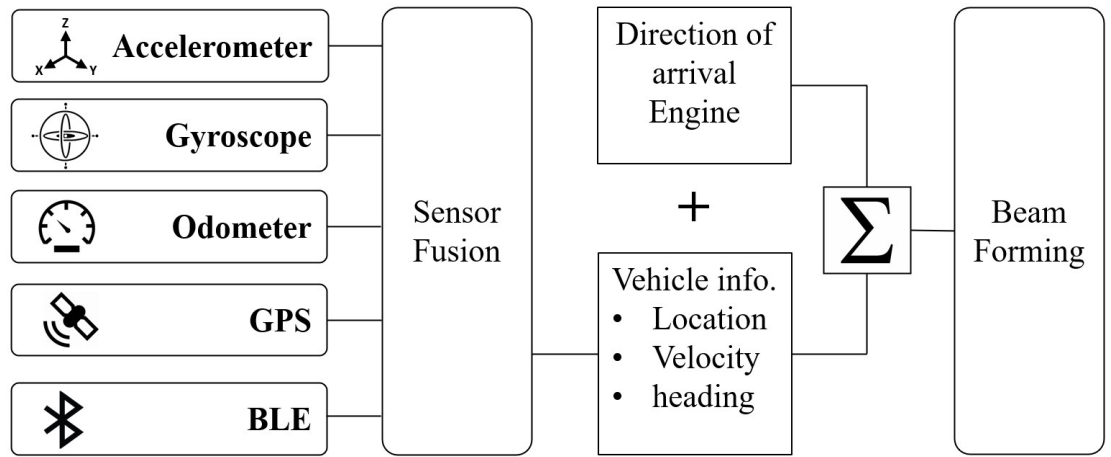
When the vehicle is moving into the underground tunnel for a short instance of time where it lost the GPS signal, the Dead Reckoning (DR) feature [110] can recover the navigation data with the aid of other sensors such as accelerometer, gyroscope, and odometer. The accelerometer detects the acceleration of the vehicle, the acceleration can be converted to velocity, micro-electro-mechanical systems (MEMS) accelerometer is the most used accelerometer in electronic devices. The gyroscope sensor is to measure the rotational angle of the moving vehicle, the deviation of the vehicle from its original orientation can be calculated. The odometer is used to measure the distance travelled by the vehicle. Most of the vehicles already have some of the sensors integrated into the vehicle's control system, the sensors information can be retrieved via the controller area network (CAN bus) interface.

### **8.1.2 Sensor Aided Beamforming System**

The vehicle is pre-loaded with a map that includes the geographical location of all the access points (AP) installed as the roadside infrastructure. When the vehicle is on the move, the sensors data is collected and through the aids of sensor fusion to produce the vehicle information such as location, speed, time, and heading, with the known location of the AP, the system can determine which AP the vehicle should connect to and at what angle the beamforming antenna should concentrate its beam to have the optimum point to point connections. When the vehicle is passed the AP, the system can predict which is the next AP and its location for the moving vehicle to roam to, while the mobile client prepared to roam over, the beamforming engine will dynamically steer its beam towards the targeted AP. The location and heading information of the moving vehicle are transmitted to the backend, the back end will use this information to determine the location and direction of the mobile vehicle with respect to the AP that is serving the connection and steers its beam toward to vehicle.

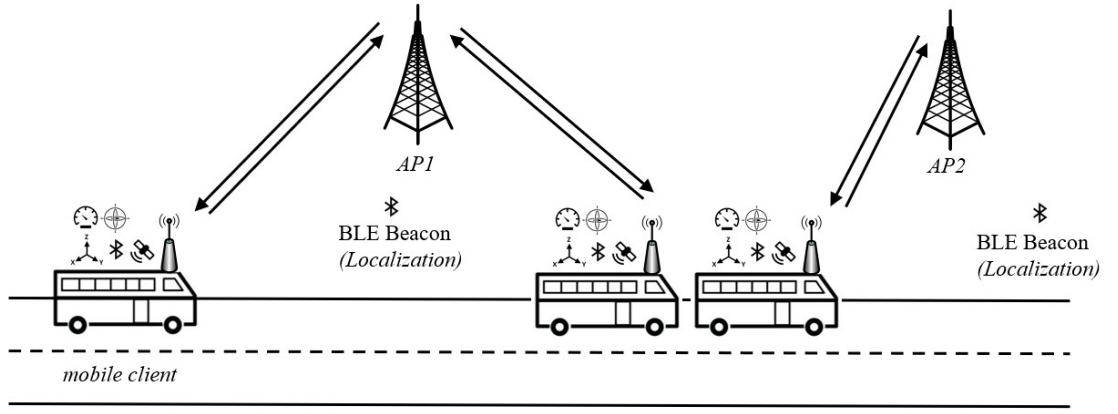


The sensors aided beamforming diagram that combined with the light direction of arrival (DOA) engine of the next generation beamforming system is presented in Fig. 8.1. With this hybrid approach by combining the sensor fusion output with the light computation output from the DOA engine, it can further improve the accuracy of the beam steering compare to the method with DOA itself. Furthermore, the existence of sensor data will reduce the processing complexity of the DOA engine, hence reducing the processing power of the DOA module.



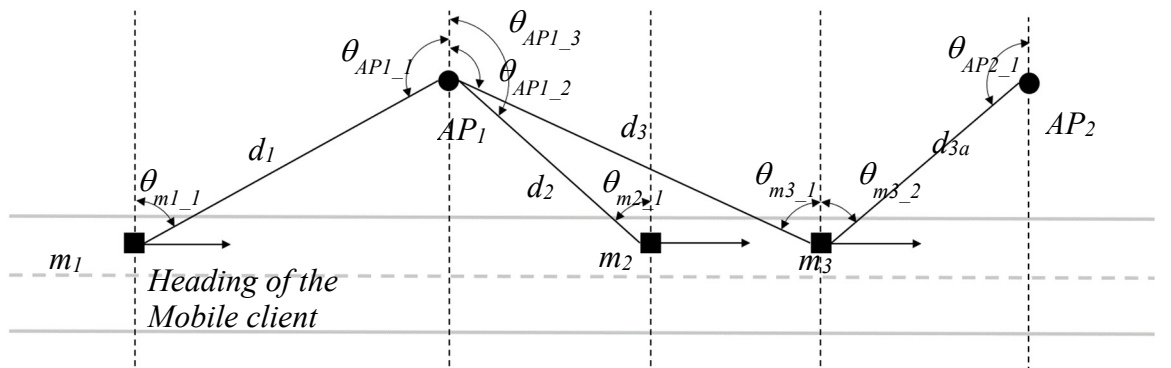
**Fig. 8.1** Combination of sensor fusion and light direction of arrival for future beamforming antenna system

The illustrations of the IoT sensors aided beamforming system is presented in Fig. 8.2. The mobile client is installed with IoT sensors and wirelessly connected to the roadside infrastructure via the smart antenna system. The localization BLE beacon is installed along the roadside to provide additional location information to improve the location accuracy of the mobile client. We would like to discuss 2 operation scenarios in this setup, i) with reliable GPS data, for example, clear sky and, ii) when GPS signal is not available such as the vehicle is inside the tunnels or its moving in the urban area with high rise building where reliable GPS signal is limited.



**Fig. 8.2** Operation scenario of the IoT sensors aided beamforming system.

For scenario i) operation with reliable GPS data, the APs that are permanently mounted at the roadside are with known geographical coordinates and the mobile clients can obtain their location information from the on-board GPS receiver. The 2 APs are located at the location  $AP_1$  and  $AP_2$  to provide communication for the passing vehicles, the vehicle with wireless mobile clients and GPS receiver installed is moving along the road heading to the right, the mobile client will roam from  $AP_1$  and  $AP_2$ , and  $m_1$ ,  $m_2$ , and  $m_3$  are the locations of the mobile client along the road. The top view of this operation scenario can be represented as a diagram in Fig. 8.3.  $\theta_m$  and  $\theta_{AP}$  are the bearings between the mobile client and the AP reference to the north,  $d$  is the actual distance between the mobile client and the AP while the mobile client is on the move.



**Fig. 8.3** Top view of the sensors aided beamforming system.

With the longitude and latitude of both AP and mobile client are known, the distance and bearing between the 2 points can be calculated [111]. The distance,  $d$  between point 1 and point 2 can be calculated using formula (8.1).

$$d = \text{acos}(\sin Lat1 \times \sin Lat2 + \cos Lat1 \times \cos Lat2 \times \cos(Lon2 - Lon1)) \times R \quad (8.1)$$

The bearing,  $be$  from point 1 to point 2 can be calculated using formula (8.2) to (8.4),

$$x = \cos Lat1 \times \sin Lat2 - \sin Lat1 \times \cos Lat2 \times \cos(Lon2 - Lon1) \quad (8.2)$$

$$y = \sin(Lon2 - Lon1) \times \cos Lat2 \quad (8.3)$$

$$be = \text{atan2}(x, y) \quad (8.4)$$

Where  $R$  is the radius of the earth (6,371 kilometers),  $d$  is the distance between 2 points in kilometers and  $be$  is the bearing from point 1 to point 2 in degree ( $0^\circ$  means heading north, the positive value represents clockwise from the north and the negative value means counterclockwise from the north),  $Latn$  and  $Lon n$  are the latitude and longitude of point  $n$  in radians.

The antenna beam direction of the mobile client,  $\theta_m$  ( $0^\circ$  denotes pointing towards the front of the mobile client) and AP,  $\theta_{AP}$  ( $0^\circ$  denote pointing to the north) can be calculated using formula (8.5) and (8.6) as shown below,

$$\theta_m = be - \text{mobile heading} \quad (8.5)$$

$$\theta_{AP} = 180^\circ - be \quad (8.6)$$

Knowing the heading of the mobile client and the bearing between the mobile client and the AP, we can determine the direction of the antenna beam, hence the antenna beam for the mobile client and the AP can be steered towards each other. The distance between the mobile client and APs are constantly monitored, to ensure it is always connected to the nearest AP, when the next AP is nearer than the current AP, the mobile client will prepare to roam over and hand over the beamforming coordination to the next nearest AP.

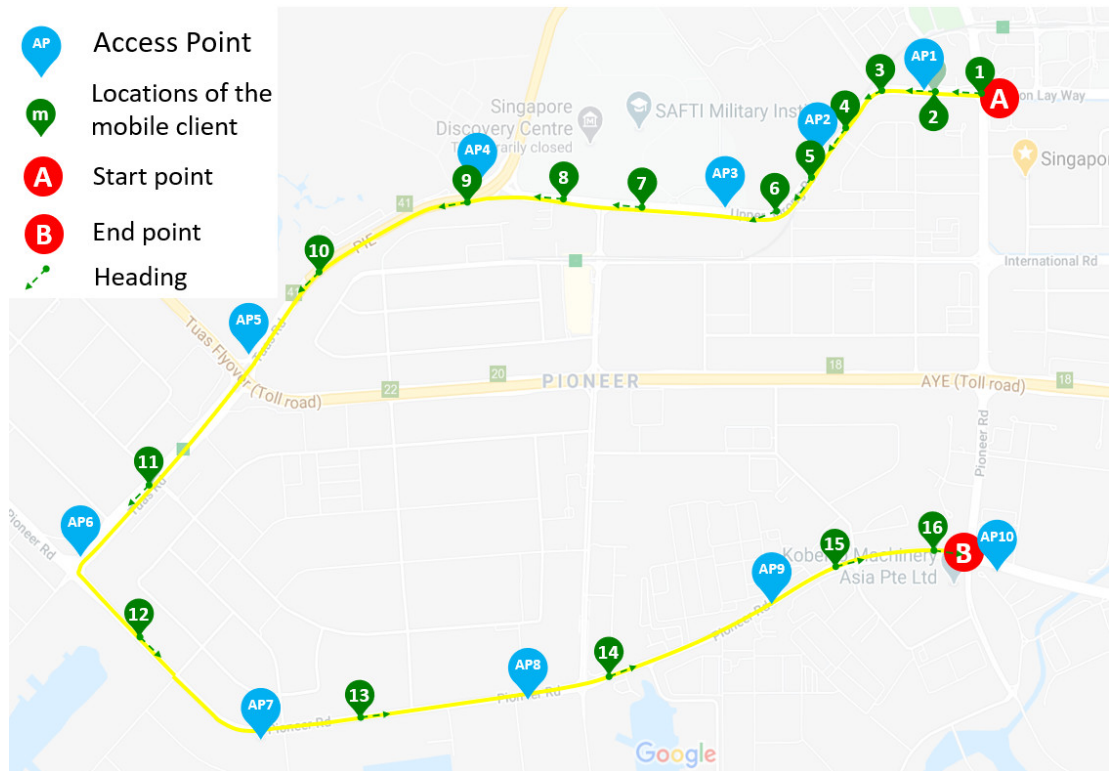
For scenario ii) where there is limited or no GPS signal coverage, the onboard IoT sensors will come to play. When the mobile terminal is moved away from the GPS coverage zone, it will make use of the last GPS fixed location with the help of DR via sensors fusion to perform the data interpolation and progressively determine the current location, speed, and heading of the mobile client, following the same approach as described earlier, the beam

steering direction can be calculated. Due to the location and heading information were obtained via interpolation from the last GPS fix and sensors fusion, the accuracy of the location and heading tend to deteriorate over time, to overcome this, the BLE beacons can be installed at the fixed locations such and lamp poles and bus stops along the stretch of road where the GPS reception is poor. Each beacon will have known coordinates, when the mobile client associate with the roadside beacon, it can reposition itself and offset the accumulated location error.

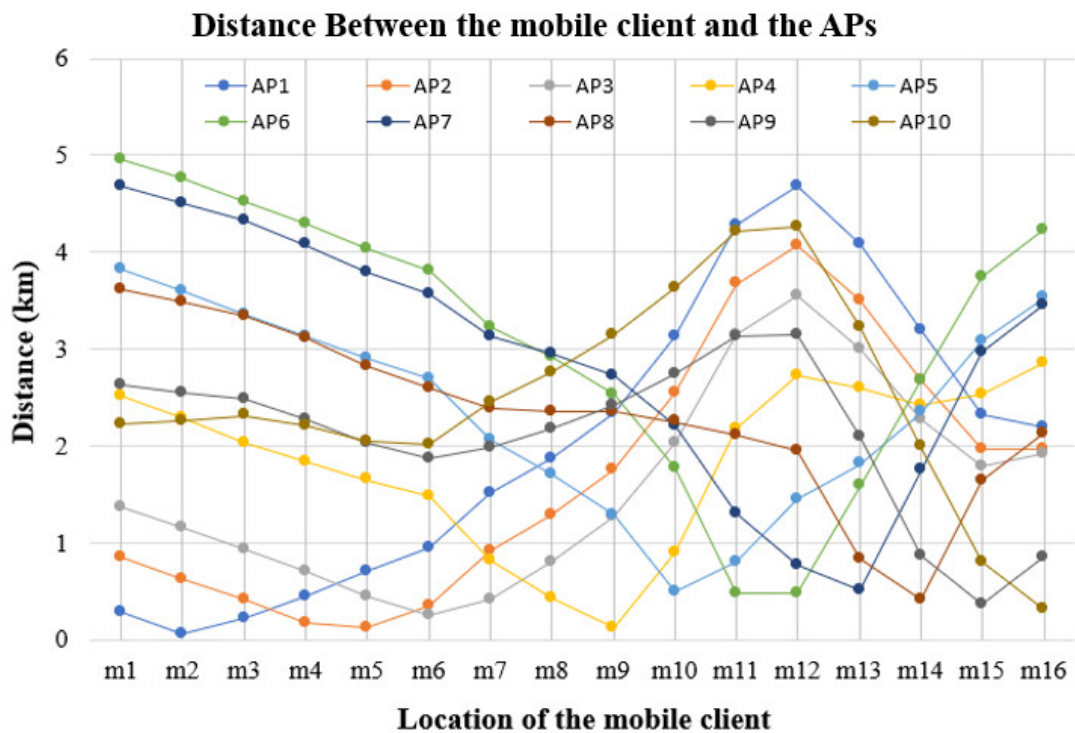
### 8.1.3 Simulation Result and Discussion

The beamforming angles and roaming between the APs and the mobile client are simulated on a sample route in Singapore around the Pan Island Expressway and Pioneer Road. 10 numbers of APs are plotted in blue waypoints, and the mobile client moves through the 16 numbers of green waypoints from point A to B. The simulated heading directions of the mobile client are indicated by the dotted green arrows as illustrated in Fig. 8.4.

When the mobile client travels from point A to point B, it will track and roam to the nearest AP. The distances between the APs and the mobile client at different waypoints are calculated using formula (8.1) and the results are shown in Fig. 8.5, the mobile client always connected to the nearest AP, in this case, the mobile client at location  $m_1$ ,  $m_2$  and  $m_3$  are connected to  $AP_1$ , and it will roam to  $AP_2$  when it moves to locations  $m_4$  and  $m_5$  and so on.

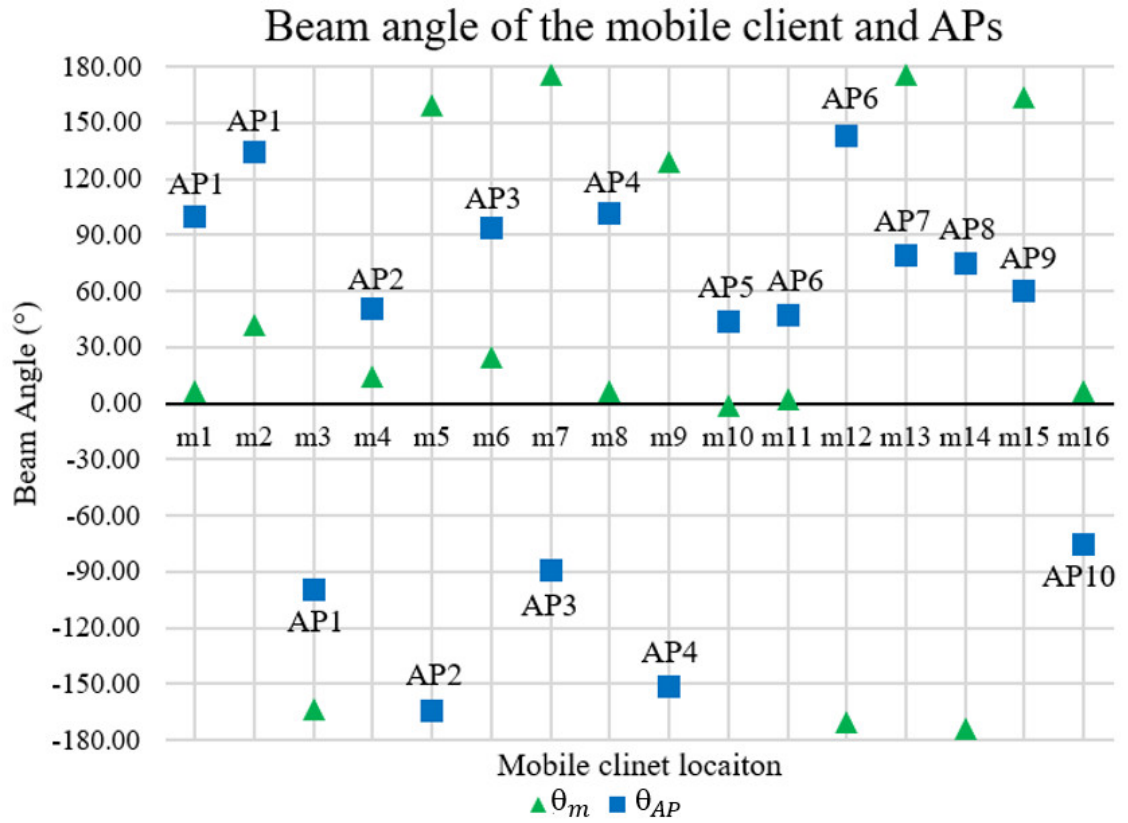


**Fig. 8.4** Access Points (blue) and mobile waypoints (green) for beamforming simulation.



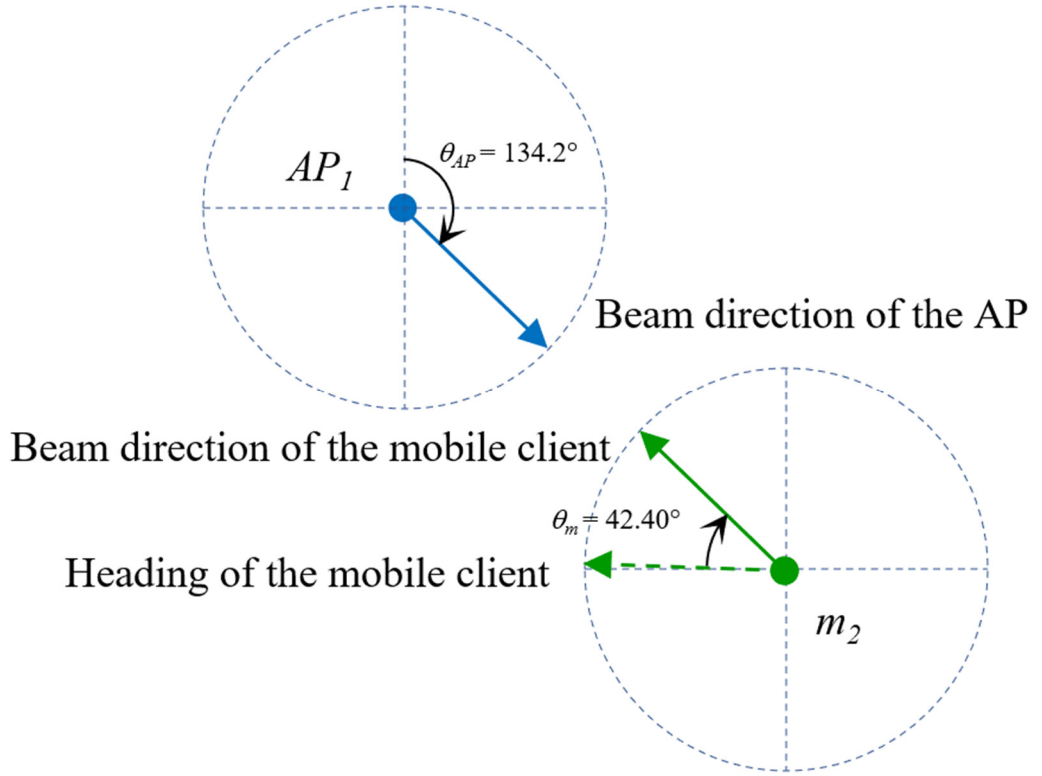
**Fig. 8.5** Distance between the mobile client and the Access points, to demonstrate the nearest AP that the mobile client is connected to while it is moving from point A to B.

The next chart indicates the calculated beamforming angle for the APs and mobile clients. When the mobile client travels from point A to point B, the antenna radiating beam of the mobile client and the APs will steer dynamically to each other and the beam angle is calculated using formula (8.5) and (8.6), the calculated  $\theta_m$  and  $\theta_{AP}$  when the mobile client is moving from point A to point B and roamed through the APs are plotted in Fig. 8.6.



**Fig. 8.6** Simulated beam angle for the mobile client and Access Points at location  $m_1$  to  $m_{16}$ .

Details of the beamforming direction can be explained using Fig. 8.7, take an example, the mobile client is at location  $m_2$  is moving at  $-88^\circ$  heading and connected to  $AP_1$ , the beam steering angle for the mobile client is  $42.4^\circ$  and  $134.2^\circ$  for the AP. When the client continues to move, the new beam angle for the mobile client and AP are calculated on the fly using the instant location of the mobile client.



**Fig. 8.7** Beamforming at location  $m_2$  where the mobile client is connected to  $AP_1$ .

The study results have proofed that the sensors aided with GPS positioning data can determine the correct angle for the antenna beam in the smart antenna system. The estimated cost for a GPS module from Quectel [112], P/N: L26-DR with built-in accelerometer, gyroscope, and wheel tick input is around U\$10, and the commercial BLE module is cost around U\$8 to U\$10 compared to the FPGA with a price tag around U\$200 and above. This technique can be deployed in the mobile terminal with lower processing power due to limited power source such as in the vehicular environment, the proposed method includes the lower-cost and faster estimation of the angle for the main beam between the mobile client and AP, the angle can be used alone or as an initial estimate to guide the DOA estimation and interference nulling.

## 9 Conclusions

The adoption of wireless communication media in the transportation sector is an unstoppable phenomenon simply due to the raising of commuter's expectation in term of internet connectivity and infotainment. The demand is expected to multiply with the recent government initiative in IoT activities. The spectrum regulator such as FCC continues to explore the possibility to allocate more frequency spectrum for unlicensed usage, however, the air space congestion issue persists due to the overwhelming demand in the wireless communications. Therefore, the research and development in the smart antenna area remains important until wireless communication can be replaced by another destructive technology that will change the wireless game entirely.

In wireless infrastructure deployment, CAPEX and OPEX are the main consideration by the stakeholder for the quickest return of investment (ROI). In this thesis, it was concluded that there is significant cost-benefit gained via practical approach and by taking advantage of the operation scenarios in the public transportation environment. It is worth considering the same approach for other types of wireless applications in transportation-related areas, such as car sharing, mobile surveillance systems, and future autonomous vehicles and robotic. The innovation in the smart antenna will continue to emerge via the similar approach by leveraging on the application scenarios instead of just focus on the smart antenna itself.

The initial study in this work provides a good overview of the practical usage scenarios and deployment know-hows that are related to the challenging field environment in the transportation area, that includes methods to ensure the robustness of the system and mitigations to overcome the challenging issues encountered in the field. The study results have motivated and set the research direction towards developing a field-friendly pre-configurable smart antenna system that is able to overcome various challenges experienced by the existing infrastructures.

A novel modern pre-configurable smart antenna system has been proposed, that consists of the  $1 \times 4$ ,  $2 \times 4$ , and  $4 \times 4$  elements for the pre-configurable gain that can be pre-configured into the smart antenna to supports coverage area of  $90^\circ$ ,  $180^\circ$ ,  $270^\circ$ , and  $360^\circ$ . The built-in beamforming feature that operates in a narrow beamwidth can be activated to support the beamforming within each  $90^\circ$  sector. A low-cost T/R module was developed and integrated into the smart antenna system to achieve the full functionality of the beamforming antenna system.



The proposed arrays delivered the gain of 11.26 dBi, 14.59 dBi, and 17.25 dBi for the  $1 \times 4$ ,  $2 \times 4$ , and  $4 \times 4$  array respectively with superior sidelobe level of -17.54 dB, -15.23 dB, and -13.79 dB for the respective low, middle and high gain antenna arrays. All the arrays exhibit the beamwidth of around  $25^\circ$  and are capable of beam steering within the  $\pm 45^\circ$  sector.

The proposed low-cost T/R module together with the recursive calibration approach can achieve  $\pm 1^\circ$  phase error and  $\pm 0.2$  dB amplitude error. The sidelobe level of the  $4 \times 4$  array is further reduced by adopting the amplitude distribution technique, the sidelobe level improvement of 11.1 dB and 5.27 dB respectively were observed at  $\pm 20^\circ$  and  $\pm 40^\circ$ . The T/R module is expected to cost around U\$85.30 for the mass volume price.

The proposed pre-configurable smart antenna system has the advantages over the state-of-the-art  $360^\circ$  smart antenna system such as i) wider operating band, (4.9 – 5.9 GHz), ii) more flexible beam steering capability (the phase of each T/R chain can be independently set), iii) pre-configurable gain (low, middle, and high gain), iv) pre-configurable sector ( $90^\circ$ ,  $180^\circ$ ,  $270^\circ$ , and  $360^\circ$ ), and v) finer beam steering angle (powered by the 6-bit digital phase shifter with  $5.625^\circ$  phase resolution).

For future research direction, it would be interesting if we consider a combination of techniques from different technology that makes the smart antenna even smarter and more reliable. In section 8, the sensor aided beamforming smart antenna system has been presented, the technique makes use of various commercially available IoT sensors to produce the sensor fusion output. The sensor fusion results can be integrated into the beamforming algorithm to produce a more reliable and less complex beamforming system. This technique provides cost-saving by reducing the system complexity, there is no doubt that the new smart antenna system can align its path and make its contribution to the smart antenna industry.

For future work, the sensor aided beamforming system together with the pre-configurable smart antenna system can be combined with the ML or AI engines, and big data such as sensors and beamforming data can be analysed to provide predictive beamforming estimation as well as improving the beamforming accuracy. Eventually, the smart antenna will continue to get smarter.

# Bibliography

- [1] 4.9 GHz Licensed Public Safety Spectrum. Available at: <https://www.fcc.gov/49-ghz-public-safety-spectrum>, [Access 11 January 2021].
- [2] Unlicensed Spectrum. Available at: <https://spectrum.ieee.org/computing/it/unlicensed-spectrum-may-be-critical-to-5g>, [Access 11 January 2021].
- [3] Masson É., Berbineau M, (2017) Railway Operators Needs in Terms of Wireless Communications. In *Broadband Wireless Communications for Railway Applications. Studies in Systems, Decision and Control*, vol 82. Springer, Cham.
- [4] W. Chen (2015) Vehicular Communications and Networks, Architectures, Protocols, Operation and Deployment, Woodhead.
- [5] F. Hu, (2018) Vehicle-to-Vehicle and Vehicle-to-Infrastructure Communications, A Technical Approach, Taylor & Grancis.
- [6] K. Zheng, Q. Zheng, P. Chatzimisios, W. Xiang and Y. Zhou, "Heterogeneous Vehicular Networking: A Survey on Architecture, Challenges, and Solutions," in *IEEE Communications Surveys & Tutorials*, vol. 17, no. 4, pp. 2377-2396, Fourthquarter 2015, doi: 10.1109/COMST.2015.2440103.
- [7] V. Kone, H. Zheng, A. Rowstron, G. O'Shea and B. Y. Zhao, "Measurement-Based Design of Roadside Content Delivery Systems," in *IEEE Transactions on Mobile Computing*, vol. 12, no. 6, pp. 1160-1173, June 2013, doi: 10.1109/TMC.2012.90.
- [8] E. Belyaev, A. Vinel, A. Surak, M. Gabbouj, M. Jonsson and K. Egiazarian, "Robust Vehicle-to-Infrastructure Video Transmission for Road Surveillance Applications," in *IEEE Transactions on Vehicular Technology*, vol. 64, no. 7, pp. 2991-3003, July 2015, doi: 10.1109/TVT.2014.2354376.
- [9] J. Heo, B. Kang, J. M. Yang, J. Paek and S. Bahk, "Performance-Cost Tradeoff of Using Mobile Roadside Units for V2X Communication," in *IEEE Transactions on Vehicular Technology*, vol. 68, no. 9, pp. 9049-9059, Sept. 2019, doi: 10.1109/TVT.2019.2925849.

- [10] M. C. Tan, M. Li, Q. H. Abbasi and M. Imran, "A smart and low-cost enhanced antenna system for industrial wireless broadband communication," *12th European Conference on Antennas and Propagation (EuCAP 2018)*, London, 2018, pp. 1-4, doi: 10.1049/cp.2018.1218.
- [11] A. Ghasemi, A. Abedi, F. Ghasemi, "Introduction to radiowaves propagation," in *Propagation Engineering in Radio Links Design*, New York, USA, Springer, 2013, ch.1, sec. 1.10.1, pp. 26-27.
- [12] A Ogunsola and A. Mariscotti. (2013) Railway Operators Needs in Terms of Wireless Communications, In *Electromagnetic Compatibility in Railways, Analysis and Management*, vol 168. Springer Science & Business Media.
- [13] IEC 61373:2010 European Standards. Available at: <https://www.en-standard.eu/iec-61373-2010-railway-applications-rolling-stock-equipment-shock-and-vibration-tests/> [Access 11 January 2021].
- [14] smartpres1.pdf (2006). Development of Smart Antenna Technology. [online] Available at: [https://www.ofcom.org.uk/data/assets/pdf\\_file/0014/36014/smartpres1.pdf](https://www.ofcom.org.uk/data/assets/pdf_file/0014/36014/smartpres1.pdf) [Access 29 May 2020].
- [15] GAO-15-775. Vehicle-to-Infrastructure Technologies Expected to Offer Benefits, but Deployment Challenges Exist. [online] Available at: <https://www.gao.gov/assets/680/672548.pdf> [Access 15 Jan 2021].
- [16] C. Gu et al., "Compact smart antenna with electronic beam-switching and reconfigurable polarizations," in *IEEE Trans. Antennas Propag.*, vol. 63, no. 12, pp. 5325-5333, Oct. 2015, doi: 10.1109/TAP.2015.2490239.
- [17] H. Boutayeb, P. R. Watson, W. Lu, and T. Wu, "Beam switching dual polarized antenna array with reconfigurable radial waveguide power dividers," in *IEEE Trans. Antennas Propag.*, vol. 65, no. 4, pp. 1807–1814, Nov. 2016, doi: 10.1109/TAP.2016.2629469.
- [18] Y. Y. Lin, C. L. Liao, T. H. Hsieh, W. J. Liao, "A novel beam switching array antenna using series-fed slots with PIN diodes," in *IEEE Antennas and Wireless Propagation Letters*, vol. 16, pp. 1393 – 1396, Dec. 2016, doi: 10.1109/LAWP.2016.2639046

- [19] Y. Yang, X. Zhu, "A wideband reconfigurable antenna with 360° beam-steering for 802.11ac WLAN applications," in *IEEE Trans. Antennas Propag.*, vol. 66, no. 2, pp. 600-608, Dec. 2017, doi: 10.1109/TAP.2017.2784438.
- [20] H. Liu, S. Gao and T. H. Loh, "Compact Dual-Band Antenna With Electronic Beam-Steering and Beamforming Capability," in *IEEE Antennas and Wireless Propagation Letters*, vol. 10, pp. 1349-1352, 2011, doi: 10.1109/LAWP.2011.2177059.7115909.
- [21] H. Liu, S. Gao and T. Loh, "Small Director Array for Low-Profile Smart Antennas Achieving Higher Gain," in *IEEE Transactions on Antennas and Propagation*, vol. 61, no. 1, pp. 162-168, Jan. 2013, doi: 10.1109/TAP.2012.2219841.
- [22] A. Narbudowicz, M. J. Ammann and D. Heberling, "Switchless Reconfigurable Antenna With 360° Steering," in *IEEE Antennas and Wireless Propagation Letters*, vol. 15, pp. 1689-1692, 2016, doi: 10.1109/LAWP.2016.2524199.
- [23] S. Krishna, G. Mishra and S. K. Sharma, "A series fed planar microstrip patch array antenna with 1D beam steering for 5G spectrum massive MIMO applications," *2018 IEEE Radio and Wireless Symposium (RWS)*, Anaheim, CA, 2018, pp. 209-212, doi: 10.1109/RWS.2018.8304989.
- [24] C. A. Balanis, "Microstrip and mobile communications antennas," in *Antenna theory analysis and design*, 4<sup>th</sup> ed., Hoboken, New Jersey, USA: John Wiley & Sons, Inc., 2016, ch.14, sec. 14.2, pp. 788-823.
- [25] G. Giunta, C. Novi, S. Maddio, G. Pelosi, M. Righini and S. Selleri, "Efficient tolerance analysis on a low cost, compact size, wideband multilayer patch antenna," *2017 IEEE International Symposium on Antennas and Propagation & USNC/URSI National Radio Science Meeting*, San Diego, CA, 2017, pp. 2113-2114, doi: 10.1109/APUSNCURSINRSM.2017.8073099.
- [26] R. Gupta and M. Kumar, "Bandwidth Enhancement of Microstrip Patch Antennas by Implementing Circular Unit Cells in Circular Pattern," *2013 5th International Conference and Computational Intelligence and Communication Networks*, Mathura, 2013, pp. 10-13, doi: 10.1109/CICN.2013.11.
- [27] K. Mondal, L. Murmu and P. P. Sarkar, "Investigation on compactness, bandwidth and gain of circular microstrip patch antenna," *2017 Devices for Integrated Circuit (DevIC)*, Kalyani, 2017, pp. 742-746, doi: 10.1109/DEVIC.2017.8074050.

- 
- [28] S. N. Ather, R. K. Verma and P. K. Singhal, "Bandwidth Enhancement for Truncated Rectangular Microstrip Antenna Using Stacked Patches and Defected Ground Structure," *2013 5th International Conference and Computational Intelligence and Communication Networks*, Mathura, 2013, pp. 55-60, doi: 10.1109/CICN.2013.21.
- [29] R. R. Selvaraju, M. R. Kamarudin, M. H. Jamaluddin, M. H. Dahri and C. Y. Low, "Compact 4-Element beam steerable printed adaptive array antenna for 5G application," *2016 IEEE Asia-Pacific Conference on Applied Electromagnetics (APACE)*, Langkawi, 2016, pp. 30-33, doi: 10.1109/APACE.2016.7916446.
- [30] Y. Wang, H. Wang and G. Yang, "Design of dipole beam-steering antenna array for 5G handset applications," *2016 Progress in Electromagnetic Research Symposium (PIERS)*, Shanghai, 2016, pp. 2450-2453, doi: 10.1109/PIERS.2016.7735012.
- [31] M. Mantash and T. A. Denidni, "Millimeter-wave beam-steering antenna array for 5G applications," *2017 IEEE 28th Annual International Symposium on Personal, Indoor, and Mobile Radio Communications (PIMRC)*, Montreal, QC, 2017, pp. 1-3, doi: 10.1109/PIMRC.2017.8292713.
- [32] J. Kim, J. Han, J. Park and J. Kim, "Design of phased array antenna for 5G mm-wave beamforming system," *2016 IEEE 5th Asia-Pacific Conference on Antennas and Propagation (APCAP)*, Kaohsiung, 2016, pp. 201-202, doi: 10.1109/APCAP.2016.7843168.
- [33] Y. Wang, L. Zhu, H. Wang, Y. Luo and G. Yang, "A Compact, Scanning Tightly Coupled Dipole Array With Parasitic Strips for Next-Generation Wireless Applications," in *IEEE Antennas and Wireless Propagation Letters*, vol. 17, no. 4, pp. 534-537, April 2018, doi: 10.1109/LAWP.2018.2798660.
- [34] S. A. Aghdam, J. Bagby and R. J. Pla, "Design and development of linear array of rectangular aperture coupled microstrip antennas with application in beamforming," *2016 17th International Symposium on Antenna Technology and Applied Electromagnetics (ANTEM)*, Montreal, QC, 2016, pp. 1-3, doi: 10.1109/ANTEM.2016.7550220.
- [35] V. G. Kasabegoudar, D. S. Upadhyay, K. J. Vinoy, "Design studies of ultra-wideband microstrip antennas with a small capacitive feed," in *International Journal of Antennas and Propagation*, Dec. 2007, doi: 10.1155/2007/67503.

- 
- [36] J. Nasir, M. H. Jamaluddin, M. R. Kamarudin, I. ullah, Y. Lo and R. Selvaraju, "A Four-Element Linear Dielectric Resonator Antenna Array for Beamforming Applications With Compensation of Mutual Coupling," in *IEEE Access*, vol. 4, pp. 6427-6437, 2016, doi: 10.1109/ACCESS.2016.2614334.
- [37] D. Pavithra, P. Ramya, K. R. Dharani and M. R. Devi, "Design of microstrip patch array antenna using beamforming technique for ISM Band," *2013 Fifth International Conference on Advanced Computing (ICoAC)*, Chennai, 2013, pp. 504-507, doi: 10.1109/ICoAC.2013.6922002.
- [38] M. S. R. Bashri, T. Arslan and W. Zhou, "A dual-band linear phased array antenna for WiFi and LTE mobile applications," *2015 Loughborough Antennas & Propagation Conference (LAPC)*, Loughborough, 2015, pp. 1-5, doi: 10.1109/LAPC.2015.7366010.
- [39] C. Cheng, H. Huxie and F. H. Su, "A compact high gain patch antenna array for IEEE 802.11ac MIMO application," *2016 IEEE 5th Asia-Pacific Conference on Antennas and Propagation (APCAP)*, Kaohsiung, 2016, pp. 327-328, doi: 10.1109/APCAP.2016.7843226.
- [40] M. U. Khan and M. S. Sharawi, "A compact 8-element MIMO antenna system for 802.11ac WLAN applications," *2013 International Workshop on Antenna Technology (iWAT)*, Karlsruhe, 2013, pp. 91-94, doi: 10.1109/IWAT.2013.6518306.
- [41] S. A. Nasir, M. Mustaqim and B. A. Khawaja, "Antenna array for 5th generation 802.11ac Wi-Fi applications," *2014 11th Annual High Capacity Optical Networks and Emerging/Enabling Technologies (Photonics for Energy)*, Charlotte, NC, 2014, pp. 20-24, doi: 10.1109/HONET.2014.7029354.
- [42] C. A. Balanis, "Fundamental Parameters and Figures-of-Merit of Antennas," in *Antenna theory analysis and design*, 4th ed., Hoboken, New Jersey, USA: John Wiley & Sons, Inc., 2016, ch.2, sec. 2.2.4, pp. 25-126.
- [43] M. C. Tan, M. Li, Q. H. Abbasi and M. A. Imran, "A Wideband Beamforming Antenna Array for 802.11ac and 4.9 GHz in Modern Transportation Market," in *IEEE Transactions on Vehicular Technology*, vol. 69, no. 3, pp. 2659-2670, March 2020, doi: 10.1109/TVT.2019.2963111.

- [44] M. C. Tan, M. Li, Q. H. Abbasi and M. Imran, "A Wideband Beam forming Antenna Array for 802.11ac and 4.9 GHz," *2019 13th European Conference on Antennas and Propagation (EuCAP)*, Krakow, Poland, 2019, pp. 1-5.
- [45] W. Chen, C. Hsu and F. Chang, "Broadband three-element MIMO antennas for IEEE802.11ac," *2016 IEEE 5th Asia-Pacific Conference on Antennas and Propagation (APCAP)*, Kaohsiung, 2016, pp. 267-268, doi: 10.1109/APCAP.2016.7843200.
- [46] T. Haynes, "A Primer on Digital Beamforming", Spectrum Signal Processing March 26, 1998.
- [47] V. Shtrom, D. T. Milton, W. S. Kish , "Circuit Board having a Peripheral Antenna Apparatus with Selectable Antenna Elements" US Patent 7,193,562 B2, Issued March 20, 2007.
- [48] Y. Lin, C. Liao, T. Hsieh and W. Liao, "A Novel Beam-Switching Array Antenna Using Series-Fed Slots With PIN Diodes," in *IEEE Antennas and Wireless Propagation Letters*, vol. 16, pp. 1393-1396, 2017, doi: 10.1109/LAWP.2016.2639046.
- [49] F. Y. Zulkifli, N. Chasanah, Basari and E. T. Rahardjo, "Design of Butler matrix integrated with antenna array for beam forming," *2015 International Symposium on Antennas and Propagation (ISAP)*, Hobart, TAS, 2015, pp. 1-4.
- [50] M. Fernandes, A. Bhandare, C. Dessai and H. Virani, "A wideband switched beam patch antenna array for LTE and Wi-Fi," *2013 Annual IEEE India Conference (INDICON)*, Mumbai, 2013, pp. 1-6, doi: 10.1109/INDCON.2013.6726150.
- [51] N. T. Pham, Gye-An Lee and F. De Flaviis, "Microstrip antenna array with beamforming network for WLAN applications," *2005 IEEE Antennas and Propagation Society International Symposium*, Washington, DC, 2005, pp. 267-270 vol. 3A, doi: 10.1109/APS.2005.1552232.
- [52] A. M. El-Tager and M. A. Eleiwa, "Design and Implementation of a Smart Antenna Using Butler Matrix for ISM-band", *Progress In Electromagnetics Research Symposium*, Beijing, China, March 23-27, 2009, pp. 571-575.

- [53] H. Liu, S. Gao and T. Loh, "Electrically Small and Low Cost Smart Antenna for Wireless Communication," in *IEEE Transactions on Antennas and Propagation*, vol. 60, no. 3, pp. 1540-1549, March 2012, doi: 10.1109/TAP.2011.2180300.
- [54] Y. Gao, M. Khaliel, F. Zheng and T. Kaiser, "Rotman Lens Based Hybrid Analogue–Digital Beamforming in Massive MIMO Systems: Array Architectures, Beam Selection Algorithms and Experiments," in *IEEE Transactions on Vehicular Technology*, vol. 66, no. 10, pp. 9134-9148, Oct. 2017, doi: 10.1109/TVT.2017.2714693.
- [55] F. Casini, R. V. Gatti, L. Marcaccioli and R. Sorrentino, "A novel design method for Blass matrix beam-forming networks," *2007 European Radar Conference*, Munich, 2007, pp. 232-235, doi: 10.1109/EURAD.2007.4404979.
- [56] D. Digdarsini, M. Kumar and T. V. S. Ram, "Design & hardware realization of FPGA based Digital Beam Forming system," *2016 3rd International Conference on Signal Processing and Integrated Networks (SPIN)*, Noida, 2016, pp. 275-278, doi: 10.1109/SPIN.2016.7566703.
- [57] F. Sohrabi and W. Yu, "Hybrid Digital and Analogue Beamforming Design for Large-Scale Antenna Arrays," in *IEEE Journal of Selected Topics in Signal Processing*, vol. 10, no. 3, pp. 501-513, April 2016, doi: 10.1109/JSTSP.2016.2520912.
- [58] C. A. Balanis, "Arrays and feed networks," in *Antenna Theory Analysis and Design*, 4<sup>th</sup> ed., Hoboken, New Jersey, USA: John Wiley & Sons, Inc., 2016, ch.14, sec. 14.8, pp. 832-837.
- [59] W. ALAN DAVIS, "Microstrip Transmission Line" in *Radio Frequency Circuit Design*, John Wiley & Sons, Inc., Hoboken, New Jersey, 2010, ch.4, sec. 4.8.4, pp. 87-88.
- [60] S. D. Assimonis, T. Samaras, V. Fusco, "Analysis of the microstrip-grid array antenna and proposal of a new high-gain, lowcomplexity and planar long-range WiFi antenna," in *IET Microwaves, Antennas & Propagation*, vol. 12, no. 3, pp. 332-338, Mar. 2018, doi: 10.1049/iet-map.2017.0548.
- [61] 3ds.com. (2019). CST Studio Suite 3D EM simulation and analysis software. [online] Available at: <https://www.3ds.com/products-services/simulia/products/cst-studio-suite/> [Accessed 29 May. 2020].



- 
- [62] M. C. Tan, M. Li, Q. H. Abbasi and M. Imran, "A Flexible Low-Cost Hybrid Beamforming Structure for Practical Beamforming Applications," *2019 IEEE International Symposium on Radio-Frequency Integration Technology (RFIT)*, Nanjing, China, 2019, pp. 1-3, doi: 10.1109/RFIT.2019.8929162.
  - [63] M. C. Tan, M. Li, Q. H. Abbasi and M. Imran, "A Recursive Calibration Approach for Smart Antenna Beamforming Frontend," *2020 14th European Conference on Antennas and Propagation (EuCAP)*, Copenhagen, Denmark, 2020, pp. 1-5, doi: 10.23919/EuCAP48036.2020.9135881.
  - [64] M. C. Tan, M. Li, Q. H. Abbasi and M. A. Imran, "Design and Characterization of T/R Module for Commercial Beamforming Applications," in *IEEE Access*, vol. 8, pp. 130252-130262, 2020, doi: 10.1109/ACCESS.2020.3009531.
  - [65] D. T. R. Liang, M. C. Tan, M. Li, Q. H. Abbasi and M. Imran, "Radome Design with Improved Aerodynamics and Radiation for Smart Antennas in Automotive Applications," *2019 IEEE International Symposium on Radio-Frequency Integration Technology (RFIT)*, Nanjing, China, 2019, pp. 1-3, doi: 10.1109/RFIT.2019.8929217.
  - [66] M. Muhammad, M. Li, Q. H. Abbasi, C. Goh and M. Imran, "Performance Evaluation for Direction of Arrival Estimation Using 4-Element Linear Array," *2019 13th European Conference on Antennas and Propagation (EuCAP)*, Krakow, Poland, 2019, pp. 1-5.
  - [67] M. Muhammad, M. Li, Q. H. Abbasi, C. Goh and M. Imran, "Direction of Arrival Estimation using Root-Transformation Matrix Technique," *2019 IEEE International Symposium on Antennas and Propagation and USNC-URSI Radio Science Meeting*, Atlanta, GA, USA, 2019, pp. 1369-1370, doi: 10.1109/APUSNCURSINRSM.2019.8889249.
  - [68] M. Muhammad, M. Li, Q. H. Abbasi, C. Goh and M. Imran, "Direction of Arrival Estimation Using Hybrid Spatial Cross-Cumulants and Root-MUSIC," *2020 14th European Conference on Antennas and Propagation (EuCAP)*, Copenhagen, Denmark, 2020, pp. 1-5, doi: 10.23919/EuCAP48036.2020.9135813.
  - [69] S. Dai, M. Li, Q. H. Abbasi and M. A. Imran, "A Fast Blocking Matrix Generating Algorithm for Generalized Sidelobe Canceller Beamformer in High Speed Rail Like Scenario," in *IEEE Sensors Journal*, doi: 10.1109/JSEN.2020.3002699.

- 
- [70] S. Dai, M. Li, Q. H. Abbasi and M. Imran, "Hardware Efficient Adaptive Beamformer Based on Cyclic Variable Step Size," *2018 IEEE International Symposium on Antennas and Propagation & USNC/URSI National Radio Science Meeting*, Boston, MA, 2018, pp. 191-192, doi: 10.1109/APUSNCURSINRSM.2018.8608636.
- [71] S. Dai, Q. H. Abbasi, M. Li and M. Imran, "Beamforming Optimization based on Kalman Filter for Vehicle in Constrained Route," *2019 IEEE International Symposium on Antennas and Propagation and USNC-URSI Radio Science Meeting*, Atlanta, GA, USA, 2019, pp. 1365-1366, doi: 10.1109/APUSNCURSINRSM.2019.8888482.
- [72] S. Han, C. I. Z. Xu and C. Rowell, "Large-scale antenna systems with hybrid analogue and digital beamforming for millimeter wave 5G," in *IEEE Communications Magazine*, vol. 53, no. 1, pp. 186-194, January 2015, doi: 10.1109/MCOM.2015.7010533.
- [73] L. Yang, Y. Zeng and R. Zhang, "Wireless Power Transfer With Hybrid Beamforming: How Many RF Chains Do We Need?," in *IEEE Transactions on Wireless Communications*, vol. 17, no. 10, pp. 6972-6984, Oct. 2018, doi: 10.1109/TWC.2018.2865313.
- [74] S. Ahmed, M. Sadek, A. Zekry and H. Elhennawy, "Hybrid analogue and digital beamforming for space-constrained and energy-efficient massive MIMO wireless systems," *2017 40th International Conference on Telecommunications and Signal Processing (TSP)*, Barcelona, 2017, pp. 186-189, doi: 10.1109/TSP.2017.8075965.
- [75] J. S. Herd and M. D. Conway, "The Evolution to Modern Phased Array Architectures," in *Proceedings of the IEEE*, vol. 104, no. 3, pp. 519-529, March 2016, doi: 10.1109/JPROC.2015.2494879.
- [76] M. Oppermann and R. Rieger, "RF modules (Tx-Rx) with multifunctional MMICs," *2017 IMAPS Nordic Conference on Microelectronics Packaging (NordPac)*, Gothenburg, 2017, pp. 57-60, doi: 10.1109/NORDPAC.2017.7993164.
- [77] B. Epstein, R. H. Olsson and K. Bunch, "Arrays at commercial timescales: Addressing development and upgrade costs of phased arrays," *2018 IEEE Radar Conference (RadarConf18)*, Oklahoma City, OK, 2018, pp. 0327-0332, doi: 10.1109/RADAR.2018.8378579.

- [78] W. Wojtasiak, D. Gryglewski, T. Morawski and E. Sedek, "Designing T/R module for active phased array radar," *14th International Conference on Microwaves, Radar and Wireless Communications. MIKON - 2002. Conference Proceedings (IEEE Cat.No.02EX562)*, Gdansk, Poland, 2002, pp. 631-634 vol.2, doi: 10.1109/MIKON.2002.1017924.
- [79] G. M. Rebeiz et al., "Highly dense microwave and millimeter-wave phased array T/R modules and Butler matrices using CMOS and SiGe RFICs," *2010 IEEE International Symposium on Phased Array Systems and Technology*, Waltham, MA, 2010, pp. 245-249, doi: 10.1109/ARRAY.2010.5613364.
- [80] T. Boles, D. J. Carlson and C. Weigand, "MMIC based phased array radar T/R modules," *2011 IEEE International Conference on Microwaves, Communications, Antennas and Electronic Systems (COMCAS 2011)*, Tel Aviv, 2011, pp. 1-4, doi: 10.1109/COMCAS.2011.6105784.
- [81] D. Conway, M. Fosberry, G. Brigham, E. Loew and C. Liu, "On the development of a C-band active array front-end for an airborne polarimetric radar," *2013 IEEE International Symposium on Phased Array Systems and Technology*, Waltham, MA, 2013, pp. 198-201, doi: 10.1109/ARRAY.2013.6731826.
- [82] A. Fina, A. Di Carlofelice and F. De Paulis, "High Power, Thermally Efficient, X-band 3D T/R Module With Calibration Capability for Space Radar," in *IEEE Access*, vol. 6, pp. 60921-60929, 2018, doi: 10.1109/ACCESS.2018.2876011.
- [83] Z. Wang et al., "An improved high-power X-band 4×4 tile-type LTCC T/R module based on liquid cooling micro-channels," *2019 IEEE MTT-S International Microwave Symposium (IMS)*, Boston, MA, USA, 2019, pp. 1042-1045, doi: 10.1109/MWSYM.2019.8701038.
- [84] Y. M. Wu et al., "An X-band Scalable 4×4 Digital Phased Array Module using RF SoC and Antenna-in-Package," *2019 IEEE Radar Conference (RadarConf)*, Boston, MA, USA, 2019, pp. 1-6, doi: 10.1109/RADAR.2019.8835499.
- [85] H. B. Zhang, Z. L. Zhou, S. T. Yu and D. M. Li, "Integrated Antenna-TR Module Design for Millimeter Band Phased-Array," *2018 International Conference on Microwave and Millimeter Wave Technology (ICMMT)*, Chengdu, 2018, pp. 1-3, doi: 10.1109/ICMMT.2018.8563982.

- [86] K. Koh, J. W. May and G. M. Rebeiz, "A Millimeter-Wave (40–45 GHz) 16-Element Phased-Array Transmitter in 0.18- $\mu\text{m}$  SiGe BiCMOS Technology," in *IEEE Journal of Solid-State Circuits*, vol. 44, no. 5, pp. 1498-1509, May 2009, doi: 10.1109/JSSC.2009.2017971.
- [87] H. M. M. Makkawi, "Comparative study of the radiation characteristics between uniform, Tschebyscheff and Binomial amplitude distributions of linear patch antenna array for x-band radar warning receivers," *2017 International Conference on Communication, Control, Computing and Electronics Engineering (ICCCCEE)*, Khartoum, 2017, pp. 1-8, doi: 10.1109/ICCCCEE.2017.7866087.
- [88] A. P. Joubko, N. M. Naumovich and O. A. Yurtsev, "Influence of amplitude distribution within a module and over a system of modules on the pattern of multimodule antenna array," *2015 International Conference on Antenna Theory and Techniques (ICATT)*, Kharkiv, 2015, pp. 1-3, doi: 10.1109/ICATT.2015.7136831.
- [89] D. Vollbracht and G. Michalek, "X-Band phase- and amplitude distribution network for phased array antenna measurements," *2016 10th European Conference on Antennas and Propagation (EuCAP)*, Davos, 2016, pp. 1-5, doi: 10.1109/EuCAP.2016.7481578.
- [90] N. Nakamoto, T. Takahashi, Y. Konishi and I. Chiba, "Phase optimization for accurate beam forming of phased array with element field errors at every phase shift," *2013 IEEE International Symposium on Phased Array Systems and Technology*, Waltham, MA, 2013, pp. 693-697, doi: 10.1109/ARRAY.2013.6731914.
- [91] Q. Fei, Y. Yu, X. Yin, L. Yang and Y. Lu, "Low-cost phase shifter and calibration solution for multi-channel receiver," *2016 IEEE International Conference on Ubiquitous Wireless Broadband (ICUWB)*, Nanjing, 2016, pp. 1-3, doi: 10.1109/ICUWB.2016.7790422.
- [92] M. C. Tan, M. Li, Q. H. Abbasi and M. A. Imran, "A Wideband Beamforming Antenna Array for 802.11ac and 4.9 GHz in Modern Transportation Market," in *IEEE Transactions on Vehicular Technology*, vol. 69, no. 3, pp. 2659-2670, March 2020, doi: 10.1109/TVT.2019.2963111.

- [93] C. A. Balanis, "Smart antennas," in *Antenna theory analysis and design*, 4<sup>th</sup> ed., Hoboken, New Jersey, USA: John Wiley & Sons, Inc., 2016, ch.16, sec. 16.8, pp. 946-959.
- [94] M. C. Tan, M. Li, Q. H. Abbasi and M. Imran, "A Flexible Low-Cost Hybrid Beamforming Structure for Practical Beamforming Applications," *2019 IEEE International Symposium on Radio-Frequency Integration Technology (RFIT)*, Nanjing, China, 2019, pp. 1-3, doi: 10.1109/RFIT.2019.8929162.
- [95] ADI HMC1133LP5E GaAs MMIC 6-BIT Digital Phase Shifter, 4.8 - 6.2 GHz datasheet. [Online] Available at: <https://www.analogue.com/en/products/hmc1133.html#product-overview> [Access 9 September 2020].
- [96] IDT IDTF2258NLGK Wideband Voltage Variable RF Attenuator datasheet. [Online] Available at: <https://www.idt.com/sg/en/products/rf-products/rf-attenuators/f2258-wideband-voltage-variable-rf-attenuator> [Access 9 September 2020].
- [97] Qorvo TQP5525 5 GHz 802.11a/n/ac Wi-Fi High Power Amplifier datasheet. [Online] Available at: <https://www.qorvo.com/products/p/TQP5525> [Access 9 September 2020].
- [98] ADI HMC717ALP3E GaAs pHEMT MMIC Low Noise Amplifier, 4.8 to 6.0 GHz 5 GHz 802.11a/n/ac Wi-Fi High Power Amplifier datasheet. [Online] Available at: <https://www.analogue.com/en/products/hmc717a.html> [Access 9 September 2020].
- [99] ADI HMC8038LP4CETR High Isolation, Silicon SPDT, Nonreflective Switch, 0.1 GHz to 6.0 GHz datasheet. [Online] Available at: <https://www.analogue.com/en/products/hmc8038.html> [Access 9 September 2020].
- [100] ADI ADRF5044 100 MHz to 30 GHz, Silicon, SP4T Switch datasheet. [Online] Available at: <https://www.analogue.com/en/products/adrf5044.html> [Access 9 September 2020].
- [101] pads.com. (2020). *PADS PCB Design Software – Mentor Graphics*. [online] Available at: <https://pads.com> [Accessed 25 Feb 2020].
- [102] M. C. Tan, M. Li, Q. H. Abbasi and M. Imran, "Sensor Aided Beamforming in Vehicular Environment," *2020 International Conference on UK-China Emerging*

- Technologies (UCET)*, Glasgow, United Kingdom, 2020, pp. 1-4, doi: 10.1109/UCET51115.2020.9205411.
- [103] R. M. Abdelmoneem, E. Shaaban and A. Benslimane, "A Survey on Multi-Sensor Fusion Techniques in IoT for Healthcare," *2018 13th International Conference on Computer Engineering and Systems (ICCES)*, Cairo, Egypt, 2018, pp. 157-162, doi: 10.1109/ICCES.2018.8639188.
- [104] S. Aygün, E. O. Güneş, M. A. Subaşı and S. Alkan, "Sensor Fusion for IoT-based Intelligent Agriculture System," *2019 8th International Conference on Agro-Geoinformatics (Agro-Geoinformatics)*, Istanbul, Turkey, 2019, pp. 1-5, doi: 10.1109/Agro-Geoinformatics.2019.8820608.
- [105] P. Kaur and R. Sobti, "Sensor Fusion Algorithm For Software Based Advanced Driver-Assistance Intelligent Systems," *2018 First International Conference on Secure Cyber Computing and Communication (ICSCCC)*, Jalandhar, India, 2018, pp. 457-460, doi: 10.1109/ICSCCC.2018.8703269.
- [106] T. Chakraborty, S. Yamaguchi and S. K. Datta, "Sensor Fusion and Adaptive Cruise Control for Self Driving Platoon," *2018 IEEE 7th Global Conference on Consumer Electronics (GCCE)*, Nara, 2018, pp. 231-235, doi: 10.1109/GCCE.2018.8574639.
- [107] Q. P. Ha, S. Metia and M. D. Phung, "Sensing Data Fusion for Enhanced Indoor Air Quality Monitoring," in *IEEE Sensors Journal*, vol. 20, no. 8, pp. 4430-4441, 15 April 2020, doi: 10.1109/JSEN.2020.2964396.
- [108] B. P. L. Lau, N. Wijerathne, B. K. K. Ng and C. Yuen, "Sensor Fusion for Public Space Utilization Monitoring in a Smart City," *IEEE Internet of Things Journal*, vol. 5, no. 2, pp. 473-481, April 2018, doi: 10.1109/JIOT.2017.2748987.
- [109] H. Agarwal, P. Tiwari and R. G. Tiwari, "Exploiting Sensor Fusion for Mobile Robot Localization," *Third International conference on I-SMAC (IoT in Social, Mobile, Analytics and Cloud) (I-SMAC)*, Palladam, India, 2019, pp. 463-466, doi: 10.1109/I-SMAC47947.2019.9032653.
- [110] U-blox positioning chips and modules with dead reckoning functions. [online] Available at: <https://www.u-blox.com/en/positioning-chips-and-modules#tab-dead-reckoning> [Access 29 May 2020].

- [111] Calculate distance, bearing and more between Latitude/Longitude points [online]  
Available at: <https://www.movable-type.co.uk/scripts/latlong.html> [Access 3 Jun, 2020]
- [112] Quectel Wireless Solutions. [online] Available at:  
<https://www.quectel.com/product/l26dr.htm> [Assess 25 Jun 2020]

# Appendix A: Permission Request Form



## Permission Request Form

---

To:

Deric Lee Chyan, Managing Director of RFNet Technologies Pte Ltd

I am preparing a thesis on my research with the following title:

**Design of Antenna Array and Data Streaming Platform for Low-Cost Smart Antenna Systems**

to be submitted to

**University of Glasgow**

James Watt School of Engineering

Room 422 James Watt South Bldg,

Glasgow

G12 8QQ

United Kingdom

and I am requesting permission to use the material described below from RFNet.

1. Cost simulation for wireless deployment in the transportation market.
2. The material was taken from the training resources that was prepared for the system integrator (SI).

I will ensure that full acknowledgement is given to your company.

Would you kindly grant permission for me to utilise the materials for thesis writing, I would like to ask you to sign below and return the form to the address given below.

Thank you very much for your kind assistance.

Date: 13 September 2020

Requested by: Tan Moh Chuan

Address:

University of Glasgow

537 Clementi Road, Ngee Ann Polytechnic,

Level 4 SIT Building.

599495 Singapore

---

Permission granted,

Date:

By:

Deric Lee Chyan

Managing Director

RFNet Technologies Pte Ltd

## **Appendix B: PCB Gerber Artwork File for the Antenna Array.**

The Antenna array was constructed by two PCBs, the top PCB, which is a single layer board and the bottom PCB, which is a 2-layer PCB, the top PCB (PCB Part number: PCB-1086-00) consists of the antenna elements at the top layer and the bottom PCB (PCB Part number: PCB-1087-00) consists of the solid ground plane on top layer and antenna feeding network at the bottom layer. The PCB specifications and the gerber artwork of the PCBs are listed below.

## PCB P/N: PCB-1086-00 Specifications

**Descriptions:** Top Side PCB (Antenna Elements)

### General Specifications:

1. This is a 1-layer PCB board
2. Substrate Material: Taizhou Wangling F4BTM-2, Dielectric Constant = 3.
3. Finishing: Immersion Gold over Electroless Nickel
4. V-cut: 2 locations.

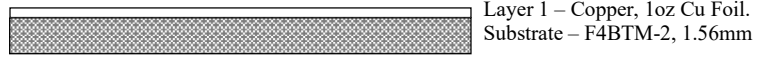


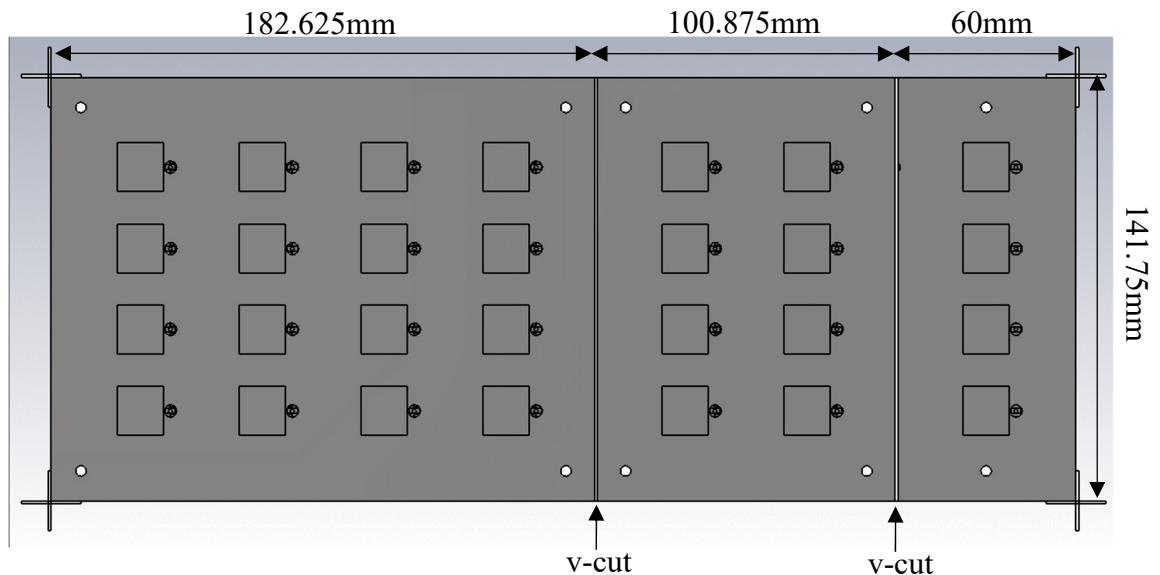
Figure1: PCB Stack up information.

5. Descriptions of gerber files.

| Gerber filename       | Descriptions  |
|-----------------------|---|
| TopPCB L1 Signal.gbr  | Layer 1   |
| TopPCB Drill List.gbr | Drilling List<br>Ø3.5 mm x 10 : NPTH<br>Ø1.3 mm x 28 : NPTH |
| V-cut.gbr             | 2 x V-cut pint  |
| Outline.gbr           | PCB Outline 343.5 x 141.75 mm                               |

Gerber Information.

### PCB dimensions



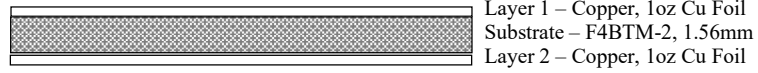
Top PCB (PCB-1086) – Top View

## PCB P/N: PCB-1087-00 Specifications

**Descriptions:** Bottom Side PCB (Solid Ground and Antenna Feeding Network)

**Note:**

1. This is a 2-layer PCB board
2. Substrate Material: Taizhou Wangling F4BTM-2, Dielectric Constant = 3.
3. Finishing: Immersion Gold over Electroless Nickel
4. V-cut: 2 locations.



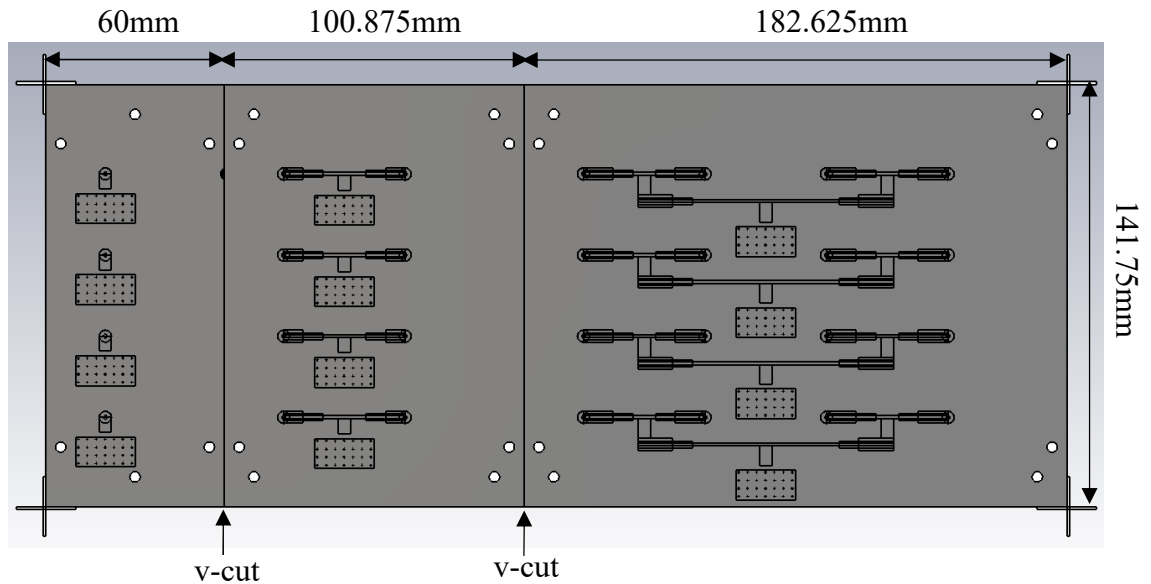
*Figure1: PCB Stack up information.*

5. Descriptions of gerber files.

| Gerber filename       | Descriptions  |
|-----------------------|---|
| BotPCB L1 Signal.gbr  | Layer 1   |
| BotPCB L2 GND.gbr     | Layer 2   |
| BotPCB Drill List.gbr | Drilling list<br>Ø3.5 mm x 22 : NPTH<br>Ø1.3 mm x 28 : NPTH<br>Ø0.5 mm x 784: PTH |
| V-cut.gbr             | 2 x V-cut pint  |
| Outline.gbr           | PCB outline 343.5 x 141.75 mm   |

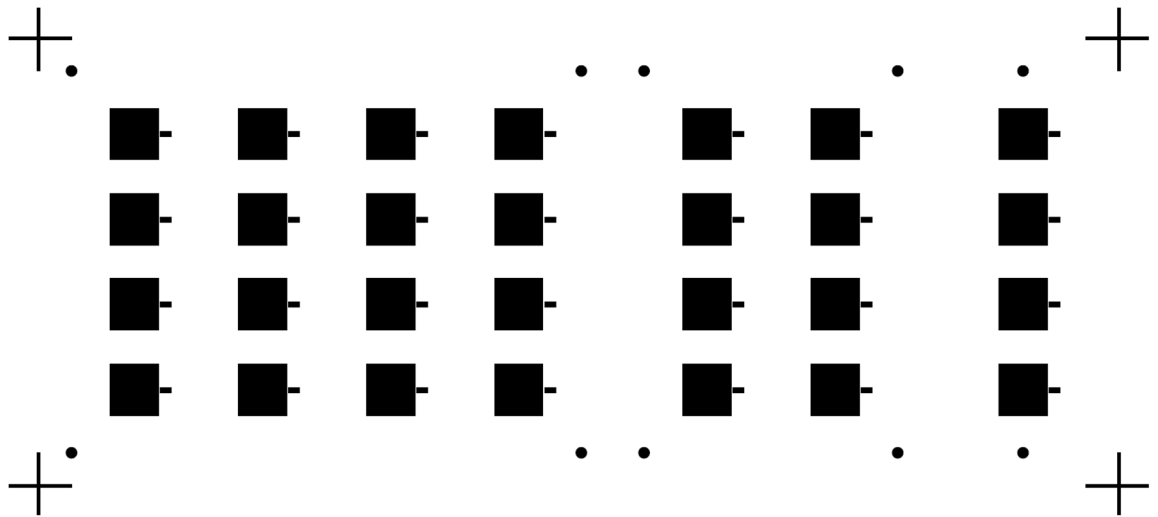
*Gerber Information.*

6. PCB dimensions

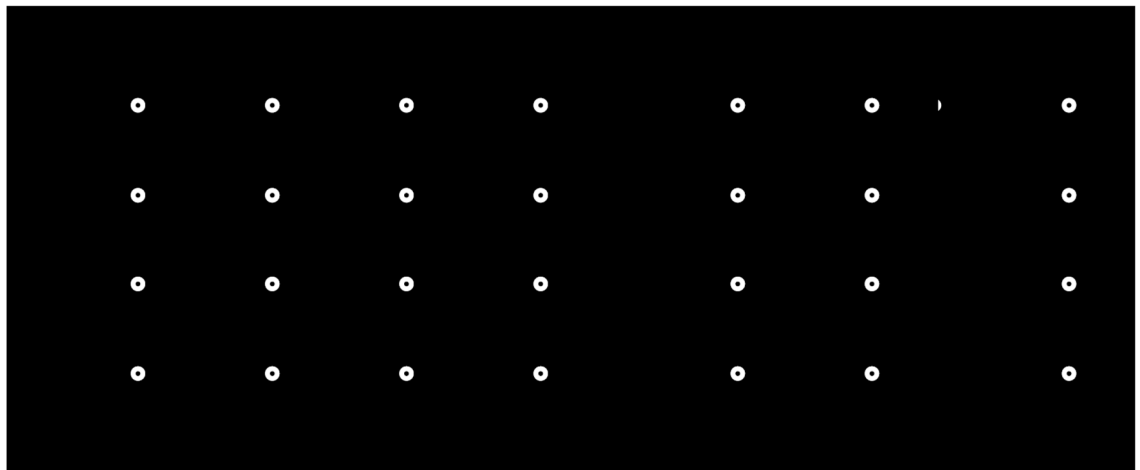


*Bottom PCB (PCB-1087) – Bottom View*

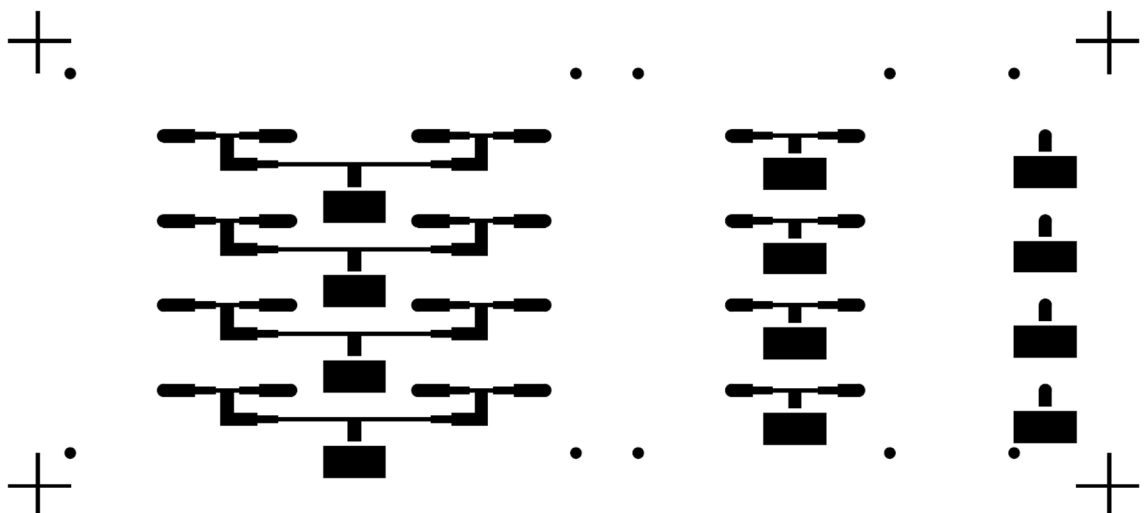
PCB Gerber Artwork for the antenna arrays



*PCB-1086 (Top Layer)*



*PCB-1087-00 (Top Layer)*



*PCB-1087-00 (Bottom Layer)*

# **Appendix C: Specification of the Antenna Substrate Material**

Following substrate material is used to fabricate the antenna array,

Substrate Part Number: F4BTM-2

Manufacturer: Taizhou Wangling

Location: Jiangsu, China

The Specification of F4BTM-2 is presented in the next page.

# Company Introduction

Established in 1984, the TAIZHOU WANGLING insulating materials factory is the professional manufacturer of the high frequency microwave printed circuit board, and is an integrated economical entity of science research、production and management in the field of electronic information material. Our company employs 86 engineering technicians, of which 15 employees own title senior professional post.. Our major products include Teflon woven glass fabric copper-clad laminates、Teflon woven glass fabric copper-clad laminates with ceramic filled、microwave composite dielectric copper-clad substrate、microwave multilayer printed circuit board、microwave electronic device and insulation 、anti-sticking fabric, etc.. Our products are widely applied to the industries of aerospace、aviation 、 satellite communication 、 navigation 、 aerospace 、 radar 、 electronic countermeasure、3G、4G、5G communication、compass navigation satellite system、textile、clothing、food and so on. Our company has an annual production capacity of 1.36 million square meters for copper-clad laminate and 50000 square meters for microwave composite dielectric copper-clad substrate. We have successfully cooperated with national key projects many times and were approved by relevant departments from navigation, aviation, China manned space project and received the honor of “National Key New product” . Our company has passed the Quality Management System certification、the Environmental management system certification、the occupational health and safety management system certification、the quality management system of weapon equipment certification、and passed through the secrecy qualification level 3 certification. UL certification was passed in 2007.

Our company was granted with Jiangsu high technology enterprise, Jiangsu AAA credit grade enterprise and “observe contracts and keep promises” enterprise. In the scientific research, we rely on the support of domestic tertiary institutions and scientific research departments and founded Provincial Research Center for Engineering Technology. With the development of this industry, we are always based on the concept of “quality-focused and customer-oriented” and continually meet customers requirements to achieve a better cooperation.

In order to let new and old customers learn more our products and have a wider choice, we specially edit this instruction.



# Contents

## Teflon (PTFE) series:

### 一. F<sub>4</sub> copper-clad laminates

- (1) Teflon woven glass fabric copper-clad laminates (F4B-1/2)
- (2) Teflon woven glass fabric copper-clad laminates with high permittivity (F4BK-1/2)
- (3) Teflon woven glass fabric copper-clad laminates with high permittivity (F4BM-1/2)
- (4) Teflon woven glass fabric copper-clad laminates with high permittivity (F4BMX-1/2)
- (5) Teflon woven glass fabric copper-clad laminates with high permittivity (F4BME-1/2)
- (6) Teflon woven glass fabric with ceramic membrane copper-clad laminates (F4BM-2-A)
- (7) Teflon woven glass fabric with ceramic membrane copper-clad laminates (F4BME-2-A)
- (8) Teflon woven glass fabric with ceramic filler copper-clad laminates (F4BTM-1/2)
- (9) Teflon woven glass fabric with ceramic filler copper-clad laminates (F4BTME-1/2)
- (10) Teflon woven glass fabric planar resistor copper-clad laminates (F4BDZ294)
- (11) Metal base Teflon woven glass fabric copper-clad laminates (F4B-1/AL、Cu)

## Teflon woven glass fabric with ceramic filler copper-clad laminates

### F<sub>4</sub>BTM-1/2

F<sub>4</sub>BTM-1/2 is laminated by laying up of the varnished glass cloth with Teflon resin and filler with the Nano-ceramic, according to the scientific formulation and strict technology process. This product takes advantages over F<sub>4</sub>BM series in the electrical performance、improves the heat dissipation effect and has the small coefficient of thermal expansion.

#### Technical Specifications:

|                                       |  |  |                                 |                                 |                                 |                                  |
|---------------------------------------|--|--|---------------------------------|---------------------------------|---------------------------------|----------------------------------|
| Appearance                            | Meet the specification requirements for the laminate of microwave PCB<br>by National and Military Standards. |  |                                 |                                 |                                 |                                  |
| Types                                 | F <sub>4</sub> BTM-1/2<br>(255)  | F <sub>4</sub> BTM-1/2<br>(265)  | F <sub>4</sub> BTM-1/2<br>(285) | F <sub>4</sub> BTM-1/2<br>(294) | F <sub>4</sub> BTM-1/2<br>(300) | F <sub>4</sub> BTM-1/2<br>(320)  |
|                                       | F <sub>4</sub> BTM-1/2<br>(338)  | F <sub>4</sub> BTM-1/2<br>(350)  | F <sub>4</sub> BTM-1/2<br>(400) | F <sub>4</sub> BTM-1/2<br>(440) | F <sub>4</sub> BTM-1/2<br>(615) | F <sub>4</sub> BTM-1/2<br>(1020) |
| Dimension<br>(mm)                     | 610×460  | 600×500  | 1220×914                        | 1220×1000                       |                                 |                                  |
|                                       | For special dimension, customized laminates is available.  |  |                                 |                                 |                                 |                                  |
| Thickness<br>and<br>Tolerance<br>(mm) | Laminate<br>thickness  | 0.254  | 0.508                           | 0.762                           | 0.787                           | 1.016                            |
|                                       | Tolerance  | ±0.025   | ±0.05                           | ±0.05                           | ±0.05                           | ±0.05                            |
|                                       | Laminate<br>thickness  | 1.27   | 1.524                           | 2.0                             | 3.0                             | 4.0                              |
|                                       | Tolerance  | ±0.05  | ±0.05                           | ±0.075                          | ±0.09                           | ±0.1                             |
|                                       | Laminate<br>thickness  | 5.0  | 6.0                             | 9.0                             | 10.0                            | 12.0                             |
|                                       | Tolerance  | ±0.1   | ±0.12                           | ±0.18                           | ±0.18                           | ±0.2                             |
| Mechanical<br>property                | Peel strength (1oz<br>copper)  | Normal state: ≥18N/cm; No bubble、delamination、peel strength≥15N/cm (in the constant humidity and temperature、and keep in the melting solder of 265℃±2℃ for 20 seconds) . |                                 |                                 |                                 |                                  |
| Thermal<br>stress                     | After solder float, 260° C, 10s, ≥3 times , no delamination and blister.                                     |  |                                 |                                 |                                 |                                  |
| Chemical<br>Property                  |  |  |                                 |                                 |                                 |                                  |
|                                       |  |  |                                 |                                 | Value                           |                                  |

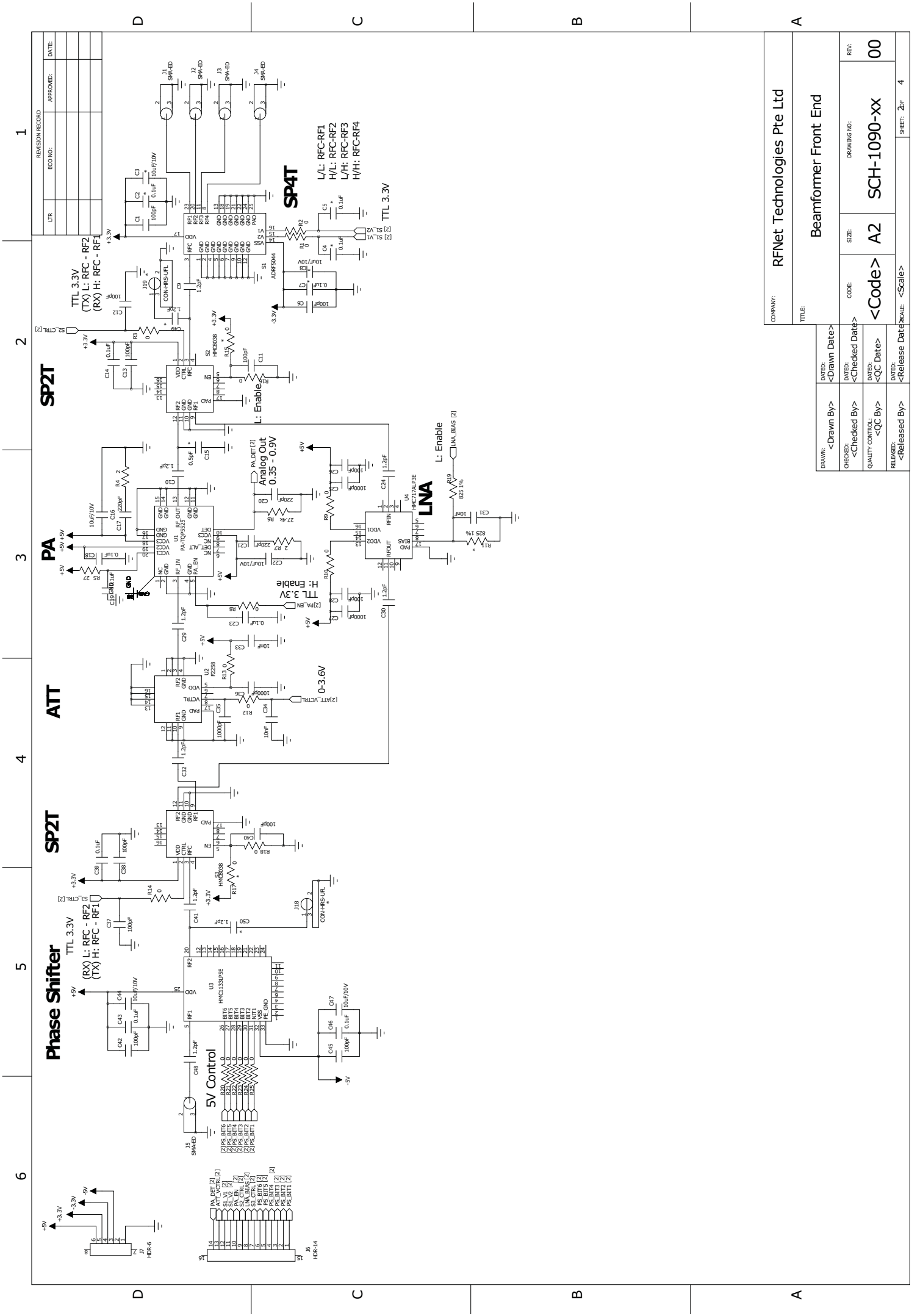
|   |                                   |   |   |   |                    |
|---|-----------------------------------|---|---|---|--------------------|
| Electrical<br>Property                                  | Density                           | Normal state  |   | g/ cm <sup>3</sup>  | 2.1～3.0            |
|   | Moisture<br>Absorption            | Dip in the distilled<br>water of 20±2℃<br>for24 hours |   | %   | ≦0.05              |
|   | Operating<br>Temperature          | High-low temperature<br>chamber                       |   | ℃   | -50℃～+260℃         |
|   | Thermal<br>Conductivity           |   |   | W/m/k   | 0.6~0.9            |
|   | CTE<br>(typical)                  | -55～288℃<br>(ε r : 2.55~3.0)                          | ppm/℃                                   | 15 (x)  |                    |
|   |                                   |   |   | 15 (y)  |                    |
|   |                                   |   |   | 65 (z)  |                    |
|   | CTE<br>(typical)                  | -55～288℃<br>(ε r : 3.2~3.5)                           | ppm/℃                                   | 15 (x)  |                    |
|   |                                   |   |   | 15 (y)  |                    |
|   |                                   |   |   | 55 (z)  |                    |
|   | CTE<br>(typical)                  | -55～288℃<br>(ε r : 4.0~10.2)                          | ppm/℃                                   | 12 (x)  |                    |
|   |                                   |   |   | 14 (y)  |                    |
|   |                                   |   |   | 50 (z)  |                    |
|   | Shrinkage<br>Factor               | 2 hours in boiling<br>water                           |   | %   | < 0.0002           |
|   | Surface<br>Resistivity            | 500V<br>DC  | Normal state                            | M・Ω   | ≧1×10 <sup>6</sup> |
|   |                                   |   | Constant<br>humidity and<br>temperature |   | ≧1×10 <sup>5</sup> |
|   | Volume<br>Resistivity             | Normal state  |   | MΩ.cm   | ≧1×10 <sup>7</sup> |
|   |                                   | Constant humidity and<br>temperature                  |   |   | ≧1×10 <sup>6</sup> |
|   | Surface<br>dielectric<br>strength | Normal state  |   | δ=1mm (Kv/mm)   | ≧1.2               |
|   |                                   | Constant humidity and<br>temperature                  |   |   | ≧1.1               |
| Dielectric<br>Constant                                  | 10GHz                             |   | ε r                                     | 2.85±0.05、2.94±0.05<br>3.00±0.05、3.20±0.05<br>3.38±0.05、3.50±0.05<br>4.00±0.08、4.40±0.10<br>6.15±0.15、10.2±0.25 |                    |
| Thermal<br>Coefficient of<br>ε r<br>(PPM/℃)<br>-50~150℃ | ε r                               |   | Value                                   |   |                    |
|   | 2.85, 2.94                        |   | -85                                     |   |                    |
|   | 3.0, 3.2                          |   | -75                                     |   |                    |
|   | 3.38                              |   | -65                                     |   |                    |
|   | 3.5                               |   | -60                                     |   |                    |
|   | 4.0                               |   | -60                                     |   |                    |
|   | 4.4                               |   | -60                                     |   |                    |
|   | 6.15                              |   | -55                                     |   |                    |

|  |                              |        |     |           |                           |
|--|------------------------------|--------|-----|-----------|---------------------------|
|  |                              | 10.2   | -50 |           |                           |
|  | Dissipation<br>Factor        | 10GHz  | tgδ | 2.55~3.0  | $\leq 1.5 \times 10^{-3}$ |
|  |                              |        | tgδ | 3.0~3.5   | $\leq 2.0 \times 10^{-3}$ |
|  |                              |        | tgδ | 4.0~10.20 | $\leq 2.5 \times 10^{-3}$ |
|  | UL<br>Flammability<br>Rating | 94 V-0 |     |           |                           |

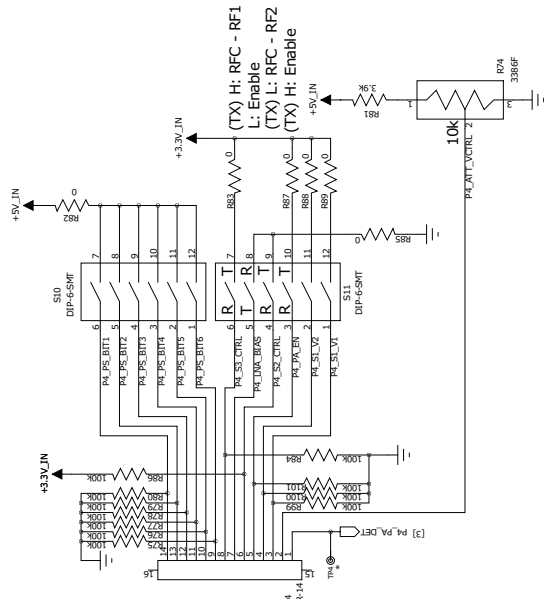
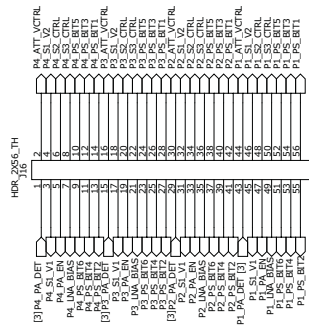
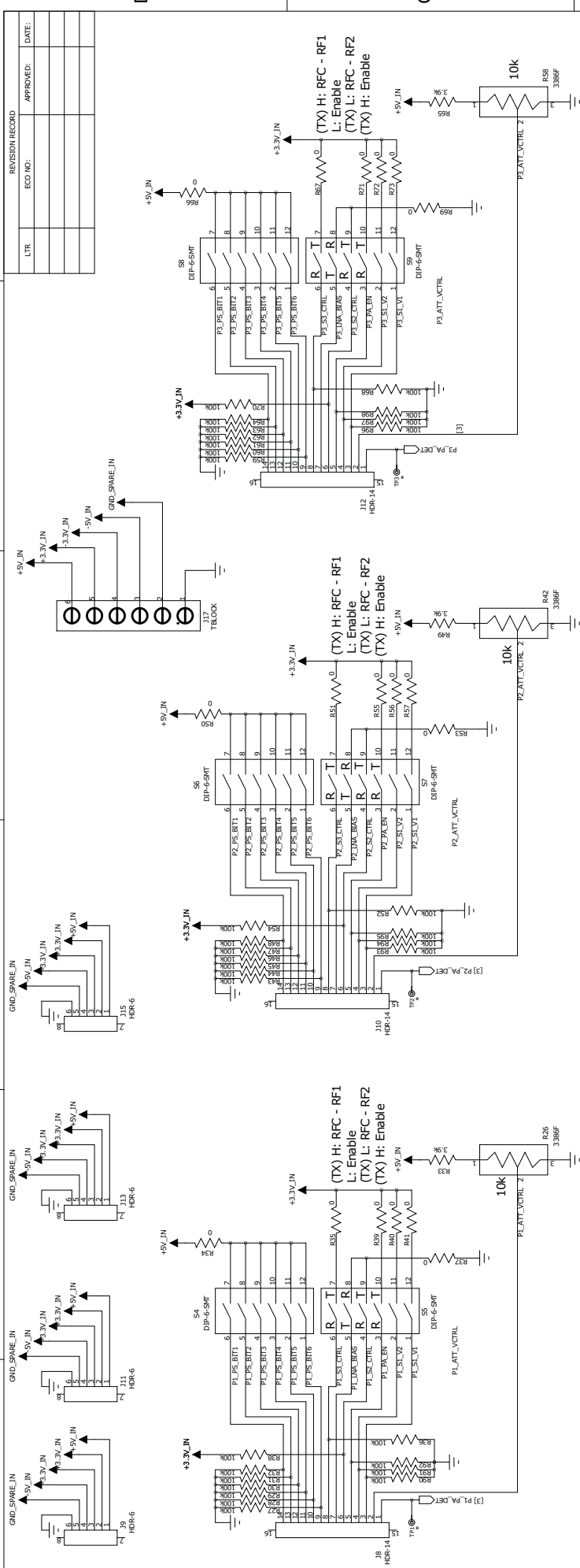
## **Appendix D: Schematic Diagram of the T/R Module**

The electronic components wiring diagram is represented in the schematic diagram generated by the CAD software from Mentor Graphic, all the components, and parts are designed into the schematic diagram and export to PADS PCB design software for PCB traces routing to route all the necessary connection between the components.





|                                     |                       |
|-------------------------------------|-----------------------|
| COMPANY: RFNet Technologies Pte Ltd |                       |
| TITLE: Beamformer Front End         |                       |
| DRAWN: <Drawn By>                   | DATED: <Drawn Date>   |
| CHECKED: <Checked By>               | DATED: <Checked Date> |
| QUALITY CONTROL: <QC By>            | DATED: <QC Date>      |
| RELEASED: <Released By>             | DATED: <Release Date> |
| CODE: <Code>                        | SIZE: A2              |
| DRAWING NO: SCH-1090-xx             | REV: 00               |
| SHEET: 2 of 4                       |                       |







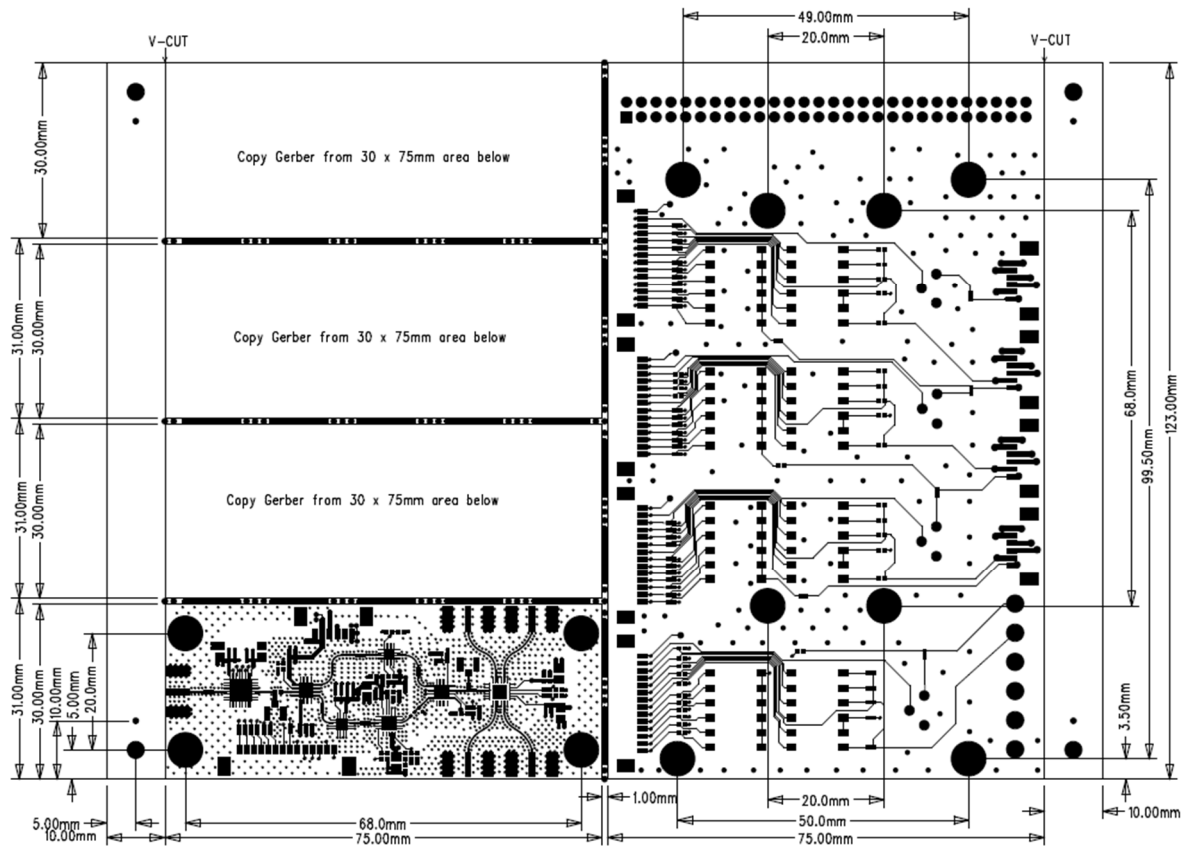
# **Appendix E: PCB Gerber Artwork File of the T/R Module**

This appendix includes the following:

1. The dimension of the beamformer T/R module PCB (PCB-1090-BF) and the Interface board (P/N: PCB-1090-IM)
2. PCB fabrication Specifications
3. PCB-1090 gerber file descriptions
4. The Gerber Artwork for T/R module, layer 1 to layer 4
5. Assembly Drawing for PCB-1090-BF and PCB-1090-IM.








- 1) PCB Dimension Drawing with penalization for both beamforming Frontend and Interface Module, each panel consists of 4 sets of PCB-1090-BF (Beamformer T/R module) and 1 set of PCB-1090-IM (Interface module).

*PCB dimension of the T/R module and interface board*



- 2) Specifications for PCB Fabrication (unless otherwise specified)
- FINISHED BOARD THICKNESS TO BE 60 MILS +/- 10%.
  - SOLDEMASK TO BE LPI, COLOR: GREEN, BOTH SIDES.
  - PLATING: IMMERSION GOLD OVER ELECTROLESS NICKEL.
  - SILKSCREEN: TOP SIDE, COLOR: WHITE
  - SEE DRILL CHART FOR FINISHED HOLE SIZES.
  - HOLE TOLERANCE IS +/- 3 MILS UNLESS OTHERWISE SPECIFIED.
  - SEE FILM FOR LAYER SEQUENCE.
  - THIS IS A 4 LAYER BOARD.
  - TRACE WIDTHS IN ARTWORK ARE FINISHED SIZES. DO NOT DEVIATE WITHOUT PRIOR AUTHORIZATION FROM RFNet.
  - REMOVE UNUSED PADS FROM INTERNAL LAYERS.
  - 50 OHMS FOR THE 16 MIL TRACE WIDTH TO BE FINISHED SIZES +/- 1 MIL ON TOP LAYERS
  - BOW AND TWIST: .75% MAX ALLOWABLE.
  - PCB MATERIAL: RO4003 OVER FR4
  - PROVIDE CROSS SECTION WITH COMPLETED BOARDS
  - COPPER THICKNESSES SHOWN ARE BEFORE PLATING.
  - FABRICATE PER IPC-6012 CLASS 2 (LATEST REVISION) UNLESS OTHERWISE SPECIFIED.
  - MATERIAL: NEMA GRADE FR-4, HI-TEMP 170 DEGREE C MIN, PER IPC-4101/24.
  - TEARDROPS: OK TO ADD AS NEEDED TO MEET 0.002 MINIMUM TRACE INTERCONNECTS AS PER IPC-6012 CLASS 2.
  - NO THIEVING ALLOWED ON THIS BOARD.
  - PANELISATION: REFER TO PANELISATION FILE FOR DETAIL
  - PLUG HOLE AT TOP AND BOTTOM SIDE FOR HOLES SIZE <= 12 MIL

- v. REMOVE PART OR PORTION OF THE SILK SCREEN IF IT IS CROSSES OVER THE PADS OR NON-PLUG PLATED THROUGH HOLE
- w. PCB LAYER STACK UP INFORMATION

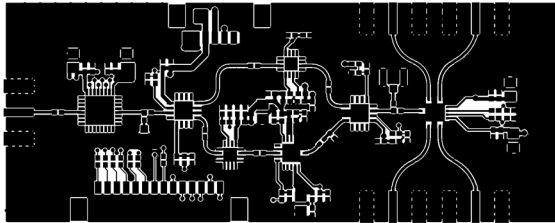
|   |  |
|---|--|
|  | TOP SIDE - LAYER 1 (1/2 oz. Cu FOIL)                         |
|  | RO4003 - 8 MILS – CRITICAL                                   |
|  | GND PLANE - LAYER 2 (1 oz. Cu FOIL)                          |
|  | FR4 - Not Critical - Adjust to meet finished board thickness |
|  | POWER PLANE - LAYER 3 (1 oz. Cu FOIL)                        |
|  | FR4 - Not Critical - Adjust to meet finished board thickness |
|  | BOTTOM SIDE - LAYER 4 (1/2 oz. Cu FOIL)                      |

3) Descriptions of gerber files.

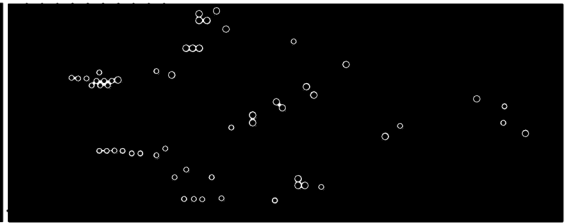
| Gerber filename     | Descriptions             |
|---------------------|--------------------------|
| 11.pho              | Layer 1 (top layer)      |
| 12.pho              | Layer 2 (inner layer 1)  |
| 13.pho              | Layer 3 (inner layer 2_  |
| 13.pho              | Layer 4 (bottom layer_   |
| smt.pho             | Solder mask top          |
| smb.pho             | Solder mask bottom       |
| pmt.pho             | Paste mask layer – top   |
| sst.pho             | Silk screen layer        |
| drill.pho           | Drill drawing file       |
| AssemblyDrawing.pho | PCB outline 170 x 123 mm |

4) The Gerber Artwork for T/R module, layer 1 to layer 4 are shown below.

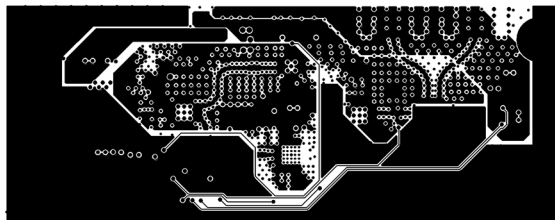
*Layer 1 (signal Layer)*



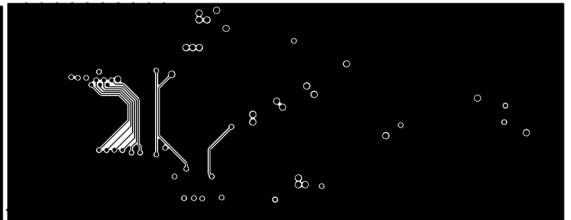
*Layer 2 (Ground Layer)*



*Layer 3 (Power Layer)*

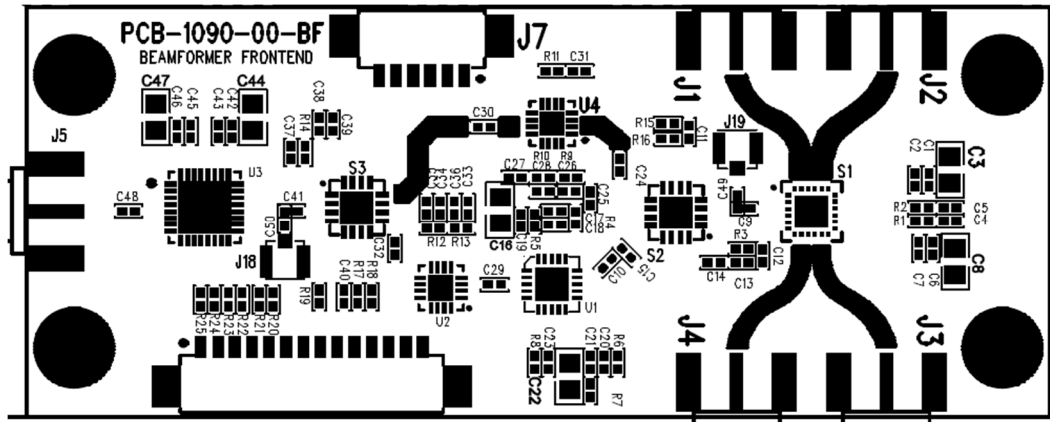


*Layer 4 (Ground and Signal Layer)*

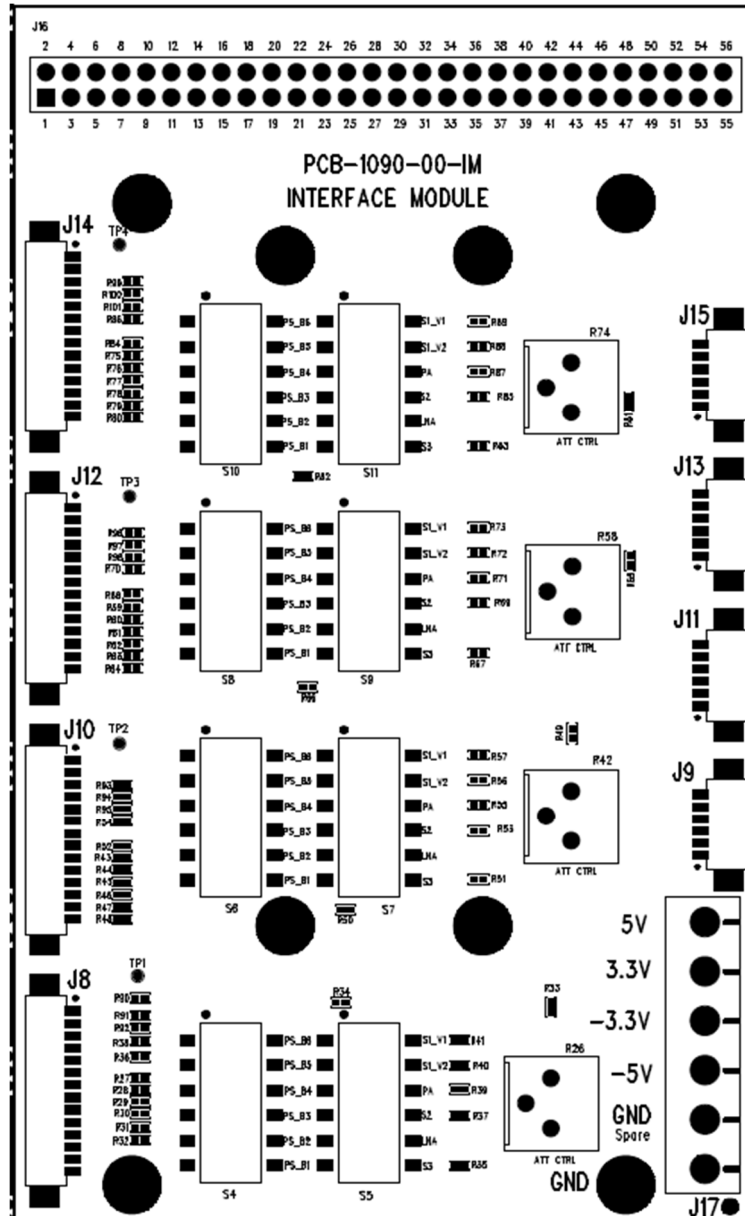


5) Assembly Drawing

Assembly Drawing for PCB-1090-BF (Beamformer board)



Assembly drawing of the PCB-1090-IM (Interface Board).



# Appendix F: Bill-of-Materials (BOM) of the T/R Module

The Bill-of-Materials (BOM) of the T/R module consists of the following 3 groups of components that are categories according to the module and process.

1. **PCBA-1090-BF (RF Beamforming Frontend T/R Module)** consists of material that is required to assemble the individual RF beamforming frontend T/R module.
2. **PCBA-1090-IM (Interface Module for RF Beamforming Frontend)** consists of material that is required to assemble the Interface module.
3. **Final Assembly (Materials for Final Assembly)**, consists of material that is required to connect between the T/R module and the interface module.

## Appendix F: Bill-of-Materials (BOM) of the T/R Module

| S/N  | BOM Level | Designator  | Description  | Value             | Mfg.                      | P/N                                       | Vendor                 | Qty |
|--|-----------|---|--|-------------------|---------------------------|---|------------------------|-----|
| <b>PCBA-1090-BF (RF Beamforming Frontend T/R Module)</b> |           |   |  |                   |                           |   |                        |     |
| 1.00   | SMT       | C1 C6 C11-13<br>C26 C28 C37-<br>38 C40 C42<br>C45 | CAP, 0402,<br>NP0, 100 pF,<br>+/-5%, 50 V  | 100 pF, 50 V      | Murata                    | GRM1555C1H101JA01D/<br>GRM1555C1H101JZ01D | Murata                 | 12  |
| 2.00   | SMT       | C14 C18-19<br>C23 C39 C43<br>C46                  | CAP, 0402,<br>X5R, 0.1 uF, +/-<br>10%, 25 V  | 0.1 uF, 25 V      | Murata                    | GRM155R61E104KA87D                        | AVnet                  | 7   |
| 3.00   | SMT       | C16 C22 C44<br>C47                                | CAP, 0805,<br>X7R, 10 uF, +/-<br>10%, 10 V   | 10 uF, 10 V       | Murata/<br>Taiyo<br>Yuden | GRM21BR71A106KE51L/<br>LMK212ABJ106KG-T   | Alphatec/<br>RS        | 4   |
| 4.00   | SMT       | C17 C20-21  | CAP, 0402,<br>COG, 220 pF,<br>+/- 5%, 50 V   | 220 pF, 50 V      | Murata                    | GRM1555C1H221JA01D                        | Alphatec               | 3   |
| 5.00   | SMT       | C25 C27 C35-<br>36                                | CAP, 0402,<br>X7R, 1000pF,<br>+/-5%, 50 V  | 1000 pF, 50<br>V  | Murata                    | GRM155R71H102JA01/<br>GRM155R71H102KA01D  | Murata                 | 4   |
| 6.00   | SMT       | C31 C33-34  | CAP, 0402,<br>X7R, 0.01 uF,<br>+/- 10%, 25 V   | 0.01 uF, 25 V     | Walsin                    | 0402B103K250CT/<br>GRM155R71E103KA01D     | GEPS                   | 3   |
| 7.00   | SMT       | C9-10 C24<br>C29-30 C32<br>C41 C48                | CAP, 0402,<br>COG, 1.1 pF,<br>+/- 0.1 pF, 50 V   | 1.1 pF, 50 V      | Murata                    | GJM1555C1H1R1BB01D                        | Alphatec               | 8   |
| 8.00   | MI        | J1-5  | RF / Coaxial<br>Connector,<br>SMA Coaxial,<br>Straight Jack,<br>Board Edge /<br>End Launch, 50<br>ohm                        | RF Con            | Samtec                    | SMA-J-P-H-ST-EM1                          | Element<br>14          | 5   |
| 9.00   | SMT       | J6  | PicoBlade™<br>Connector<br>System 1.25<br>mm Pitch<br>PicoBlade™<br>Header, Surface<br>Mount, Right<br>Angle, 14<br>Circuits | 14 contacts       | Molex                     | 0532611471                                | Element<br>14          | 1   |
| 10.00  | SMT       | J7  | PicoBlade<br>Connector<br>System,<br>1.25mm Pitch<br>PicoBlade<br>Header, Surface<br>Mount, Right-<br>Angle, 6<br>Circuits   | 6 contacts        | Molex                     | 0532610671                                | Element<br>14          | 1   |
| 11.00  | SMT       | R1-3 R8-10<br>R12-14 R16<br>R18 R20-25            | RES, 0402, 0<br>OHMS, 1/16 W   | 0 ohm             | Walsin/<br>KOA            | WR04X000PTL/<br>RK73Z1ETTP                | GEPS/<br>RS            | 17  |
| 12.00  | SMT       | R19   | RES, 0402, 825<br>OHMS, +/-1%,<br>1/16 W   | 825 ohms,<br>1%   | Walsin/<br>Vishay         | WR04X8250FTL/<br>CRCW0402825RFKED         | GEPS/<br>Element<br>14 | 1   |
| 13.00  | SMT       | R4 R7   | RES, 0402, 2<br>OHMS, +/-1%,<br>1/16 W   | 2 ohms            | Walsin/<br>Kamaya         | WR04X2R0JTL/<br>RMC1/16S-2R0FTH           | GEPS/<br>RS            | 2   |
| 14.00  | SMT       | R5  | RES, 0402, 27<br>OHMS, +/-5%,<br>1/16 W  | 27 ohms           | Walsin/<br>Vishay         | WR04X270JTL/<br>CRCW040227R0FKED          | GEPS/<br>RS            | 1   |
| 15.00  | SMT       | R6  | RES,<br>0402, 27.4K<br>OHMS, +/-1%,<br>1/16 W  | 27.4K ohms,<br>1% | Walsin/<br>Multicom<br>p  | WR04X2742FTL/<br>MCMR04X2742FTL           | GEPS/<br>Element<br>14 | 1   |
| 16.00  | SMT       | S1  | 100 MHz to 30<br>GHz, Silicon,<br>SP4T Switch  | SP4T              | ADI                       | ADRF5044BCCZN                             | Arrow                  | 1   |
| 17.00  | SMT       | S2-3  | High Isolation,<br>Silicon SPDT,<br>Nonreflective<br>Switch, 0.1<br>GHz to 6.0 GHz   | SPDT              | ADI                       | HMC8038LP4CE                              | Arrow                  | 2   |

## Appendix F: Bill-of-Materials (BOM) of the T/R Module

| S/N   | BOM Level | Designator  | Description  | Value         | Mfg.           | P/N                           | Vendor     | Qty       |
|---|-----------|---|--|---------------|----------------|-------------------------------|------------|-----------|
| 18.00   | SMT       | U1  | 4.9-5.9 GHz PA   | PA            | Qorvo          | TQP5525                       | RFMW       | 1         |
| 19.00   | SMT       | U2  | Voltage Variable RF Attenuator 50 to 6000 MHz  | ATT           | IDT            | IDTF2258NLGK                  | Digikey    | 1         |
| 20.00   | SMT       | U3  | GaAs MMIC 6-BIT Digital Phase Shifter, 4.8 - 6.2 GHz   | Phase Shifter | ADI            | HMC1133LP5E                   | Arrow      | 1         |
| 21.00   | SMT       | U4  | 4.8 – 6 GHz LNA  | LNA           | ADI            | HMC717ALP3E                   | Arrow      | 1         |
| <b>Total SMT Components Count</b>                         |           |   |  |               |                |                               |            | <b>77</b> |
| <b>PCBA-1090-IM (Interface Module for RF beamforming)</b> |           |   |  |               |                |                               |            |           |
| 22.00   | SMT       | R26 R42 R58 R74   | RES, 10 k ohms Through Hole Trimmer Resistor 0.5 W Finger Adjust Bourns 3386 series                  | 10k ohms      | Bourns         | 3386F-1-103TLF                | RS         | 4         |
| 23.00   | MI        | S4-11   | DIP / SIP Switch, 6 Circuits, Slide, SMD, SPST, 24 VDC, 25 mA  | 6 Dip         | Omron          | A6S6104H                      | Element 14 | 8         |
| 24.00   | SMT       | J9 J11 J13 J15  | PicoBlade Connector System, 1.25 mm Pitch PicoBlade Header, Surface Mount, Right-Angle, 6 Circuits   | 6 contacts    | Molex          | 0532610671                    | Element 14 | 4         |
| 25.00   | SMT       | J8 J10 J12 J14  | PicoBlade™ Connector System 1.25 mm Pitch PicoBlade™ Header, Surface Mount, Right Angle, 14 Circuits | 14 contacts   | Molex          | 0532611471                    | Element 14 | 4         |
| 26.00   | MI        | J17   | Standard Terminal Block, Wire to Board, CTB5000 Series, 6 Contacts, 5 mm, Terminal Block, PCB        | 6 contacts    | Camden Boss    | CTB5000/6                     | Element 14 | 1         |
| 27.00   | SMT       | R34-35 R37 R39-41 R50-51 R53 R55-57 R66-67 R69 R71-73 R82-83 R85 R87-89 | RES, 0402, 0, 1/16 W   | 0             | Walsin         | WR04X000PTL                   | GEPS       | 24        |
| 28.00   | SMT       | R27-32 R36 R38 R43-48 R52 R54 R59-64 R68 R70 R75-80 R84 R86 R90-101     | RES, 0402, 100K OHMS, +/-5%,1/16 W   | 100K ohms     | Walsin         | WR04X104JTL/ RC0402JR-07100KL | GEPS       | 44        |
| 29.00   | SMT       | R33 R49 R65 R81   | RES, 0402, 3.9K OHMS, +/-5%,1/16 W   | 3.9K ohms     | Walsin/ Vishay | WR04X392JTL/ CRCW04023K90FKED | GEPS/ RS   | 4         |



## Appendix F: Bill-of-Materials (BOM) of the T/R Module

| S/N  | BOM Level | Designator   | Description  | Value | Mfg.                                    | P/N                  | Vendor                                  | Qty       |
|--|-----------|--|--|-------|---|----------------------|---|-----------|
| 30.00  | SMT/MI    |  | PCB  | PCB   | Precision Circuit Manufacturers Pte Ltd | PCB-1090-00          | Precision Circuit Manufacturers Pte Ltd | 3         |
| <b>Total MI Components Count</b>                     |           |  |  |       |   |                      |   | <b>96</b> |
| <b>Final Assembly (Materials for Final Assembly)</b> |           |  |  |       |   |                      |   |           |
| 31.00  | FA        | Cable assembly between -BF and -IM module for data.  | Cable Assembly, PicoBlade 14 Position Receptacle, PicoBlade 14 Position Receptacle, 3.9", 100 mm             | --    | Molex                                   | 15134-1401           | Element 14                              | 4         |
| 32.00  | FA        | Cable assembly between -BF and -IM module for Power. | PicoBlade-to-PicoBlade Off-the-Shelf (OTS) Cable Assembly, Single Row, 100.00 mm Length, 6 Circuits, Natural | --    | Molex                                   | 0151340601           | Element 14                              | 4         |
| 33.00  | FA        | SMA adaptor  | RF / Coaxial Adapter, 50 ohms, 18 GHz, SMA, Plug, SMA, Plug, Straight Adapter, 50 ohms                       | --    | Multicom p                              | 19-22-2-TGG          | Element 14                              | 4         |
| 34.00  | FA        | 4-way power splitter                                 | Coaxial 30 W 0° 4-Way Power Divider 4 - 8 GHz  | --    | Quotana                                 | DBPD0404000800A      | Quotana                                 | 1         |
| 35.00  | FA        | Stand-off between T/R module                         | 10 mm M3 metal stand-off (M) - (F)   | --    | Harwin                                  | R30-3001002          | Element 14                              | 4         |
| 36.00  | AF        | Spring washer for stand-off                          | M3 Spring Washer, 2.36 mm compressed to 1 mm.  | --    | TR FASTENINGS                           | DM3 - DSSA2WA - S100 | Element 14                              | 4         |
| 37.00  | FA        | Power Supply for +5 V and -5 V                       | Power supply unit AC to +12 V / 2.8 A, +5 V / 6 A, -5 V / 0.5 A 65 W   | --    | Meanwel l                               | RT-65A               | RS Components                           | 1         |
| 38.00  | FA        | Power Supply for +3.3 V and -3.3 V                   | Power Supply unit 12 V to +3.3 V / 151 mA, -3.3 V / 151 mA, 1 W  | --    | XP Power                                | IHA0112D03           | Element 14                              | 1         |
| <b>Total FA Components Count</b>                     |           |  |  |       |   |                      |   | <b>23</b> |

Note:

BOM: Bill of Material

Mfg.: Manufacturer

P/N: Part Number

Qty: Quantity

SMT: Surface Mount Technology Part

MI: Manual Insert Part

FA: Final Assembly Part